



Munich School of Engineering

The Combined Smart Energy Systems Laboratory

Franz Christange, M. Sc.

Vollständiger Abdruck der von der Munich School of Engineering der Technischen Universität München zur Erlangung des akademischen Grades eines

Doktor-Ingenieurs (Dr.-Ing.)

genehmigten Dissertation.

Vorsitzender: Prof. Dr.-Ing. Jörg Ott

Prüfende der Dissertation:

1. Prof. Dr. Thomas Hamacher
2. Prof. Dr.-Ing Rolf Witzmann

Die Dissertation wurde am 09.06.2020 bei der Technischen Universität München eingereicht und durch die Munich School of Engineering am 15.02.2021 angenommen.

Preamble

I would like to take the chance to give a little personal note to this technical work. While visiting a market in Venice, together with my wife, a picture suddenly caught my eye - on a beautiful royal blue background with the moon and stars sparkling and a child pointing upwards to the sky, there was written in yellow letters:

*Don't tell me the sky's the limit
when there are footprints on the moon.*

read in Venice, by Paul Brandt

This aphorism may be slightly overblown, but it was one key aspect which made me to persevere and finally to manage this project with all its specific challenges: From the initial concept, to financing, laboratory design, purchase of the components and the laboratory construction.

I would like to thank all my colleagues, my family and friends and other supporters for their great support during this project. My work would not have been possible without them. I would like to highlight some persons who had a vital importance for me and the success of the project: First, I would like to highlight the role of my wife. She agreed to me doing this project, although it meant a high additional burden for the family in a difficult time. She tolerated me being angry or sad when things did not work as I expected, or when challenges seemed unsolvable to me. She supported me faithfully during a hard time.

Second, I would like to thank Prof. Hamacher. I came as a young man with a fresh degree without much practical experience into his office to advertise for a doctoral position. He did not just give me the chance for making this project, but he also trusted in me by giving me much freedom to realize my visions and to manage the project. This amount of trust cannot be taken for granted.

And I would like to thank my mother for spending many hours for proofreading and the linguistic support. Finally, I would like to thank my two small kids for always making me feel happy and laughing.

Abstract

The present work describes the design concept for the Combined Smart Energy Systems (CoSES) experimental microgrid research laboratory. The key aspect is the energy system model interconnection framework (ESMIF), which structures the different energy system processes, and with it, also the control and operation challenges in five consecutive layers. The first layer describes the processes of energy supply of the different locations in the grid in a 15 min time scale. The second layer specifies the power distribution of multiple different appliances across the physical phases in a time scale of 1 s. The third layer integrates the interaction of voltage and current magnitudes at 5 ms, while the fourth layer integrates the interaction of instantaneous voltages and currents at $100 \mu\text{s}$. At the fifth layer the four abstracted layers are realized as true physical actions.

The basis of the experimental microgrid research laboratory is the analysis of the research requirements in the context of the energy transition especially at the level of distribution grids. The fundamental transition is the replacement of the centralized power plants, which control large parts of the energy system through their synchronous generators, by distributed, mainly renewable energy sources. The result are upcoming challenges at all five ESMIF layers, from fluctuating generation to active harmonics damping, which have to be solved in the years to come. The microgrid laboratory provides a universal tool to analyze physical processes and to validate developed strategies and solutions at all five ESMIF layers in the context of low voltage grids.

The key aspect of the laboratory design is to flexibly allow to investigate different scenarios by considering all relevant processes. This leads to design the experimental systems for electricity, heat and communication and control, as these interact in the context of sector coupling and digitalization. The extent of the microgrid laboratory is five houses with a low voltage grid of about 2 km cable length and two further extensions. Multiple different generation, storage and sector coupling facilities are available, like photovoltaic, battery, combined heat and power and heat distribution grid systems. The electricity consumption is emulated through a power electronic load emulation facility. True weather conditions as well as artificial modeled conditions can be applied for the different scenarios.

The emulation of the electricity consumption requires algorithms to compute the load behavior. The proposed solution of this work describes the interaction of measured grid voltages and simulated load behavior which results in the consumption current setpoints at a time range of $4 \mu\text{s}$. The five ESMIF layers allow the algorithm to distinguish the differently abstracted processes of electricity consumption in time scales from $100 \mu\text{s}$ to 15 min. These layers represent the electro-physical behavior of the consumption devices and the behavior of humans, when they use various devices. Artificial weather is generated by the simulation of a parametric weather model. That allows to flexibly investigate scenarios at different locations with multiple weather conditions. The analysis and validation of these models show the model accuracy critically, based on comparisons with real measurements.

Contents

Abstract	2
Contents	3
List of Figures	5
List of Tables	8
1 Introduction	15
1.1 The future role of low voltage grids	17
1.2 Research in the context of microgrids	19
1.3 Microgrid laboratories and experimental facilities	22
1.4 Problem statement and contributions	23
2 Research Requirements	25
2.1 Fundamental physical-technical principles of energy system operation	25
2.2 Energy system model interconnection framework (ESMIF)	28
2.2.1 General framework description	28
2.2.2 Framework process description	30
2.3 Fundamental laboratory requirements	33
2.3.1 General laboratory requirements	34
2.3.2 Specific laboratory requirements	35
3 Laboratory Design	39
3.1 Overall design	40
3.1.1 Laboratory layout and dimension	40
3.1.2 Electric energy system	43
3.1.3 Thermal energy system	46
3.1.4 Communication and control system	48
3.2 Component design	49
3.2.1 Mean voltage system	49
3.2.2 Low voltage grid	51
3.2.3 Electricity load	58
3.2.4 Utility generators	60
3.2.5 Domestic electricity system requirements	61
3.2.6 Domestic heat systems	63

3.2.7	Measurement and real time control system	72
4	Laboratory HIL Models	75
4.1	Electricity consumption model of conventional households	75
4.1.1	Introduction to load modeling	76
4.1.2	System layer model	77
4.1.3	Provision layer	83
4.1.4	Distribution layer	89
4.1.5	Supply layer	92
4.2	Weather model	93
4.2.1	Introduction to weather modeling	93
4.2.2	Weather model methodology	94
5	Analysis and Validation of HIL Models	101
5.1	Conventional consumption model	101
5.1.1	Experimental setup	101
5.1.2	Experimental results	102
5.1.3	Analysis and interpretation of the results	121
5.2	Weather model	127
5.2.1	Experimental results	128
5.2.2	Analysis and interpretation of the results	130
5.3	Model based laboratory scenario analysis	132
5.3.1	Full load scenario	132
5.3.2	Generation and consumption feeder scenario	135
5.3.3	Mixed generation and consumption scenario	137
6	Conclusions	141
6.1	Summary of contributions	141
6.2	Future research	142
6.3	Concluding remarks	142
A	Mathematical Derivations	145
A.1	Derivation of the electricity load switching behavior process equation	145
A.2	Transformation from normal to Weibull distribution	146
A.3	Derivation of the amplitude error compensation factor for filtered white noise	148
B	Irradiation Factors	151
B.1	Normal-to-horizontal factor	151
B.2	Horizontal-to-sloped factor	151
B.3	Scattering factor	152
C	Impressions of the Laboratory Realization	153
	Bibliography	159

List of Figures

1.1	Final energy consumption of Germany	16
1.2	Renewable electricity generation in Germany	18
1.3	This work's contributions	24
2.1	Overall energy system behavior in five consecutive layers	29
2.2	Interactions between the ESMIF layers	31
3.1	Microgrid laboratory overview	41
3.2	Dimensioning of the electrical power rating	42
3.3	Microgrid laboratory's active electric components	44
3.4	Microgrid laboratory's electricity system	45
3.5	Microgrid laboratory's heat system	46
3.6	Possible district heating configurations	48
3.7	Mean voltage bus bar system	50
3.8	Patch panel approach for grid configuration	51
3.9	Technical setup of the low voltage system	54
3.10	Technical setup of the experimental electricity grid configuration facility	55
3.11	Pi-circuit diagram of cables	56
3.12	Electricity measurement concept	57
3.13	Emulated load system behavior	59
3.14	Utility generators	61
3.15	Flexible configuration mechanism for PV and BEV	62
3.16	Circuit diagram of flexible inverters	63
3.17	Schematic of the CHP and the boiler	66
3.18	Schematic of the heat pump	66
3.19	Schematic of the air heat pump	67
3.20	Schematic of the HIL heat source	67
3.21	Schematic of the heat storages	68
3.22	Schematic of the HIL heat load emulator	70
3.23	Schematic of the grid transfer station	71
3.24	Schematic of the pipe emulator	71
4.1	Electricity consumption as PHIL approach	76
4.2	Load model - system layer	78
4.3	Resistive load circuit diagram	80

4.4	Switched-mode power supply circuit diagram	80
4.5	Motor circuit diagram	82
4.6	Load model - provision layer	84
4.7	Step response of first order linear high-pass	86
4.8	Load model - distribution and supply layer	89
4.9	Block diagram of the distribution layer load model	90
4.10	Step response of first order linear low-pass	91
4.11	Weather model methodology	94
4.12	Weather magnitude's interaction	95
4.13	Diurnal and Seasonal variation	97
5.1	Electric energy consumption	103
5.2	Step response of electric power consumption of water cookers	104
5.3	Step response of electric power consumption of different water cookers	105
5.4	Distribution layer's random process model	106
5.5	Distribution layer's process to compute reference power	107
5.6	Distribution layer's random process model	108
5.7	Current consumption of an exemplary resistive consumer	108
5.8	Current consumption of an exemplary SMPS consumer	109
5.9	Current consumption of an exemplary universal motor consumer	110
5.10	Current consumption of an exemplary induction motor consumer	110
5.11	Worst case model accuracy example	111
5.12	Step response of the notebook charger	112
5.13	Current peaks of the notebook charger	112
5.14	Step response of the vacuum cleaner	113
5.15	Step response of the waste water pump	113
5.16	Worst case model accuracy	114
5.17	Current peaks of the vacuum cleaner	115
5.18	Current peaks of the waste water pump	115
5.19	Current peaks $I_m^\# = I_m^* - \text{peak}(I_m)$ of the waste water pump - frequency	116
5.20	Steady state current of multiple different household devices	117
5.21	Step response of multiple different household devices	117
5.22	Step response of multiple different household devices - frequency	118
5.23	Current peaks of multiple different household devices	118
5.24	Notebook charger's current reaction	119
5.25	Notebook charger's current reaction	119
5.26	Notebook charger's current reaction	120
5.27	Waste water pump's current reaction	120
5.28	Waste water pump's current reaction	121
5.29	Waste water pump's current reaction	121
5.30	Multiple different household devices' current reaction	122
5.31	Multiple different household devices' current reaction	122
5.32	Multiple different household devices' current reaction	122
5.33	Maximum daily global horizontal irradiation	128

5.34	Hourly global horizontal irradiation	129
5.35	Daily ambient temperature	129
5.36	Hourly ambient temperature	130
5.37	Daily horizontal wind speed	131
5.38	Hourly horizontal wind speed	131
5.39	CoSES standard electricity grid topology	133
5.40	Possible scenery based on the standard grid topology	134
5.41	Per unit current flows of full load scenario	134
5.42	Per unit grid voltages of full load scenario	135
5.43	Grid limit violations of the full load scenario	136
5.44	Per unit current flows of the generation and consumption feeder scenario	136
5.45	Per unit grid voltages of the generation and consumption feeder scenario	137
5.46	Grid limit violations of the generation and consumption feeder scenario	138
5.47	Per unit current flows of the mixed generation and consumption scenario	138
5.48	Per unit grid voltages of the mixed generation and consumption scenario	139
5.49	Grid limit violations of the mixed generation and consumption feeder scenario	140
C.1	Mean voltage room	153
C.2	OLTC room	154
C.3	Electricity grid configuration system	154
C.4	PHIL load emulator	155
C.5	Electricity and control system of SFH-3	155
C.6	Patch-panel system	156
C.7	Heat modules of SFH-2	157
C.8	Heat modules of MFH	157
C.9	The brine heat pump	158






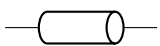
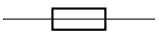

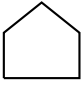

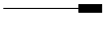
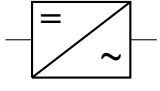
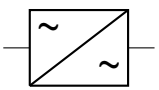
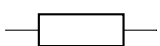


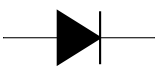
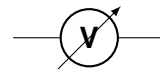



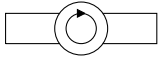
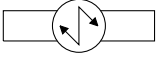
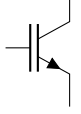
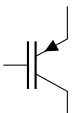
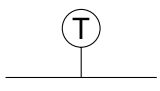
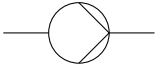
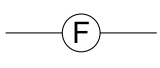
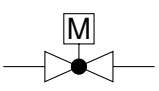
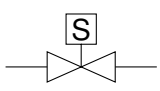
List of Tables

3.1	Electricity grid edges	53
3.2	Electricity grid nodes	54
3.3	Heat system facilities	65
4.1	Provision layer's steady state motor load parameters	88
5.1	Electric devices under test	103
5.2	Parameters for the supply layer's electricity consumption model	104
5.3	Parameters for the distribution layer's recovery dynamics model	105
5.4	Parameters for the distribution layer's random process model	105
5.5	Parameters for the distribution layer's random process model	107
5.6	Parameters for the provision layer's SMPS model	109
5.7	Parameters for the provision layer's universal motor model	109
5.8	Parameters for the provision layer's induction motor model	110
5.9	Parameters for the provision layer's multiple different household devices	116
5.10	Parameters for the weather model	127

Abbreviations

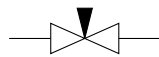
Abbreviation	Description
HV	high voltage
MV	mean voltage
LV	low voltage
AC	alternating current
DC	direct current
PV	photovoltaic system
BEV	battery electric vehicle
CHP	combined heat and power system
MG	microgrid
OSI	open system interconnection (model)
EMS	energy management system
CoSES	center for combined smart energy systems
ESMIF	energy system model interconnection framework
OLTC	on-load tap changing transformer
RT	real-time
HIL	hardware-in-the-loop
PHIL	power-hardware-in-the-loop
DLMP	distributed locational marginal price
SFH	single family house
MFH	multi family house
EXT	extension (only for electric grid extension)
CB	circuit breaker
GEN	generator
STOR	storage
THD	total harmonic distortion
BB	bus-bar
FPGA	field programmable gate array
IGBT	insulated-gate bipolar transistor
HT	high temperature
LT	low temperature

Symbols

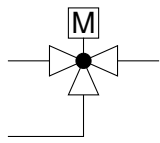
Symbol	Description	Symbol	Description
	circuit breaker		load breaker
	current transducer		voltage transducer
	transformer		transmission line, cable (resp. grid)
	fuse		ground
	emulated houses		socket
	plug		inverter
	back-to-back inverter / converter		resistor
	capacitor		inductor
	diode		voltage measurement
	current measurement		motor
	generator		rotational speed sensor
	torque sensor		n-igbt
	p-igbt		temperature meter
	pump		flow meter
	motor/control valve		solenoid valve



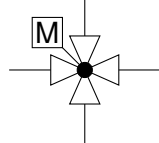
checkvalve



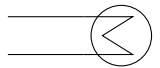
needle valve



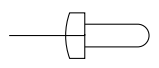
three way valve, mixer



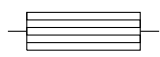
four way valve



heat exchanger in tank



heater rod in tank



heater rod in pipe

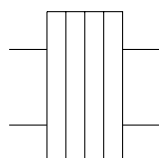
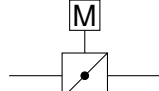


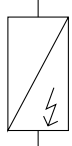
plate heat exchanger



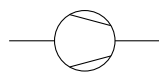
open flow



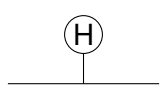
ventilation flap



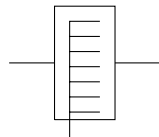
electric air heater



fan



humidity sensor



steam humidifier

Nomenclature

Modifiers

Symbol	Description
\bar{x}	mean value, low-pass filtered value
$x^\#$	specific modifier
\tilde{x}	estimation, approximation
\hat{x}	measured value
$\dot{x}, \ddot{x}, \overset{\cdot\cdot\cdot}{x}$	first, second, third temporal derivative
$x', x'', x^{(n)}$	n-th local modified variable
x^*	limit, value for $t \rightarrow \infty$, explicit steady state value

Variables and parameters

Symbol	Description
$\mathbb{1}$	heaviside function
\mathcal{I}	irradiance
\mathcal{A}	ambient temperature
\mathcal{W}	windspeed
d	disturbance variable
e	Euler number, control error
f, g, h	general functions
i	instantaneous current
j	complex number
k, l	iterators
m, n	series length
t	time
u	control variable
v	voltage
x	system theoretic state
y	system theoretic process variable
x, y, z	standard general variables
C	capacitance
D	distortion
E	energy

G	transfer function
\underline{G}	transformation matrix
\overline{I}	RMS current
L	inductance
P	active Power
Q	reactive Power
Q_9	heat (reference: °C)
R	resistance
R_9	thermal resistance
T	time constants
T	transformation function
V	RMS voltage
W	weight function
ϵ	small number
ζ	parameter
η	efficiency
ϑ	temperature
μ	mean value function
π	circular number
ρ	relative resistance
σ	standard deviation function
τ	time for integral over time
φ	angle of polar coordinates, phase
χ	modified standard general variable
ψ	flux
ω	angular velocity
Δ	difference

Indexes

Symbol	Description
d	desired value, set point variable
m	motor
r	reference value
r	resistance
s	switched mode power supply
u, v, w	special coordinates, three phases
x, y, z	standard Cartesian coordinates

Chapter 1

Introduction

One of the most characterizing challenges of the 21st century is to achieve an ecologically sustainable, economically affordable and technically reliable energy system. The human made global warming through energy generation driven green house gas emissions is proven without any doubt [88]. Promising environmental friendly technologies to generate electric energy are biomass, including waste and sewer gas, solar energy, water power, wind power and geothermal energy. Nuclear power is not considered, as it is an ecologically and environmentally risky technology: An accident like Fukushima Daiichi for instance causes huge uninhabitable regions and costs of about 100 Billion Euros [88].

Germany's overall energy demand is approximately $3,700 \text{ TWh/a}$ primary energy according to numbers from 2017, with a share of 12.4% renewable energy carriers [10]. This splits up to the end energy consumption of 660 TWh/a (26,2%) for households, 750 TWh/a (29.7%) for traffic, 720 TWh/a (28.7%) for industry and 390 TWh/a (15.4%) for other commercials [10], as illustrated in Fig. 1.1. The overall share of electricity is 520 TWh/a or 20.6% of the entire end energy consumption [10], which is only a low electrification proportion. Biomass and water power generation capacities are limited to 54.3 TWh/a [6] respectively 24.0 TWh/a [8]. Expansion capabilities are assigned to geothermal power with a magnitude of 8.7 TWh/a electricity and $43,5 \text{ TWh/a}$ heat [33]. The intermittent solar and wind energy sources are anticipated as the most important driving forces for renewable energy generation [6], due to their high, almost unlimited availability. Beneath electricity, energy is mainly consumed for heating (and cooling) purposes, which have a proportion of 56% of Germany's overall energy consumption and for traffic with a proportion of 29.7% [88]. The most promising concept for the heating and traffic transformation to be supplied through renewable energies, is to utilize electric energy through heat pumps and battery electric vehicles (BEV), as well as synthetic fuels which are produced through electric energy. Beside the feature, that these technologies can be supplied through solar and wind electric energy, they also allow to significantly assist balancing the intermittency of solar and wind electric generation and of conventional electricity consumption. This finally means by disregarding synthetic and biofuel imports an electrification of the overall energy sector, which is an increase from 20.6% to values approaching to 100%.

Today, we have a profound understanding of the fundamental functionality of the

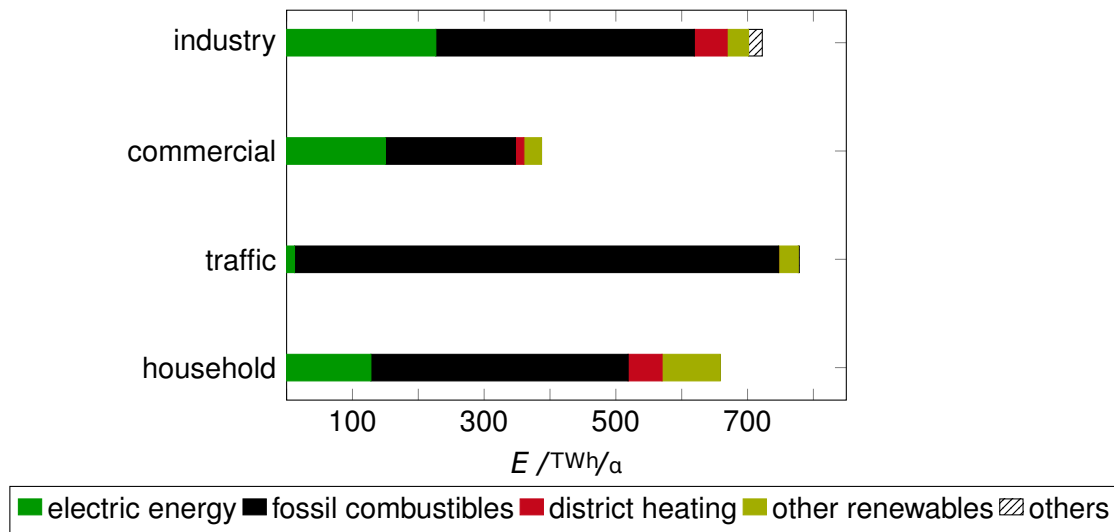


Figure 1.1: Illustration of the final energy consumption of Germany in 2017, for each sector, with the electric energy proportion. Data from [10] - Industry is described as mining and manufacturing, commercial is described as professional, trade and services

conventional electricity system. The fundamental concept of electric energy supply is to provide widely spread distributed electricity sources with specified voltages and frequencies for the spatially independent drawing of the required amount of power. It is achieved through centralized power plants with synchronous generators, generating power which is transmitted and distributed to the consumers through the appropriate high (HV), mean (MV) and low voltage (LV) grids. An unbalance between generated and consumed power physically causes voltage drops, such that the consumer would automatically adapt to the generated amount of power. But the voltage is kept constant by adapting the synchronous generators' excitations, such that more active and reactive power is supplied if the voltage drops. The extra required active power is physically drawn from the kinetic energy of the rotating shaft, which causes a decreasing electric frequency. This process directly couples the balance of generated and consumed power and the electric frequency, such that frequency deviations are a direct indicator for the balance of generation and consumption. An outer control loop cascade, the so-called frequency control, controls the prime mover to accelerate the shaft, such that the electric frequency is kept within operating limits. The synchronization of these voltage and frequency control actions among the power plants is achieved by droop control strategies. In many countries, especially in Germany, the coordination and billing of the overall energy generation is achieved through balancing responsible entities trading energy on markets and grid operators compensating occurring deviations through balancing power.

The present energy transition means to switch off the power plants with the synchronous generators and replace them by distributed generators, like photovoltaic systems (PV), combined heat and power systems (CHP) and wind power. Many distributed generators are based on fluctuating sources, which means to feed exactly the meteorologically available amount of energy into the grid, without significant consideration of voltage and frequency or balancing generation and consumption. This causes a stepwise

reduction of voltage and frequency control capabilities, as well as a stepwise reduction of the coupling between frequency and power balance, which is one of today's fundamentals of power system control. This process is accompanied by a multitude of new emerging consumer appliances, mainly based on power electronic technologies. These enable the efficient transition from alternating (AC) to direct current (DC), but are typically characterized by a highly nonlinear and typically capacitive dynamic behavior. This causes disturbances, like injecting higher harmonics.

The following sections motivate the importance of microgrid (MG) research and provide a short overview about actual research activities in this context. This includes a separate overview about MG research laboratories and the detailed problem statement of this thesis about designing a MG laboratory appropriate to the research requirements.

1.1 The future role of low voltage grids

This work focuses on MGs as intelligently controlled LV grids with multiple distributed generation, storage and active consumption technologies. The main active consumption technologies are BEV charging and electrical heating and cooling. The LV and MV distribution grids see the largest challenges due to their changing role from passive distribution systems to active grids which generate large amounts of electric energy and provide system services, like control reserve, spinning reserve, short circuit power, reactive power supply, blackstart and islanding abilities as well as redispatch [6].

Today's overall electricity consumption of about 520 TWh/a [10] split mainly up to the industrial, commercial and household sector as illustrated in Fig. 1.1. The fundamental change for future renewable energy systems is that the fossil combustibles have to be replaced to avoid their carbon dioxide emissions. In the household and commercial sector fossil combustibles are mainly used for heating, which will be replaced by renewable combustibles, solar thermal, district heating, synthetic fuels and a high share of heat pumps due to its unlimited availability, its high mean efficiency of 300% [88] and the ability to assist balancing the fluctuating electricity system. Assuming today's commercial and household fossil combustible energy carriers to be replaced by such heat pumps means an additional electricity consumption of 196 TWh/a . District heating with an actual energy consumption of 113 TWh/a will be supplied by geothermal and other energy carriers, such that changes can be assumed to carry no significant weight. In the traffic sector, the fossil combustibles are mainly used for road, ship and air traffic. Assuming that the BEV technology prevails means that fossil combustibles of the road traffic could be approximately replaced by BEV charging. The combustion engine has a typical efficiency of 10 to 35% [88]. The required electric energy demand after conventional combustion vehicles have been replaced by BEVs can hence be estimated as 25% of the combustion technology's energy demand. According to numbers from [18] 85.1% of the traffic combustibles are consumed by road traffic, which means an additional BEV charging electricity demand of 156 TWh/a . This could mean a potential of 352 TWh/a electricity consumption increase in total, which would mainly affect the low voltage system, as BEV charging stations and distributed heat pumps are typically connected to the LV grid. This finally could mean an approximate doubling of today's LV electricity consumption, by

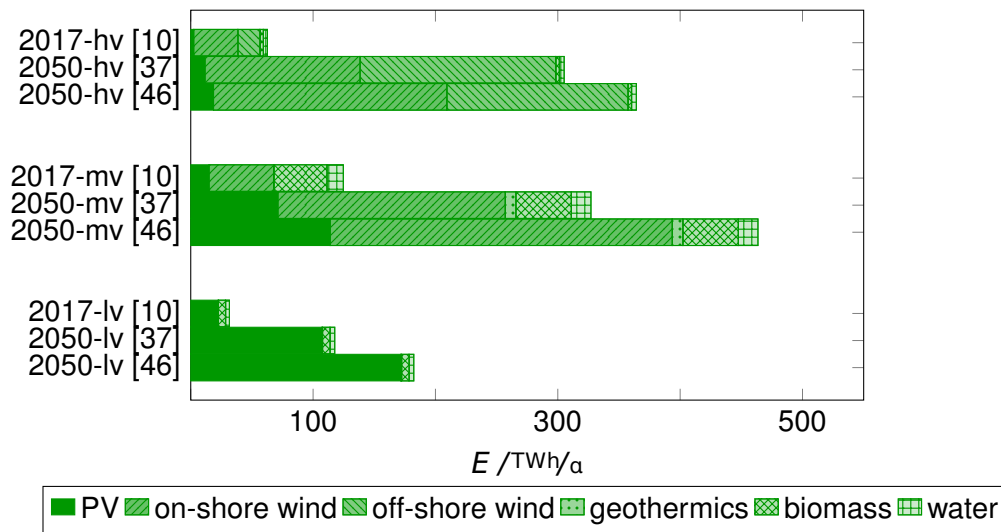


Figure 1.2: Illustration of the renewable electricity generation in Germany in 2017 [10] and in 2050 for PV and wind [46][37], divided into the three fundamental voltage layers proportional to 2017th data [19]. Assumed fully developed geothermics [33], water [8] and biomass [6] in 2050

considering today's household and commercial electricity consumption as LV proportion.

A further fundamental transformation process is caused by the generation of electricity. Studies for about-90%-renewable energy scenarios of the year 2050 show significantly different results. In [37] an optimal PV generation of 190 TWh/a , an optimal on-shore wind generation of 320 TWh/a and an optimal off-shore wind generation of 250 TWh/a is analyzed. In [46] an optimal PV generation of 304 TWh/a , an optimal on-shore wind generation of 471 TWh/a and an optimal off-shore wind generation of 148 TWh/a is analyzed. Geothermal energy has a maximum potential of 8.7 TWh/a [33], biomass has a maximum potential of 54.3 TWh/a [6] and water has a maximum potential of 24.0 TWh/a [8]. Considering today's shares of renewable generation in the LV/MV/HV grid layers leads to a future LV electricity generation share of about 100 to 200 TWh/a , a MV share of about 300 to 500 TWh/a and a HV share of about 300 to 400 TWh/a as indicated in Fig. 1.2. This means a share of about 10 to 20% of the electricity generation at the LV level, but a share of 55 to 70% at the LV/MV distribution grid level.

The future important role of LV grids is primarily indicated by the increased electricity consumption and generation in the LV grid. The consumption will increase by a factor of about 2 and additionally there will be a significant energy generation proportion of about 10 to 20%. Aggravating this situation, PV generation and BEV charging as well as heat pumps are characterized by high power flows with low full load hours and partly extreme simultaneities. The conventional LV system is originally not designed for the resulting high peak powers and the added energy generation. Increasing the utilization of the LV system, which is conventionally in a range of 1.2 to 11.2% measured through the utilization of LV distribution transformers [72], could provide a solution without requiring large LV grid expansions. For this reason the high amounts of available flexible loads through heat pumps and BEV charging have to be intelligently coordinated such that

peak PV generation is consumed locally and does not strain the LV grid and such that consumption peaks are avoided. The true capacity of LV grids is mainly limited through line voltage drops [51], which requires to additionally consider voltage control strategies. The increasing number of nonlinear consumers, especially in the LV grid, cause harmonic disturbances which cause avoidable losses, additional capacity limitations and can cause system instabilities. Considering islanding and blackstart capabilities for the LV grid could make the saved capacity reserves through the $(n + 1)$ -redundancy available for normal energy supply, which could increase the available MV operating capacity by about 65% [6]. Furthermore, heat pumps and BEV charging at the LV level is a large proportion of the overall available flexible load, which has to be utilized for balancing the overall fluctuating generation and consumption.

The exact extent of the future LV grid role is not finally clear. The replacing of centralized power plants by fluctuating renewable generation requires most available active components as flexibilities, to undertake significant parts of the control of the entire energy system. Especially the high amounts of available flexibilities at the LV level, consisting of big parts of the BEV charging and domestic heat pumps, could play an important role. Furthermore limitations at the LV level have to be handled. These tasks require the utilization of digital communication and control technologies to coordinate available flexible technologies. Their utilization in the LV grids finally allows them to become intelligent MGs. These challenges motivate the specific investigation of LV grids, which are exclusively considered in this work. Furthermore, achieved research results can partly be mapped to higher voltage levels, especially to the overall LV/MV distribution system, as they have similarities due to their former passive and in future intelligent nature.

The interaction of electricity, heating and cooling, traffic and digital communication and control cannot entirely be investigated based on models and simulations. Appropriate models are simply not available and due to their complexity only in a simplified manner imaginable. An appropriate laboratory allows reference measurements especially for model design and validation tests for verifying developed coordination, management and control strategies. This motivates to design the CoSES LV MG research laboratory. This work contributes by developing the technical laboratory concept based on research requirements.

1.2 Research in the context of microgrids

Microgrid research goes back to the works of Bob Lasseter [55] and Robert H Lasseter [56] which introduce MGs as a solution for the reliable integration of distributed energy generation, by utilizing flexibilities like storages and controllable loads. An overview to the concept of MGs and especially their challenges and available solutions in the context of control approaches is given in [68]. A fundamental research question addresses the overall operation and control structure of the MG. Literature shows a strong analogy about structuring the multiple different research aims in different layers. The probably most wide spread multi layer model is the well known open system interconnection (OSI) model in the context of communication engineering. Motivated by it, [95] describes the energy internet, which is a five layer structure from the access layer, with the interface to the

physical appliances, to the application layer, with an energy transaction platform. The OSI model serves also as a reference in [21], which describes a seven layer structure, from the physical layer including the real technical equipment to the intelligence layer, which includes advanced data processing applications. Literature in the close context of MGs distinguishes typically three layers. A common structure separates local controllers from the MG energy management system (EMS) and the distribution system operator level [67][68][76]. Other allocations are local inner loops, synchronization and main grid [40][63] or frequency and voltage control, restoration to nominal values and import and export of power [83]. The similarity of these multilayer approaches is that they structure challenges with regard to different hierarchical system sections. An alternative approach is the energy system model interconnection framework (ESMIF) concept, described in the previous work [22], which distinguishes five layers structuring the overall physical energy system behavior in different abstraction layers.

In literature exist different fundamental characteristics of MG topologies. One discussion is whether MGs should be based on AC, DC or hybrid grid architectures with their individual advantages [40][67][76][94]. The overall trend for the close future goes to AC MGs because of the available infrastructure. For future applications, DC MGs are under discussion. The initial idea of MG topologies includes to distinguish critical and uncritical supply feeders, which means to provide uninterrupted power supply for the consumers of the critical supply feeder [56] [58][90]. The typical agreement is that true MGs include the ability to connect and disconnect from the utility grid [40][83][90][94]. The fundamental aim of the MG concept is to allow the integration of a high amount of distributed energy sources. The overall aim for mainly renewable energy generation requires the integration of large numbers of PV sources into the LV grid, but also micro water and micro wind power, as well as CHP units. The majority of the water and wind power generation will be connected to grids of higher voltages. Other technologies which could be available in the LV grid are power-to-heat (or -cooling) technologies like heat pumps, BEV charging stations and battery storages. Power-to-heat and -cooling technologies, like heat pumps and air conditioners, promise to provide a high amount of flexibility for the electricity system. The low temporal requirements of the thermal sector, due to the buildings' high heat capacity, and the good storage properties of thermal energies can be utilized by the electricity system, by adapting thermal energy generation to the availability of electricity. Specific research in this field focuses for instance on the integration of heat pumps and BEV charging as flexible demand in electricity markets [70], or on quantifying the electric flexibility of buildings [26]. Especially early MGs include this concept of heat driven electric flexibilities [56][58]. The charging process of BEV is controlled by the car, but influenced through limitations specified by the charging station. This mechanism allows to consider electric vehicle charging as flexibility, such that the car is charged when electricity is available. Utilizing the battery through vehicle-to-grid applications is discussed as a storage opportunity in the context of MGs [68]. This requires charging stations with an implemented communication standard of ISO 15118. This standard also allows to provide charging status data, like battery capacity or charge level. Battery storages are a flexibility for the electricity system per se. Its drawback is that it is an additional investment, without co-benefit like BEV or power-to-heat technologies. This makes batteries a comparably

expensive technology, but due to the increasing market penetration battery prices are falling. One of the major technical advantages of batteries is its fast reactivity, which allows for instance to provide primary reserve [91].

Research about energy system operation, especially in the context of MGs is varied, as it is a "complex multi-objective control system that deals with issues from different technical areas, time scales and physical levels" [63]. A unique standard for connecting distributed generation units to the electricity grid to manage these complexities is not available [76]. Fundamental research topics are energy management [68][63][90], voltage control [40][62][68][76][83][94], damping of system perturbations [39][66], inverter control [35][54][92][53][74] and disturbance management through islanding [67][83] including black start strategies [90]. Energy management concepts, which mainly come along with unit commitment and economic dispatch, are typically market driven approaches [12][34][44][63][68][90]. Local market approaches like distribution locational marginal pricing (DLMP) incorporate the consumer's location and its transmission limitations into the market mechanisms [43].

Voltage control is one of the central research topics in MG literature, especially distributed generator's droop control methods for voltage control and power sharing [40][68][76][83][94] and adapted methods like considering storage's state of charge [40]. Traditional droop methods, especially reactive power - voltage droop control, have several disadvantages, like slow reactions especially under transient conditions or poor impact in LV grids due to the low impedance content of the LV power cables [68]. Indirect droops could solve this voltage control problem, which would contradict active power dispatch [31]. Strategies to control voltages in the LV grid by mainly compensating voltage drops along power lines are switching strategies of on-load tap changing (OLTC) transformers and line voltage regulators [62], reactive power feed-in strategies [62], or controlling active power flows [31]. System perturbations like harmonics can be actively damped through power electronic devices [39][66]. There are multiple different inverter control strategies, like those based on carrier based pulse width modulation [53] or space vector modulation [92][35], or like model predictive control strategies [54] as well as different advanced inverter configurations like four-leg inverters [92][53][35], multilevel inverters [35] or impedance source inverters [74]. Further research in this field focuses on synchronization strategies, like online estimation of power quality parameters [42]. Managing disturbances in the main grid, like voltage dips or blackout, through islanding and reconnecting is described in [67][83]. Strategies to carry out black starts in the MG are mentioned in [90]. Other research topics are protection of the distribution grid under distributed generation [62][65][76]. Various problems are entirely solved by numerous different specific strategies, including genetic algorithms, swarm algorithm, mixed integer linear and nonlinear optimizers, rule based systems, machine learning systems [63], master slave control, peer to peer control [94] or multi agent systems [62][63][94] and many others.

Energy system research also includes many diverse topics without any direct relation to MG operation. Technology research for instance aims for developing new and improving existing technologies. Exemplary works are alternative PV materials with promising properties like hydrocarbons [52], or battery technologies like redox flow, which store electric energy in liquids [75]. Other works for instance focus on studies about the

overall energy system configuration, like the amount of required generation, storage and transmission capacities. This is often based on specific scenarios, like studies about flexibility requirements in Europe [48]. A frequently discussed topic is the suggestion to apply DC grids [27] with its specific advantages. Research in the context of system analysis typically investigates the properties of specific technologies in the overall system context. Exemplary studies in this context of system analysis are quantifying the impact of BEV charging on power quality [38] or describing fundamental characteristics of electricity load behavior [80].

1.3 Microgrid laboratories and experimental facilities

Numerous different laboratories and testbeds in the context of MGs are already realized. A detailed review about MG testbeds around the world is given in [47][59] and [76]. A survey about mainly cyber physical testbeds in the context of MGs is presented in [25]. Real live field tests in Japan are introduced in [36].

A typical design of MG testbeds is based on real distributed generation devices connected to an emulated system. The DeMoTec testbed in Kassel includes multiple distributed generation and emulated grid and consumption facilities [14]. The fundamental design of the CERTS MG laboratory testbed involves mainly emulated generation and consumption facilities which are connected through real grid cables with a significant impedance [32][57]. A further testbed is the Tianjin University MG testbed (TUMT), which comprises multiple distributed generation and storage technologies, forming with emulated cables and loads an experimental single phase LV MG [87]. A third example is the flywheel test rig of the University of Manchester, which focuses on experiments with a flywheel, connected to distributed generation devices and a load emulator [14]. The MG of the Distributed Electrical Systems Laboratory (DESL) of the EPFL in Lausanne 'EPFLSMARTGRID' comprises parts of the local university campus grid with the unspecified university's electricity consumption [2]. The Center for Grid Integration and Storage Technologies of the RWTH Aachen has a MG laboratory with the outstanding property of a real, flexibly configurable low voltage grid [1]. Other similar, mainly smaller testbeds are described for instance in [14][49][50][63][93]. The similarity of these testbeds are their focus on power dispatch and voltage control. They are based on highly emulated system behavior. Most allow to experimentally investigate strategies to disconnect and reconnect to the utility grid.

Other testbeds focus on the information technology part of MG operation. The Grid 5000 project combines 5000 distributed computing units for a highly performant grid simulation [20]. Another example is the RTDS realtime (RT) simulator used for hardware in the loop (HIL) simulation of MG behavior and testing control strategies [89]. Other testbeds which simulate physical system behavior and focus on digital data processing and communication, like information management systems, are for instance [61][79][84].

Systems, which are realized with limited power ratings allow to emulate fundamental principles of MG behavior. Explicitly scaling down the power rating of an entire feeder is described in [15]. Smaller scaled systems have the advantage of lower budget and space

requirements. Typically such laboratories utilize power electronic devices to emulate larger generation devices. Such testbeds are for instance described in [41][60][82][86].

There are various experimental test sites for thermal energy supply in the context of electricity and heat sector coupling. Diverse laboratory infrastructures in research and development institutes are used to investigate specific properties of individual technologies and strategies, like HIL systems for heat pumps [30] or for CHP units [29]. The emulation of heating consumption in a laboratory environment through a HIL co-simulation approach is described in [29]. Real live test sites are used to validate new strategies in research projects especially in the context of advanced district heating systems, like in Hamburg-Wilhelmsburg [4] or in 'Auf dem Zanger' in Kempten [3].

1.4 Problem statement and contributions

The present work addresses emerging challenges of the transition from a centralized power plant controlled electricity system to an intelligent decentralized network controlled system. Its focus is LV distribution systems, which will develop to MGs as defined in Def. 1.1. The LV distribution system will see the largest evolution from a passive, unidirectional consumer system to an active bidirectional system with many intelligent distributed generation, storage and consumption devices. It will play a significant role in future overall electricity system operation and control. The fundamental challenge of MG research is to find operational concepts and strategies to ensure a reliable energy supply which is environmentally and economically sustainable. The MG has to integrate into the overall future energy system operation strategy. The vision of this work is to provide a MG laboratory as a realistic reference system for investigations to model and understand physical system behavior and to test and validate developed strategies in a realistic environment. The scope of this laboratory is the LV grid, by considering the important impact of heating (and cooling), BEV charging and digital communication and control technologies.

Definition 1.1 *A microgrid (MG) is defined throughout this work as a LV grid, with a high share of intelligent controlled distributed generation, storage and consumption devices, to undertake significant parts of the overall electricity system operation and control.*

This work aims for designing a MG laboratory concept which considers electricity at low voltages and the impact of heating (and cooling), BEV charging and digital communication and control technologies. The laboratory should allow to flexibly investigate the energy system behavior to its full extent under normal operation conditions which means to consider the impact of the complete spectrum of possible control and operation strategies. These flexible investigation capabilities require the laboratory to allow to flexibly implement different operation strategies at all levels, from pure unit commitment to internal power electronic control strategies. This allows to flexibly use the MG laboratory for investigating most of the actual and future research questions in the context of energy system operation.

The first essential contribution of this work is a systematic analysis of the physical-technical principles of energy system operation and their systematic structuring. Its aim is to derive technical laboratory requirements to allow to flexibly investigate most of the actual

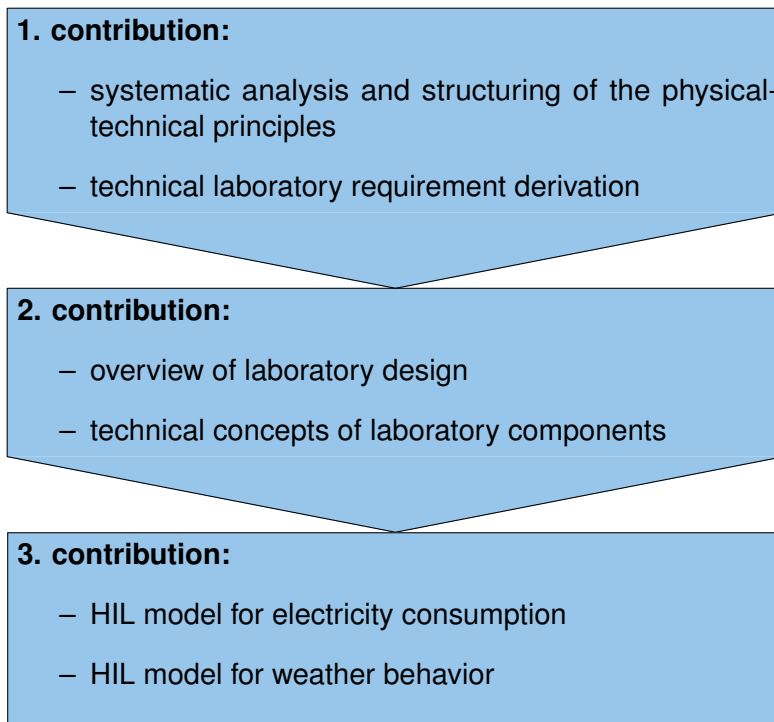


Figure 1.3: Overview to this work's contributions to the final aim of designing a flexible MG research laboratory

and future MG research challenges. It also allows to develop solutions and to flexibly operate the laboratory in a target oriented manner. The second essential contribution is to give an overview of the laboratory design and to describe the technical-functional concept of the laboratory components. The laboratory especially requires components which allow to emulate external parts of energy system. These external parts, like human behavior influencing electricity consumption or weather conditions influencing renewable energy generation, cannot be entirely integrated as real components in the laboratory. The third essential contribution of this work is to design HIL models to realistically emulate these components, which cannot be part of the laboratory in reality. Weather and human controlled electricity consumption are the most influential external components, which are not yet well modeled in literature. These HIL models are required to flexibly apply multiple different external conditions in the laboratory, including artificial scenarios, different electricity consumption characteristics, different climatic conditions, or winter scenarios in summer. An overview of these contributions is given in Fig. 1.3.

Chapter 2

Research Requirements

This chapter analyzes and structures the physical-technical principles of energy system operation and derives technical laboratory requirements, which is the first main contribution of this work. As illustrated in Sec. 1.2, MG research is a manifold field, which is based on various physical principles and time scales. The first part of this chapter describes five fundamentally different physical-technical principles of energy system operation which when taken together represent the complete physical-technical process of electric energy supply. The second part of this chapter describes the ESMIF [22] which structures the first part's physical-technical principles in five consecutive layers. The third part derives the fundamental technical laboratory requirements as the fundamental basis for the following chapter.

2.1 Fundamental physical-technical principles of energy system operation

This section describes the fundamental physical-technical principles of energy system operation to structure the manifold field of MG research in this context. The physical-technical principles are the immutable commonality of MG system behavior while considering the investigation of various different operation and control strategies. These principles enable the design of one unique structure for the entire manifold tasks of energy system operation, independent from the underlying technologies and strategies.

The fundamental principle of electric energy supply is to provide an ideal sinusoidal voltage source for the consumer as presented in Axm. 2.1. In reality this aim is only reached in between specific limits. The following part of this section describes five consecutive measures as physical-technical principles, which are necessary and sufficient to ensure the idealized or close to ideal electric energy supply.

Axiom 2.1 *The idealized electric energy supply in the context of MGs is the provision of an ideal three phase voltage source with a sinusoidal signal shape, a constant frequency of 50 Hz, an amplitude of $\sqrt{\frac{2}{3}}400$ V per phase and a relative phase shift of $\frac{2\pi}{3}$ rad.*

The provision of a sinusoidal voltage source is not naturally given, and has to be actively controlled. Therefore, the first physical-technical principle states that the physical

coupling of voltages and currents, especially through Ohm's law and the capacitive and inductive effects, allows to influence voltages through currents. This requires **electrical technologies which are capable of feeding in specific currents** as a control input.

The second physical-technical principle is to specify the shape of the current feed-in **to ensure the sinusoidal voltage signal shape** with a frequency of 50 Hz. This plays a subordinate role in the traditional electric energy supply as the sinusoidal shape is automatically ensured through the synchronous generation and not affected through the mainly linear consumption devices. The synchronous generators physically couple the electric frequency and the balance of generated and consumed power, such that the frequency is indirectly controlled through balancing power generation and consumption. In future, more and more power electronic consumption devices with non-linear system properties disturb the sinusoidal shape through their injection of current harmonics which interact with the voltage. But distributed actively controlled power electronic devices would be able to restore the sinusoidal signal shape with appropriate control strategies. These strategies would consider the phase and amplitude of the current as a control input.

The third physical-technical principle is to specify the phase and amplitude of the currents to feed in a specified power and **to ensure a nominal voltage magnitude**. Voltage magnitudes on a local scale are mainly influenced through voltage drops along the grid and its facilities, and through active and reactive power flows. Voltage magnitudes on a global scale are influenced by over- or undersupply of electrical power. The conventional synchronous machine induced behavior, especially the underlying voltage control mechanisms, ensures a steady voltage magnitude, which utilizes kinetic energy reserve of the shaft's rotation. This means that the synchronous generator's voltage control redirects the impact of over- or undersupply of power from the voltage magnitude to the frequency. Future power electronic based technologies could utilize for instance stored electric energy in the intermediate circuit capacitors to control grid voltages through specifying reactive powers, and through modifying the specified active power feed-in, which is its control input.

The fourth physical-technical principle is to specify the active power feed-in **to achieve a reliable and efficient power dispatch and distribution**. The underlying physical law is the conservation of energy. It states that each grid node's power in- and outflows have to be balanced. The underlying technologies cause considerable transmission and distribution losses and are subject to their technical capacity limits. The main challenge is to limit flowing currents to their technological limit and to prevent protection devices from tripping, while allowing for the economic dispatch of available generation and flexible consumption capacities. Strategies to achieve this are mainly based on adapting the powerflow of generation, storage and consumption devices, which affects efficiency in the long run. The limited impact of voltage control through reactive power has to be considered in these strategies. This principle considers the specification of the available generation and flexible consumption capacities as its control input.

The fifth physical-technical principle is to specify the available generation and flexible consumption capacity **to ensure the appropriate amount of energy for the consumers' needs**. The partly unpredictable generation and consumption requires sufficient controllable prosumers to be balanced out. Conventional mechanisms of adapting generation to

the consumers' needs are not efficiently possible for fluctuating renewable energy sources. Fluctuating weather conditions, like sunshine or windspeed, and fluctuating energy consumption cause high diurnal and seasonal variations in generation and consumption balance. The electric power grid breaks the regional dependency of this balancing until reaching its transmission capabilities by slightly reducing efficiency. There are four fundamental strategies to achieve balancing of energy consumption and generation, with their individual properties:

1. The conventional approach is to adapt the energy generation to the energy consumption. During an oversupply, PV and windpower can only curtail generation which finally means to discard energy without any other savings. This concept works efficiently for biomass or within some limits for water power generation, as saved fuels can be used later on. In emergency cases, curtailment is also a viable strategy for PV and wind generation.
2. The demand side management approach adapts the energy consumption to match the energy generation. Assuming that it does not try to influence human behavior, this strategy is only applicable for automated parts of the entire energy consumption. Adapting traditional household consumption through human end-users requires its social acceptance, which contradicts the fundamental idea of a readily available energy supply. Autonomously adapting the consumption to the energy generation involves shifting the energy consumption in time as long as the consumer is not affected. Besides industrial or commercial applications, mainly power-to-heat, power-to-cooling and BEV-charging applications are suitable under this approach. From this view, these three concepts can thus have a significant positive impact on the electric power system due to their flexibility, but they also increase the electric energy demand.
3. The storage-based approach flexibly stores and withdraws energy in a typically chemical storage. Although it is a flexible strategy, it requires additional cost-intensive technologies which significantly increases the investment for batteries, which means it to be an expensive approach.
4. The efficiency increment approach reduces losses among the electric power supply network. It has only an indirect impact, as using more efficient technologies makes balancing generation and consumption less energy demanding. From a system operation view this mainly minimizes lossy energy transmission and preferably operates more efficient generation, storage and consumption technologies. This means placing generation close to the consumption, using efficient scales of technologies and to optimize the system operation efficiency.

These five principles cover the entire physical-technical process of electric energy supply. The answers to the underlying general research questions for each of the five principles provide technologies which supply sufficient energy generation capabilities, generate and distribute the appropriate amount of power and ensure standardized voltage signal shapes and magnitudes which allow to draw power in a regulated manner.

Summary: The entire physical-technical process of electric energy supply is covered by

- having appropriate electric technologies available,
- maintaining the sinusoidal voltage signal shape,
- maintaining a nominal voltage magnitude,
- achieving a reliable and efficient power dispatch and distribution and
- providing the appropriate amount of energy.

2.2 Energy system model interconnection framework (ESMIF)

This section describes the ESMIF, which is the foundation for the later structural specification of laboratory performance and dimensioning. The ESMIF structures the energy system's processes and tasks in five consecutive layers with different levels of abstraction, based on the five fundamental physical-technical principles of the previous section.

The ESMIF is originally developed to structure the different overall control tasks to allow the flexible interoperation of different technologies. This is especially valuable for the diverse technology manufacturers by specifying standardized control interfaces at different abstraction layers [22]. This means that technologies like CHP, heat pumps, PV inverters or batteries could be controlled by one joint energy management system. All these devices would expect the same physical control command at same sampling rates, e.g. each second, a new active power setpoint.

2.2.1 General framework description

The key idea of the modular framework is to structure the overall energy system behavior into five consecutive layers based on the five physical-technical principles of electric energy system operation as illustrated in Fig. 2.1. This leads to specific processes for each layer with the aim to comply with the underlying physical-technical principle. The process of an overlying layer is based on the assumption, that the underlying layer's task is largely accomplished, like a strategic robo-soccer team play is based on the assumption that the robots can perform coordinated movements. Starting with real system components, the abstraction concept of assuming accomplished tasks of underlying layers, ensures that the framework considers the energy system processes to its full extent. The challenge is to define the tasks such that the resulting process is compactly described by mathematical models while being temporally decoupled. This means that the lower layer's task needs to be accomplished much faster than the higher layer's process dynamics.

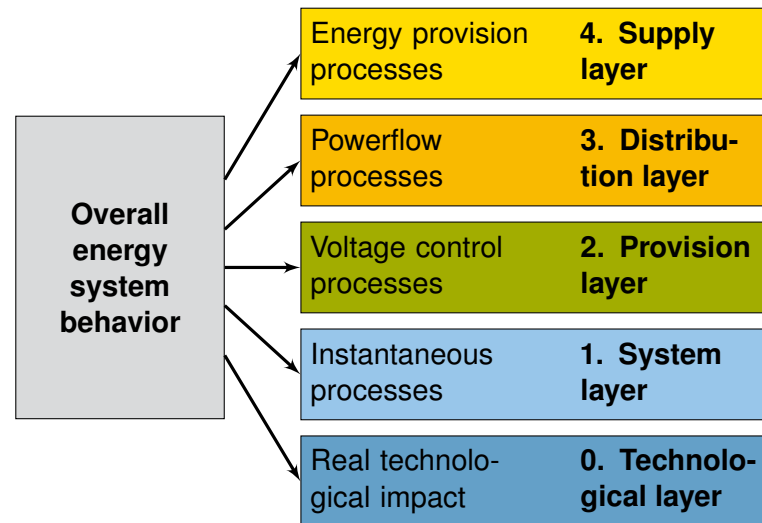


Figure 2.1: Illustration of structuring the overall energy system behavior into five consecutive layers

The ESMIF comprises five consecutive layers related to the five aforementioned physical-technical principles. The bottom layer, called **technological layer**, comprises the real technologies, without simplification or abstraction. Its specific task is to transform control commands, being typically reference instantaneous currents i_d of the upper layer under real conditions into real physical actions.

The first abstraction layer is called **system layer** as its process consists of the dynamical interaction of the system's instantaneous magnitudes. Its specific task is to comply with the second physical-technical principle by controlling the sinusoidal signal shape of the instantaneous grid voltage v , which characterizes the AC system. It is mainly influenced by the control strategies of power electronic devices like PV inverters, and the physical properties of directly connected other energy conversion technologies, like synchronous generators or transformers. Power electronic control algorithms typically operate in a sampling range of 10 to 100 kHz. A standardized sampling rate of $100\ \mu\text{s}$ allows to consider up to the 50th harmonics in a pseudo continuous manner.

The second abstraction layer is called **provision layer**¹, as its fundamental process is to enable the specified provision of power by coordinating grid voltages and voltage drops along the power lines. Its specific task is to comply with the third physical-technical principle by controlling the voltage RMS magnitude V all over the grid. It is mainly influenced by physical grid properties, the active and reactive power flows and imbalances of generation and nominal consumption. The main control focus is put on active and reactive power feed-in to control the grid voltages. To consider fast processes in a pseudo continuous manner, a standardized sampling rate of 5 ms is useful. Significantly faster rates get into conflict with the processes of the system layer, because variations beyond one period of 20 ms are effectively affecting the sinusoidal signal shape. Significantly slower sampling rates would not allow to consider changing amplitudes of one period

¹The term 'provision layer' replaces the term 'transmission layer' of previous works, as the similarity with the term 'transmission grid' could be confusing.

in a pseudo continuous manner. Typically voltage control systems operate slower, as large systems with many users behave slow due to the mutual stochastic compensation of individual transient processes. Following the strict theory of the ESMIF, this mutual stochastic compensation is part of the provision layer's strategy. Especially small island systems and uninterrupted power supplies have to actively control these quick processes.

The third abstraction layer is called **distribution layer**, as its fundamental process is the distribution of the available energy to the consumers according to their needs. Its specific task is to comply with the fourth physical-technical principle by requesting the available energy prosumer capacities to achieve a reliable and efficient power distribution and supply. Especially in terms of highly fluctuating generation and consumption devices like PV or human controlled household devices, the balance between power feed-in and draw has to be actively controlled through available flexibilities especially on a short term by ceasing available inertia. These flexibilities can be storages like batteries, controllable generation devices like water power or chp plants, or controllable consumption devices, like electric heating, heat pumps or BEV charging stations. The temporal resolution of the underlying processes typically depends on the considered system dimension, as stochastic fluctuations of multiple prosumer devices balance each other. The clear temporal separation between voltage control processes and this layer's control process requires a standardized sampling rate of e.g. 1 Hz. This allows to consider typical fluctuations which depend on external processes like consumer or weather behavior, but neglect internal fluctuations like the dynamical reaction on voltage deviations, which are considered in the provision layer's processes.

The fourth layer is called **supply layer**, as its fundamental process is the reliable and efficient supply of sufficient energy generation and flexible consumption capacities. Its specific task is to comply with the fifth physical-technical principle by specifying sufficient flexibilities to be available for balancing fluctuating generation and consumption. This allows to supply the appropriate amount of energy to balance the consumed and lost energy by making flexible generation, storage and consumption facilities available. This task is the foundation of the distribution layer's task, which dispatches power from these supplied energies. A specified sampling rate of 15 min allows to consider the diurnal and seasonal variations in a pseudo continuous manner. Higher frequent variations are typically stochastic fluctuations, which are treated in the distribution layer. Furthermore, the sampling of 15 min complies with the German law in the context of energy billing.

2.2.2 Framework process description

This subsection describes specifically the behavior of electric energy systems as a process by structuring it into the ESMIF framework. Each component of the energy system, from the energy generation through the distribution to the energy consumption, is a part of each layer. These parts of one system component interact vertically through standardized interfaces, which are physical set points and measurements. Each layer is actively manipulated by the control action of its overlying layer, while it assumes the underlying layer's aim to be fulfilled. Considering grid connected devices and facilities, their supply layer's set points are desired energies ΔE_d , their distribution layer specifies powers P_d ,

their provision layer specifies current magnitudes I_d with phase angles φ_d and their system layer specifies the instantaneous currents i_d which are realized in the technological layer. The modular multitier framework with its physical interfaces between the layers for grid connected devices is illustrated in Fig. 2.2.

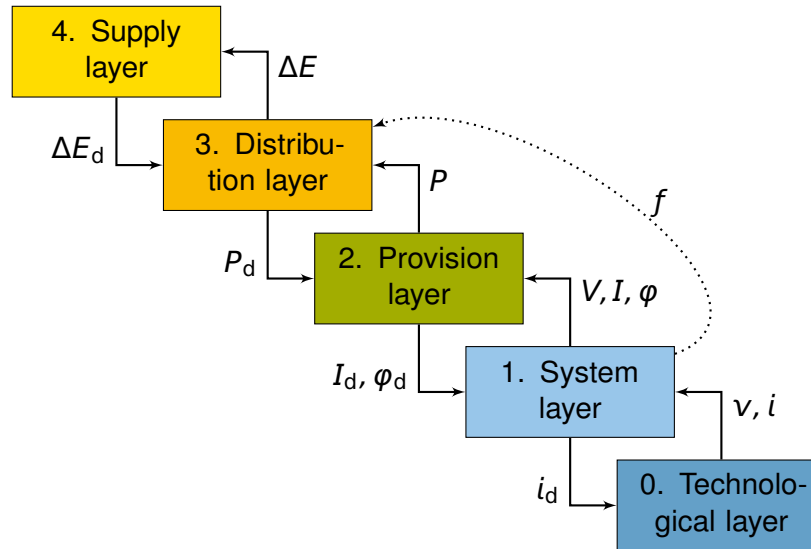


Figure 2.2: Illustration of the fundamental interactions between the individual ESMIF layers of devices connected to the grid, upwards are measurements, downwards are control set points; dotted frequency measurement f is an example for application depending additional measurements: e.g. frequency is conventionally used in the 3. layer to indicate the balance between generation and consumption

The fundamental aim of the **supply layer** is to procure sufficient energy generation capabilities ΔE_d to balance generation and consumption. This requires sufficient controllable prosumers, so called flexibilities like heat pumps, water power, combustion engines, BEV charging stations or batteries, which allow to adapt generation and consumption during the days in time intervals of few minutes. An overall strategy needs to coordinate these flexibilities to balance overall generation and consumption. It specifies the amount of energy of flexible generation and consumption facilities to feed into the energy system in one 15-minute interval.

The conventional strategy on a global scale are global markets, which means that all consumed and generated energies are traded. Balancing groups are virtual subsystems which need to balance purchase, generation and consumption. This approach assumes that always sufficient transmission capacities are available such that no regional distinctions are necessary. Transmission restrictions are manually handled through redispatch. Local market approaches, like DLMP [43] promise to provide a solution to incorporate the location and transmission restrictions into the energy market. Smaller island systems, like those used to supply remote cottages, are often based on diesel generators which automatically adapt the fuel combustion and hence the electricity generation to balance the energy consumption. Island systems based on fluctuating generation like PV typically do have a battery which balance energy generation and consumption until it is empty

which means an outage.

The upper layer provides sufficient energy to supply the consumer based on 15 min intervals. The fundamental aim of the **distribution layer** is to dispatch the available flexible energy prosumer capacities as active power flow P in second intervals and to distribute the generated power efficiently and reliably to the consumer. The efficiency mainly focuses on the reduction of transmission and distribution losses. Reliability indicates not to exceed technical limits like transmission capacity restrictions. Short term fluctuations and disturbances, arising from consumer or weather behavior considered as stochastic processes with uncertainties have to be compensated through adapting the active power flow.

The conventional approach is to use frequency as an indicator for imbalances between generation and consumption. The droop controllers increase or decrease the electricity generation through prime mover actions for stabilizing the system. Remaining deviations are compensated by requesting operating reserves which are traded on a specific market. The last option in emergency cases is load shedding. Further strategies could be developed or tested. Conventionally, besides redispatch there are sufficient transmission reserves designed such that power lines cannot be overloaded through these stochastic fluctuations.

After an ensured balance of power generation and consumption, the **provision layer** aims for ensuring a specified nominal voltage amplitude V_n . Its control strategies adapt the current magnitudes I with their phase angles φ to stabilize the grid voltage V close to its nominal value V_n . The mutual dependency of the voltages, the currents and their phase angles show a dynamic behavior. Without considering these dynamics in the control strategies, there is a true risk of dynamic instabilities, oscillations or even destruction of components.

In conventional systems, voltages are controlled through the excitation of the synchronous generators in centralized power plants. This finally causes the aforementioned relation between the power balance and the frequency. A power over- or undersupply is compensated through the synchronous generator's voltage controller by the kinetic energy of the shaft. This finally leads to an increasing or decreasing rotation and hence also decreasing electricity grid frequency. The coordination between the multiple power plants is realized through a voltage - reactive power droop. Stability investigations including the upper layer's power balancing control (traditionally called frequency control) are based on highly simplified swing equation models. The local distribution of voltage drops can be compensated through OLTC typically used on a high voltage level, but also used more and more in low voltage applications to compensate for voltage range deviations mainly caused by PV feed-in. Local active or reactive power feed-in influences local voltages mainly through the feedback on voltage drops along inductive power lines, which allows to actively control local voltages through active and reactive power feed-in. Its usage in distribution systems is conventionally not realized and still content of active research. The fundamental advantage of reactive power is that it does not impact the balance of power generation and consumption.

The provision layer controls the amplitude of the sinusoidal voltages, the **system layer** aims for ensuring its sinusoidal signal shape. Its control strategies adapt the instantaneous

currents i such that voltages v result in sinusoidal signal shapes. As long as predominantly linear consumption devices exist, sinusoidal generation is sufficient to ensure sinusoidal voltages. The current shape can actively be adapted in power electronic devices like PV inverters, which could be used to actively damp the disturbances of nonlinear consumption devices, which are on the rise.

The active control of the sinusoidal signal shape is conventionally not investigated. Mainly linear consumption devices cause no disturbances of the sinusoidal signal shape and synchronous generators naturally inject sinusoidal currents into the grid through their rotors' rotation and their windings' arrangement. Power electronic generation devices actively control the currents' sinusoidal signal shapes with different qualities. Modern inverters typically use voltage source inverter control strategies, which generate a comparatively accurate sinusoidal signal shape through filtered high frequent transistor switching. Adaptions in their control strategies would allow to modify the signal shape, which could compensate other harmonics or disturbances, similar as today's active power filters.

The system layer provides instantaneous set points which the **technological layer** aims to realize. Its control strategies adapt internal processes like modulation techniques for switching transistors in power electronic devices, to modulate and realize the upper layer's references. This layer's tasks are faced with real conditions, which include disturbances and other technological limitations.

Summary:

- The ESMIF structures the overall energy system behavior into 5 consecutive layers according to five physical-technical principles
- The supply layer incorporates energy provision processes based on 15 min sampling
- The distribution layer incorporates powerflow processes based on 1 s sampling
- The provision layer incorporates voltage control processes based on 5 ms sampling
- The system layer incorporates instantaneous processes based on 100 μ s sampling
- The technological layer incorporates the real technological impact

2.3 Fundamental laboratory requirements

This section describes technical requirements as the fundamental basis for the design concept of the MG research laboratory. Beneath general laboratory requirements, specific

requirements are based on MG research topics, being structured through ESMIF as described in the previous section.

2.3.1 General laboratory requirements

This subsection describes general requirements for the CoSES MG laboratory. Experimental laboratories aim in general for three research applications. Science fundamentally requires real reference systems to study and finally describe the physical system behavior. This means that the MG laboratory is required to measure and observe the physical behavior of its components to design and validate appropriate models. This requires besides a sophisticated measurement system many different reference technologies and the ability to flexibly configure diverse system layouts and scenarios. The second fundamental laboratory research application is to provide a platform which incorporates the technical complexity to its full extent. Typically complex mechanisms, like measurement errors, environmental impacts, but also communication, sampling and computation cannot be realistically implemented in models or simulations. This means, that the laboratory finally requires real technologies including communication and control to investigate the complex interaction of the individual MG system components. The third fundamental laboratory research application is to validate developed methodologies and operation strategies. Generating reliable and convincing results requires the real implementation of the underlying strategies under realistic conditions. This requires besides the possibility to flexibly implement diverse MG operation and control strategies the ability to flexibly configure diverse system layouts and scenarios, especially sector coupling technologies as heat pumps, CHP and BEV charging, including the entire heat system. This means that the laboratory requires to be designed for being a modeling reference, an experimental testing facility and a validation tool for new operation strategies.

The fundamental laboratory concept must take different partly conflicting design requirements into account. The fundamental requirement is that it has to be designed to allow investigating the most relevant research questions in the context of MG operation. An further fundamental requirement is the laboratory to be technically realizable especially including monetary and technical aspects, but also its complexity has to be limited to allow efficient research. The limited complexity is partly in conflict with requiring the laboratory being flexibly usable. This means that it requires flexible configuration mechanisms to allow emulating multiple different scenarios.

Summary:

The laboratory generally requires

- a sophisticated measurement system
- many different realistic reference technologies
- the ability to flexibly configure layouts and scenarios
- real technologies, including communication and control
- a possibility to flexibly implement operational control strategies
- sector coupling technologies

2.3.2 Specific laboratory requirements

This subsection describes specific MG laboratory requirements, which are based on MG research topics through the ESMIF. It raises fundamental research questions for each ESMIF layer, which have to be solved in future investigations with the aid of the laboratory. These research questions result in the specific technical laboratory requirements.

The supply layer raises the question how generation and consumption in future energy systems can be balanced. To investigate different strategies to develop reliable answers to this question, the laboratory initially requires fluctuating generation and consumption devices to emulate the challenge at all. Solutions are based on so called flexibilities, which are controllable generation, storage and consumption devices. Distributed computation devices and an experimental communication system allow to implement distributed control and management strategies to control these flexibilities and finally to balance generation and consumption.

The supply and the distribution layer raises the question how heat and electricity interact through CHP, electric heating and heat pumps realistically. Its investigation requires to incorporate the heat system into the laboratory. It has to be flexibly configurable, to allow multiple different scenarios. This includes heat generation, storage and consumption, but also a heat grid could have a major impact on the electricity system.

The supply and the distribution layer raises the question how BEV mobility and electricity interact through BEV charging stations realistically. Its investigation requires different charging stations to be able to incorporate their behavior. The human factor has to be emulated, as no human can live in this laboratory.

The distribution layer raises the question how additional distributed generation and consumption devices, like heat pumps, BEV charging stations and PV can be realized in preexisting grids without exceeding distribution capacity limits. This question is especially relevant for house connection cables, because of the high power rating and simultaneity of BEV charging stations and PV plants. The alternative solution to grid expansion is to coordinate flexibilities such that the distribution capacity limits are not exceeded. This

requires such distributed flexibilities, which are controllable to be able to coordinate the dispatch of these technologies.

The provision layer raises the question how voltage range deviations can be compensated to ensure a reliable energy supply. The main reason for over- or undervoltages is the voltage drop along the distribution system. This requires a sufficiently large distribution grid with appropriate long realistic cables, to emulate these critical grid conditions. Incorporating the impact of harmonics and transient processes requires real grid cables, as cable emulators only focus on sinusoidal steady state conditions. Voltage drops of the mean voltage distribution grid have to be emulated by a HIL approach, which requires an adaption of the transformers voltages. These voltage drops can be compensated by injecting active or reactive power. This requires to have facilities available which allow to control active and reactive power, which could be the aforementioned flexibilities.

The system layer raises the question how the impact of harmonics and other mainly dynamic effects can be compensated to ensure a reliable electricity system operation. Its investigation requires to allow to implement such effects by a highly dynamic load emulator which can operate in the sub-periodic range of microseconds. Power electronic devices, which allow to implement specific control algorithms could allow to test new control strategies to damp harmonics etc.

The technological layer raises the question how to ensure using realistic HIL models. The validation of HIL models requires measuring real references, like a weather station and a real PV plant. It allows to validate HIL PV generation. The reference for the consumption is not possible in the laboratory, external real measurements of remote field tests are required.

A cross layer research question is which impact global non-technical factors, like national electricity markets, have on the local MG and how can these be utilized. These investigations are beyond the focus of the laboratory and have to be emulated. This requires an overall computational performance to calculate the emulation models.

Another cross layer research question is which impact the overall grid state has on the MG and vice versa. This question involves questions about frequency control, but also the impact of mean voltage harmonics, voltage drops and other disturbances on higher voltage levels. Treating this question requires to emulate the mean voltage grid behavior through power hardware in the loop (PHIL) facilities, which involves high costs.

A further cross layer research question is how the overall electricity system can restart after a major blackout without centralized power plants. Research for this question requires island capabilities of the MG to emulate blackout conditions and to implement the black start process. Controllable inverters, which allow to implement specific control approaches could be the fundamental basis to allow such a black start, as well as controllable rotating generators.

Summary:

The laboratory specifically requires

- fluctuating generation devices, incl. a real PV plant
- highly dynamic load emulator
- flexibilities, like controllable generation, storage and consumption devices
- distributed computation devices with overall computational performance
- experimental communication system
- a flexibly configurable heat system, including heat generation, storage, consumption and a heat distribution grid
- different charging stations
- sufficiently large distribution grid with appropriate long real cables
- facilities which allow to control active and reactive power
- controllable power electronic devices
- a weather station
- mean voltage grid emulator, if affordable
- island capabilities

Chapter 3

Laboratory Design

This chapter describes the technical concept of the experimental MG laboratory design of the Technical University of Munich's research group 'Center for Combined Smart Energy Systems' (CoSES). It is located at the Center for Energy and Information ("Zentrum für Energie und Information") in Garching. The laboratory design is based on the laboratory requirements which are elaborated in Sec. 2.3. The technical design process itself is based on heuristic methods and available products of the market, which is not part of this work. Rather this work elaborates the result of the design process, by giving an overview to the overall laboratory design and describing the concept of the individual laboratory components. For clarity of the following work, the important terms 'grid users', 'topology', 'configuration', 'setup' and 'scenario' are defined in Def. 3.1 to Def. 3.5.

Definition 3.1 *The term grid user is defined throughout this work as a technical system, which is physically connected to an energy utility grid to consume, store or generate electric energy and which is no energy utility grid itself. Grid users are for instance the electric infrastructure of buildings, centralized battery storages or power plants.*

Definition 3.2 *The experimental grid topology is defined throughout this work as the properties of a specific experiment, which describe the length and the arrangement of the grid connections, the location of the grid users and the location of connections to other utility grids.*

Definition 3.3 *The experimental configuration is defined throughout this work as a specific topology with specified technical properties of the utility grid, like cable types and transformer properties.*

Definition 3.4 *The experimental setup is defined throughout this work as a specific configuration with specified external conditions, like weather conditions or available water flow for water power generation.*

Definition 3.5 *The experimental scenario is defined throughout this work as a specific setup with specified generation, storage and consumption technologies.*

3.1 Overall design

This section gives an overview to the overall laboratory design, which is motivated by the technical requirements of Sec. 2.3. Analyzing these requirements results in two partly opposing laboratory properties. Some experiments require to be as realistic as possible for the validation of new strategies, other experiments require to be flexibly configurable and replicable. For this purpose, the MG concept intends two fundamental operation modes, the

1. laboratory operation mode (HIL mode), which is independent of real external impacts like weather etc., which are emulated by HIL approaches, to achieve replicable and flexibly configurable experiments and the
2. validation operation mode (VAL mode), which implements real appliances like PV which are based on real external conditions, to achieve as realistic and reliable results as possible.

The MG consists of an electric low voltage grid by considering heating and cooling, as well as communication networks. This work focuses on the energy sectors, by only considering interfaces to the experimental communication system. The laboratory setup in the electricity, the thermal and the digital layer is illustrated in Fig. 3.1. The fundamental limitation of the laboratory is that it is a test site and not entirely real, which means that it does not contain real buildings with real humans. This requires conventional energy consumption to be emulated, independent of the specified operation mode.

Summary:

- HIL and VAL laboratory mode for specifiable or real experimental scenarios
- Microgrid laboratory involves the electric, thermal and digital layer

3.1.1 Laboratory layout and dimension

The MG laboratory layout fundamentally aims for emulating realistic scenarios in a realizable dimension. The final dimension highly depends on the available local preconditions, which allow to fundamentally involve the energy facilities of five houses, the real electricity grid and some further facilities. Four houses have each a power rating of conventional multifamily houses with five flats and one house with a typical power rating of a multifamily house with 30 flats. For a clear termination this work labels the four smaller houses as single family houses (SFH)¹ and the bigger house as multi family house (MFH). Each of these buildings comprise the real electrical, heating and cooling system, from the grid

¹The term single family house is reasonable, as it has the identical power rating if BEV charging and electricity heating were considered.

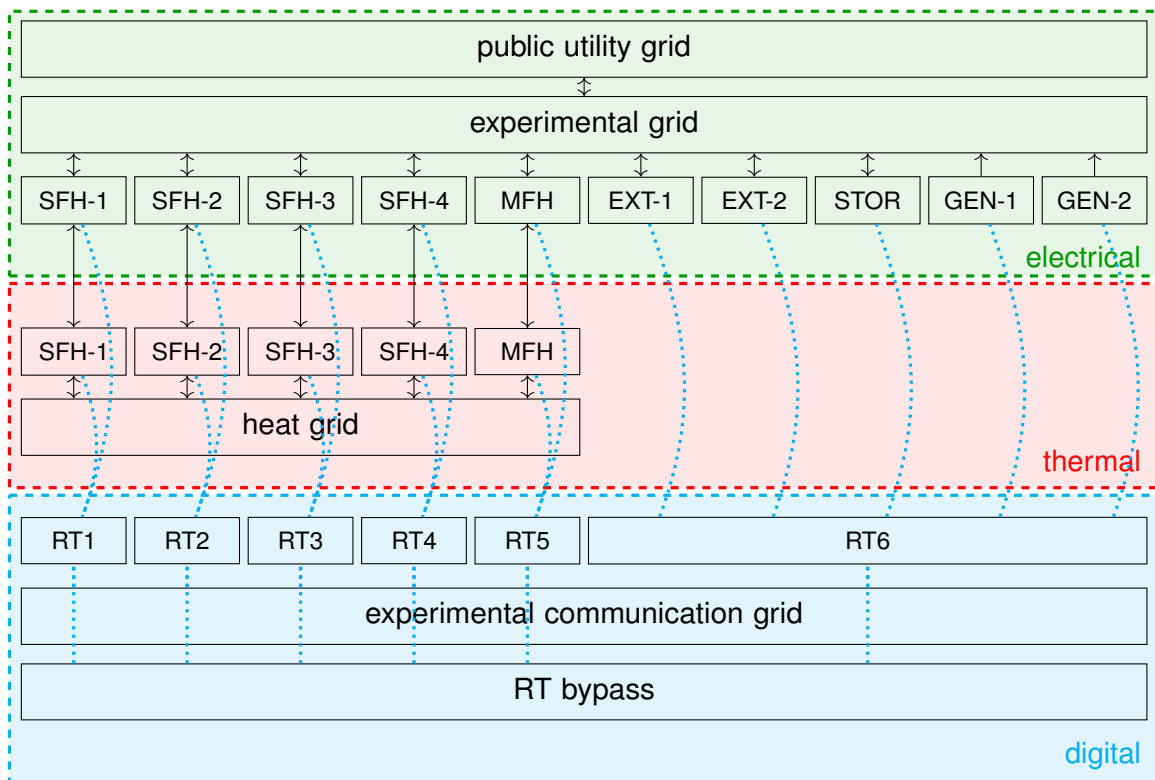


Figure 3.1: Overview over the general structure of the MG laboratory with the electrical, thermal and digital layer

access to real storages until the emulated consumption. A virtual extension (EXT) of two nodes of the electricity grid can flexibly emulate either a separate virtual section of the distribution grid or two further multi family houses without consideration of real heating. Furthermore the laboratory has two generators (GEN) to emulate micro wind or water power sources, as well as one centralized storage (STOR). These extensions allow to flexibly configure further scenarios in the MG laboratory. Hence, the overall laboratory setup consists of the four SFHs, one MFH, two EXTs, two GENs and one STOR in an electricity, thermal and digital layer as illustrated in Fig. 3.1. This setup is a good compromise between the aforementioned research requirements and realizability, based on multiple heuristic analyses and computations.

The electric power rating of the 30-flats MFH results from a conventional dimensioning according to German standard DIN 18015-1, illustrated in Fig. 3.2. The superior available standard power rating for the MFH is $I_{n,MFH} = 125$ A. The appropriate power rating for the SFH is $I_{n,SFH} = 63$ A. Considering BEV charging or electric hot water generation would require a higher power rating, which requires to interpret the SFHs as smaller houses because the power ratings are technically fixed laboratory parameters. An alternative is to consider experimental scenarios with the challenge of subsequent BEV charging and electric heating retrofitting. The power rating of the two emulated electric EXTs is dimensioned to a minimum power of $P_{n,EXT} = 100$ kVA, to allow to configure realistic scenarios with a sufficient impact on the grid's line voltage drops. The power rating of

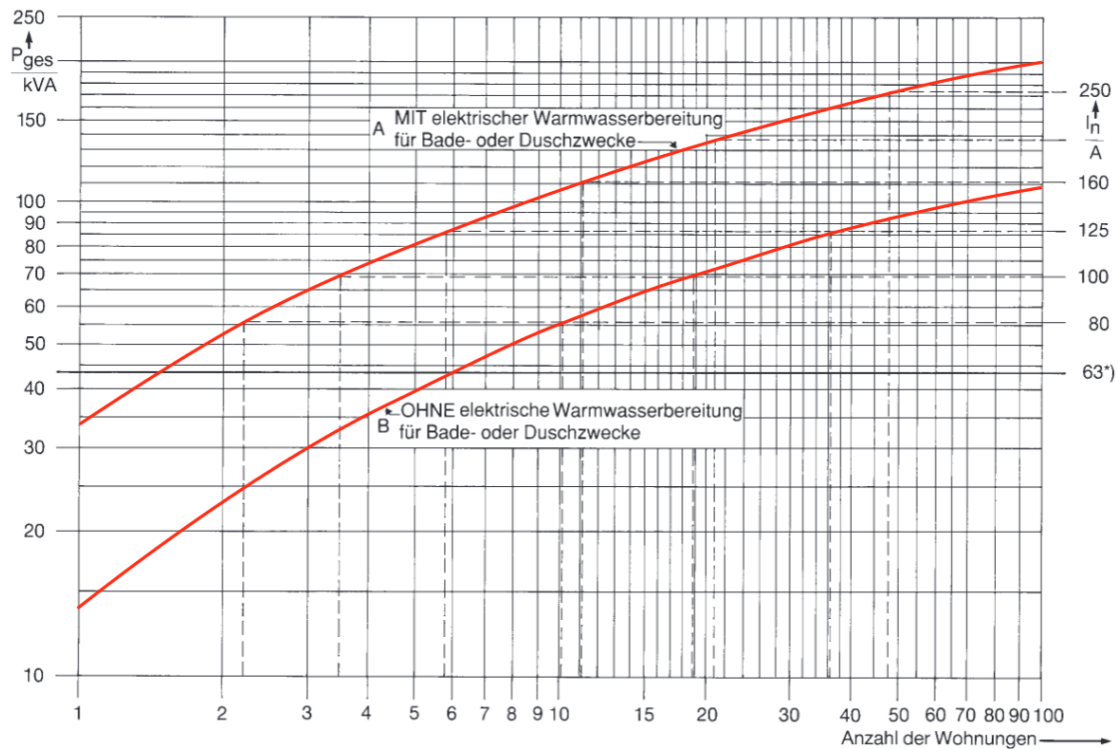


Figure 3.2: Dimensioning of the electrical power rating of house connections according to German standard DIN 18015-1: number of flats in argument axis, power rating in value axis, higher/lower graph with/without electric hot water generation, © DIN 18015-1, Beuth Verlag GmbH

the STOR connection is $P_{n,STOR} = 173$ kVA and of the GEN connections are $P_{n,GEN} = 44$ kVA.

Two parallel transformers allow to flexibly investigate multiple different experimental configurations and scenarios. The fundamental power rating of the grid without considering simultaneity factors, GENs and the STOR

$$P_{n,grid} = P_{n,MFH} + 4P_{n,SFH} + 2P_{n,EXT} = 458 \text{ kVA}$$

splits up to two transformers, with a power rating of $250 \text{ kVA} \leq \frac{P_{n,grid}}{2}$. This means that considering experimental configurations with one transformer means to assume a simultaneity factor of 0.5 and considering both transformers means to assume a simultaneity factor of 1.0, by only considering energy consumption.

The heat power rating of the five buildings consists of the space heating and hot fresh water power demand. The heating demand is typically determined through the heating load calculations, described in European standard EN 12831. This approach is based on highly location specific data, like the buildings location and construction. Emulating flexibly different houses makes a rough calculation of the heating load requirements sufficient. Considering future scenarios requires to assume highly insulated buildings. Fundamental assumptions are to generally consider 70 m^2 floor area for each flat, including heated general floor areas like hallways. Assuming a maximum relative heating load for the MFH

of 30 W/m^2 results entirely in the MFH's heating load of $P_{\text{hl,MFH}} = 30 \times 70 \text{ m}^2 \times 30 \text{ W/m}^2 = 63 \text{ kW}$. Considering a slightly higher maximum relative heating load for the smaller SFHs of 35 W/m^2 results entirely in the SFHs' heating load of $P_{\text{hl,SFH}} = 5 \times 70 \text{ m}^2 \times 35 \text{ W/m}^2 = 12 \text{ kW}$. The hot water system dimensioning is typically based on the demand number (German: Bedarfskennzahl) which is defined in German standard DIN 4708-2. Considering the mentioned standard configuration of one bathtub and two further hot water taps with 3.5 residents in each flat means demand numbers of $N_{\text{hw,MFH}} = 30$ and $N_{\text{hw,SFH}} = 5$, which specify the required power rating of the fresh water heater. The mean energy demand for hot water is estimated by assuming a daily mean hot water consumption of 40 l/d per person. Heating water up by 50 K requires 0.058 kWh/l , which means a mean energy demand for hot water for the SFHs of $5 \times 3.5 \times 40 \text{ l/d} \times 0.058 \text{ kWh/l} = 41 \text{ kWh/d}$ and for the MFHs of $30 \times 3.5 \times 40 \text{ l/d} \times 0.058 \text{ kWh/l} = 244 \text{ kWh/d}$.

Summary: The MG consists of 4 SFHs, 1 MFH, 2 GEN, 2 EXT and 1 STOR:

- SFH's power rating is electrically 63 A, for heating 12 kW and for hot water generation $N_{\text{hw,SFH}} = 5 \hat{=} 41 \text{ kWh/d}$
- MFH's power rating is electrically 125 A, for heating 63 kW and for hot water generation $N_{\text{hw,MFH}} = 30 \hat{=} 244 \text{ kWh/d}$
- GEN's power rating is 63 A
- EXT's power rating is electrically 160 A
- STOR's power rating is electrically 250 A

3.1.2 Electric energy system

The experimental electricity grid of the MG laboratory connects the grid users through the distribution transformer to the local mean voltage utility grid. The grid users are the aforementioned 5+2 houses (4 SFH, 1 MFH and 2 EXT) and central utility generation (GEN) and storage (STOR) facilities. The functional connection from the MV through the transformer and the grid to the grid users is illustrated in Fig. 3.3. An important aim is to be able to have full control abilities over the entire path, from the mean voltage to the grid users, which allows the flexible implementation of multiple scenarios with different operational control strategies.

Mean voltage PHIL systems would allow to implement digitally computed artificial MV system behaviors. Its application is prepared but not executed due to the high cost of the required MV power electronic systems. Artificial MV behaviors allow to flexibly configure multiple different scenarios and flexibly implement operational control strategies. It is required for investigations which stand in a conflict with the local grid properties, like over- or undervoltages at the MV layer, different MV stiffnesses or experiments with specific requirements for the overall grid behavior.

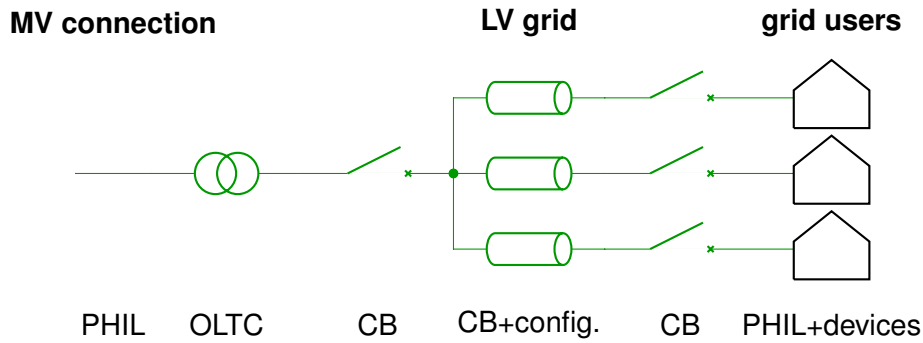


Figure 3.3: Illustration of the MG laboratory electricity system's active components: From the mean voltage (MV), through the low voltage (LV) grid to the grid users, with the ability to actively control all components through HIL facilities, OLTC and CB switching and an offline flexibly adjustable grid configuration, which allows radial, ring and meshed grid topologies

The flexible operation of the MG motivates to specify the MV transformer as two parallel undersized transformers, connecting the experimental low voltage grid with the local 20 kV MV grid. This allows experimental configurations with differently localized transformer feed-in, as well as experimental configurations with one undersized transformer, with a sufficient strong transformer or even two individual experiments with each one half of the laboratory at the same time. A possibility to switch the connection to the MV is applied to allow grid connected and island experiments, as well as their transitions. Both transformers are OLTCs, to be able to configure different static transformer tapplings or to investigate strategies including OLTCs.

The requirement for realistic reference technologies and to flexibly configure scenarios motivates to use real grid cables. These, in contrast to cable emulators, allow a more realistic behavior which is required for convincing investigations to verify control strategies, as well as model reference investigations, especially by considering harmonics and transient processes. The lengths and diameters of these cables are an important factor for the grid behavior due to the cable's voltage drops under load. Flexible grid configurations require to provide different types and lengths of cables which can flexibly be connected to each other, to allow to configure multiple grid topologies, including the grid users.

Voltage measurements at each grid node and current measurements of all power lines, which allows to gather the accurate electric system state, realize the required sophisticated measurement system. Remote controlled circuit breakers (CB) at all grid users and one CB which can flexibly be allocated to any grid cable allow to flexibly emulate trips and to flexibly apply load shedding strategies.

Beneath the five houses, the grid comprises further grid users. The two EXTs are realized by a PHIL system, which allows to flexibly implement any system behavior within technological limits. The other grid users comprise two rotating generators (GEN), whose propulsion is externally controlled by a HIL approach through a torque controlled motor to emulate either micro wind or water power sources. The grid users additionally comprise the ability to connect a real centralized battery storage or other external centralized

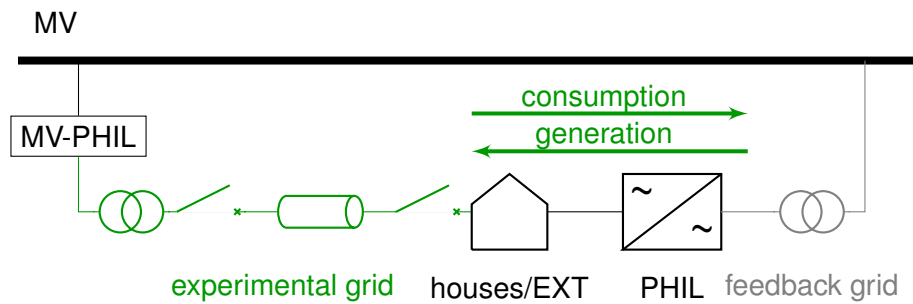


Figure 3.4: Functional schematic of the MG laboratory electricity system: Experimental grid, PHIL consumption and feedback grid

facilities for specific research projects.

The electricity consumption of the five houses has to be emulated, as the houses, their walls, rooms and habitants, do not exist in reality. The energy system facilities of these houses are only realized in a laboratory hall, except the real energy consumption devices, which highly depend on the human behavior. The electric consumption is emulated through a PHIL approach, which requires the appropriate power electronic facilities for each house. A bidirectional PHIL system as used for the EXTs, allows to flexibly emulate consumption including distributed generation and storage units. The PHIL systems mainly draw electric energy from the experimental grid with specified physical properties to emulate its consumption. The consumed energy is fed back into the local utility grid through a separate LV grid, the feedback grid. It also allows to emulate generation in each house by supplying the required energy through the feedback grid. This setup is illustrated in Fig. 3.4.

The five houses comprise real electric energy appliances, to provide the required reference technologies for modeling which allows to realistically emulate the behavior of further such technologies. The major pure electric technologies to be considered are PV generation, batteries, appropriate inverters and BEV charging stations. The ability to allocate these technologies flexibly to the five houses allows to flexibly configure multiple scenarios. Conventional inverters do not allow for influencing the physical feed-in-behavior. The requirement for flexibly implementing operational control strategies includes investigations about the voltage signal shape. Also controlling the voltage amplitudes require to control this feed-in-behavior flexibly. This means that additional experimental inverters are applied which allow to directly control the switching of the power transistors, such that different behaviors can be realized flexibly.

One of the most promising strategies to apply the required sector coupling to shift electric consumption and generation to balance each other is coupling heat and power. Available technologies are to burn fuels and generate electricity and heat (CHP) or to generate heat by using electric energy in heat pumps or electric heaters. Investigations in this context about sector coupling requires the application of different heat pump, electric heating and CHP technologies with different power factors in the five houses. The allocation of these technologies characterize the individuality of each house, other technologies and the location of the houses in the grid are flexibly allocatable.

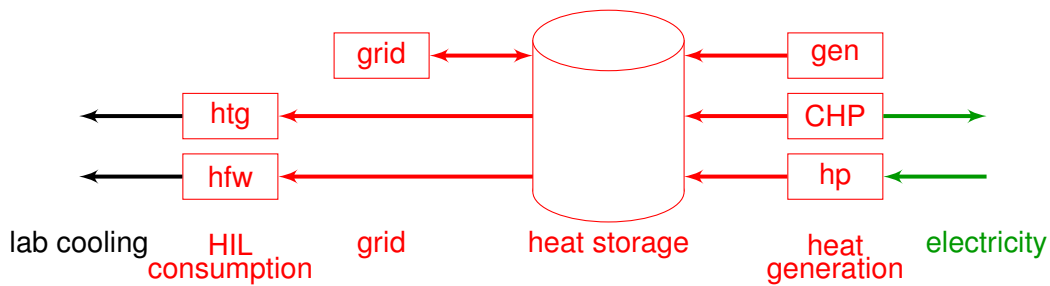


Figure 3.5: Functional schematic of the MG laboratory's heat system of each house: house central heat storage, heat generation through HIL generator (gen), CHP and heat pump (hp), connection to the heat grid, and HIL consumption through emulating heating (htg) and hot fresh water (hfw)

Summary: The electricity system consists of

- MV PHIL systems
- two parallel undersized MV transformers, including appropriate CBs
- real grid cables with different lengths and diameters
- voltage measurements at each grid node, current measurements of all power lines
- Remote controlled CBs at all grid users and one flexibly allocatable
- two EXTs as PHIL systems
- two rotating generators
- connection for a real centralized battery storage
- PV generation, batteries, BEV charging stations and appropriate inverters allocatable to 5 houses
- controllable experimental inverters
- heat pump, electric heating and CHP technologies

3.1.3 Thermal energy system

The heat system consists of the domestic thermal energy system of the five houses and the thermal distribution grid. This work focuses on the heat system with the requirement to simply allow the extension of a cooling system for future experiments. The required ability to flexibly investigate different system topologies, scenarios and operational control strategies motivates to design the heat storage as a house central appliance, which connects

the local heat generation, the grid transfer station and the heat consumption, as illustrated in Fig. 3.5. This design decouples different heat generation and consumption facilities, such that different scenarios through using only some of the available technologies can be investigated. The consumption of heat through hot fresh water and heating is emulated through a HIL approach, due to the laboratory based approach without real consumers. This requires the laboratory cooling system to apply the required heat sinks. The individual appliances, like the consumption or CHP, are modularly manufactured such that individual appliances can be moved to another house to apply further flexibilities.

The thermal distribution grid allows to investigate strategies which exchange heat energy between different houses. The inducement of such strategies is to combine the advantages of different heat generation technologies throughout the grid. This means that the grid and the heat transfer stations have to be able to flexibly transfer heat in multiple directions throughout different temperature levels. Scenarios, which aim for separating different temperature levels, for instance heating and hot water or heating and cooling, need to separate two flow pipes and one return pipe, which requires a flexible three pipe heat grid. Conventional district heating systems require two pipes and circular designs require one pipe, such that the technical setup of the heat grid, especially the number of used pipes has to be flexibly configurable.

The requirement for the ability to flexibly configure the topology of the grid means that different types and lengths of pipes and different interconnections have to be applicable to flexibly connect different houses in different configurations. The dependency of the physical properties of pipes on external conditions like ambient temperature makes it necessary to emulate the pipe behaviors with a HIL approach to allow investigations of different experimental setups. The emulation of the pipe behaviors allows to flexibly specify the pipe lengths under multiple different conditions. Flexibility of the configuration of the connections among the houses, meaning which house is directly connected to which other house, is reached by providing six different connections among the houses, which can flexibly be activated. Different possible configurations are exemplary illustrated in Fig. 3.6.

Summary:

The heat system consists of

- heat storages as a house central appliance
- heat consumption being emulated through a HIL approach
- a possibility for the extension of the cooling system
- a multi directional heat grid and transfer stations for flexible temperature levels
- a flexible three-pipe heat grid with emulated pipe behavior
- 6 flexibly activatable heat grid connections

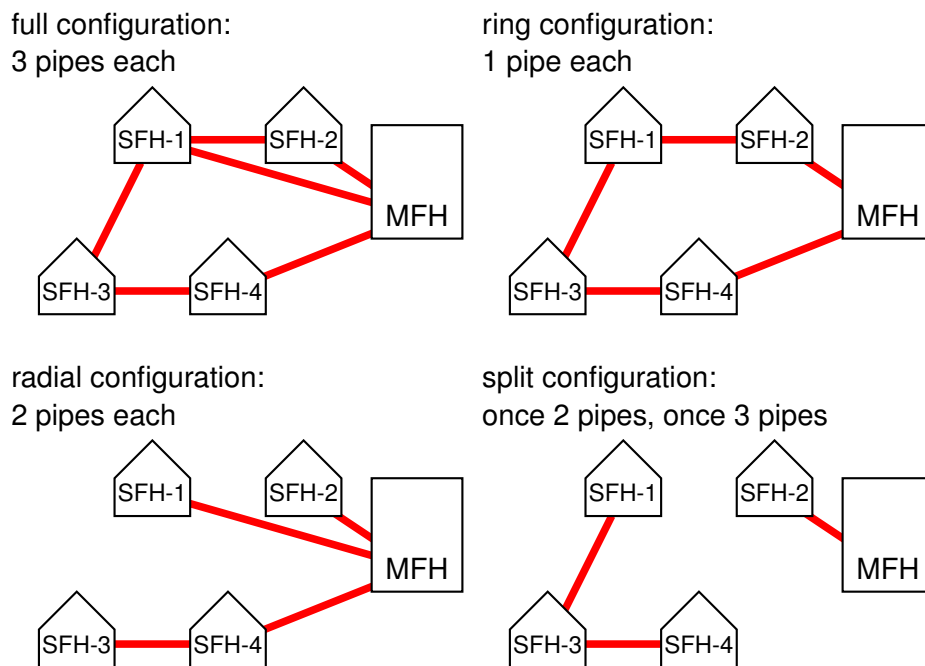


Figure 3.6: Overview over different possible district heating configurations - four examples

3.1.4 Communication and control system

One of the fundamental requirements is to have sufficient distributed RT computation devices to process recorded measurement and control data and to compute the experimental control and operation strategies. Distributed computational units, such that each house has at least its own computational device for electricity and one for heat allow to flexibly operate the electricity and the heat system of each house individually or in different configurations combined. This allows to use the laboratory flexibly and efficient, as several experiments can be carried out at the same time with parts of the entire laboratory, like considering each energy carrier or each house individually. A RT bypass allows the reliable intercommunication of the distributed computational devices to operate the laboratory through one centralized algorithm. The host computer system with an appropriate human interface applies the visualization, configuration and human interaction with the control system. The overall RT computation devices are used as the required sophisticated measurement system, which records analog and digital measurement and control data at a data server for post processing in the context of the evaluation of experimental results. The measurement over the distributed computational system has a sophisticated time synchronization to generate accurate time stamps for the measurement data, which is required to compare records of individual measurement systems.

Digitized MGs will utilize communication systems to share measurement, control and other important data as required from multiple different MG operation strategies. In this view, communication delays, uncertainties and performance limitations as well as communication system disturbances and outages have a significant impact on the energy system operation. The communication system itself lies outside of the focus of this work, but is still an important part of the MG laboratory. This requires the control

systems to be able to send and receive experimental data. The most flexible opportunity to allow this throughout multiple communication technologies is to use standardized ethernet interfaces. Ethernet communication protocols can flexibly be translated into other communication technologies, such that this is a reasonable compromise between flexibility and realizability. The requirement for flexibility means also to be able to make investigations without consideration of the communication system impact, which is allowed by utilizing the aforementioned RT bypass.

Summary:

The communication and control system consists of

- distributed computational units
- a RT bypass
- a host computer system with an appropriate human interface
- a measurement system with a data server
- a sophisticated time synchronization
- standardized ethernet interfaces to send and receive experimental data through the experimental communication system

3.2 Component design

This section describes the technical concept of the individual laboratory components, with a focus on their operational aspects. It is based on the technical laboratory design, topology and dimensioning. Safety and other technical and operational aspects are beyond the scope of this work and are only partly included, as far as they influence MG operation strategies.

3.2.1 Mean voltage system

The MV system connects the MG laboratory with the public MV utility grid. Its setup is illustrated in Fig. 3.7. The available utility MV system is designed as delta circuit. It consists of one three-phase bus-bar (BB) which is connected through the feed-in with a load-break switch with the utility grid. A power quality watchdog facility is installed before the feed-in, to avoid grid interferences from the laboratory. In case of grid interferences, an appropriate filter system, connected to the second feeder, protects the MG laboratory from tripping through the watchdog. The third feeder supplies the feedback grid. There is one feeder reserve for future applications. This BB's last feeder connects a transformer, with a PHIL facility and a further transformer to a second BB. This BB's voltage is directly controlled through the PHIL facility to allow for emulating flexibly mean voltage grid behaviors in the

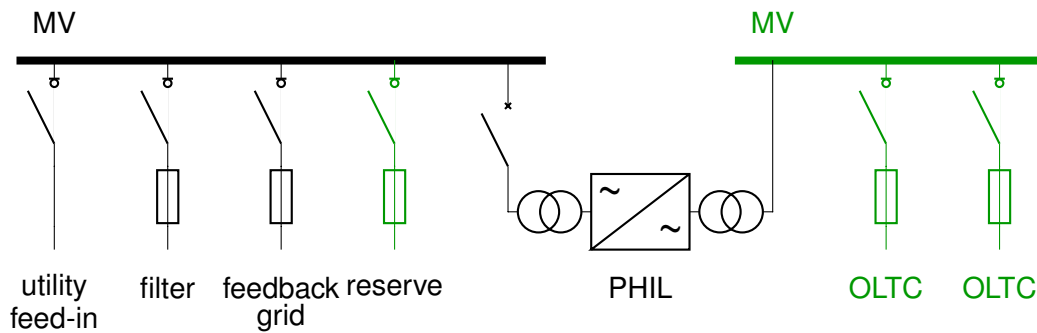


Figure 3.7: Technical illustration of the mean voltage BB system - parts of the experimental electricity system are illustrated in green

second BB. This BB connects two feeders which supply one experimental transformer each which are designed to be OLTC transformers.

The MV PHIL facility, which is not yet executed, has to be dimensioned for the second BB's power rating, which means 500 kVA for both OLTCs. Connecting one OLTC to the first BB's reserve feeder allows a power rating of 250 kVA for this PHIL facility, which means that experiments with modified MV behaviors are limited to electricity system configurations with one transformer. For considering higher harmonics, the controllable frequency spectrum of the PHIL facility needs to reach the 40th harmonics, which is the range of total harmonic distortion (THD) definition in European standard EN 50160:1999. Practically, this means an actively controllable band width of at least up to 2.5 kHz, including possible base frequency deviations and a safety margin. Higher harmonics, especially interactions with other laboratory facilities are negligible, because of the OLTC's low-pass filtering characteristics. The PHIL facility needs to control the three phase voltages and measure their currents. Through the RT system, it needs to allow a closed loop voltage control up to the aforementioned 2.5 kHz oscillations, to allow to implement the dynamic interaction between the emulated grid and the real experimental MV grid. According to the Nyquist-Shannon sampling theorem and considering a safety factor of 2, there is only $100 \mu\text{s}$ for the feedback loop, from the measurement through the control algorithm computation to the control action realization. This period needs to be allocated into the three subprocesses

1. measurement, digitization and data provision in $25 \mu\text{s}$,
2. data reception, control loop computation, control data provision in $25 \mu\text{s}$ and
3. control data reception and realization of control action in $50 \mu\text{s}$, which is typically the longest lasting subprocess.

The OLTC transformers are 20 kV-0.4 kV delta-star transformer with a nominal power rating of 250 kVA. The transformer ratio can be switched from $\frac{0.4 \text{ kV}}{20 \text{ kV}}$ in $\pm 4 \cdot 2.5\%$ steps, which is a commonly used configuration. The switching is actively controllable by the RT system through an open ethernet based communication protocol. A conventional operation mode, which automatically controls the secondary winding's voltage is available

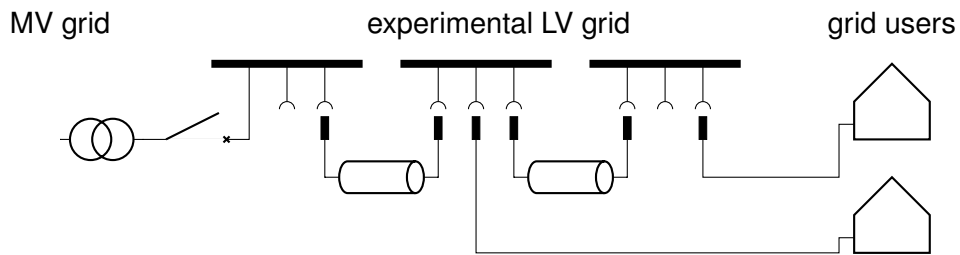


Figure 3.8: Patch panel approach for the experimental grid configuration system: BBs with only sockets are grid nodes, cables with plugs are grid edges and the grid users with one plug are the grid leaves.

as a reference behavior. The efficiency of the OLTC is specified to be high, which means a short circuit voltage of $u_k = 4\%$, to consider a high technological standard. The feedback transformer is a standard 20 kV-0.4 kV delta-star transformer. Its nominal power rating results from the power demand of electric heaters, the PHIL loads and the BEV charging stations. A reasonable standard power rating of 630 kVA allows for reserves for future applications. All transformers have a temperature warning and a temperature tripping, which acts on the low and high voltage CBs. All transformers are protected against overload with high voltage fuses.

Summary:

The mean voltage system consists of

- MV system as illustrated in Fig. 3.7
- PHIL facility is not yet executed
- two OLTC transformers with a nominal power rating of 250 kVA, switched from $\frac{0.4 \text{ kV}}{20 \text{ kV}}$ in $\pm 4 \cdot 2.5\%$ steps
- feedback transformer is a standard 630 kVA 20 kV-0.4 kV transformer

3.2.2 Low voltage grid

The low voltage grid system mainly consists of protection devices and the grid configuration system, which is applied in a set of cabinets. The key functionality is to freely configure the grid topology, which is applied by a manual patch panel approach. The key idea is to freely combine different grid edges, realized as cables with plugs at both ends, and grid nodes, realized as BBs only with appropriate sockets, as illustrated in Fig. 3.8. The grid users can also be connected through a connection cable with one plug to the BBs.

The grid cables are dimensioned such that realistic grid configurations and significant impacts on system behavior especially on voltage drops are achieved. Typically aluminum non-shielded cables with diameters in a range of 120 mm^2 to 300 mm^2 are used

in German LV grids, especially 150 mm² [72]. Copper cables are favorable for the laboratory, because of the much more complex cable installation. The main advantage of copper cables are the about 50% lower possible bending radii for cables with similar electrical characteristics. Other advantages are the 30 – 40% smaller diameters and the lower sensitivity for cable breaking due to multiple bending during laboratory installation. Shielded cables are required to minimize mutual influences of close cables, which would be remote in reality. These arguments lead to specify shielded copper cables with diameters of 70 mm², 95 mm² and 150 mm², which have a similar electric behavior as the typically used aluminum cables and hence are a close compromise between realism and feasibility.

The grid cables need to be protected against overload, which is a risk for fire, especially in the experimental context. As high packing densities have to be expected, the cables cannot be overloaded for a long term in the laboratory. This reasons to specify overload protection devices for each cable with the following properties

- 70 mm²-cables are protected with a nominal current of 125 A, which means a tripping in about 1 s at a current of 900 A and in about 1 h at a current of 190 A
- 95 mm²-cables are protected with a nominal current of 160 A, which means a tripping in about 1 s at a current of 1050 A and in about 1 h at a current of 230 A
- 150 mm²-cables are protected with a nominal current of 250 A, which means a tripping in about 1 s at a current of 1900 A and in about 1 h at a current of 410 A

according to the international standard IEC/EN 60269-2.

The lengths of these individual grid cable segments result from a compromise between a non-negligible impact on electricity grid behavior and still realistically short connections. Considering pure resistive impacts mean relative voltage drops of

- 13.81 %/km for 70 mm²-cables with the nominal current load of 125 A
- 13.02 %/km for 95 mm²-cables with the nominal current load of 160 A
- 12.89 %/km for 150 mm²-cables with the nominal current load of 250 A.
- 10.31 %/km for 150 mm²-cables with the current load of 200 A.

Considering a significance level of 0.5% voltage drop means cables with different lengths are only distinguishable if they have a minimum length difference of 40 m, which conforms at least 0.5% voltage drop at nominal current load. A minimum length of 100 m means about 1.3 – 1.4% voltage drop under nominal load for each grid cable, such that entirely sufficient voltage drops can occur. The 150 mm²-cables are dimensioned by considering a current load of 80% of the nominal current load, to give the lower probability of high current loads credit. Typically higher diameters are used for longer distances, which motivates a minimum length of 150 m for the 150 mm² cables and increments of 50 m, which conforms 0.5% voltage drop. Three different lengths of each diameter provide a sufficient flexible selection of grid cables. The most typical cable type with 95 mm² is

Table 3.1: List of all available grid edges as grid cables and connection cables, with their affiliation, diameter, current rating, length, and connection to the grid nodes through 250 A power-lock (pl-250) and 125 A CEE (CEE-125) plugs

cable-id	assignment	diameter	current rating	length	connection
C-1	grid	150 mm ²	250 A	250 m	2 pl-250
C-2	grid	150 mm ²	250 A	200 m	2 pl-250
C-3	grid	150 mm ²	250 A	150 m	2 pl-250
C-4	grid	95 mm ²	160 A	180 m	2 pl-250
C-5	grid	95 mm ²	160 A	180 m	2 pl-250
C-6	grid	95 mm ²	160 A	140 m	2 pl-250
C-7	grid	95 mm ²	160 A	140 m	2 pl-250
C-8	grid	95 mm ²	160 A	100 m	2 pl-250
C-9	grid	95 mm ²	160 A	100 m	2 pl-250
C-10	grid	70 mm ²	125 A	180 m	2 pl-250
C-11	grid	70 mm ²	125 A	140 m	2 pl-250
C-12	grid	70 mm ²	125 A	100 m	2 pl-250
C-13	STOR	150 mm ²	250 A	> 20 m	1 pl-250
C-14	EXT	70 mm ²	160 A	< 15 m	1 pl-250
C-15	EXT	70 mm ²	160 A	< 15 m	1 pl-250
C-16	GEN-1	16 mm ²	63 A	> 20 m	1 CEE-125
C-17	GEN-2	16 mm ²	63 A	> 20 m	1 CEE-125
C-18	SFH-1	16 mm ²	63 A	> 20 m	1 CEE-125
C-19	SFH-2	16 mm ²	63 A	> 20 m	1 CEE-125
C-20	SFH-3	16 mm ²	63 A	> 20 m	1 CEE-125
C-21	SFH-4	16 mm ²	63 A	> 20 m	1 CEE-125
C-22	MFH	50 mm ²	125 A	> 20 m	1 CEE-125

provided twice. This leads to the set of twelve grid cable segments, which are specified in Tab. 3.1.

The connection cables, which connect the grid users to the grid are dimensioned with 16 mm² copper equivalent for 63 A supply, which is applicable to the SFHs and the GENs. The grid extensions with nominal current rating of 125 A are connected through a 70 mm² copper grid cable. The MFH connection cable is appropriately dimensioned with 50 mm² copper. Lengths of at least 20 m are specified for all connection cables which means a significant voltage drop with nominal current load. The EXT connection cables should not have significant impact on the EXT behavior, such that the HIL emulation is not distorted. This means shorter than 15 m cable length, which equals 0.25% voltage drop, fulfilling a safety margin of 2 according to the aforementioned significance level.

The grid and connection cables are connected through BBs to establish the electricity grid. These connections are realized through sockets at the BBs and plugs at the cables. Applying without loss of flexibility a permanent connection of the OLTCs to each one BB and grouping two sets of plugs and sockets with different power ratings reduce on the one hand the challenges of limited current ratings of sockets and plugs and on the other hand the disproportional high space demand and monetary cost of plugs and sockets

Table 3.2: List of all available grid nodes as BBs (bb), with available 250 A power-lock (pl-250) and 125 A CEE (CEE-125) sockets, the BB current rating and their supply connection

bb-id	pl-250	CEE-125	current rating	supply
bb-1	3	1	360 A	OLTC-1
bb-2	2	2	360 A	OLTC-2
bb-3	3	2	360 A	none
bb-4	3	2	360 A	none
bb-5	4	1	360 A	none
bb-6	1	2	250 A	none
bb-7	2	2	360 A	none
bb-8	3	1	360 A	none
bb-9	3	1	360 A	none
bb-10	2	1	250 A	none

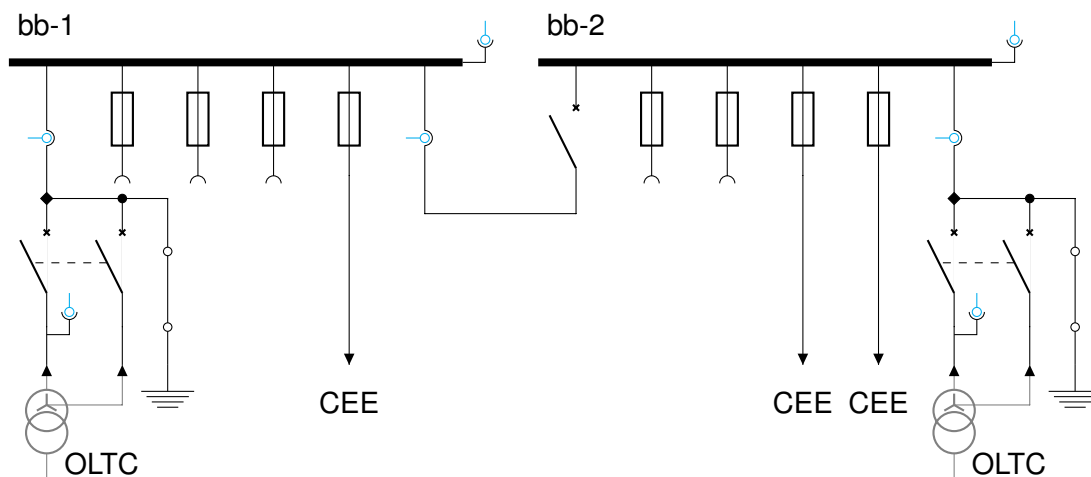


Figure 3.9: Illustration of the technical setup of the low voltage OLTC protection and BB cabinets; voltage and current transducers are in light blue, diamond shaped connection combines 3-phase and neutral to 3-phase+neutral;

with high current ratings. The permanent connection of the OLTCs allows a maximum current rating of the remaining cables of 250 A, which is realized by powerlock plugs and sockets with a nominal current rating of 250 A. The connection cables of the five houses and the two generators C-16 to C-20 of Tab. 3.1 are realized with CEE plugs and sockets with a nominal current rating of 125 A. Ten grid nodes are considered to be sufficient for connecting the 12 available grid edges with a high degree of freedom. This specifies ten different BBs as these grid nodes, as listed in Tab. 3.2. The first two of them are directly connected to each one OLTC. Five BBs contain three 250 A sockets, three contain two 250 A sockets and two BB contain one and four 250 A sockets respectively. All BBs contain one to two 125 A sockets. This allows up to two houses or generators to be connected to one node, and nodes with up to four connected edges. A direct connection of two nodes can be used to increase the number of sockets.

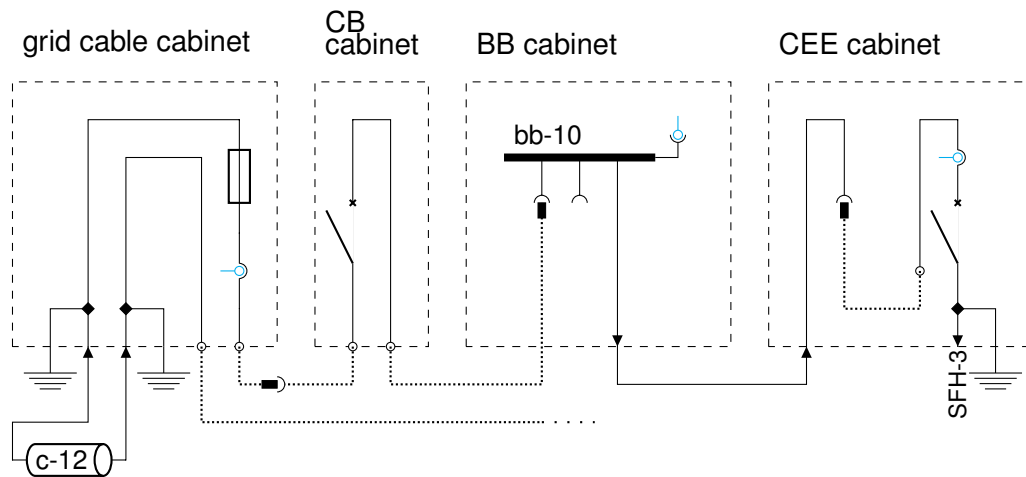


Figure 3.10: Illustration of the technical setup of the experimental electricity grid configuration facility in parts; voltage and current transducers are in light blue, diamond shaped connection combines 3-phase+neutral and PE to 3-phase+neutral+PE; the illustrated configuration connects SFH-3 to bb-10, which is connected through the grid CB to c-12 which is connected to a further not illustrated BB.

The electric structure of the OLTC protection and connection to the BBs is illustrated in Fig. 3.9. The neutral point grounding can be removed to allow isolated neutral grounding experiments. The OLTC is connected through a remote controlled 3-phase+neutral CB to switch between grid isolated and grid connected operation modes. The CB is also required for protection tasks, which requires different protection tripping mechanisms. The OLTC temperature tripping prevents the transformer from burning after getting hot. An emergency tripping is required to cut off electricity for safety reasons. The mean voltage intertripping is required to avoid reverse voltages and to avoid to switch under load, as only a MV load break switch is available. An overload tripping protects the cables and other facilities from overload through exceeding current limits.

The aforementioned OLTC protection and BB cabinets affiliate through their BBs bb-1 and bb-2 into the experimental electricity grid configuration facility. Its mechanism is partly illustrated in Fig. 3.10, covering grid cable c-12, BB bb-10 and connection to grid user SFH-3. Each end of the twelve grid cables are connected to a cabinet. Their shields are grounded. Their phases and neutral are connected to highly flexible cables ending with powerlock plugs. One side of each cable is protected against overload through fuses and their currents are measured by a three phase+neutral current transducer. Connection cables from grid users to the grid are protected against overload through a CB, their currents are measured with an appropriate transducer and they are connected through a highly flexible cable to either CEE or powerlock plugs. The grid CB cabinet contains one remote controlled CB, with one end connecting through a highly flexible cable a powerlock socket, and the other end a powerlock plug. This can be plugged in between any grid cable and any BB. All highly flexible cables with powerlock sockets can be flexibly connected to any BB. The CEE sockets in the CEE cabinets are fixed connected to the appropriate BBs. In the CEE cabinet the flexible CEE connection cables can flexibly be connected to the

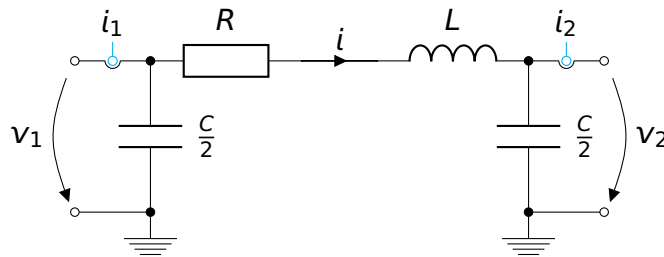


Figure 3.11: Pi-circuit diagram of cables with theoretically required current measurements at both ends

CEE sockets of the BBs. The current rating of the BBs is 360 A or 250 A as listed in Tab. 3.2, considering a simultaneity factor of 0.7.

A major property of the experimental MG laboratory is to have sophisticated measurement and control capabilities. Active control capabilities in the low voltage grid system are the CBs and the tap changer of the OLTC transformer. The CB and the tap changer have to be actuated through control commands from the RT system. The measurement system is based on current and voltage transducers which have to be read through the RT system. To allow to gather the entire system state, each node's voltage and each edge's current needs to be measured. This requires voltage transducers at each BB, and current transducers at each grid cable. Theory requires a current measurement at each end of the cable because these currents differ. The electrical behavior of a cable is simplified illustrated for one entirely isolated phase as a pi-circuit diagram in Fig. 3.11. Mainly the leakage currents through the capacities cause differences between both sides' currents i_1 and i_2 . Typical capacities of low voltage grid cables are in a low range of nF/km. Assuming an exaggerated worst case scenario of $1 \mu\text{F}$ for one cable, would mean a leakage current lower than $I_{\text{leakage}} = 2UC\omega < 0.25 \text{ A}$, by considering a safety factor of 2 for the impact of higher harmonics. It is calculated with frequencies of 50 Hz and voltages of 400 V, higher harmonics have a proportionally higher impact, but with typically significant lower amplitudes, which balance each other. Currents lower 0.25 A mean a proportion of lower than 0.2% of the nominal values, which is hardly accurately measurable, due to limited accuracy of the transducer, the limited resolution of the digitization process and the finally limited impact on system behavior. This means to only apply one current measurement for each cable by assuming this current to be the central current i of Fig. 3.11, which means an exaggerated worst case measurement error of 0.1% relative to the current measurement range, which appears acceptable. The impact of the leakage capacity on the entire grid is not neglected, as it is measured from one cable to another, it is only not measurable in one cable segment. Longer cables with higher leakage capacity impact are configured by cascading individual cable segments, what means that leakage currents are measured because there is one measuring point per single cable segment.

The specific interconnection of voltage and current transducers, meaning which voltages and currents are measured in a 3 phase+neutral+pe system, have a high impact on the research capabilities of the laboratory. Investigations considering ground currents require a realistic distribution of grounding potentials and resistances. This means each house requires its own grounding remote of the grounding of other houses. Realizing

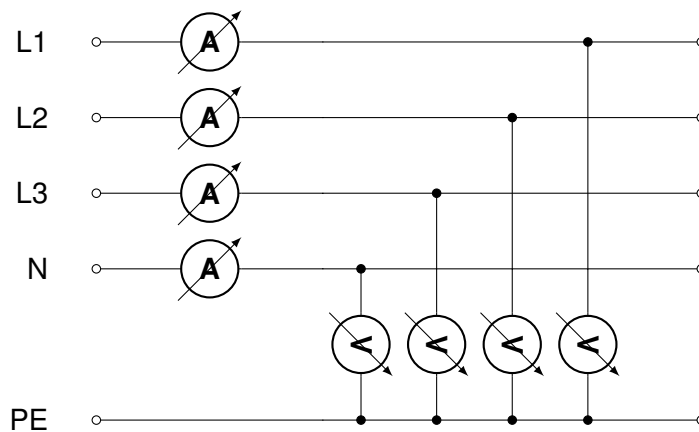


Figure 3.12: General measurement concept of voltages and currents

realistic and flexibly different grounding resistances is hardly imaginable. Furthermore this means that PE cannot be fixed connected to one joint earthing, which contradicts basic electricity safety principles for one central laboratory. For these reasons it appears useful not to investigate ground currents, which mainly are relevant for failure and protection investigations. This means not to measure ground currents as well as ground potentials, which leads to the preferred measurement concept as illustrated in Fig. 3.12. Four currents of the three phases and the neutral conductor remain for measurement. Neglecting ground currents could theoretically allow not to measure the neutral current due to $i_{L1} + i_{L2} + i_{L3} + i_N = 0$, which causes no redundancies. For practical accurate measurement tasks redundancies can be applied to increase accuracy and to gain a measure for parts of the inaccuracies, which motivates to apply a four current measurement. Having one overall grounding potential over the grid allows to use this as a joint measurement reference potential. Measuring neutral voltages is essential for investigations of neutral-potential-shifts due to unsymmetrical grid loads. This motivates to specify four voltage measurements, from the three phases L1 to L3 and the neutral conductor relative to ground potential. Significant balancing currents have a direct impact on voltage measurement accuracy due to the PE impedances, which means that balancing currents have to be avoided and PE conductors require an adequate dimension. Further specific measurements are required to gather the grid system's entire state, like the balancing current between the first two BBs, the transformer currents and the transformer voltages to allow resynchronization and reconnection after islanding. All grid measurements are illustrated in Fig. 3.9 and Fig. 3.10.

Summary:

The low voltage grid involves:

- grid configuration system by a manual patch panel approach as illustrated in Fig. 3.8
- set of twelve grid cable segments as specified in Tab. 3.1
- ten different BBs as grid nodes as listed in Tab 3.2
- OLTC connection as a remote controlled CB to switch grid isolated and grid connected modes
- grid CB
- sophisticated measurement and control capabilities

3.2.3 Electricity load

The key component of the experimental laboratory is the electric load emulator. It finally realizes the electricity consumption of the five houses, appropriate generation technologies and the two EXTs. To be able to use it flexibly for multiple different tasks, it is important that it realizes any software defined load and generation behavior. The only physical technology which can be used for this task is a four quadrant frequency converter with an appropriate control strategy. It is a power electronic device which is closed loop controlled such that the desired behavior can be flexibly realized. This control loop means that the frequency converter itself is a dynamical system, which dynamically interacts with the desired behavior, which typically is another dynamical system. But also dynamical interactions with other devices which are electrically connected to the load emulator, like a PV inverter will occur. The interaction of incautiously connected dynamical systems has in general to be initially considered as instable, which means physical parameters can diverge, which can lead to system shut downs or even their destruction. The typical phenomenon is the joint swing up or undesired oscillations. These phenomena have to be precluded by system design. The only possibility to absolutely preclude swing ups, undesired oscillations or other system diverges, is to mathematically proof dynamical stability. To ensure the desired behavior, an asymptotic stability proof is required. These proofs require entire system knowledge, which is not available. The solution is to define specifications and mechanisms to preclude these phenomena as far as possible.

The initial question is how to apply a specific flexible system behavior on a frequency converter. Assuming a stiff grid means that voltage is almost fixed by the grid, and currents are controlled by the converter. This means that the converter measures the voltage v and current i , its controller computes a control action for the power electronics which cause a flowing current i . The control goal is to equal the flowing current i and a specific reference current i_d . The load model provides the reference current i_d , based on the voltage measurement v , which means it to be an admittance model. The entire system

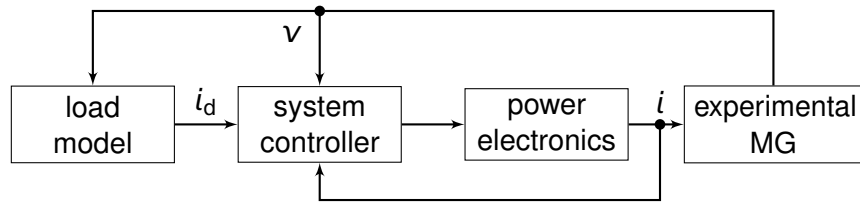


Figure 3.13: Block diagram of the system behavior of emulated load dynamically interacting with the experimental MG; reference current i_d , actual current i , actual voltage v

structure is illustrated in Fig. 3.13.

Considering the mutual interaction of the three system parts, the load model, the frequency converter and the MG individually allows their specific analysis. The interaction between the load model and the MG is desired, as it would also exist in reality, assuming an accurate load model. Having complete system knowledge of the frequency converter allows to consider its system behavior in the load model, as required to avoid instabilities and to ensure a realistic overall system behavior. The difficulty of the interaction between the frequency converter and the MG is the unknown system behavior of the MG. The MG is required to be flexible, which means to investigate multiple different setups, and it is generally complex and partly unknown, depending on the used mainly proprietary devices. One opportunity to avoid undesired oscillations between such devices and the frequency converter is to operate them on distinct frequency spaces. This means that the short control action of the fast system has only a minor impact on the control of the slower system, which breaks this critical feedback loop. An unstable interaction among the frequency converter and the overall grid, typically by ensuring a high control performance with a weak grid, can only be prevented by adapting control parameters by knowing the control strategy and the power electronic behavior.

The load emulator system has seven outputs. The four outputs for the SFHs require a minimum peak current rating of ± 90 A each, which correspond to the current rating of the house connections. The same leads for the MFH and the two EXTs to a minimum peak current rating requirement of ± 180 A. The maximum emulator's output peak voltage-to-ground rating is ± 902 V, which allows a 15% overvoltage, a 100% neutral conductor offset and a 20% safety offset for the nominal peak neutral phase voltage $400\text{ V}\sqrt{\frac{2}{3}}$. The maximum peak voltage operating range is 716 V, which allows a 15% overvoltage, the maximum peak phase voltage difference factor of a three phase system of $\sqrt{3}$ and a 10% safety offset for different neutral offsets and phase angles of the different outputs for the nominal peak neutral phase voltage $400\text{ V}\sqrt{\frac{2}{3}}$. The frequency operating range from 0 to 2.75 kHz for voltages and currents allows to consider the 50th harmonic. The system can operate voltages and currents whose shapes are within the aforementioned limits.

Preventing the aforementioned system instabilities and undesired oscillations, requires extreme system performance parameters like settling time. Products with such performance parameters are not available on the market. For this reason safety margins have to be reduced to a minimum, such that at least one product is available. Considering the 50th harmonic in the laboratory means a Nyquist sampling period of $200\ \mu\text{s}$, whereby the load emulator has to be faster. Allocating 25%-50%-25% of the available period for the con-

trol delay - rise time - final settling, means to require the emulator's 10-to-90% rise time of maximum $100 \mu\text{s}$ and the initial 0-to-10% control delay of $50 \mu\text{s}$. The 90-to-100% settling cannot be specified, because this time period theoretically lasts infinite, but is veiled by noise and limited measurement accuracy. The sampling rate of 250 kHz of the internal load emulator controller, and the load model allows to divide the initial 0-to-10% control delay of $50 \mu\text{s}$ into more than ten samples, to enable pseudo-continuous system consideration. The load model is computed in the external RT system, such that measurement and setpoint data have to be communicated to the load emulator. The fibre-optical communication between the load emulator and the RT system precludes disturbances and inaccuracies through electro-magnetic couplings between the power cables and the communication cables because of the possible high frequency power components.

Summary:

The load emulator has

- a maximum output peak voltage-to-ground rating of $\pm 1000 \text{ V}$ allows a 15% overvoltage, a 100% neutral conductor offset and a 20% safety offset
- maximum peak voltage operating range allows a 15% overvoltage and a 10% safety offset
- frequency operating range from 0 to 2.75 kHz
- 10-to-90% rise time of maximum $100 \mu\text{s}$, 0-to-10% control delay of $50 \mu\text{s}$ avoids system instabilities and undesired oscillations
- sampling rate of 250 kHz allows a pseudo-continuous system consideration

3.2.4 Utility generators

The utility generator systems (GENs) consist of two real generators, which are driven by a motor with a frequency converter to allow to emulate wind or water generation units. One GEN is a synchronous generator with a power rating of 30 kVA and one pole pair. The second GEN is an asynchronous squirrel cage machine with a power rating of 30 kVA and one pole. The one pole allows to emulate realistic shaft velocities of 3000 rpm which are typically used for micro wind plants or micro water power plants. The functional schematic of the GENs is illustrated in Fig. 3.15. The rotational velocity and torque measurement, including the frequency converter and the asynchronous machine are used as a controlled actuator to apply the appropriate torque, depending on the model behavior and the shaft velocity. The generators' currents and voltages are measured. A CB allows to separate or connect the generator to the experimental grid. An additional grid side voltage measurement allows to synchronize the generator and the grid for a smooth switch. For the synchronous generator, the excitation voltage is generated through a rectifier,

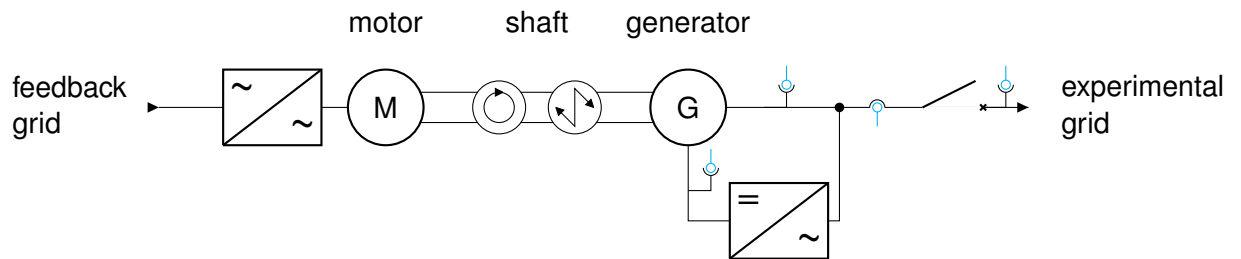


Figure 3.14: Functional schematic of the utility generators: Feedback grid supplies a motor through a converter, the motor drives the generator through the coupled shaft with rotational velocity and torque measurements. The generator's excitation is controlled through a rectifier (only for synchronous generator), voltages and currents are measured, the connection to the experimental grid can be switched through a CB including the required grid voltage measurement.

which is supplied from the generator. A black-start can be applied through the residual magnetism of the rotor.

3.2.5 Domestic electricity system requirements

The domestic electricity system consists of different real generation, storage and consumption facilities, especially PV, batteries and BEV charging stations. These can be flexibly allocated to different houses, such that not each house requires each one facility. The similarity of PV and batteries is that both require inverters, which allows to apply one joint allocation mechanism as illustrated in Fig. 3.15. The inverters' AC side can flexibly be connected through plugs to the five houses, which provide each one four sockets. The current rating of these connections is each one 32 A which is typically not utilized. The inverters' DC side can similarly be connected to the available batteries and PV strings with a similar current rating. The laboratory location allows to apply four PV strings, which are mounted on a walkable platform with a flexible elevation mounting. The azimuth is fixed to southern direction². The peak power rating is 4.6 kW for each PV string. The two applied battery systems have a capacity of 13 kWh and a power rating of 6 kW with a lithium-nickel-manganese-cobalt-oxide (NMC) technology. All these facilities have different appropriate state of the art inverters. Furthermore two flexible inverters are applied.

The flexible inverters are controlled through an FPGA in the RT system by switching the IGBTs. The inverters' circuit topologies have to allow unsymmetrical currents for allowing to implement strategies to balance unsymmetric grid loads. For this task, there are two fundamental topologies, the split DC intermediate circuit and the four legged topology, as illustrated in Fig. 3.16. There are multiple multi layer topologies which require more complex control strategies, which have to be retrofitted on demand. The inverters work with a typical nominal DC voltage of 750 V. Lower or higher battery and PV voltages have to be realized with a DC-DC converter. The inverter's power rating is dimensioned as 6 kVA for efficiently meeting the requirements of the PV and having an overhead for unbalanced feed-in or reactive power control. Beneath the inverter circuit, appropriate

²located in Garching, close to Munich, southern Germany

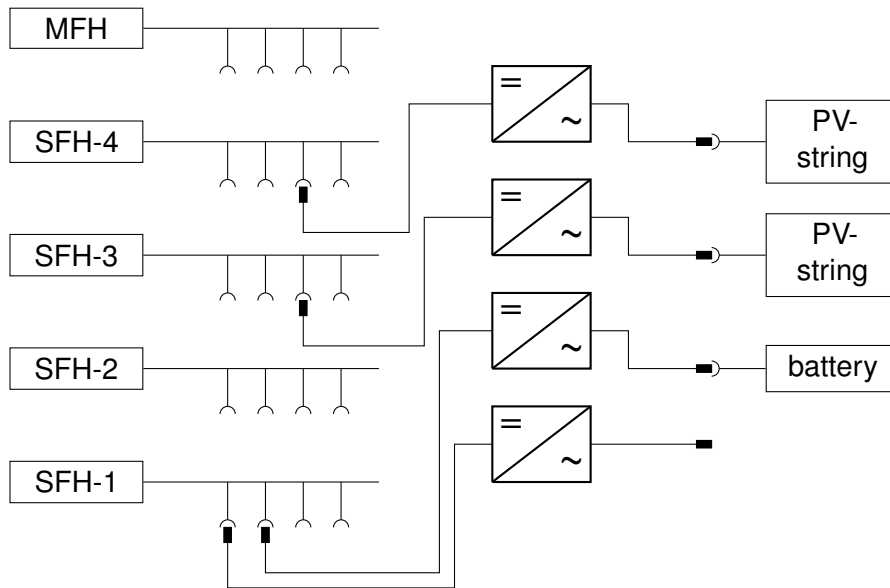


Figure 3.15: Functional schematic of the flexible configuration mechanism (not complete number of devices are illustrated) to allocate different facilities like PV strings or batteries through different types of inverters to different houses; illustrated example: one inverter is configured to SFH-4, one to SFH-3 and two to SFH-1; two PV strings and one battery are connected to each one inverter such that one PV string is allocated to SFH-4, one to SFH-3 and the battery to SFH-1

grid filters and safety equipment are available. The inverters are located in a separate electromagnetic compatibility housing, to avoid disturbances through the high frequent switching of the transistors.

The location's capabilities allow four BEV charging stations, dimensioned with 32 A, which is the highest available AC charging standard. Two BEV charging stations are constructed for semi public spaces and two BEV charging stations of different manufacturers are constructed for domestic applications and are compatible to the ISO 15118 vehicle-to-chargepoint-communication standard. The major requirement for the charging stations is that the charging power can be online limited through the RT system. All charging stations can be flexibly allocated to the five houses and the feedback grid through a plug-socket patch panel system, equivalent to that one used to allocate the inverters which is illustrated in Fig. 3.15 on the left side.

The BEV charging station socket connections, the inverter socket connections, the electric connections to the heat systems and spare sockets and clamps are connected through a power distributor. The heat system connection can be switched to the feedback grid to be able to decouple heat and electric experiments.

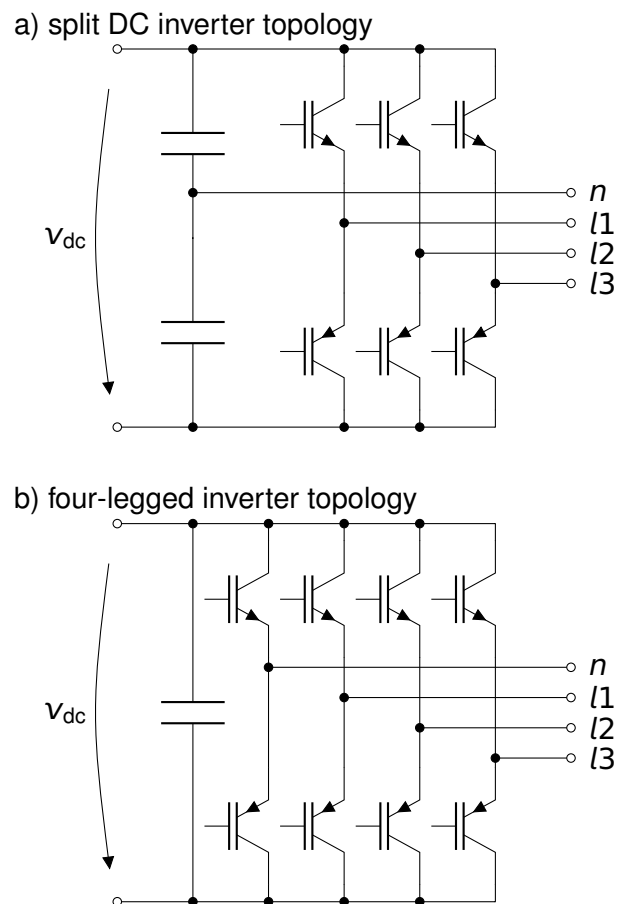


Figure 3.16: Functional circuit diagram of flexible inverters: topology a) with a split DC circuit and topology b) with a fourth leg

Summary:

The domestic electricity system consists of

- four 5 kW PV strings
- two 6 kW and 13 kWh battery systems
- two 6 kVA controllable flexible inverters
- two BEV charging stations for semi-public spaces
- two BEV charging stations for domestic applications compatible to the ISO 15118 standard

3.2.6 Domestic heat systems

The components of the domestic heat systems have been developed in cooperation with Dr. Peter Tzscheuschler and Daniel Zinsmeister. The fundamental idea is to provide

different heat generation technologies at each house to allow to configure different scenarios. All heat technologies are constructed in individual modules, such that individual generation technologies can be connected to other buildings with acceptable effort, if the provided flexibility is not sufficient. A major focus is put on providing sufficient technologies which couple power and heat, as CHP, heat pumps and heat coils. All available facilities are listed in Tab. 3.3.

The SFH-1's heat system is based on a micro CHP unit. It is dimensioned such that it is able to supply the hot water demand in summer, which is 41 kWh/d . Calculating 8 h full load results in 5.1 kW heating power requirement of the CHP unit. The heating demand in winter of 12 kW requires an additional gas boiler. The HIL heat generation system is mainly meant to emulate a solar thermal plant, with a peak power of 9 kW, which can take over the hot water generation during sunny summer days. This allows for two fundamental heating configurations for the SFH-1:

1. A CHP unit generates mainly the hot water and parts of the heating demand during the year, and a heating boiler assists when it is not sufficient.
2. A solar thermal plant generates mainly the hot water during summer, while heating demand is taken over by a heating boiler.

A separate solar hot water storage, which can buffer hot water during the night utilizes the solar thermal plant. The daily hot water demand $5 \times 3.5 \times 40 \text{ l/d} = 700 \text{ l/d}$ motivates to dimension the hot water storage at 500 l to be sufficient over the night. A 850 l heating buffer tank is sufficient to decouple heating generation and demand during some days. The gas engine CHP unit with a flexible modulation between $3.8 - 5.2 \text{ kW}_{\text{th}}$ and $1.1 - 2.0 \text{ kW}_{\text{th}}$ ensures hot water supply during summer, but can also be realistically used for smaller buildings. The heating boiler with 20 kW power can provide the entire heating.

The SFH-2's heat system is based on an air heat pump, which is dimensioned to supply the hot water demand during the day by 8 kW thermal power rating during cold weather, which means slight more during warm weather. It assists hot water generation by a 6 kW heating coil. The possibility of a 9 kW flexible solar thermal HIL emulator extends the system. For the heating demand during winter, there is a heating boiler with 20 kW power rating. A stratified tank with 500 l stores heat for hot water during the day and buffers heating and hot water during the winter for some hours.

The SFH-3's heat system is based on a brine heat pump with a power rating of 10 kW to meet the hot water and parts of winter's heating demand. A 9 kW HIL heat generator can emulate a solar thermal plant mainly for summer's hot water generation. A standard 850 l buffer tank with an external fresh water station for hot water heating allows to investigate systems with simpler storages.

The SFH-4's heat system's heat generation is similar to that one of SFH-1, but with a different CHP technology. The Stirling CHP unit has a 6 kW_{th} thermal and 1 kW_{el} electrical power rating. The CHP unit additionally integrates a spare boiler with 26 kW power rating. A further variation is provided by applying a 1000 l combination storage tank for heating and hot water.

Table 3.3: Overview over the heat system facilities and their location

location	component	electric power rating	heat power rating/capacity
SFH-1	gas engine CHP	2 kW	5.2 kW
	gas boiler		20 kW
	HIL generation		9 kW
	heat storage		0.8 m ³
	solar hot water tank		0.5 m ³
SFH-2	air heat pump	3 kW	10 kW
	gas boiler		20 kW
	HIL generation		9 kW
	heat storage		0.8 m ³
SFH-3	brine heat pump	3 kW	10 kW
	HIL generation		9 kW
	heat storage		0.9 m ³
SFH-4	Stirling CHP incl. boiler	1 kW	32 kW
	heat and hot water storage		0.9 m ³
MFH	gas engine CHP	5 kW	11.9 kW
	gas engine CHP	18.3 kW	34 kW
	gas boiler		50 kW
	heat storage		2 m ³

The MFH's heat system is based on two different CHP units. One is dimensioned such that it is able to drive high full load hours for only the MFH, the other one is dimensioned such that it additionally assists the grid as a central generation unit. The hot water demand of the MFH is 244 kWh/d which, assuming 20 h full load, requires a generation power of 12.2 kW which motivates the smaller CHP unit with a modulated power rating of 9.2 – 12 kW_{th} and 2.9 – 5.0 kW_{el}. The larger CHP unit is dimensioned based on 12 h full load for the entire grid with a hot water heat demand of $4 \times 41 \text{ kWh/d} + 244 \text{ kWh/d} = 408 \text{ kWh/d}$ which leads to a required power rating of 34 kW. The CHP unit with a power rating of 34 kW_{th} and 18.3 kW_{el} allows to compensate for grid and storage losses. The large 2 m³ sophisticated stratified heat tank with an external fresh water station, allows to balance heat demand fluctuations of the grid and the MFH itself. The heating demand of 63 kW is met by assistance of a 50 kW boiler.

Realization

The pipe system modules of the **CHP units and the heating boilers** are similar. The only technical difference is the additional electricity output of the CHP unit. The functional schematic of the pipe system is illustrated in Fig. 3.17. The fundamental idea of these modules is, that a pump pumps cooler water from the return through the CHP or the heating boiler to the flow, to get heated. The flow rate and the temperatures before and after heating up are measured, to be able to determine the gained heat energy. The fuel for the heating process is natural gas which is burned. Its consumption is measured, as well as the gas temperature and the exhaust temperature to be able to determine exactly the energy in and outflow.

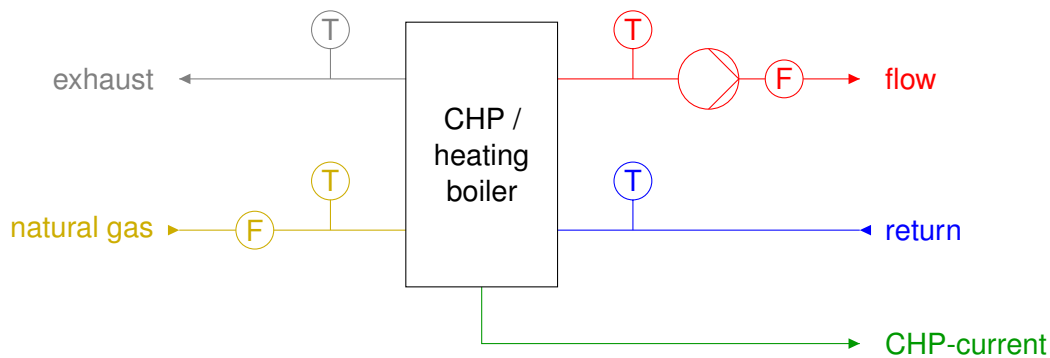


Figure 3.17: Functional schematic of the CHP and the boiler (without electricity generation) connection.

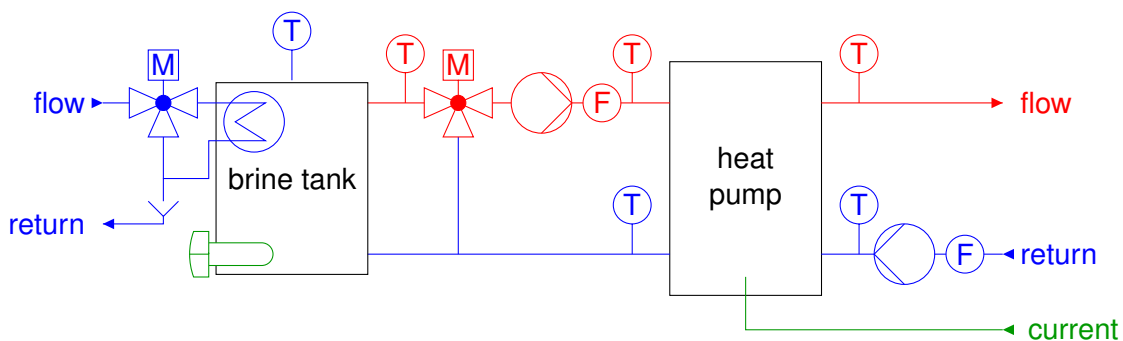


Figure 3.18: Functional schematic of the heat pump connection.

The **brine heat pump** module is based on a brine heat pump with an emulated brine source out of a tank through a conventional HIL approach. Its circuits are illustrated in Fig. 3.18. The heat pump consumes electricity to heat the water from the return to the flow through the heat pump cycle. That water has to be pumped, its flow rate and flow and return temperatures are measured to compute the thermal energy output of the heat pump. The heat pumps' main energy source is the brine circuit, whose power is measured through one flow meter and two temperature meters. The brine comes out of a tank, its outflow temperature is measured and actively controlled mixed with the brine return, for cooling to the desired temperature. The desired temperature is calculated through a HIL model. The brine tank's temperature is heated from low temperatures by a medium warm cooling water source through a three way valve to control the flow through the tank, and to bypass the remaining flow. An electric heater in the brine tank is a backup heater, if the cooling water is not sufficient due to its limited temperature.

The **air heat pump** is based on a hygroscopic air conditioner to emulate the desired air conditions for the heat pump. It utilizes ambient laboratory air and indirectly the laboratory heat losses as the main energy source, and an electric air heater, as well as a steam humidifier to emulate artificial air conditions for the heat pump. The functional schematic is illustrated in Fig. 3.19. A fan compensates the windage through the hygroscopic air conditioner, three ventilation flaps allow a continuous mixing of ambient air and cold and dry air, outflowing of the heat pump. The electric heater allows to emulate temperatures

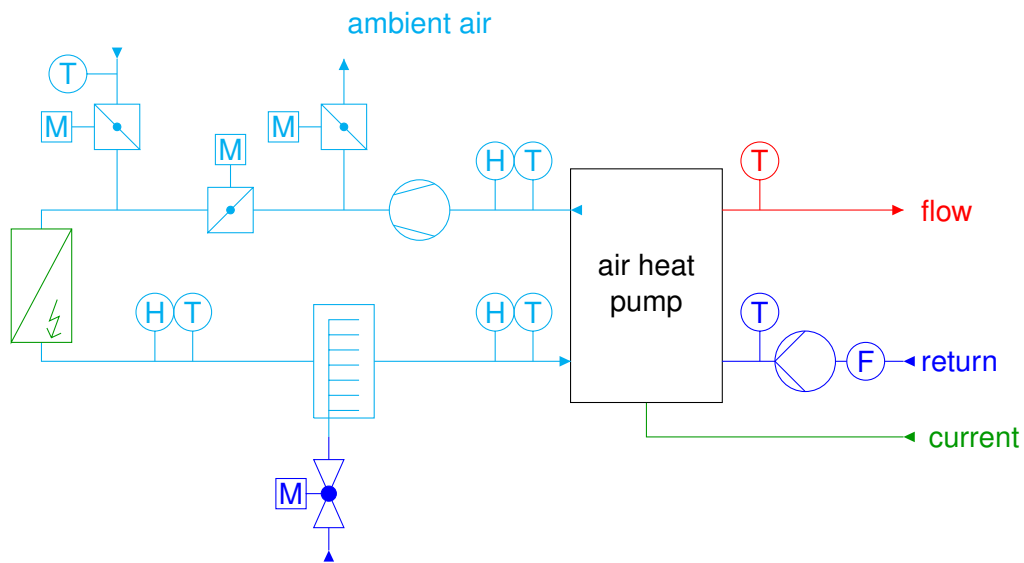


Figure 3.19: Functional schematic of the air heat pump

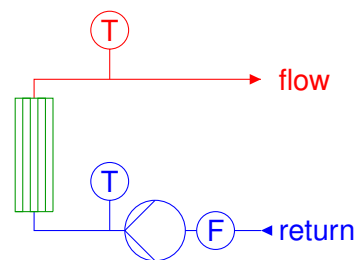


Figure 3.20: Functional schematic of the HIL heat source

higher than the laboratory itself, especially by considering the laboratory air humidity. The steam humidifier allows to humidify the air even at negative temperatures in a controlled manner. Humidity and temperature sensors directly at the inflow allow to exactly control the emulated air conditions. Sensors at the outflow allow to specifically investigate the behavior of the heat pump. The laboratory air temperature sensor allows to control the admixed air, such that the desired air temperature and air humidity are not exceeded. The third humidity sensor decouples the impact of the ambient air and the steam humidifier. The required control strategy is based on a non-linear multi-in-multi-out control approach.

The **HIL heat source** is based on an electric heater, whose power can be controlled. The module's pipe circuit is illustrated in Fig. 3.20. A pump ensures the waterflow, the hydro-thermal state is measured by one flow meter and two temperature sensors. The HIL heat source can also be used as a HIL emulation of cooling demand.

The five **storage** modules of the houses are similar, with main differences in the provision of hot water. The circuit of the five modules are jointly illustrated in Fig. 3.21. The SFH-1 has a hot water tank, which is heated through a heat exchanger within, which is fed through a pump from the heat storage. The hydro-thermal state is measured. The SFH-2, SFH-3 and MFH replace that tank by a pure heat exchanger, which is a traditional fresh water station circuit. The SFH-4 heats its hot water directly through a heat exchanger

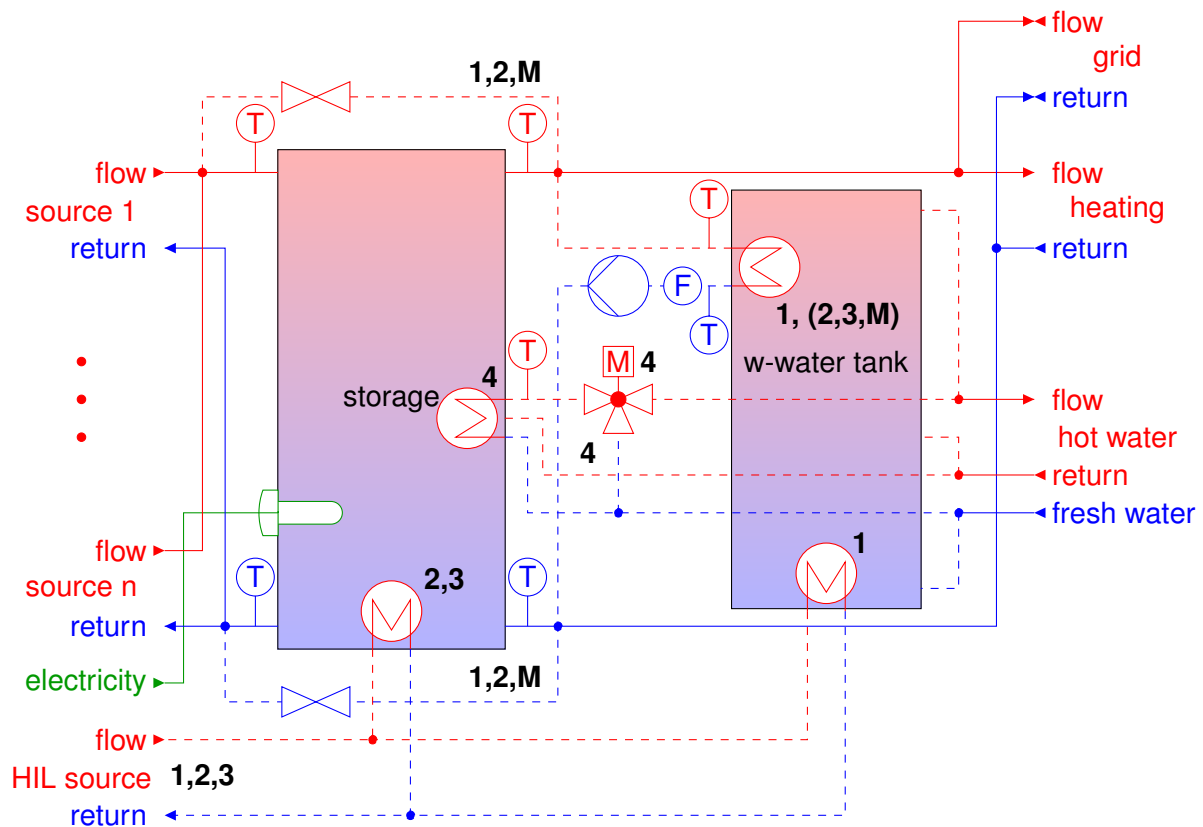


Figure 3.21: Functional schematic of the storages; Dashed parts only exist in some houses, labeled with black numbers (1-4, M); SFH-1 has the illustrated hot water tank, SFH-2, SFH-3 and MFH have a heat exchanger (so fresh water station) instead of the tank, SFH-4 heats hot water in its storage; SFH-1, SFH-2 and MFH have a direct coupling between sources (left side) and consumption/grid (right side); the HIL source (mainly solar thermal) is in SHF-1, SFH-2 and SFH-3; all other sources are in parallel on the left side.

in the heat storage, with the possibility to control the outflow temperature through a three way valve by admixing cold water. Heating, hot water and the grid transfer station are connected to one joint circuit but heating water can alternatively be connected directly to the storage at a lower height for utilizing stratification effects. The HIL sources are directly connected through a heat exchanger to the hot water tank or the storage. All other heat sources are connected in parallel through one circuit to the storage. Storage in- and outflow temperatures are measured, as well as the stratification through multiple outlying temperature sensors. The SFH-1, SFH-2 and MFH have the option to directly link the source and the consumption circuit.

The pipe circuit of the **HIL load emulator** cools the heating circuit, pipes away consumed hot water and implements the hot water circulation losses. Its functional schematic is illustrated in Fig. 3.22. A pump drives the heating circuit, whose flow temperature is controlled through a three way valve with return admixture. The hydro-thermal state on both sides of that valve are measured with each two temperature and one flow sensor. The heating flow is split up to two different cooling heat exchangers by a controlled three

way valve, to allow to control high and low heating losses accurately. These two plate heat exchangers for cooling the heating circuit are fed by cooling water. The cooling flow rate is controlled by a control valve, and split up to the two heat exchangers through a three way valve. The return of the cooling is open, which means pressureless. There is a flow and a return temperature sensor for control purposes.

The hot water circulation losses are implemented by a further plate heat exchanger. The hydro-thermal state is measured through those three sensors. The circulation is driven by a pump. Consumed hot water is piped away by opening a combination of three solenoid valves, which are manually configured through each one needle valve with different flow rates. Fresh water is required for refilling the consumed hot water in the hot water generation module. It is directly taken out of the cooling circuit. A cooling circuit feeds the cooling of the circulation. A control valve and two temperature sensors allow the control of the cooling flow through the heat exchanger, which means to control the cooling.

The **grid transfer station** connects a high temperature (HT) and a low temperature (LT) circuit bidirectionally to a three pipe grid. The system schematic is illustrated in Fig. 3.23. Two plate heat exchangers realize the system separation between the grid and the house circuits. The house side of both exchangers are equal. Directly at the heat exchanger there is a hydrothermal state measurement with three sensors. The high temperature side is directly connected. The low temperature side is connected through two pumps in parallel for both circulation directions. A three way valve controls through which pump the water flows. This allows to feed energy into the grid by pumping water from the high temperature to the low temperature and to receive energy from the grid by pumping water in the opposite direction.

The grid side is based on a grid with three temperature levels. The high and the medium temperature pipes are connected to the high temperature heat exchanger, the medium and the low temperature pipes are connected to the low temperature heat exchanger, which is especially meant for cooling. The grid sides of both exchangers have a hydro-thermal state measurement with three sensors each. The higher temperature side of both exchangers are directly connected to the appropriate pipes. The lower temperature sides are connected through a valve for regulating the consumption flow from the higher to the lower temperature pipe, or a pump for realizing the feed-in flow in the opposite direction. This means for the entire grid, if no feed-in pump is operated, that no consumption is possible, independent whether the valve is open or closed. For the feed-in, the valve has to be closed to prevent to short circuit the pump. Simpler, more realistic and especially conventional transfer stations can be emulated by operating only parts of the available transfer station.

The HIL circuit of the **district heating grid pipe emulator** controls the physical properties of the pipes, especially its temperature and pressure losses and the virtual volume of the pipe. The functional schematic of one pipe emulator is illustrated in Fig. 3.24. As the pipe can be operated in both flow directions, four check valves enable an unidirectional flow through the active part of the pipe circuit, which is physically modified to emulate the virtual pipe's properties. The pressure losses of the pipe are realized through a control valve. The continuing hot water outflow of a virtually longer pipe, after a cold inflow gradient is realized through a controlled high power electric heater. A four way valve allows to

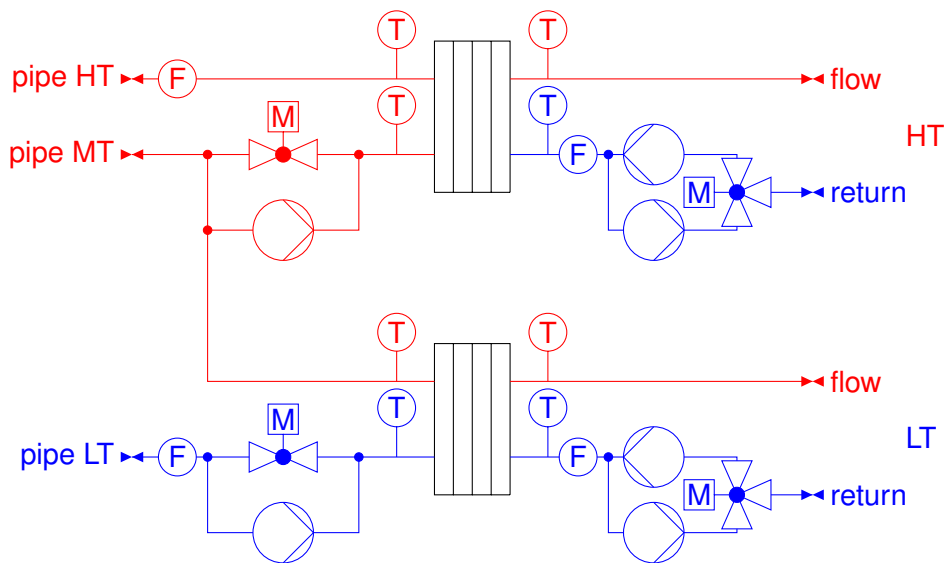


Figure 3.23: Functional schematic of the grid transfer station

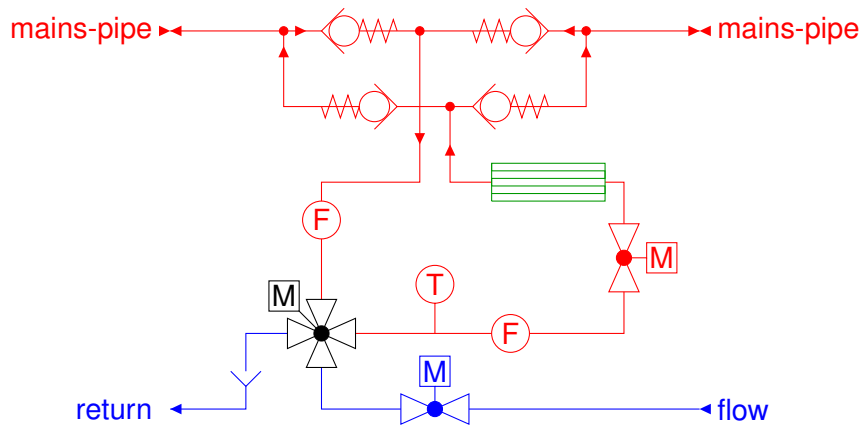


Figure 3.24: Functional schematic of the grid's pipe emulator

Summary:

The domestic heat systems consists of

- CHP and boiler modules according to Fig. 3.17
- brine heat pump module according to Fig. 3.18
- air heat pump module according to Fig. 3.19
- HIL heat source modules according to Fig. 3.20
- heat storage modules according to Fig. 3.21
- emulated heat load modules according to Fig. 3.22
- grid transfer station modules according to Fig. 3.23
- grid's pipe emulator modules according to Fig. 3.24

3.2.7 Measurement and real time control system

The measurement and RT control system is the fundamental computational instance of the laboratory. It consists of 12 different computational units, for the electricity and the heat system of each house and each one general grid operator controller. The flexible inverters are controlled by separate FPGAs.

The controllers interact with the laboratory system through different analog-digital-input-output (ADIO) and serial or parallel digital communication interfaces. The strategy to implement the required digital communication interfaces is to have Ethernet ports which can be transformed through individual converters to the required communication technology. This allows to avoid installing numerous different communication ports in spare. For the analog interfaces, a 16 Bit digital resolution is specified, which is about 65,000 samples. An assumed worst case utilization of 30% and considering positive and negative values results in about 10,000 actively used samples which leads to a relative quantization error of 0.01%, which leads to a relative quantization error proportion of $\frac{0.01\%}{1\%} = 1\%$ at an overall measurement and control accuracy of 1%. The quantization error has not to be considered, as it is not significant at a significance level of 5%. Furthermore, an appropriate fibre-optical communication technology is required to control the PHIL load emulator.

The electricity controllers run at a fundamental frequency of 1 kHz which fulfills the provision layer's requirements, which are explained in Sec. 2.2.1. The current and voltage measurements require a sampling of 10 kHz, which allows to analyze the 50th harmonic with a nominal frequency of 2.5 kHz by considering an oversampling factor of 2 to the required Nyquist-frequency according to the Nyquist-Shannon sampling theorem. The FPGAs to control the power electronic inverters are based on an up to 1 MHz sampling to allow to implement high switching model predictive control strategies. Traditional pulse width modulation control strategies should be calculated up to 300 kHz which is a fast switching rate for today available power electronic devices. The heat system is much slower, with a specified base sampling rate of 100 Hz, which represents no technical limitation. A major property of the distributed controllers is that measurements are recorded time synchronous. Otherwise, the time base of individual measurements could deviate, which would make an accurate comparison of different measurements impossible. The synchronization accuracy of the controllers of the electronic system is specified as 1 μ s, by allowing a resolution of 1° of the 50th harmonic, with a base frequency margin of 10%. A synchronization of 1 ms for the heat system is a sufficient and not limiting standard.

At least 4 ethernet ports are required for each house, one for the experimental wide area network, one for domestic facilities and devices, one for the domestic local area network and one spare for future applications. Each RT computer requires in addition one connection to the laboratory LAN for the host computer communication and measurement data transfer to a central data storage. Its performance is specified up to 1.3 times of all ADIO samples to be transmittable. It is sufficient, because the 10 kHz current samples need not to be stored and hence transmitted all the time. Typically an online analysis and down-sampling is implemented.

The operation of the laboratory without considering the experimental WAN requires a RT bypass. Its specification is that each ADIO data needs to be uploaded and downloaded

such that maximum one sample delay occurs. Assuming 50% of the time to be required for sampling and processing, means that 0.5 sample times remain for communication. This means that all ADIO samples need to be communicated within $500\ \mu\text{s}$ for the electricity system and within 5 ms for the heat system. The ADIO data of the FPGA is counted within the electricity system, but appropriately downsampled.

Summary:

Measurement and RT control involves

- 12 computational units and two FPGAs
- four ethernet ports as digital communication interfaces for each house
- 16 Bit overall digital resolution
- 1% overall measurement and control accuracy
- electricity controllers run at 1 kHz sampling
- current and voltage measurements require 10 kHz sampling
- FPGAs require an up-to 1 MHz sampling
- heat system base sampling is 100 Hz
- synchronization accuracy of $1\ \mu\text{s}$ and for the heat system 1 ms
- host computer communication and measurement data transfer network
- RT bypass to up- and download each ADIO data within $500\ \mu\text{s}$ and 5 ms for the heat system

Chapter 4

Laboratory HIL Models

The key challenges of the MG laboratory are that no energy consuming residents can live in it and that highly weather-dependent technologies will be investigated, while local weather conditions in general do not coincide with research requirements. This chapter describes two fundamental HIL models to emulate the human influenced consumption behavior and the required weather conditions. The consumption behavior is calculated through this model in the RT system and realized by the aforementioned electric load emulator. It is the key component of the experimental laboratory, as it provides the ability to apply conventional electricity consumption. The weather emulation allows to investigate multiple different weather conditions, which also means to allow to investigate scenarios of regions with different climatic conditions, extreme weather conditions or seasonal aspects, like investigating winter scenarios in local summer.

4.1 Electricity consumption model of conventional households

The electric energy consumption of conventional households consists of multiple electric devices which consume electric energy by converting it into a tertiary energy carrier to perform the intended action. This means an interaction between the electricity grid providing the voltage $v(t)$ and the consumption devices which consume a current $i(t)$ as illustrated in Fig. 4.1. In real households, the behavior of the consumption devices highly depend on the human behavior. As no humans can live in the laboratory, the electricity consumption is replaced by a PHIL load emulator, which realizes the desired current $i_d(t)$, which is calculated in the electricity consumption model described in this section. The resulting laboratory interaction between the grid, the PHIL facility and the model is also illustrated in Fig. 4.1.

This section focuses on the uncontrolled conventional electric consumption, which finally is the current $i(t)$ of all consumer devices, which depend on the measured grid voltage $\hat{v}(t)$. The model which is described in this section calculates the desired current $i_d(t)$, depending on the measured grid voltage $\hat{v}(t)$. In the laboratory, the calculated current $i_d(t)$ is commanded to the electric load emulator, which is described in Sec. 3.2.3, to realize the current $i(t) \stackrel{!}{=} i_d(t)$.

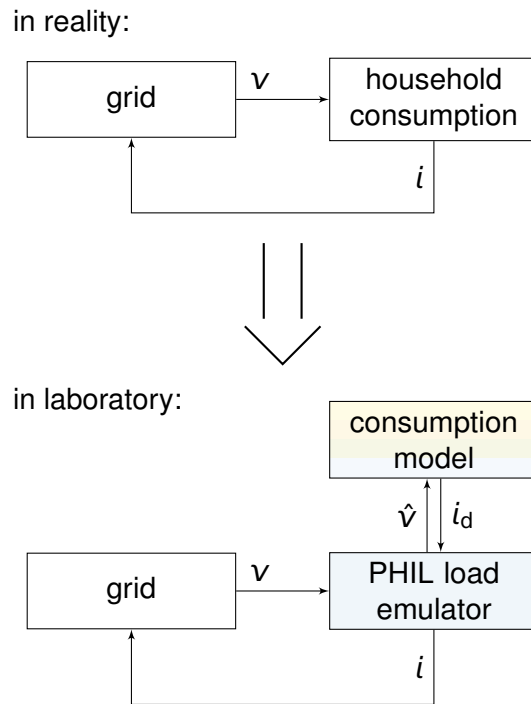


Figure 4.1: Electricity consumption in the MG laboratory as PHIL approach, to realistically emulate household consumption; the five ESMIF layers are indicated in the consumption model block (supply layer to system layer) and the PHIL load emulator block (technological layer)

The purpose of this model is to describe the processes on a regional level. This means to focus on the realistic behavior on a house level, but not to emulate the behavior of each individual appliance separately. The goal of this section is to describe the mathematical model, based on the ESMIF framework as the fundamental operational basis of the laboratory. This section is fundamentally based on the previous work [24].

4.1.1 Introduction to load modeling

Electricity load modeling is a frequently discussed, important research topic in the context of electric energy system research [77]. The conventional electricity load is an aggregation of individual devices of daily domestic or commercial use like stoves, lights and other electrical appliances, which are not actively controlled to behave in accordance with the electricity grid. Traditional load models consider the physical interdependency of grid voltage and load currents [77].

The specific characteristics of already existing load models is that accurate models do not exist, in contrast to generation and transmission systems. This is caused by the various different available technologies and the dependency on human behavior. Existing load models simplify the behavior through being based on standard load profiles, lumped parameters or abstractions devoid of dynamics [78]. Realistic investigations in the laboratory without real consumers require a robust and detailed dynamical load model. This includes the interdependency of voltages and currents devoid of RMS simplifications.

4.1. ELECTRICITY CONSUMPTION MODEL OF CONVENTIONAL HOUSEHOLDS 77

Arif et. al. distinguish in their load model review [11] the static and dynamic load models and their composite. These traditional modeling methods include the interaction of active and reactive power consumption with the RMS grid voltage. Exemplary dynamic models, like induction motor or exponential recovery load models only include specific properties of the entire dynamic interactions, especially the dynamic interaction of active and reactive power consumption based on the RMS grid voltage. Exemplary static modeling strategies, like ZIP, exponential or frequency load models neglect dynamic behavioral patterns, which mainly affect closed loop investigations. The composition of individual dynamic and static load models combine the properties of both, which does not cover all fundamental behavioral patterns of conventional loads. Literature also describes transient load models, like [69][5] which describe transient grid voltage and load current interactions. The limitation of existing models is the missing consideration of human triggered time variant model features, frequency dependency or the fast dynamical processes in the context of higher harmonics. Especially the combination of all behavioral patterns in one combined model has not been found in literature. An alternative to load models is to apply measured and recorded data with the disadvantages of its underlying inflexibilities and the missing ability to interact with the grid. The previous work [24] being described in the following subsections incorporates the fundamental dynamics of electricity loads.

Fundamental dynamics is a concept which has been previously developed by this author et.al. in the context of robotics to handle unknown objects with partly unknown internal dynamics [28]. This concept simplifies highly complicated dynamical behaviors as far as possible to gain a simple mathematical description of all behavioral patterns, which have a dominant impact on the overall behavior. The swing equation in the context of dynamic electricity system description could be interpreted as a part of the fundamental dynamics of electricity systems.

4.1.2 System layer model

The fundamental content of the system layer is to consider the instantaneous interaction of currents $i(t)$ and voltages $v(t)$. The overlying layer provides RMS current references $I_d(t)$ and the measured RMS voltage $\hat{V}(t)$, as well as their phase angle $\varphi_d(t)$. The goal of the system layer's model proportion is to incorporate these behavioral patterns, which affect instantaneous magnitudes, but not RMS magnitudes under its fundamental assumption of sinusoidal voltages. Behavioral patterns, which affect the RMS magnitudes are incorporated by using them as references from the overlying layer, which could be imagined as illustrated in Fig. 4.2.

The conventional load refers to agglomerated numerous devices which consume electric energy. It is assumed that the energy consumption process of this conventional consumption model cannot be actively controlled. Typical examples of appliances which are included in this category are for instance refrigerators, cookers, vacuum cleaners, illumination, computers, chargers, televisions, pumps and more. Electric energy is predominantly used

- to drive mechanical forces and movements. Different kinds of motors use electric

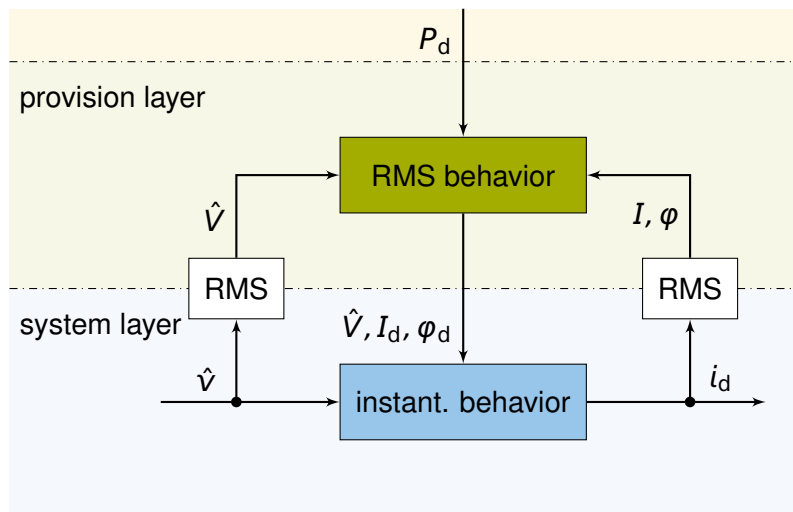


Figure 4.2: Functional schematics of the system layer's interaction of the load model

energy to exert forces to mass-containing objects, which often result in acceleration and finally in movement. The three most common electric motors are the induction motor, the direct current motor and the universal motor. Other types are for instance the synchronous motor, linear motors or reluctance machines. Induction motors are classically driven by three phase alternating current, but typically the single phase induction motor is more often used in household applications. Direct current motors are based on direct current, which needs to be artificially generated from the alternating current power system. Universal motors are typically used for household appliances, because of their high starting torque and their ability to simply specify rotational speed.

- to generate chemical energy. Chemical energy is generated through electric energy in rechargeable batteries and in electrolysis applications. As electric vehicle charging, and battery charging for grid applications are separately considered, chemical energy generation is only a rarely implemented process. But still generating chemical energy through electric energy is typically a direct current consuming process.
- to carry information. Electric energy as information carrier is an application of growing importance. The basis for these processes is typically direct current.
- to generate heat. A major effect of electricity is its tendency to emit heat through thermodynamic processes. The diverging electric energy is converted into thermal energy, which is used for different purposes. The main purpose is to use it for heat demanding applications. A further typical example is to heat up the thin wire of a light bulb to glow, which causes it to illuminate as an indirect effect through generating heat.
- to generate radiation. Most radiation applications, which comprise illumination, radio communication, microwave, ultraviolet, radar and röntgen applications are based on direct current supply. Exemplary applications are LED and neon lighting,

4.1. ELECTRICITY CONSUMPTION MODEL OF CONVENTIONAL HOUSEHOLDS 79

mobile communication, microwaves, disinfection, detection, ranging and diagnostic radiology applications. The most common illumination applications are typically driven by low voltage direct currents. Radiation with higher frequencies are typically supplied by high voltage direct currents, which are typically generated through transformers and HV rectifiers.

- to generate magnetic fields. Magnetic fields are used for manipulating and sensing moving charge carriers, nuclear magnetic resonance imaging and to apply forces on magnetic material, for instance for transport purposes. These applications play a subordinate role in the overall energy system, especially in households.
- to generate electric fields. Electric fields are used for manipulating and sensing charge carriers and for chemical and ionization applications. These applications play a subordinate role in the overall energy system, especially in households.
- to generate electric arcs. Electric arcs are typically used for illumination purposes and high temperature applications, including melting metal and welding. Electric arc applications are not such common and can be approximated by a resistive behavior with some limits. They are typically not used in household applications.
- to generate sounds and vibrations. Sounds and vibrations are typically supplied through direct current.

There are multiple technical solutions to generate direct current from alternating voltages. The most common solution is to use switched mode power supplies (SMPS), which dominate already the actual market due to their efficient operation and cost effective technology. That analysis of different household devices motivates to assume that conventional load mainly consists of resistive, SMPS and motor load components. This allows to model the subordinate differently characterized consumption devices by these three standard characteristics. The modeling idea is first to describe the behavior of one device of each component, then to extend the model to an agglomerated load component model, which emulates any number of similar devices. Other occurring load components are approximated as a combined resistive-SMPS-motor load. The approximation errors are assumed not to be influential, because of the rare occurrence of the underlying appliances. This results in the postulate 4.1, which means mathematically for the overall load model that the entire instantaneous load current

$$i_d(t) = i_{r,d}(t) + i_{s,d}(t) + i_{m,d}(t) \quad (4.1)$$

consists of the resistive $i_{r,d}(t)$, the SMPS $i_{s,d}(t)$ and the motor $i_{m,d}(t)$ current proportion.

Postulate 4.1 *Each aggregated electric load on a household level can be modeled as a combination of resistive, switched mode power supply and motor load characteristics.*

System layer: Resistive load model

A resistive load device mainly consists of a resistance, which is constant in the system layer's time scope, for at least short periods of time, independent of the possibly changing

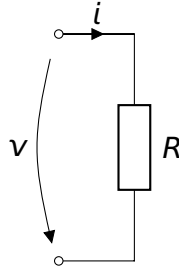
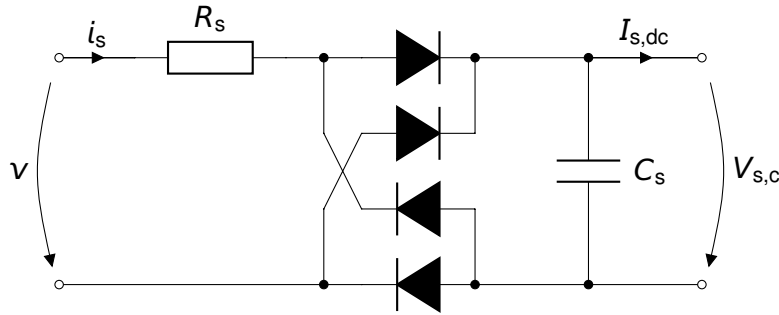


Figure 4.3: Circuit diagram of resistive load characteristics

Figure 4.4: Circuit diagram of the rectification circuit of a switched-mode power supply, with grid voltage v and current i_s

applied voltage. The resistive load device is modeled by the circuit diagram in Fig. 4.3 which leads to the instantaneous current equation

$$i_{r,d}(t) = \frac{\hat{v}(t)}{R_r} \quad (4.2)$$

with the resistance R_r . This equation is a linear relation between the instantaneous voltage $\hat{v}(t)$ and current $i_{r,d}(t)$, which allows to consider multiple different resistive load devices as the resistive load component by (4.2) with linearly adapting the resistance parameter R_r . The resistance parameter $R_r(\hat{V}, I_{r,d})$ implements the upper layer's behavior by being adapted through its root mean square voltage $\hat{V}(t)$ and desired current $I_{r,d}(t)$. The conventional resistance equation leads to

$$R_r(\hat{V}, I_{r,d}) = \frac{\hat{V}(t)}{I_{r,d}(t)}, \quad (4.3)$$

which ensures the same instantaneous behavior under sinusoidal conditions as specified through the RMS magnitudes of the provision layer.

System layer: SMPS load model

There is a trend towards devices which are supplied by low DC voltages. These DC voltages are predominantly generated by SMPS, which draw their power from the AC grid. The typical grid connected part of the SMPS circuit diagram is illustrated in Fig. 4.4. The circuit after the DC rectification capacitor C_s is not illustrated.

4.1. ELECTRICITY CONSUMPTION MODEL OF CONVENTIONAL HOUSEHOLDS 81

Assuming a lossless process to generate the constant DC voltage out of the available DC rectification voltage $V_{s,c}$ means a constant power consumption through the DC current $I_{s,dc} \cdot V_{s,c} = \text{const}$ from the energy consuming device. Considering the nominal efficiency η_s of the rectification circuit of Fig. 4.4 leads through the nominal power consumption $P_{s,d}$ to that constant power consumption

$$I_{s,dc} \cdot V_{s,c} = \eta_s \cdot P_{s,d} \Rightarrow I_{s,dc} = \frac{\eta_s \cdot P_{s,d}}{V_{s,c}}. \quad (4.4)$$

The nominal power consumption $P_{s,d}$ is the reference magnitude of the distribution layer.

The rectification circuit of the SMPS could be modeled with the Shockley equation to model the diodes, which results in

$$i_s = I_{\text{sat}} \left(e^{\frac{\hat{v} - R_s i_s - V_{s,c}}{2n_s V_{s,T}}} - 1 \right) - I_{\text{sat}} \left(e^{\frac{-\hat{v} + R_s i_s - V_{s,c}}{2n_s V_{s,T}}} - 1 \right)$$

with the reverse bias saturation current I_{sat} , the thermal voltage $V_{s,T}$ and the ideality factor n_s , being model parameters. It is a non-linear implicit equation referring to the current. This equation cannot easily be solved analytically for the instantaneous grid current $i_{s,d}(t)$. Numerical solutions are not practicable due to their time consuming iterations. This leads to requiring a further approximation. Simplifying the diodes' non-linearities to an ideal behavior results in

$$i_{s,d}(t) = \begin{cases} \frac{\hat{v}(t) - V_{s,c}}{R_s} & \forall \hat{v}(t) > V_{s,c} \\ \frac{\hat{v}(t) + V_{s,c}}{R_s} & \forall \hat{v}(t) < -V_{s,c} \\ 0 & \forall \text{ other} \end{cases} \quad (4.5)$$

which is a simple non-differentiable equation. This simplification mainly appears on the sharp transition from $i_{s,d}(t) = 0$ to $i_{s,d}(t) \neq 0$, which would be marginally smoother by solving the more realistic Shockley equation. Considering the dynamic behavior of the capacity $\dot{V}_{s,c} = \frac{i_{s,c}}{C_s} = \frac{|i_{s,d}| - I_{s,dc}}{C_s}$, and the capacity current $i_{s,c}$ consisting of the rectified grid current $|i_{s,d}|$ and the DC current (4.4) leads to the capacity voltage

$$\dot{V}_{s,c} = \frac{|i_{s,d}| - \frac{P_{s,d}\eta_s}{V_{s,c}}}{C_s} \quad (4.6)$$

which is required in (4.5) to compute the instantaneous current $i_{s,d}(t)$.

Many parallel SMPS devices mean a linear relation between their overall current $i_{s,d}$ and their reference power $P_{s,d}$ from the distribution layer, indicating the number of active devices in the SMPS load component. The current equation (4.5) contains the inverse resistance $\frac{1}{R_s}$ as a linear factor. This allows the implementation of the SMPS reference power $P_{s,d}$ to calculate the resistance parameter

$$R_s = \frac{\rho_s}{P_{s,d}} \quad (4.7)$$

with the constant relative resistance ρ_s . A hinger number of active devices also results in a higher joint capacity of all these devices. This means that the capacity C_s in (4.6) has

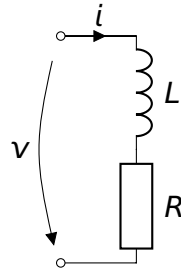


Figure 4.5: Circuit diagram of induction motor load characteristics

to be proportional to the SMPS power $P_{s,d}$, which represents the number of active devices $C_s \propto P_{s,d}$, which allows to define the time constant

$$T_s := \frac{P_{s,d}}{C} = \text{const} \quad (4.8)$$

as the constant proportionality constant. Behind these calculations is the joint assumption, that all SMPS devices have the same technical characteristics. Devices with different characteristics could not be scaled due to their non-linear behavior in (4.5) and (4.6). This model incorporates finally the characteristics of all SMPS devices as equal.

System layer: Motor load model

Single phase motor loads are predominantly characterized by the inductive effect of grid connected windings. A sudden change in grid voltage v would not cause an immediate reaction in the current i_m because the magnetic field in the winding would keep the current continuously flowing. Modeling this effect requires an inductance in serial connection to the grid. To allow to realistically emulate active and reactive power, at least a serial resistor is required. This leads to the circuit diagram illustrated in Fig. 4.5. More complex circuits, like considering non-linearities or circuits parallel to the resistor do not provide better results for individual motor types. Considering many differently behaving motor types motivates to use that simple model to incorporate these fundamental behavioral patterns. Electrical machines typically show negligible non-linear patterns like harmonics, which allows to focus on linear circuit elements.

Modeling the agglomeration of multiple different motor types, especially single phase induction motors and universal motors, requires to focus on the fundamental behavioral patterns. Further modeling details improve the accuracy for one type at cost for other types. The important focus of modeling the entire household by one compact model is the fundamental dynamics, which assume that other behavioral patterns have negligible impact on the overall behavior as they balance each other or can simply be compensated by controllers.

The required circuit to model motor loads for instantaneous voltages $\hat{v}(t)$ and currents $i_{m,d}(t)$ consists of the resistance R_m and inductance L_m in series. The circuit's behavior is formulated as a differential equation

$$\frac{d}{dt} i_{m,d} = \frac{1}{L_m} (\hat{v}(t) - R_m i_{m,d}(t)) \quad (4.9)$$

with the resistance R_m and inductance L_m to be adapted for different provision layer conditions. The provision layer provides the RMS voltage $\hat{V}(t)$ and current $I_{m,d}(t)$ and its phase angle $\varphi_{m,d}(t)$. The resistance and inductance parameters result through

$$R_m(\hat{V}, I_{m,d}, \varphi_{m,d}) = \frac{\hat{V}}{I_{m,d}} \cos \varphi_{m,d} \quad (4.10)$$

$$L_m(\hat{V}, I_{m,d}, \varphi_{m,d}) = \frac{\hat{V}}{I_{m,d} \omega_n} \sin \varphi_{m,d} \quad (4.11)$$

from the provision layer's magnitudes. The linearity of (4.9) allows the transition from one device to the agglomerated motor load component through the linear parameter adaption in (4.10) and (4.11).

Summary:

The instantaneous load model

- interacts with its environment as illustrated in Fig. 4.2
- consists of a linear combination (4.1) of a resistive $i_{r,d}$, an SMPS $i_{s,d}$ and a motor $i_{m,d}$ load component
- the resistive load component model is described through (4.2) and (4.3)
- the SMPS load component model is described through (4.5), (4.6), (4.7) and (4.8)
- the motor load component model is described through (4.9), (4.10) and (4.11)

4.1.3 Provision layer

The fundamental content of the provision layer is the dynamical interaction of RMS magnitudes. It provides the RMS voltage $V(t)$ and the RMS reference current $I_d(t)$ with its phase angle $\varphi_d(t)$ for the underlying supply layer.

The goal of the provision layer's model proportion is to incorporate these behavioral patterns, which affect RMS magnitudes, but not the power consumption under the fundamental assumption of nominal voltage amplitudes. This layer's fundamental assumption is that processes on the supply layer ensure sinusoidal voltages. The behavioral patterns which affect power are only directly considered in the distribution layer, but affect the RMS behavior through the reference power P_d . An overview about the interactions and dependencies of the provision layer is given in Fig. 4.6.

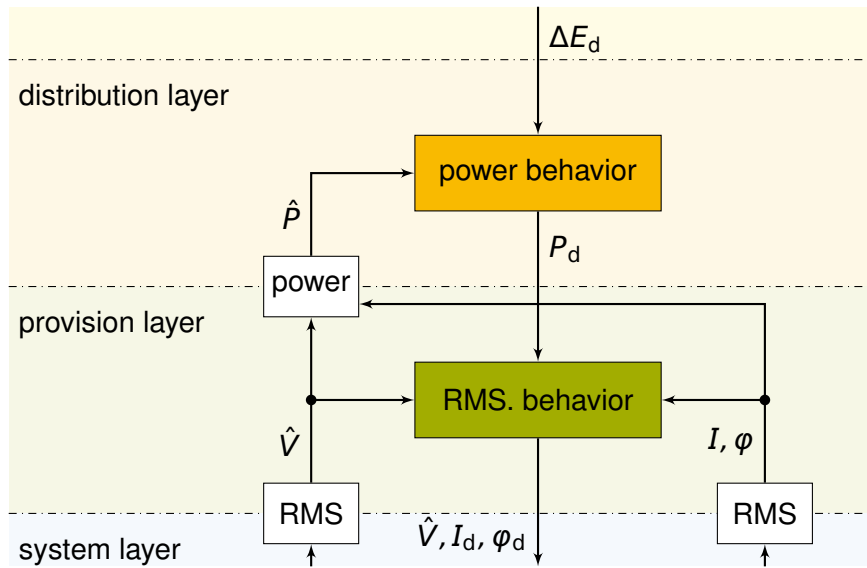


Figure 4.6: Functional schematics of the provision layer's interaction of the load model

Provision layer: Resistive load model

The instantaneous behavior of the resistances of (4.2) are directly transferred to RMS voltage $\hat{V}(t)$ and current $I_{r,d}(t)$

$$I_{r,d}(t) = \frac{\hat{V}(t)}{R_r}. \quad (4.12)$$

The distribution layer's reference power $P_{r,d}$ equals the actual power $\hat{P}_r = \hat{V}(t) \cdot I_r(t) = \frac{\hat{V}^2(t)}{R_r}$ under nominal conditions $\hat{P}_r|_{\hat{V}=V_n} = P_{r,d}$, which leads to the resistance parameter equation

$$R_r(t) = \frac{V_n^2}{P_{r,d}}, \quad (4.13)$$

which represents the agglomeration of multiple individual devices.

Provision layer: SMPS load

The fundamental characteristics of the SMPS load behavior is its voltage independent power consumption after the rectification. The RMS behavior is mainly characterized by the impact of the rectification capacity C_s , which buffers the energy from the grid to the appliance. The non-linear rectification circuit causes current harmonics, which do not carry active power through the provision layer's fundamental assumption of sinusoidal shaped voltages. The relation between RMS voltages $\hat{V}(t)$, currents $I_{s,d}(t)$, and the power $P_{s,d}(t)$ is characterized by the powerfactor pf through $P = UI \cdot pf$. Considering the system layer's behavior equation in (4.5) shows a relation between the current $i_{s,d}$ and the voltage difference $\hat{v}(t) - V_{s,C}$. Their equivalent magnitudes in the provision layer are the current $I_{s,d}$ and the voltage difference $\sqrt{2}\hat{V}(t) - V_{s,C}$. Considering a linearization of (4.5)

4.1. ELECTRICITY CONSUMPTION MODEL OF CONVENTIONAL HOUSEHOLDS 85

for RMS magnitudes and adapting the resistance parameter to compensate linearization errors leads to

$$I_{s,d} = \begin{cases} \frac{P_{s,d}}{\rho'_s pf} (\sqrt{2}\hat{V}(t) - V_{s,C}) & \forall \sqrt{2}\hat{V} \geq V_{s,C} \\ 0 & \forall \text{ other} \end{cases} \quad (4.14)$$

with $R'_s = \frac{\rho'_s}{P_{s,d}}$ and the power factor pf to account for the additional deformed power currents.

The remaining unspecified parameter is the capacitor voltage $V_{s,C}$. Considering the capacity's energy content

$$E_{s,C} = \frac{1}{2} C_s V_{s,C}^2$$

leads to the change of energy content by its differentiation

$$P_{s,C} = \frac{dE_{s,C}}{dt} = \frac{1}{2} V_{s,C}^2 \dot{C}_s + C_s V_{s,C} \dot{V}_{s,C}$$

which leads to the capacity voltage

$$\dot{V}_{s,C} = \frac{P_{s,C}}{C_s V_{s,C}} \quad (4.15)$$

by assuming constant capacities $\dot{C}_s = 0$. A changing reference power $P_{s,d}$ means a changing number of active appliances, which proportionally increases the overall capacity $C_s \propto P_{s,d}$. This justifies the approximation of $\dot{C}_s = 0$ as $P_{s,d}$ does not change in the temporal scope of the provision layer. The mentioned proportionality motivates to apply the SMPS time constant T_s as defined in (4.8) to calculate the capacity $C_s = \frac{P_{s,d}}{T_s}$. The capacity's power flow $P_{s,C}$ consists of its power in- and outflow. The power inflow $\hat{V}(t)I_{s,d}(t) \cdot pf - R'_s I_{s,d}^2(t)$ consists of the actual grid power $\hat{V}(t) \cdot I_{s,d}(t) \cdot pf$ subtracted by the resistance's power losses $R'_s I_{s,d}^2(t)$. The capacitor's outflow $P_{s,d} - R'_s I_{s,n}^2(t)$ consists of the nominal power demand $P_{s,d}$ subtracted by the nominal resistor's losses $R'_s I_{s,n}^2$. The nominal current $I_{s,n}$ would cause the nominal power flow $P_{s,d}$ under nominal voltage conditions $P_{s,d} = pf \cdot I_{s,n} V_n$, which results in

$$pf \cdot I_{s,n} = \frac{P_{s,d}}{V_n}. \quad (4.16)$$

Combining these terms for the in- and outflow results in the capacitor's power flow

$$P_{s,C} = \hat{V}(t)I_{s,d}(t) \cdot pf - R'_s I_{s,d}^2(t) \cdot pf^2 - (P_{s,d} - R'_s I_{s,n}^2(t) \cdot pf^2) \quad (4.17)$$

by neglecting the resistive losses of the deformed power currents through considering pf^2 . This neglectation prevents instabilities through resistive losses exceeding the power inflow $-R'_s I_{s,d}^2(t) > \hat{V}(t)I_{s,d}(t) \cdot pf$ due to linearization errors. Consistently neglecting the resistive losses of the deformed power currents for the actual $R'_s I_{s,d}^2(t) \cdot pf^2$ and the nominal $R'_s I_{s,n}^2(t) \cdot pf^2$ case compensates the error of each other for $I_{s,d} \approx I_{s,n}$.

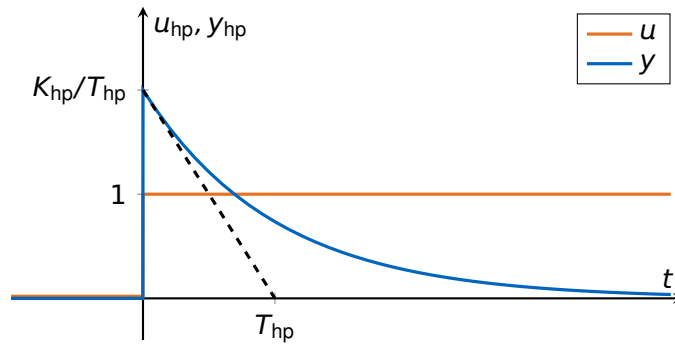


Figure 4.7: Step response of first order linear high-pass, with output y_{hp} and input u_{hp} , as well as the time constant T_{hp} and the gain parameter K_{hp} .

Applying (4.8), (4.16) and $R'_s = \frac{\rho'_s}{P_{s,d}}$ in (4.17) and (4.15) finally leads through simple algebraic reformulations to the rectification capacitor voltage dynamics

$$\frac{d}{dt} V_{s,c}(t) = \frac{T_s}{V_{s,c}(t)} \left(\frac{\hat{V}(t) I_{s,d}(t) \cdot pf}{P_{s,d}} - 1 + \rho'_s \left(\frac{1}{V_n^2} - \frac{I_{s,d}^2(t) \cdot pf^2}{P_{s,d}^2} \right) \right). \quad (4.18)$$

Provision layer: Motor load model

The dynamical behavior of different motor types are characteristically similar: after a voltage $\hat{V}(t)$ or frequency $\hat{\omega}(t)$ change, there is a significant initial reaction of the current $I_{m,d}(t)$, which settles according to its specific time constant to an adapted steady state value $I_{m,d}^*(\hat{V}(t), \hat{\omega}(t); P_{m,d})$. Assuming the dynamic dependency on voltage magnitude $\hat{V}(t)$ and frequency $\hat{\omega}(t)$ is orthogonal, finally means both dependencies can be independently modeled and finally added.

The fundamental basis for all behavioral patterns is a linear first order high-pass filter with the transfer function

$$G_{hp}(s) = \frac{K_{hp}s}{1 + T_{hp}s}, \quad (4.19)$$

whose step response is illustrated in Fig. 4.7. It responds to a unit step with an initial step up to $\frac{K_{hp}}{T_{hp}}$, and settles to a steady state value of zero. The time constant T_{hp} implements the characteristic duration of that settling process. Because of the high-pass characteristics of $G_{hp}(s)$, or in time domain the settling to zero, constant offsets of the input do not affect the output's behavior.

Considering current deviations of its steady state values $\Delta I_{m,v}(\hat{V}, t) = I_{m,d}(t) - I_{m,d}^*(\hat{V}(t); P_{m,d})$ and $\Delta I_{m,\omega}(\hat{\omega}, t) = I_{m,d}(t) - I_{m,d}^*(\hat{\omega}(t); P_{m,d})$ which settle to zero creates the prerequisites for applying the first order high-pass filter transfer function for the motor

4.1. ELECTRICITY CONSUMPTION MODEL OF CONVENTIONAL HOUSEHOLDS 87

load model, which results in

$$G_{m,v} = \frac{\Delta I_{m,v}(\hat{V}, s)}{\hat{V}(s)} = \frac{K_{m,v}s}{1 + T_{m,v}s}$$

$$\Rightarrow \Delta I_{m,v}(\hat{V}, t) = \frac{1}{T_{m,v}} \left(K_{m,v} \hat{V}(t) - \int \Delta I_{m,v}(\hat{V}, \tau) d\tau \right) \quad (4.20)$$

$$G_{m,\omega} = \frac{\Delta I_{m,\omega}(\hat{\omega}, s)}{\hat{\omega}(s)} = \frac{K_{m,\omega}s}{1 + T_{m,\omega}s}$$

$$\Rightarrow \Delta I_{m,\omega}(\hat{\omega}, t) = \frac{1}{T_{m,\omega}} \left(K_{m,\omega} \hat{\omega}(t) - \int \Delta I_{m,\omega}(\hat{\omega}, \tau) d\tau \right) \quad (4.21)$$

including their formulation in time domain.

The overall steady state RMS current

$$I_{m,d}^*(t) = I_{m,v}^*(\hat{V}, t) + I_{m,\omega}^*(\hat{\omega}, t) + I_{m,n}(P_{m,d}) \quad (4.22)$$

consists of the nominal RMS current $I_{m,n}(P_{m,d})$, and of the steady state deviations caused by voltage $I_{m,v}^*(\hat{V}, t)$ and frequency deviations $I_{m,\omega}^*(\hat{\omega}, t)$. Considering the dynamical RMS current component (4.20) and (4.21), as well as the steady state current $I_{m,d}^*(t)$ results in the final RMS current of the motor load model

$$I_{m,d}(t) = \Delta I_{m,v}(V, t) + \Delta I_{m,\omega}(\omega, t) + I_{m,d}^*(t). \quad (4.23)$$

The initial reaction of the RMS current immediately after a voltage or frequency step at t_0 from V_0 to V_+ or ω_0 to ω_+ , respectively, consists of the response of G_{hp} and the new steady state values $I_{m,v}^*(\hat{V}, t)$ or $I_{m,\omega}^*(\hat{\omega}, t)$, respectively. The response of G_{hp} , being the overshoot, is assumed to be proportional to the voltage $\Delta V = V_+ - V_0$ respectively frequency step $\Delta\omega = \omega_+ - \omega_0$ and to the nominal current $I_{m,n}$

$$\frac{K_{m,v}}{T_{m,v}} \Delta V \propto \Delta V \cdot I_{m,n}$$

$$\frac{K_{m,\omega}}{T_{m,\omega}} \Delta\omega \propto \Delta\omega \cdot I_{m,n}$$

Considering the nominal current as the current causing the active power flow $P_{m,d}$ under nominal voltage conditions $V_{m,n}$

$$I_{m,n} = \frac{P_{m,d}}{V_{m,n} \cos \varphi_{m,n}} \quad (4.24)$$

allows to formulate the proportionalities as

$$K_{m,v} = \kappa_{m,v} \cdot T_{m,v} \cdot I_{m,n} \quad (4.25)$$

$$K_{m,\omega} = \kappa_{m,\omega} \cdot T_{m,\omega} \cdot I_{m,n} \quad (4.26)$$

with $\kappa_{m,v}$ and $\kappa_{m,\omega}$ as the appropriate proportionality constants.

Table 4.1: List of the provision layer's steady state motor load model parameters for induction and universal motor driven devices

parameter	induction motor	universal motor
$\kappa_{m,V}^*$	0	1
$\kappa_{m,\omega}^*$	1	0

The relative deviations of the steady state RMS current $I_{m,V}^*(\hat{V}, t)$ respectively $I_{m,\omega}^*(\hat{\omega}, t)$ from its nominal value $I_{m,n}$ is assumed to be proportional to the relative voltage $\hat{V}(t)$ or frequency $\hat{\omega}(t)$ deviation

$$\frac{I_{m,V}^*(\hat{V}, t) - I_{m,n}}{I_{m,n}} \propto \frac{\hat{V}(t) - V_n}{V_n}$$

$$\frac{I_{m,\omega}^*(\hat{\omega}, t) - I_{m,n}}{I_{m,n}} \propto \frac{\hat{\omega}(t) - \omega_n}{\omega_n}$$

which results through (4.24) in

$$I_{m,V}^*(\hat{V}, t) = \frac{I_{m,n}}{V_n} \cdot \kappa_{m,V}^* (\hat{V}(t) - V_n) \quad (4.27)$$

$$I_{m,\omega}^*(\hat{\omega}, t) = \frac{I_{m,n}}{\omega_n} \cdot \kappa_{m,\omega}^* (\hat{\omega}(t) - \omega_n) \quad (4.28)$$

with the steady-state proportionality constants $\kappa_{m,V}^*$ and $\kappa_{m,\omega}^*$.

Multiple experiments with induction and universal motor driven devices show, that the proportionality constants can be specified as listed in Tab. 4.1, which describes a proportional dependency of universal machines on voltage and of induction machines on frequency in steady state.

Summary:

The RMS load model

- interacts with its environment as illustrated in Fig. 4.6
- consists of a combination of a resistive $I_{r,d}$, an SMPS $I_{s,d}$ and a motor $I_{m,d}$ load component by considering power angles
- the resistive load component model is described through (4.12) and (4.13)
- the SMPS load component model is described through (4.14) and (4.18)
- the motor load component model is described through (4.23), (4.20) with (4.25), (4.21) with (4.26), (4.22), (4.27), (4.28) and (4.24)

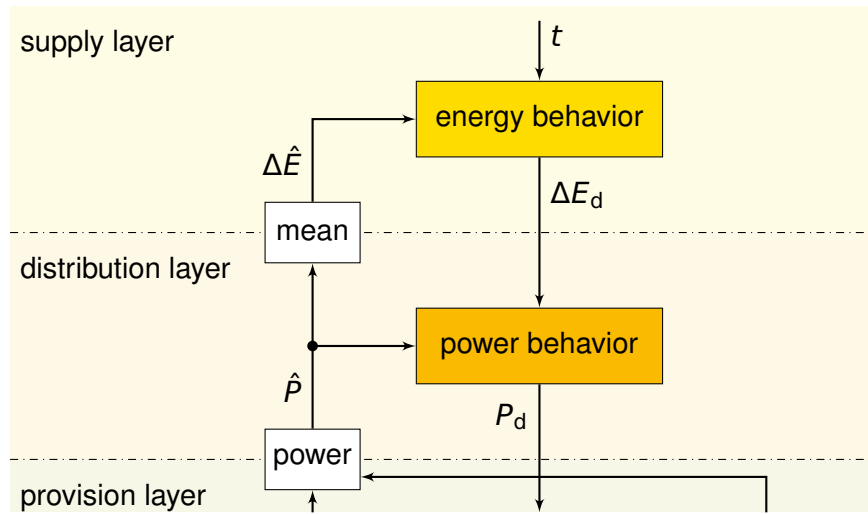


Figure 4.8: Functional schematics of the distribution and the supply layer's interaction of the load model

4.1.4 Distribution layer

The fundamental content of the distribution layer is the dynamical interaction of active powers in the grid, especially for economic dispatch. This means for the load model to calculate the reference power P_d for the underlying layer's process.

The goal of the distribution layer's load model proportion is to incorporate these behavioral patterns, which affect active power flows in a time span of seconds, but not the fundamental time variant behavioral patterns of energy consumption. This layer's fundamental assumption is that there are processes of underlying layers which achieve nominal voltages V_n . The behavioral patterns which affect time variant energy consumption along the day are only directly considered in the supply layer, but affect the power behavior through its reference energy consumption ΔE_d . These fundamental interactions and dependencies are illustrated in Fig. 4.8.

The reference energy consumption ΔE_d refers to the entire location. Assuming a constant proportional relation between the three phases u , v and w leads to

$$\Delta E_{d,u} = \kappa_u \Delta E_d \quad (4.29)$$

$$\Delta E_{d,v} = \kappa_v \Delta E_d \quad (4.30)$$

$$\Delta E_{d,w} = \kappa_w \Delta E_d \quad (4.31)$$

with $\kappa_u + \kappa_v + \kappa_w = 1$. Throughout this work the phase indexes u , v and w are for simplicity reasons not explicitly notated. An overview to the distribution layer load model is given in Fig. 4.9 for one phase.

The first step is to implement the power recovery, which means that power deviations $\hat{P} - P_d$ caused mainly by voltage deviations in the provision layer, recover partly after some time. The reason for this effect is that power controlled processes, like a temperature controlled oven compensates the reduced power draw through the lower voltage, by finally

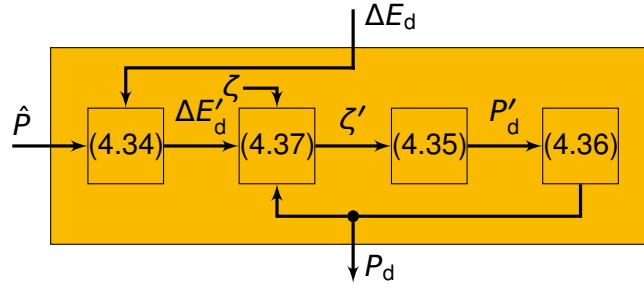


Figure 4.9: Block diagram of the distribution layer load model for a single phase: Equations and their relation

drawing more power through for instance longer heating cycles. Assuming a constant proportion K_P of the power to recover, means that the reference energy consumption ΔE_d has to be increased to $\Delta E'_d$, such that its steady state value $\Delta E'_d^*$ causes the recovery of the K_P -proportion of the actual power \hat{P} . The relative extra reference power $\frac{\Delta E'_d - \hat{P}}{\hat{P}}$, which is required to compensate power deviations $\hat{P} - \Delta E'_d$ is this power deviation negative and divided by the power consumption \hat{P} . Adding to the reference energy consumption ΔE_d the recovery proportion K_P of the reference energy consumption ΔE_d multiplied by the relative extra reference power results in the steady state reference energy consumption

$$\Delta E'_d^* = \Delta E_d + K_P \cdot \frac{\Delta E'_d - \hat{P}}{\hat{P}} \cdot \Delta E_d \quad (4.32)$$

which recovered the K_P -th part of the energy deviations.

Considering the mean power behavior of multiple consumers allows to describe it as one joint mean process, which contains the reaction on changing energy consumption references ΔE_d and the recovery of power deviations $\hat{P} - \Delta E_d$. A linear first order discrete state system with low-pass characteristics can be described with its system equation

$$y_{lp}[k+1] = y_{lp}[k] + \frac{T_s}{T_{lp}}(u_{lp} - y_{lp}[k]) \quad (4.33)$$

with the sampling time T_s and the time constant T_{lp} , which adjusts the system's settling time. Its step response is illustrated in Fig. 4.10. Considering it as a sufficient approximation for the dynamical part of the mean power behavior and considering the steady state power deviation recovery (4.32) as system input u_{lp} results in

$$\Delta E'_d[k+1] = \Delta E'_d[k] + \frac{1}{T_P} \left(\Delta E_d - \Delta E'_d[k] + K_P \frac{\Delta E'_d[k] - \hat{P}[k]}{\hat{P}[k]} \Delta E_d \right) \quad (4.34)$$

with the mean power dynamics time constant T_P and the recovery proportion K_P .

The interaction of external processes with the electric load devices is typically characterized by a switching behavior. A random process, based on the standard normal distributed white noise $\zeta[k]$ simulates this interaction of external processes. The final

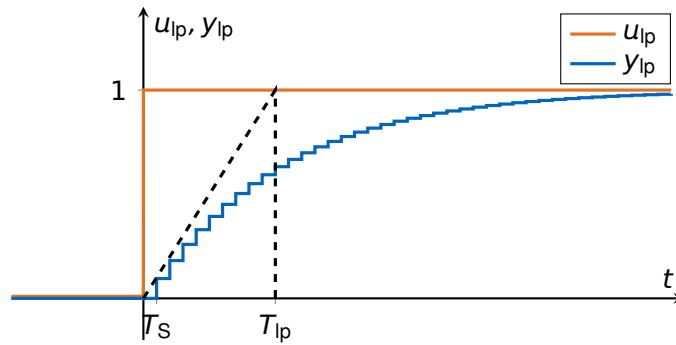


Figure 4.10: Step response of first order linear low-pass, with output y_{lp} and input u_{lp} , as well as the time constant T_{lp} .

process equation

$$P'_d[k] = P'_d[k-1] + P_\Delta \cdot \zeta'[k] \left(\frac{\arctan(\alpha(\zeta'^2[k] - \beta^2))}{\pi} + 0.5 \right), \quad (4.35)$$

with the switching height parameter P_Δ , the switching rate parameter β and the blur parameter α is a result of multiple heuristic trials. A detailed derivation of this function is given in the appendix A.1. The switching height parameter P_Δ directly affects the height of the individual steps, the switching rate parameter β affects how often a switching event occurs and the blur parameter α adjusts the clarity of the individual steps, which can be described as the ratio between ideal steps and noisy blur.

Assuming the resulting reference power P'_d to be normal distributed, means that negative powers could occur. Especially the typical characteristics of low mean powers with high spikes, but never values beyond a certain base load level $P_{d,0}$ cannot be considered as normal distributed. Assuming values above the base load $P_{d,0}$ to be Weibull distributed, allows to apply a transformation from standard normal to standard Weibull distributed random variables N2W, which is in detail explained in appendix A.2. This transformation and the base load assumption finally results in the reference power

$$P_d = P_{d,0} + N2W(P'_d; \mu[P], \sigma[P]) \quad (4.36)$$

with the overall mean $\mu[P]$ and standard deviation $\sigma[P]$ of the power consumption.

The adjustment of the noise samples $\zeta[k]$

$$\zeta'[k] = \zeta[k] + K_{\Delta E}(\Delta E'_d[k] - P_d[k-1]) \quad (4.37)$$

allows to track the reference $\Delta E'$. The tracking error $\Delta E'_d[k] - P_d[k-1]$ multiplied by the energy tracking stiffness $K_{\Delta E}$ as an offset to the noise $\zeta[k]$ implements through (4.35) the tracking of the reference power P_d with respect to the reference energy consumption $\Delta E'_d$.

Summary:

The power load model

- interacts with its environment as illustrated in Fig. 4.8
- considers three phases u, v and w individually as described in (4.29), (4.30) and (4.31)
- the power load model is described through (4.36), (4.35), (4.37) and (4.34) as illustrated in Fig. 4.9

4.1.5 Supply layer

The fundamental content of the supply layer is the time variant energy supply, especially the unit commitment. This means for the load model to calculate the reference energy consumption ΔE_d for the underlying layer's process.

The goal of the supply layer's load model proportion is to incorporate these behavioral patterns, which affect energy consumption in a time scale of 15 min. This layer's fundamental assumption is that there are processes of the underlying layers which achieve the power dispatch and distribution. The supply layer focuses on the energy consumption of one location, neglecting to distinguish the three phases. Its fundamental interactions and dependencies are illustrated in Fig. 4.8.

The fundamental property of the supply layer's model is that it is time variant, but without dependence on other magnitudes. This is subject to assuming no impact of external magnitudes like weather, and assuming no feedback from the actual energy consumption $\Delta \hat{E}$ on the reference energy consumption ΔE_d . The simplest way to implement the supply layer is to use recorded data ΔE_d . An alternative approach is to apply a random process to stochastically generate the time variant behavior. This random process is based on a standard normal distributed white noise ζ_E input. The process equation is a standardized time-discrete first order low-pass dynamics

$$\zeta'_E[k+1] = \zeta'_E[k] + \frac{15 \text{ min}}{T_E} \left(\sqrt{\frac{2T_E}{15 \text{ min}}} \zeta - \zeta'_E[k] \right) \quad (4.38)$$

with a time constant T_E and the 15 min sampling time. The standardization coefficient $\sqrt{\frac{2T_E}{15 \text{ min}}}$ ensures a standard normal distribution of ζ'_E , which means to compensate the impact of the filter dynamics on signal power, as attached in Sec. A.3. The typical behavior of only positive consumption is identical to the power behavior of the distribution layer (4.36) implemented as transformation to the Weibull distribution, which results in

$$\Delta E_d = \Delta E_{d,0} + N2W(\zeta'_E; \mu[\Delta E], \sigma^2[\Delta E]) \quad (4.39)$$

with a constant base load ΔE_0 and the overall mean $\mu[\Delta E]$ and standard deviation $\sigma^2[\Delta E]$ of the energy consumption. Details about this transformation function are attached in Sec. A.2.

Summary:

The energy load model

- interacts with its environment as illustrated in Fig. 4.8
- the energy load model is described through (4.39) and (4.38)

4.2 Weather model

Weather has a high impact on future energy systems, as solar irradiation is the energy source for PV, wind speed is the source for wind power and ambient temperature mainly affects the heating demand, but also PV efficiency. This section describes a methodology which allows to generate artificial weather data which could be based on realistic, remote, extreme or future climatic conditions. The model is fundamentally based on the requirements of the supply layer, but can be up-sampled to generate data for the distribution layer. The content of this section highly depends on the preceding work [23].

4.2.1 Introduction to weather modeling

The high dependency of renewable energy systems on weather effects results in the dependency of numeric and analytic models on weather data input. Utilizing measured weather time series and specific weather models, which are known as weather generators [7], meet this requirement. Using weather models has specific different consequences than using measured time series. Weather models enable emulating scenarios, which are not measurable. There are several exemplary application scenarios: future weather conditions due to the climate change, regions without weather station or with limited data access, or considering artificial scenarios for investigating robustness of the energy system. As each model is based on simplifications and assumptions, measured time series are more accurate. Accurately expressed, weather models address artificial weather conditions and measured time series address past real conditions.

Literature covers numerous fundamentally different methods to implement weather generator models. Weather generator models significantly differ from the concept of numerical global climate models, as they are computationally fast and focus on small regions instead of simulating the global weather system [7]. There is a distinction between sequential and nonsequential methods, addressing the correlation of each value on its preceding value. A typical approach for sequential methods is to utilize Markov chains [71] [9] [16] for modeling the stochastic data generation process. Nonsequential approaches result in uncorrelated time series. Adjusting the distribution function [13] or distinguishing the four seasons [64] allows exemplary to consider time variance. Such weather models can be designed for artificial data generation [71] or for forecast [81]. Exemplary motivations for weather generator models without context of energy system operation are propagation of wild fire [81], agriculture [73] or reliability of technical facilities, especially the electrical power distribution system [16]. In the context of renewable energy

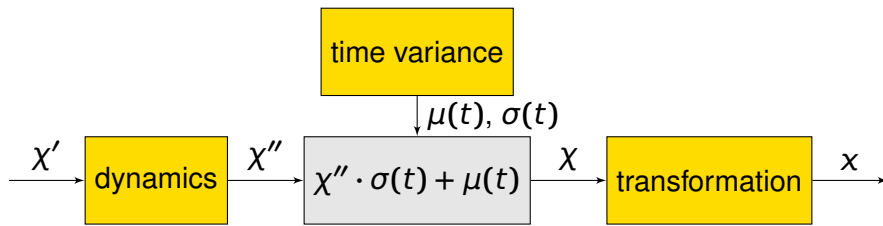


Figure 4.11: Weather model methodology based on three modules

systems, weather generators are exemplary used for scheduling the operation of MGs [85] or modeling PV [64] and wind power generation [71].

The focus of this section is to refine the preceding work [23]. The goal is to describe an analytical weather generator which involves irradiation, wind speed and ambient temperature. The time variance of the real weather causes a significant diurnal and seasonal variation of the external conditions for energy systems. The dynamical behavior of the real weather limits the rate of change of weather phenomena, which mainly affects the duration of requiring backup power from storages and hence their size. The correlation of different phenomena, like irradiation and ambient temperature, highly affects the synergies of different renewable energy technologies. Other phenomena are simplified by applying a random process.

4.2.2 Weather model methodology

The weather model aims for generating data on solar irradiation \mathcal{I} , ambient temperature \mathcal{A} and wind speed \mathcal{W} data. Its methodology is based on a modeling approach with three modules as illustrated in Fig. 4.11. The central idea of the concept is to generate normal distributed time series and to apply a transformation to an appropriate weather distribution function. Normal distributed time series χ have the crucial advantage of existing simple mathematical methods to modify its characteristics, like its mean, standard deviation or its frequency spectrum, which are used to implement the dynamical and the time variant behavioral patterns. The following three subsections describe these three methodological modules in a general manner, by neglecting indexing the different weather magnitudes.

Modeling weather dynamics

The first module of the modeling concept, illustrated in Fig. 4.11, is to incorporate the weather dynamics. The weather dynamics refer to the typical behavior that weather doesn't change arbitrarily, but in a typical manner. This means that the actual weather highly depends on the recently preceding weather. This effect is expressed as an ordinary differential equation, which implements two fundamental goals:

1. To limit the rate of change, meaning that the actual value of the weather data depends on its preceding values
2. To introduce a causal relation between different types of weather data, like irradiance and temperature.

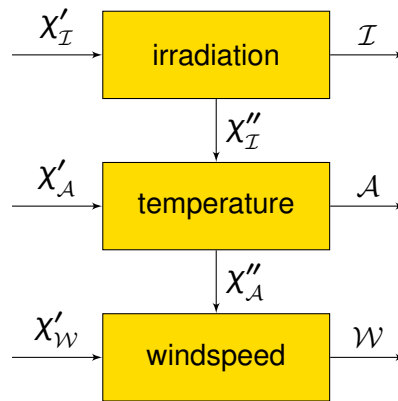


Figure 4.12: Modeling the weather magnitudes irradiation \mathcal{I} , ambient temperature \mathcal{A} and windspeed \mathcal{W} , such that they are correlated. The system input is standard normal distributed noise for each magnitude.

The limited rate of change is equivalent to applying a low-pass filter.

The input to the dynamics is a time series of standard normal distributed random numbers χ' , which are band limited white noise. White noise has an equal distributed frequency spectrum, which requires higher frequencies to be damped. The most simple dynamical equation to damp high frequencies is a linear first order low-pass system with a transfer function

$$G(s) = \frac{K}{1 + T \cdot s}, \quad (4.40)$$

the gain K and the time constant T . This system has to be extended to incorporate the causal relation between the different types of weather data. This relation is simplified such that irradiation impacts temperature $\mathcal{A}(\mathcal{I})$ and temperature impacts wind speed $\mathcal{W}(\mathcal{A})$, as illustrated in Fig. 4.12. This conforms to simplified natural relations. The output χ'' of the differential equation (4.40) is still standard normal distributed, but with a specific frequency spectrum which results in colored noise.

The suppression of high frequency components leads to a decreased signal energy content which needs to be compensated, such that the distribution function of the resulting noise χ'' is not affected by the differential equation (4.40). For this reason the differential equation needs to be standardized through the compensation factor $\sqrt{\frac{2T}{T_s}}$ with the sampling time T_s . This leads for the **irradiation** \mathcal{I} to

$$\dot{\chi}''_{\mathcal{I}} = \frac{1}{T_{\mathcal{I}}} \left(\sqrt{\frac{2T_{\mathcal{I}}}{T_s}} \chi'_{\mathcal{I}} - \chi''_{\mathcal{I}} \right), \quad (4.41)$$

with the time constant $T_{\mathcal{I}}$ as a model parameter. The standardization is elaborated in the attachment Sec. A.3. The output signal $\chi''_{\mathcal{I}}$ is ensured to be standard normal distributed.

The **ambient temperature** \mathcal{A} respectively the **wind speed** \mathcal{W} depend on the solar irradiation \mathcal{I} respectively the ambient temperature \mathcal{A} . These correlations are implemented by the fraction $\frac{\zeta_{\mathcal{A}/\mathcal{W}} \chi'_{\mathcal{I}/\mathcal{A}} + \chi'_{\mathcal{A}/\mathcal{W}}}{\zeta_{\mathcal{A}/\mathcal{W}} + 1}$ with the correlation factors $\zeta_{\mathcal{A}/\mathcal{W}}$ which adjusts the result

closer to the appropriate time series $\chi'_{\mathcal{A}/\mathcal{W}}$ or the underlying time series $\chi'_{\mathcal{I}/\mathcal{A}}$

$$\lim_{\zeta_{\mathcal{A}/\mathcal{W}} \rightarrow \infty} \frac{\zeta_{\mathcal{A}/\mathcal{W}} \chi'_{\mathcal{I}/\mathcal{A}} + \chi'_{\mathcal{A}/\mathcal{W}}}{\zeta_{\mathcal{A}/\mathcal{W}} + 1} = \chi'_{\mathcal{I}/\mathcal{A}}$$

$$\lim_{\zeta_{\mathcal{A}/\mathcal{W}} \rightarrow 0} \frac{\zeta_{\mathcal{A}/\mathcal{W}} \chi'_{\mathcal{I}/\mathcal{A}} + \chi'_{\mathcal{A}/\mathcal{W}}}{\zeta_{\mathcal{A}/\mathcal{W}} + 1} = \chi'_{\mathcal{A}/\mathcal{W}}.$$

This correlation fraction, together with the standardized first order low-pass system leads to the dynamical equation for the ambient temperature $\chi''_{\mathcal{A}}$ and wind speed colored normal distributed noise $\chi''_{\mathcal{W}}$

$$\dot{\chi}''_{\mathcal{I}} = \frac{1}{T_{\mathcal{I}}} \left(\frac{\zeta_{\mathcal{A}/\mathcal{W}} \chi'_{\mathcal{I}/\mathcal{A}} + \chi'_{\mathcal{A}/\mathcal{W}}}{\zeta_{\mathcal{A}/\mathcal{W}} + 1} \sqrt{\frac{2}{T_{\mathcal{I}} T_s}} \chi'_{\mathcal{I}} - \chi''_{\mathcal{I}} \right). \quad (4.42)$$

This equation implements a dependency of the temperature \mathcal{A} on irradiation \mathcal{I} and of the wind speed \mathcal{W} on the temperature \mathcal{A} . The resulting temperature's and wind speed's time series $\chi''_{\mathcal{A}/\mathcal{W}}$ are standard normal distributed.

Modeling time variance

The second module of the modeling concept, illustrated in Fig. 4.11 is to implement time variance. Time variant stochastic processes feature time dependent expected value $\mu(t)$ and standard deviation $\sigma(t)$ functions. Both are applied to the model by

$$\chi = \chi'' \cdot \sigma(t) + \mu(t) \quad (4.43)$$

which indicates, that the expected value $\mu(t)$ and standard deviation $\sigma(t)$ functions can be considered as separate inputs, which allows to use artificially designed functions as well as functions based on measurements. This separateness is established by depending only on constant parameters, but not on process variables. The resulting time series χ is normal distributed, time variant colored noise.

The time dependent expected value $\mu(t)$ and standard deviation $\sigma(t)$ functions feature a diurnal and a seasonal variation. These two variations, the seasonal and the diurnal variation, can be considered orthogonal by two separate time dimensions. One dimension is the time period during a day and the other dimension is the continuous interpolation of days during a year. This leads to a bent surface as exemplarily illustrated in Fig. 4.13. A simple version of an artificially designed function is based on the same parameter based function $z(t)$ to describe the surface for all different types of time series $\mathcal{I}, \mathcal{A}, \mathcal{W}$ and for both stochastic magnitudes $z(t) \in \{\mu(t), \sigma(t)\}$, but with different parameter values to satisfy the need of individually different shapes.

The parameter based function $z(t)$ is based on two different kinds of parameters, the amplitudes A and phases φ . The function $z(t)$ consists of a constant offset A_0 , a first order diurnal harmonic component $A_d \cos(\omega_d t - \varphi_d)$, a first order seasonal component $A_y \cos(\omega_y t - \varphi_y)$ and a crossed seasonal-diurnal component $A_{dy} \cos(\omega_d t -$

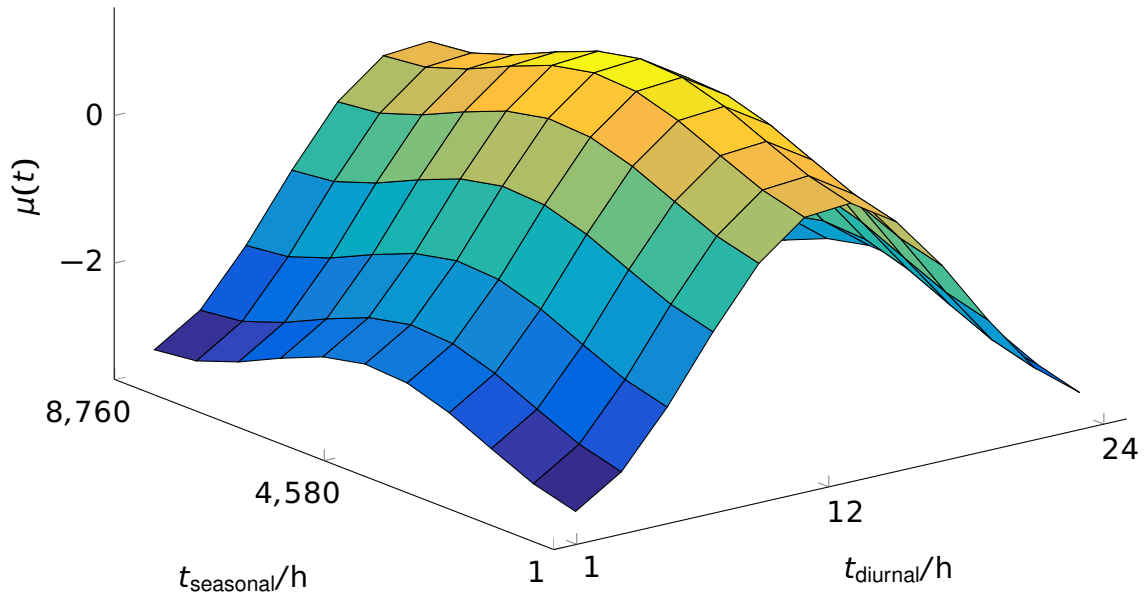


Figure 4.13: Illustration of the diurnal and the seasonal variation of the mean $\mu(t)$ by two distinct axis: Artificial example.

$\varphi_d) \cos(\omega_y t - \varphi_y)$. The overall expected value is termed A_0 , the amplitude of the expected diurnal variation A_d , the amplitude of the expected seasonal variation A_y and the amplitude of the crossed seasonal-diurnal variation A_{dy} . There is a phase φ_d and φ_y describing the time shift of the diurnal and the seasonal peak. The function $z(t)$ results in

$$z(t) = A_0 + A_d \cos(\omega_d t - \varphi_d) + A_y \cos(\omega_y t - \varphi_y) + A_{dy} \cos(\omega_d t - \varphi_d) \cos(\omega_y t - \varphi_y) \quad (4.44)$$

with the diurnal frequency $\omega_d = 2\pi/24$ h and the seasonal frequency $\omega_y = 2\pi/8760$ h. A typical shape of this function is illustrated in Fig. 4.13.

Transformation into weather space

The third module of the modeling concept, illustrated in Fig. 4.11 is to transform the time series χ into the final weather time series $\{\mathcal{I}, A, W\}$. The transformation, which leads to the final time series

$$x(t) = T(\chi(t)) \quad (4.45)$$

is in general non-linear and strongly affects the frequency spectrum.

The transformation of the **irradiation** \mathcal{I} is based on transforming the time variant stochastic time series $\chi_{\mathcal{I}}$ to the atmospheric transmission η_0 . The atmospheric transmission η_0 is defined as the relative proportion of the sunlight, which passes the atmosphere

$$\eta_0(t) := \frac{\mathcal{I}_{gn}}{\mathcal{I}_0}, \quad (4.46)$$

hence the global normal irradiation \mathcal{I}_{gn} relative to the normal radiation reaching the upper atmosphere, known as solar constant $\mathcal{I}_0 = 1362 \text{ W/m}^2$. The atmospheric transmission η_0 is a unitless ratio which accepts values between 0 and 1. Transmission rates of more than 90% are unrealistic due to the filtration effect of the clear atmosphere. The implementation of the atmospheric transmission

$$\eta_0(t) = \frac{\eta^*}{e^{-\chi_I(t)} + 1} \quad (4.47)$$

maps the time variant stochastic time series $\chi_I(t)$ with a domain from $-\infty$ to ∞ to the atmospheric transmission ratio with a domain from 0 to 1, but with a limited codomain of 0 to η^* . This allows to compute through (4.46) the global normal irradiation \mathcal{I}_{gn} .

The atmospheric transmission η_0 is based on absorption, reflection and scattering effects. The global normal radiation \mathcal{I}_g is the entire radiation reaching the earth. It consists of the direct radiation \mathcal{I}_{drn} , which is the proportion of the upper atmospheric radiation \mathcal{I}_0 , which is not interacting with the atmosphere. The proportion of the solar radiation, which is scattered in the atmosphere, such that it reaches the earth, is the diffuse radiation \mathcal{I}_{dfn} . Bindi et. al. analyze the diffuse fraction η_{df} , the relative proportion of the diffuse normal radiation \mathcal{I}_{dfn} of the global normal radiation \mathcal{I}_{gn} , which is defined as

$$\eta_{df}(t) := \frac{\mathcal{I}_{dfn}(t)}{\mathcal{I}_{gn}(t)}. \quad (4.48)$$

The result of [17] is an accurate approximation of the diffuse fraction

$$\eta_{df}(t) \approx \min\left(1, -\frac{10}{6}\eta_0(t) + 1.5\right), \quad (4.49)$$

which results through (4.48) in the diffuse normal irradiation $\mathcal{I}_{dfn}(t)$. Neglecting reflected radiation leads through the direct fraction $1 - \eta_{df}(t)$ to the direct normal radiation

$$\mathcal{I}_{drn}(t) = (1 - \eta_{df}(t)) \cdot \mathcal{I}_{gn}(t). \quad (4.50)$$

The global horizontal irradiation \mathcal{I}_{gh} results from the normal-to-horizontal factor

$$\eta_{h/n}(t) := \frac{\mathcal{I}_{drh}(t)}{\mathcal{I}_{drn}(t)}, \quad (4.51)$$

defined as the relative proportion of the direct horizontal radiation \mathcal{I}_{drh} of the direct normal radiation $\mathcal{I}_{drn}(t)$. The peak proportion of the diffuse radiation is aligned with the direct radiation, which allows to approximate

$$\begin{aligned} \mathcal{I}_{dfh}(t) &\approx \eta_{h/n}(t)\mathcal{I}_{dfn}(t) \\ \Rightarrow \mathcal{I}_{gh}(t) &= \eta_{h/n}(t)\mathcal{I}_{gn}(t). \end{aligned} \quad (4.52)$$

The resulting approximation error gets partly compensated, as it is also used in the process to determine the model parameters. In this sense, the model parameters compensate for this approximation error. The normal-to-horizontal factor $\eta_{h/n}(t)$ can be

determined through geometric calculations which depend on the location's latitude and on time [45]. Details are attached in B.

The global sloped radiation $\mathcal{I}_{gs}(t)$ is the final output of the transformation

$$\mathcal{I}(t) = \mathcal{I}_{gs}(t) \quad (4.53)$$

which is the entire radiation on a sloped surface. It consists of the direct \mathcal{I}_{drs} and the diffuse \mathcal{I}_{dfs} proportion

$$\mathcal{I}_{gs}(t) = \mathcal{I}_{drs} + \mathcal{I}_{dfs}. \quad (4.54)$$

The direct sloped radiation \mathcal{I}_{drs} depends on the direct horizontal radiation \mathcal{I}_{drh} and on the horizontal-to-sloped factor, defined as

$$\eta_{s/h}(t) := \frac{\mathcal{I}_{drs}}{\mathcal{I}_{drh}}. \quad (4.55)$$

This factor $\eta_{s/h}(t)$ can be determined through geometric calculations which depend on the location's latitude, time and the alignment of the slope [45]. Details about its computation are attached in B. The diffuse sloped radiation \mathcal{I}_{dfs} depends on the horizontal diffuse radiation and on the atmospheric scattering factor

$$\eta_{sc}(t) := \frac{\mathcal{I}_{dfs}(t)}{\mathcal{I}_{dfh}(t)}. \quad (4.56)$$

This factor can be approximated by a diffuse radiation model [45], which is attached in B. The final radiation leads to

$$\mathcal{I} = (\eta_{s/h}(t) \cdot \eta_{h/n}(t) \cdot (1 - \eta_{df}(t)) + \eta_{sc}(t) \cdot \eta_{h/n}(t) \cdot \eta_{df}(t)) \cdot \eta_0 \mathcal{I}_0. \quad (4.57)$$

The transformation of the **ambient temperature** \mathcal{A} is trivial, as the temperature is assumed to be normal distributed [23]

$$\chi_{\mathcal{A}} = \chi_{\mathcal{A}}. \quad (4.58)$$

The transformation of the **wind speed** \mathcal{W} is based on the assumption of the wind speed to be Weibull distributed. This allows to apply a transformation from normal to Weibull distributed random variables

$$\mathcal{W}(t) = \text{N2W}(\chi_{\mathcal{W}}; A_{\mathcal{W},\mu,0}, A_{\mathcal{W},\sigma,0}) \quad (4.59)$$

with the overall mean expectation value $A_{\mathcal{W},\mu,0}$ and mean standard deviation $A_{\mathcal{W},\sigma,0}$. Details about this transformation are attached in A.2.

Summary:

The weather model

- distinguishes three fundamental magnitudes, the solar irradiation \mathcal{I} , the ambient temperature \mathcal{A} and the wind speed \mathcal{W}
- consists of three fundamental calculation steps, the weather dynamics, the time variance and the transformation as illustrated in Fig. 4.11
- irradiation dynamics module is described through (4.41) and the ambient temperature and wind speed dynamics through (4.42)
- time variance module features time dependent expected value $\mu(t)$ and standard deviation $\sigma(t)$ functions through (4.44) and (4.43)
- irradiation transformation module is described through (4.57)(4.49)(4.47) and calculations from literature, attached in B
- ambient temperature transformation module is described through (4.58) and the wind speed transformation is described through (4.59)

Chapter 5

Analysis and Validation of HIL Models

This section describes the performance of the HIL model approaches, based on comparing simulated and measured data. The HIL models include the conventional consumption model described in Sec. 5.1 and the weather model described in Sec. 5.2.

5.1 Conventional consumption model

The investigation of the performance of the conventional consumption model is fundamentally based on the ESMIF framework described in Sec. 2.2.1. This section describes the experimental setup to investigate the consumption model's performance at the different ESMIF layers, as well as the experimental results and their analysis and interpretation.

5.1.1 Experimental setup

The experimental setup to investigate the consumption model's performance at the different ESMIF layers is based on three different fundamental approaches. The human impact, which is modeled as stochastic processes, is investigated by comparing the model's stochastic approach with measured household loads. The recovery dynamics is individually investigated. The technical interaction with the grid through voltages is investigated based on a dynamic measurement test bench for electric devices.

Household measurements

Several different exemplary electricity consumptions are considered to define a reference system behavior, which allows to compare and validate the load model. Measurements of the entire household consumption and of individual flats of different single and multi family houses in the south Bavarian region are executed. The focus of these measurements is set on conventional, uncontrolled electricity consumption, which means to exclude measurements which include controlled electricity consumption, like heat pumps or electric vehicle charging. Additionally, measurements with special electricity consumers, like swimming pools, are excluded. The finally chosen measurement of a single family house is

a realistic reference measurement, which allows a critical model validation. It incorporates all grid connected appliances. The chosen measurement avoids to gloss over results as steep gradients and highly fluctuating behaviors are not avoided by using multi family house measurements with a higher impact of stochastic balancing of individual consumer behaviors.

The measurements are executed with the power analyzer 'Qualistar+ C.A 8336' from Chauvin Arnoux with the current probe 'MN93A'. This power analyzer allows to record all typical power quality aspects, including higher harmonics up to the 50th order, as well as direct voltages and currents. The electricity consumption of the single family house is executed with a 15 min sampling for two weeks. The ten sample days during the week allow to calculate the time variant mean and standard deviation of the electric energy consumption. These calculated values are filtered with the symmetric 6th-order discrete time filter with the weight vector (0.5 1 1.5 2 1.5 1 0.5) to avoid the remaining fluctuations. The resulting filtered mean and standard deviations are illustrated in Fig. 5.1.

Recovery dynamics experimental setup

The recovery dynamics are based on the process of recovering energy demand after a voltage step. The experimental setup is based on water cookers, which boil 1 l water. The nominal power rating of the water cooker is 2.2 kW. If the cooker is supplied with a voltage of 180 V, it consumes a power of 1.3 kW. The cooking process lasts at nominal voltages of 230 V about 140 s and at 180 V about 230 s. Similar measurements are executed for a light bulb, which consumes 60 W at 230 V and 37 W at 180 V. These measurements of the water cooker and the light bulb are superimposed to calculate the behavior of multiple water cookers and light bulbs operating at the same time, which is required as reference behavior for the recovery dynamics validation.

Dynamic measurement test bench for electric devices

The dynamic measurement test bench for electric devices consists of a controllable voltage source and a voltage and current measurement device. The measurement device is the aforementioned power analyzer 'Qualistar+ C.A 8336' from Chauvin Arnoux. The controllable voltage source is a 'COMPISO' system of Egston. It allows to configure arbitrary voltages. Unless specified differently, the system supplies a pure sinusoidal (THD < 1%) RMS voltage of 230 V, with a frequency of 50 Hz. Voltage or frequency steps are in phase, which means without coincident phase step. Higher harmonics are in phase with the fundamental oscillation. Measurements are sampled for RMS experiments each 10 ms, and for instantaneous measurements each 300 μ s. There is a set of household devices listed in Tab. 5.1 which are available for experimental investigations.

5.1.2 Experimental results

This section compares modeled load behavior with the recorded behavior of different exemplary experimental scenarios. The experimental results, the simultaneity and the differences of the model and the measurements highly depend on the model parameterization. Heuristic methods have been applied to find appropriate model parameters.

Table 5.1: List of available electric devices to be used for experimental investigations in the dynamic measurement test bench for electric devices.

name	construction type
light bulbs	mainly resistive heating
notebook charger	switched mode power supply
mobile phone charger	switched mode power supply
LED	switched mode power supply
mixer	mainly universal motor
vacuum cleaner	mainly universal motor
cooling fan	mainly universal motor
induction motor at idle	mainly single phase induction motor
waste water pump	mainly single phase induction motor

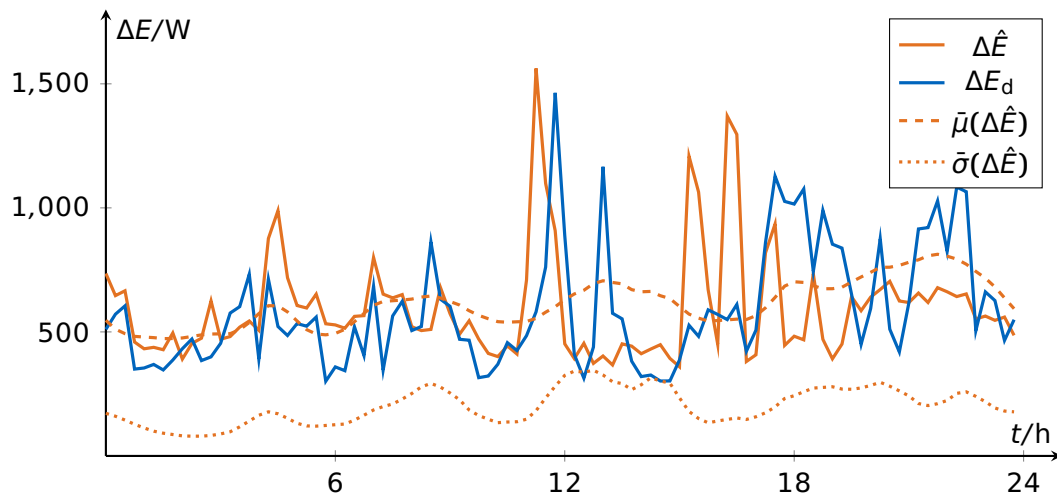


Figure 5.1: Electric energy consumption for a single family house: Exemplary measured $\Delta\hat{E}$ and modeled random process ΔE_d consumption and calculated mean $\bar{\mu}(\Delta\hat{E})$ and standard deviation $\bar{\sigma}(\Delta\hat{E})$ (calculated over 10 measured sample days during the week, filtered with a 6-dimensional discrete filter)

Supply layer analysis

The load model at the supply layer includes the stochastic and time variant electric energy consumption. It is sampled each 15 min. The measured electricity consumption of an exemplary single family house is illustrated in Fig. 5.1 for one day, including its time variant mean and standard deviation. This illustration also shows the model behavior, which highly depends on stochasticity and on the model parameters listed in Tab. 5.2. The stochastic process means to expect not similar modeled and measured trajectories, but similar trajectory characteristics.

The model behavior's trajectory is significantly different from the measured trajectory, due to their stochastic nature. The fundamental behavior appears similar. Fluctuations with similar amplitudes result at similar times. Similar high overshooting, but similarly few undershooting peaks occur. The overshooting peaks' durations and slew rates are similar.

Table 5.2: List of parameters for the supply layer's electricity consumption model part, which leads to the stochastic behavior illustrated in Fig. 5.1.

variable	value	variable	value
T_E	30 min	μ	see Fig. 5.1
σ	see Fig. 5.1		

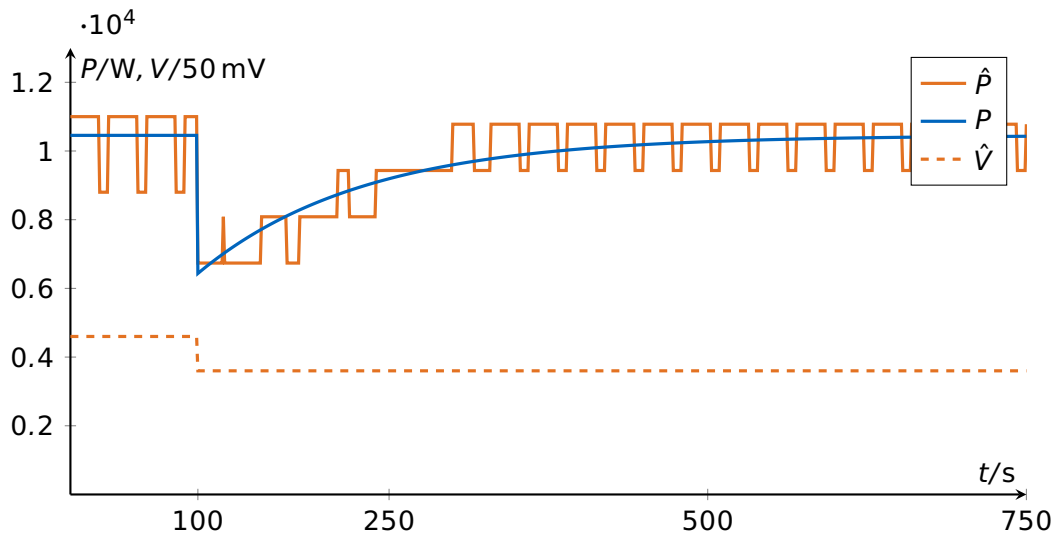


Figure 5.2: Electric power consumption of each 30 s starting one water cooker: Exemplary reference \hat{P} and modeled P consumption, measured voltage \hat{V}

Distribution layer analysis

The distribution layer load model mainly consists of the recovery dynamics and the stochastic load process. The recovery dynamics are based on the natural process of recovering parts of the energy demand after a voltage step. The reference system is the artificial system of each 30 s starting one water cooker, which boils 1 l water. After 100 s a voltage step for all water cookers from 230 V to 180 V is applied. The resulting power consumption \hat{P} is illustrated in Fig. 5.2, including the voltage step. The power consumption switches when one water cooker is finished or a new one starts, which results in the observable pulsing behavior. After the voltage step the power consumption collapses due to the mainly resistive behavior of the water cookers. The power consumption recovers after about 180 s to the previous power consumption, with slightly flatter switching heights.

The model behavior is also illustrated in Fig. 5.2. It shows a continuous process output, with a collapse after the voltage step at $t = 100$ s to a similar value as the reference measurement. The recovery process is similar to the recovery of the measured reference, but with a longer lasting final settling of about 400 s. After 180 s recovery, about 75% of the power collapse is recovered.

An experiment, which considers more different kinds of consumption devices is illustrated in Fig. 5.3. Each two seconds starting one water cooker, which a third having only half, a third having full and a third having double nominal power. Additionally 500 light bulbs are operating. After 100 s a voltage step for all devices from 230 V to 180 V

Table 5.3: List of parameters for the distribution layer's recovery dynamics model part (4.34), which leads to the voltage step response illustrated in Fig. 5.3

variable	value	variable	value
ΔE_d	187 kW	T_P	130 s
K_P	0.83		

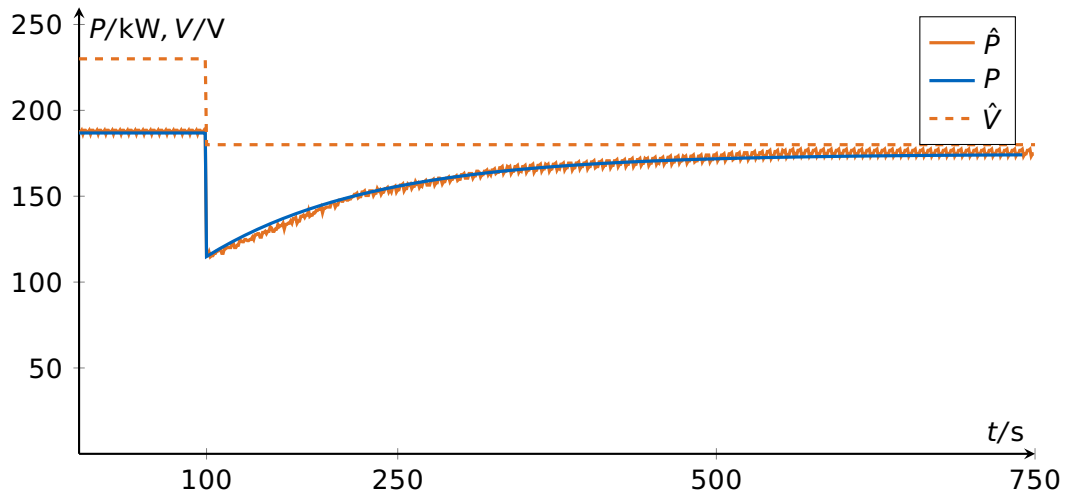


Figure 5.3: Electric power consumption of each 2 s starting one water cooker, with half, full and double power in equal shares: Exemplary measured and multiplied \hat{P} and modeled P consumption, measured voltage \hat{V}

Table 5.4: List of parameters for the distribution layer's random process model, as illustrated in Fig. 5.4

variable	value	variable	value
T_P	130 s	$K_{\Delta E}$	0.005 1/W
P_{Δ}	140 W	α	15
β	3		

is applied. The resulting reference trajectory is calculated by appropriately halving or doubling the measured power and the measured duration. The used model parameters for calculating the appropriate model behavior are listed in Tab. 5.3. The reference and the modeled trajectory are largely congruent, besides the reference trajectory having some jitter. Its recovery from $t = 100$ s to $t \approx 600$ s consists of three mainly straight parts.

The random load dispatch process of the distribution layer transforms the recovery dynamics filtered 15 min-samples of the supply layer into a 1 s-sampled random process. This process is characterized by the automatic and manual switching of individual devices, which cause load trajectories with steps, spikes and flat trajectory elements, as illustrated in Fig. 5.4. Neglecting the feedback of the random process equation on the recovery dynamics, for instance by assuming the recovery proportion $K_P = 0$, leads to the adapted energy consumption $\Delta E'_d$ being the low-pass filtered reference ΔE . It is illustrated in Fig. 5.4 based on parameters listed in Tab. 5.4, including an exemplary random process

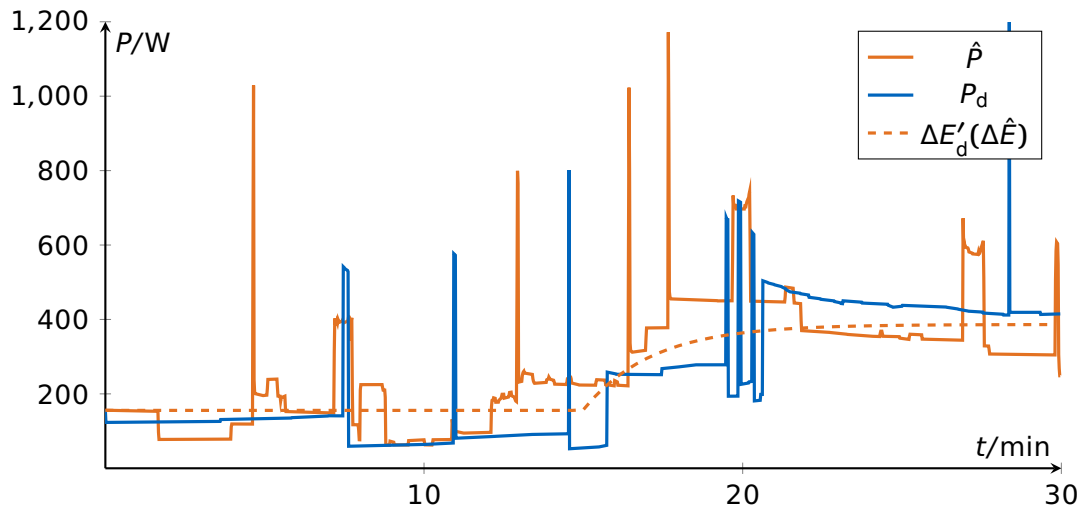


Figure 5.4: Distribution layer's random process model based on neglecting the feedback of the random process equation on the recovery dynamics, by assuming $K_P = 0$. Measured data \hat{P} and modeled data P_d , based on parameters from Tab. 5.3

output P_d . This output shows random steps, spikes and flat trajectory elements with a drift towards the adapted energy consumption $\Delta E'_d$. At about $t = 20$ min the output shows a marginally stable oscillation, a pulsing of about 600 W with random pulse width and random absolute pulse height. Spikes of real measurements show a different height and a different width, as for instance at $t = 5$ min a 800 W pulse for about 2 s and at $t = 27$ min a 300 W pulse for about 40 s. Similarly different patterns are spikes of the model, at $t = 7$ min a 400 W spike for about 10 s and at $t = 28$ min a 800 W pulse for about 1 s. There are patterns with similar and with different power levels before and after spikes, similarly in the measured and the modeled trajectory.

The impact of the different parameters on the model behavior is illustrated in Fig. 5.5. It shows as reference in blue the previously discussed model output of Fig. 5.4. The model output with varied parameters uses the identical random numbers as noise input and the identical parameters, besides the individual parameter variation. The top left diagram shows the impact of the energy tracking stiffness, which is decreased from $K_{\Delta E} = 0.005 \text{ 1/W}$ to $K_{\Delta E} = 0.001 \text{ 1/W}$. The effect is a significantly reduced number of peaks and steps, and a significantly increased height and width of these peaks. The drift back to the adapted energy consumption $\Delta E'_d$ is decreased, especially at $t = 20$ min to $t = 30$ min, which leads to a weaker tracking of the reference adapted energy consumption $\Delta E'_d$. The pulsing at $t = 20$ min is vanished. The top right diagram shows the impact of the switching height parameter, which is decreased from $P_{\Delta} = 140 \text{ W}$ to $P_{\Delta} = 50 \text{ W}$. The effect is a significantly reduced height of the individual peak and step events, and a significantly increased width of the lower peaks. The pulsing at $t = 20$ min is vanished. The bottom left diagram shows the impact of the blur parameter, which is decreased from $\alpha = 15$ to $\alpha = 1$. The effect is a significantly decreased flatness of individual trajectory segments, individual steps and flat segments turn into a typical noisy random process. Individual spikes show slightly decreased height. The pulsing at $t = 20$ min is reduced.

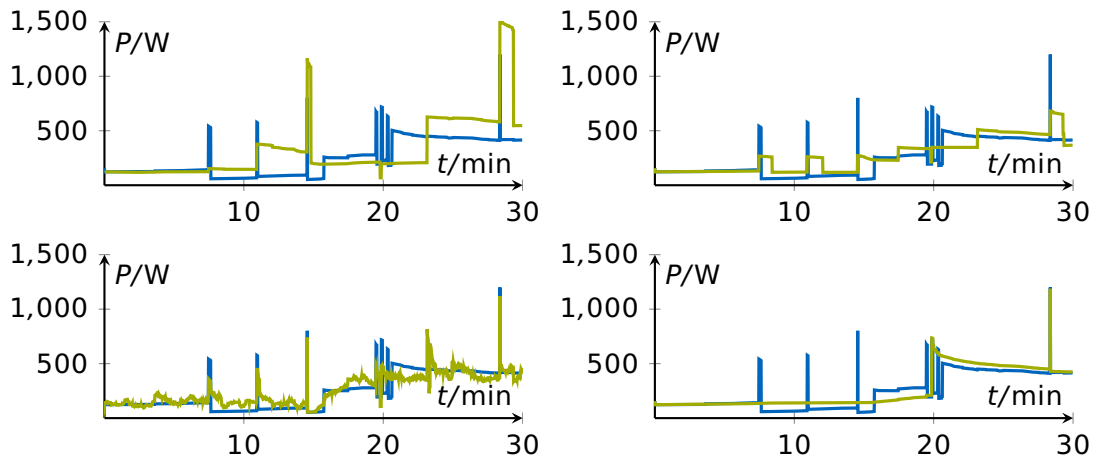


Figure 5.5: Distribution layer's process to compute reference power P_d with modified parameters: top left: decreased energy tracking stiffness $K_{\Delta E} = 0.001 \text{ 1/W}$, top right: decreased switching height parameter $P_{\Delta} = 50 \text{ W}$, bottom left: decreased blur parameter $\alpha = 1$ and bottom right: increased switching rate parameter $\beta = 3.5$. The four identical blue graphs are based on the original parameters as listed in Tab. 5.3, the random input of all graphs is identical to that one used in Fig. 5.4

Table 5.5: List of parameters for the distribution layer's random process model, as illustrated in Fig. 5.6

variable	value	variable	value
T_P	130 s	$K_{\Delta E}$	0.01 1/W
P_{Δ}	140 W	α	15
β	3	K_P	0.83

The bottom right diagram shows the impact of the switching rate parameter, which is increased from $\beta = 3.0$ to $\beta = 3.5$. The effect is a significant reduced amount of spikes and steps. The pulsing at $t = 20 \text{ min}$ turns into an individual step.

Multiple simulations show that the energy tracking stiffness $K_{\Delta E}$ increases the overall tracking of the reference and causes increased amounts of spike and step events, which last shorter. The switching height parameter P_{Δ} mainly increases the height of the spike and step events and decreases the spike width. The blur parameter α mainly increases the flatness of the segments between the individual spikes and steps. The switching rate parameter β mainly decreases the amount of peak and step events.

The random load dispatch process including the true impact of the recovery dynamics by assuming $P = P_d$ is illustrated in Fig. 5.6, based on the parameters of Tab. 5.5. It shows entirely 1 h of 1 s-sampled measured and model generated data. Previous reference measurement data is this period's segment from $t = 23 \text{ min}$ to $t = 53 \text{ min}$. From $t = 0 \text{ min}$ to $t = 4 \text{ min}$ the measured data shows a pulsing of about 1200 W with different heights and durations. The model behavior shows diverse patterns, including random pulsing, steps, approximately flat and drifting segments, and pikes with random heights and widths, which show similar stochastic properties as the previously described

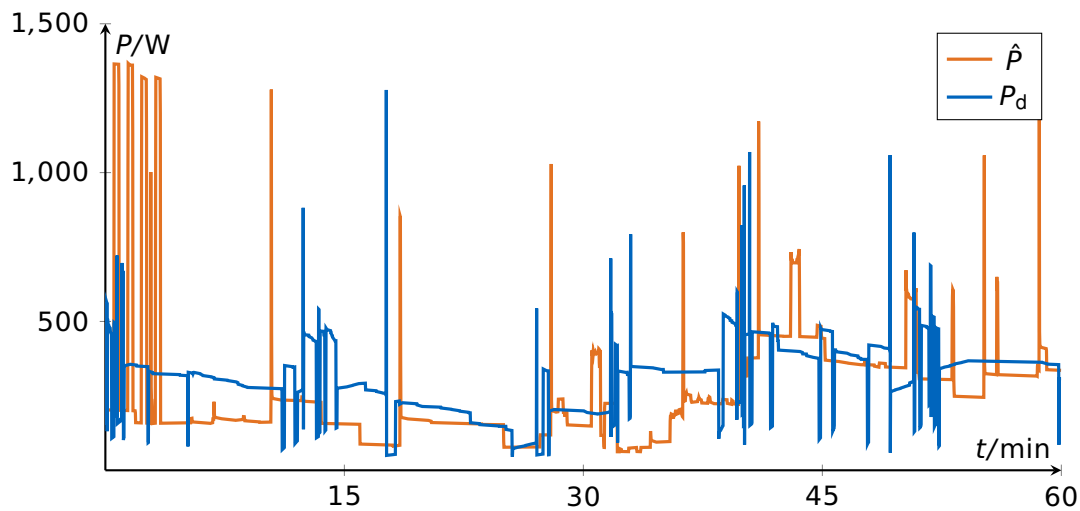


Figure 5.6: Distribution layer's random process model including the feedback of the random process equation on the recovery dynamics, by assuming $P = P_d$. Measured data \hat{P} and modeled data P_d , based on parameters from Tab. 5.5

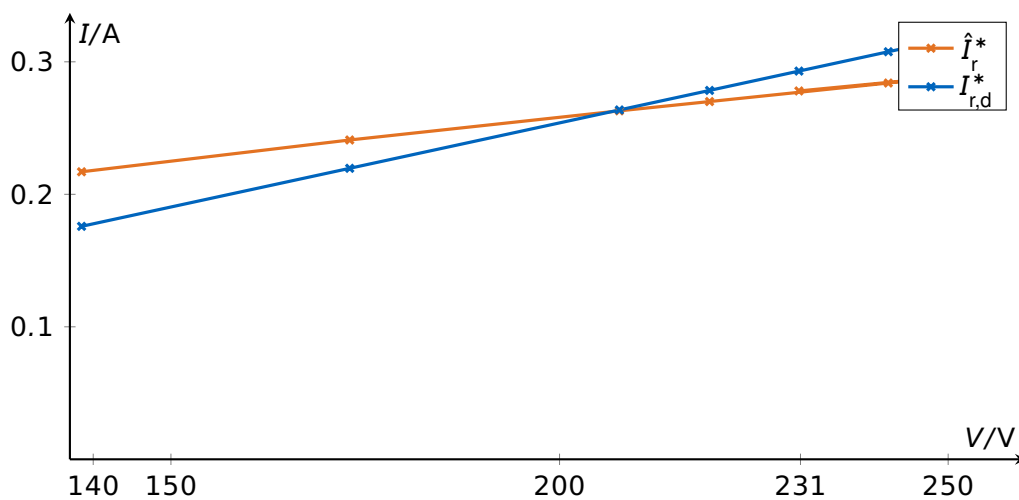


Figure 5.7: Current consumption of an exemplary resistive consumer: Measured steady state current I_r^* depending on given voltage V of the light bulbs from Tab. 5.1

pure random process analyses. The consideration of the recovery dynamics through the recovery proportion K_P has an impact on the system behavior, which requires an adaption of the energy tracking stiffness $K_{\Delta E}$.

Provision layer steady state analysis

The provision layer mainly distinguishes resistive, SMPS and motor loads, while motor loads consist of universal and induction motor load components. The steady state of these devices consists of the current magnitude after settling I^* depending on the given voltage V . Resistive loads are trivial and show high model accuracies, as exemplarily illustrated in Fig. 5.7. Different SMPS devices are investigated, the exemplary steady state results

Table 5.6: List of parameters for the provision layer's SMPS model, as illustrated in Fig. 5.8

variable	value	variable	value
T_s	195 W/mF	ρ	900 Ω /W
$P_{s,d}$	33 W		

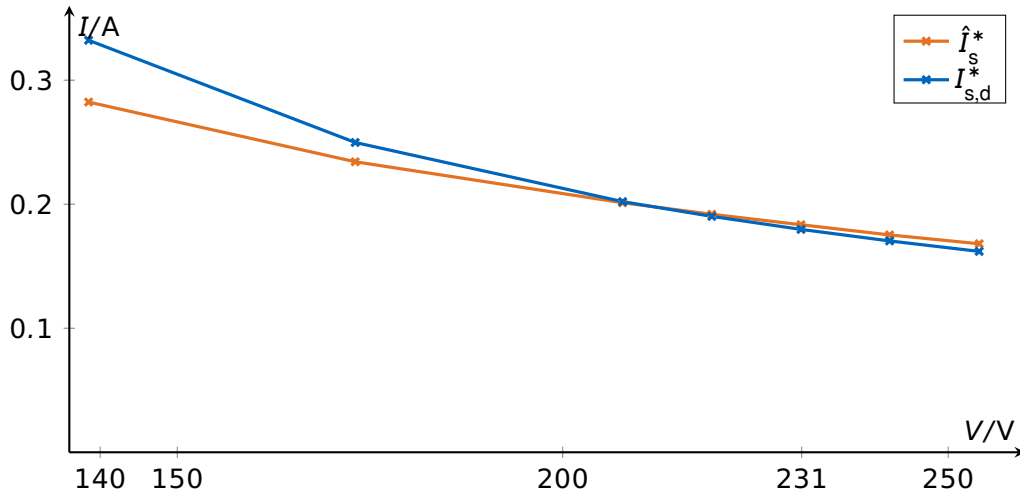
Figure 5.8: Current consumption of an exemplary SMPS consumer: Measured steady state current I_s^* depending on given voltage V of the notebook charger from Tab. 5.1 - a small pure resistive component of 6 W has been subtracted

Table 5.7: List of parameters for the provision layer's universal motor model, as illustrated in Fig. 5.9

variable	value	variable	value
$P_{m,d}$	802 W	$\cos \varphi_{m,n}$	0.9
$K_{m,V}^*$	1	$K_{m,\omega}^*$	0
$K_{m,V}$	4.5 Ams/V	$K_{m,\omega}$	0 Ams/rad
$T_{m,V}$	0.34 s	$T_{m,\omega}$	0 s

of the notebook charger from Tab. 5.1 are illustrated in Fig. 5.8. Analyses have shown a 6 W resistive component, which is subtracted for all investigations with this device. The result shows the typical current drop for higher voltages. The measurement and the model I^* - V -trajectory have a similar shape, with limitations in the different slope. The point of intersection and the local similarity depends on the model parameters. Voltages below 140 V typically cause diverse different reactions, like disabling of the devices or highly nonlinear, not predictable behaviors.

The steady state behavior of motor loads highly depend on whether it is an universal or an induction motor. Universal motors typically show a mainly linear increase of the current consumption with increasing voltages. An exemplary modeled and measured trajectory of the vacuum cleaner mentioned in Tab. 5.1 is illustrated in Fig. 5.9. The voltage trajectories show a similar behavior. Differences in the flatness of the trajectory are not visible. The

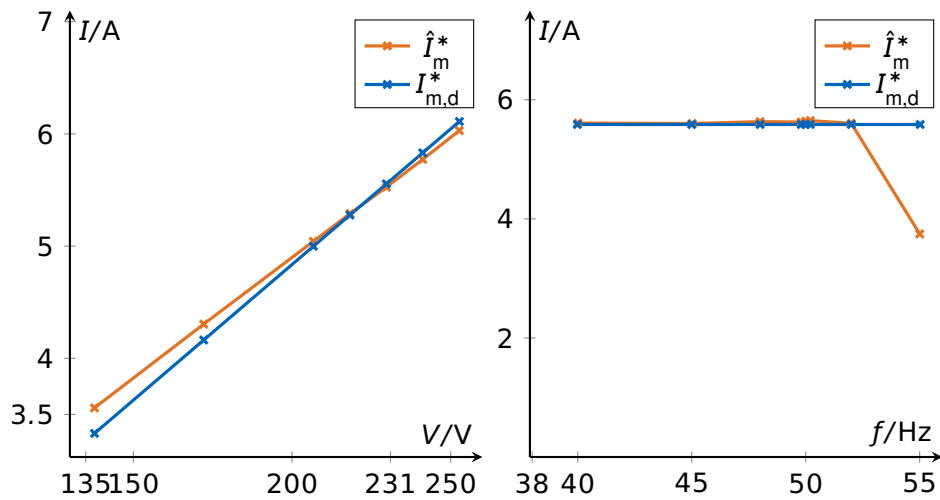


Figure 5.9: Current consumption of an exemplary universal motor consumer: Measured steady state current I_m^* depending on given voltage V or frequency f of the vacuum cleaner from Tab. 5.1

Table 5.8: List of parameters for the provision layer's induction motor model, as illustrated in Fig. 5.10

variable	value	variable	value
$P_{m,d}$	140 W	$\cos \varphi_{m,n}$	0.9
$K_{m,V}^*$	0	$K_{m,\omega}^*$	1
$K_{m,V}$	8 Ams/V	$K_{m,\omega}$	3.3 Ams/rad
$T_{m,V}$	0.014 s	$T_{m,\omega}$	0.02 s

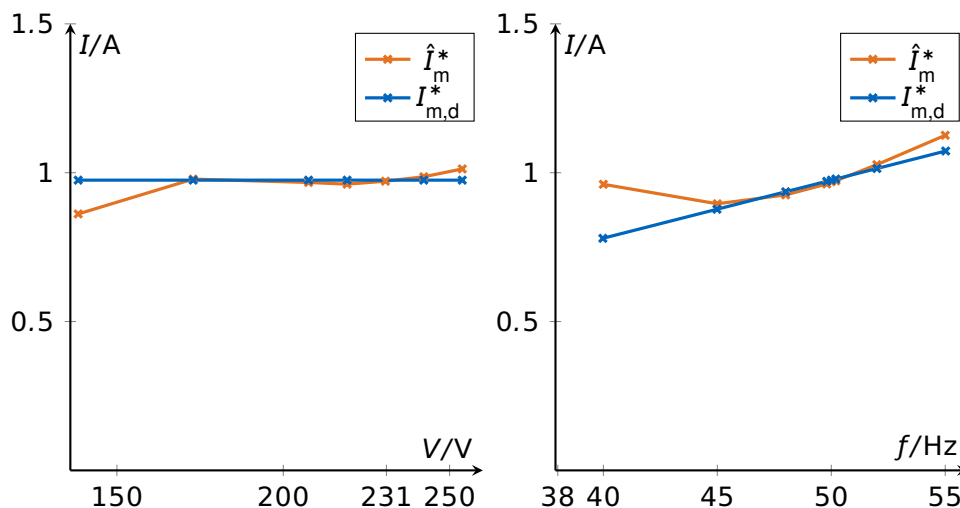


Figure 5.10: Current consumption of an exemplary induction motor consumer: Measured steady state current I_m^* depending on given voltage V or frequency f of the waste water pump from Tab. 5.1

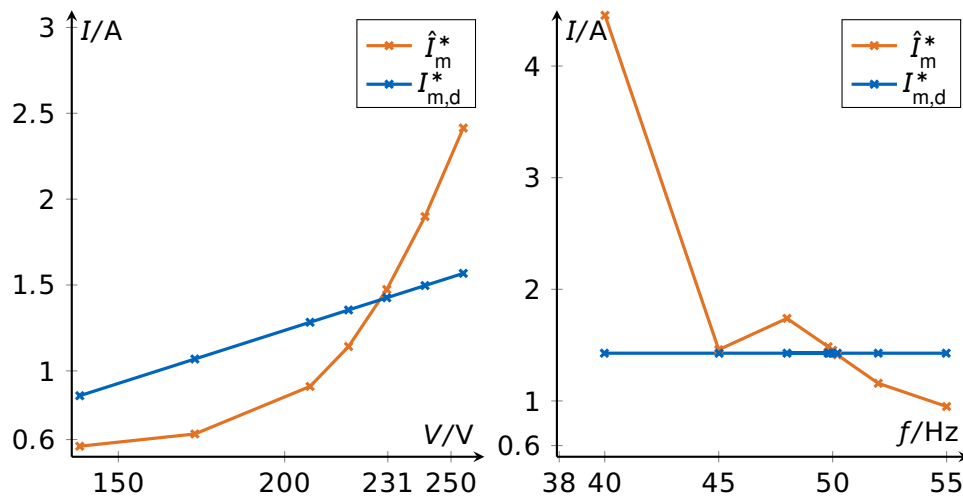


Figure 5.11: Worst case model accuracy: Measured steady state current I_m^* depending on given voltage V or frequency f of the pure induction motor at idle from Tab. 5.1: modeled as universal motor for slightly better results

difference between both trajectories is that the measured data illustrates a flatter slope with a small offset, which results in only an affine relation between current and voltage. The linear model behavior compensates part of the error by the slightly steeper slope. There is no visible frequency dependency, except at high frequencies of 55 Hz, which causes an about 33% reduced current. Induction motors typically consume a mainly voltage independent amount of current. An exemplary modeled and measured trajectory of the waste water pump mentioned in Tab. 5.1 is illustrated in Fig. 5.10. Only at extreme high or low values, voltage dependencies are visible. The frequency dependency is linear, besides low frequencies in a range of about 40 Hz. Also high frequencies in a range of 55 Hz show significant model inaccuracies. All investigated other consumer devices show similar accurate behaviors as the illustrated vacuum cleaner and the waste water pump. An exemplary device with a low modeling accuracy is the pure induction motor at idle. It is illustrated with the better fitting universal motor model in Fig. 5.11, showing significant different behavioral patterns.

Provision layer distinct devices dynamic analysis

The dynamic behavior of the provision layer's model components is separately analyzed for the individual devices, based on different step responses. Resistive components are trivial and due to their ideal behavior not further illustrated. SMPS devices show a significant voltage dependency, which is exemplarily illustrated in Fig. 5.12 for the notebook charger at a -25% voltage step. Larger negative voltage steps cause a decreasing of the current consumption until zero, which lasts longer. Positive voltage steps cause an approximately proportional increasing of the current. Significant limitations of the model are mainly based on steady state deviations, which are discussed in the previous section. A significant frequency dependency is not observable. The global validity of the dynamic model accuracy is evaluated based on multiple step responses and comparing modeled

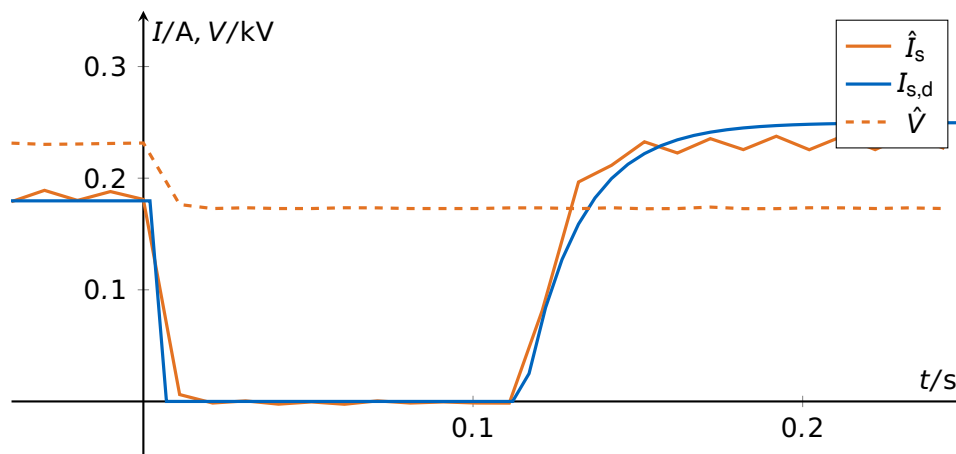


Figure 5.12: Step response of the notebook charger from Tab. 5.1 as an SMPS load component, with a pure resistive component of 6 W being subtracted: A -25% voltage step \hat{V} , the measured \hat{I}_s and modeled $I_{s,d}$ current response

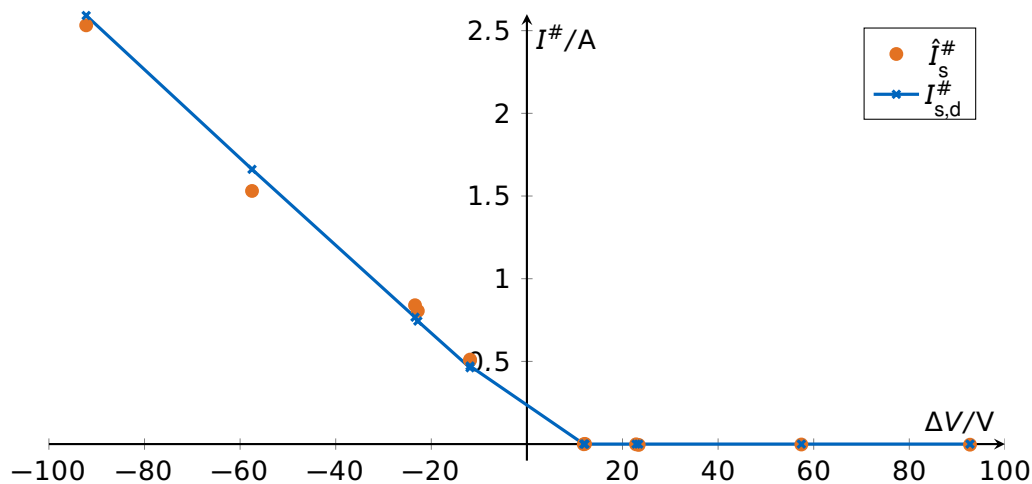


Figure 5.13: Current peaks $I_s^\# = \text{peak}(I_s)$ of the notebook charger from Tab. 5.1, depending on voltage step $\Delta V = V_0 - V^*$: Measured $\hat{I}_s^\#$ and modeled $I_{s,d}^\#$ values

and measured current absolute peak heights $I_s^\# = \text{peak}(I_s)$. This current peak values $I_s^\#$ are compared against the voltage step heights, which are calculated as the value before the step subtracted by the value after the step

$$\Delta V = V_0 - V^*.$$

The peaks are typically zero for decreasing voltage steps $\Delta V > 0$ and linearly increasing for increasing steps. The model shows globally accurate step heights.

Motor loads typically are sensitive on voltage and frequency changes. The response on a voltage and frequency step of an universal motor load is exemplarily illustrated in Fig. 5.14. Except the minor noise of the measured current signal and steady state deviations, the voltage step responses show no significant modeling deviations. The modeled and the measured step responses settle after an initial peak to their steady

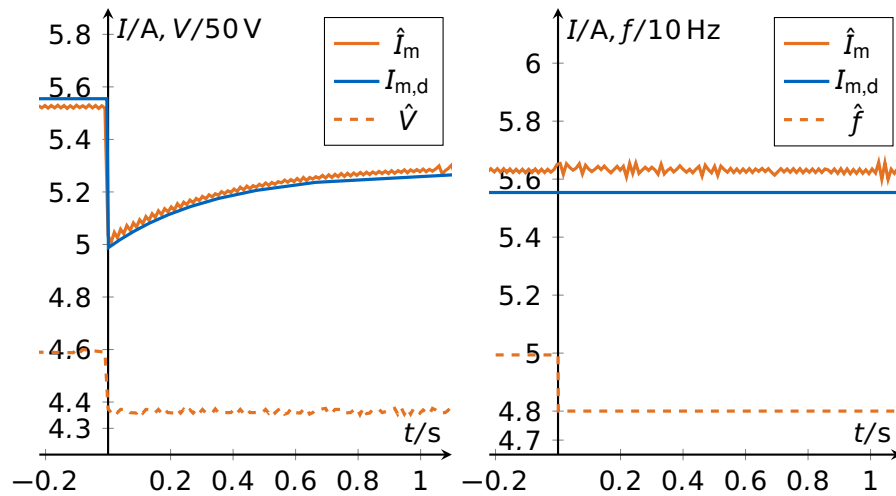


Figure 5.14: Step response of the vacuum cleaner from Tab. 5.1 as a universal motor load component: A -25% voltage step \hat{V} , a -4% frequency step \hat{f} and the appropriate measured \hat{I}_m and modeled $I_{m,d}$ current responses

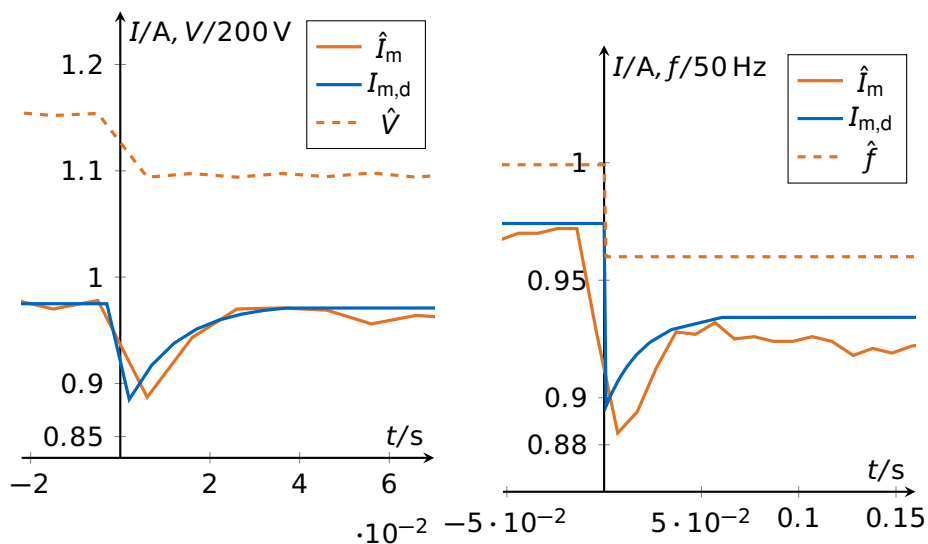


Figure 5.15: Step response of the waste water pump from Tab. 5.1 as an induction motor load component: A -25% voltage step \hat{V} , a -4% frequency step \hat{f} and the appropriate measured \hat{I}_m and modeled $I_{m,d}$ current responses

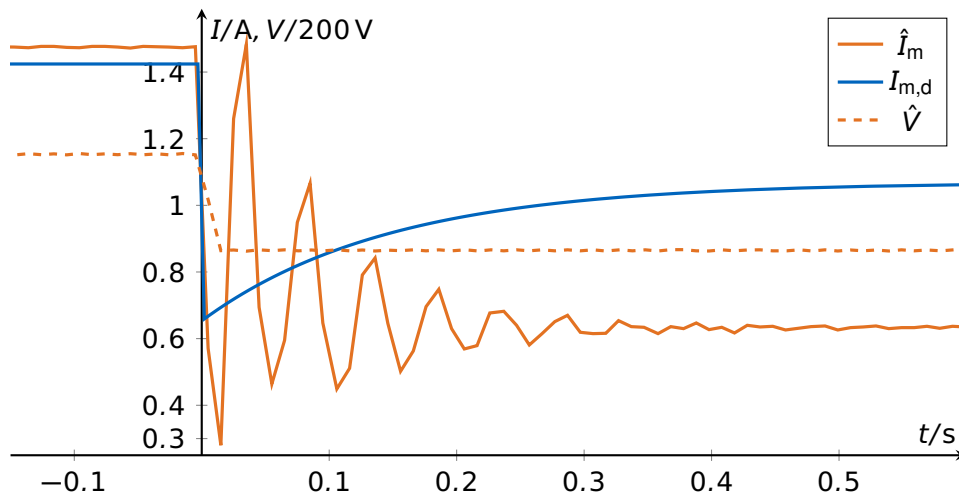


Figure 5.16: Worst case model accuracy: Step response of the pure induction motor at idle from Tab. 5.1 as a universal motor load component: A -25% voltage step \hat{V} and the appropriate measured \hat{I}_m and modeled $I_{m,d}$ current responses

state value. The only significant current reaction on a frequency step from 50 Hz to 48 Hz is an increasing noise. The model also shows no frequency dependency due to the appropriate proportionality parameter equals zero $K_{m,\omega} = 0$. The response on a voltage and frequency step of an induction motor load is exemplarily illustrated in Fig. 5.15. The most significant difference to the previous illustration is the faster settling process. Sampling deviations and measurement noise cause significant deviations between the measured and the modeled current trajectories. The frequency behavior of the induction motor is significant. Considering only the steady state, the induction motor does not show significant voltage dependencies, but still a dynamic reaction on voltage steps as a short current peak is observable. An extreme worst case scenario is illustrated in Fig. 5.16 which shows the current response of the pure induction motor at idle on a voltage step. Beneath the above discussed steady state deviations, this motor shows a significant oscillating settling process, which is not included in the model. All other investigated real motors show results similar to that ones from Fig. 5.14 or Fig. 5.15.

The global validity of the dynamic model accuracy is evaluated based on multiple step responses and comparing modeled and measured current peak heights. The current peak height is calculated as the steady state value, subtracted by the peak current

$$I_m^\# = I_m^* - \text{peak}(I_m).$$

This current peak height $I_m^\#$ is compared against voltage or frequency step heights $\Delta V = V_0 - V^*$ respectively $\Delta f = f_0 - f^*$. The peak heights for the exemplary universal motor load are illustrated in Fig. 5.17. Significant deviations result mainly for high voltage steps in a region of $\Delta V = 60\text{ V}$ and larger, which corresponds to steps from high values to lower values. Similar results are obtained for the induction motor load in Fig. 5.18. A fundamental observation is that the current peak height $I_m^\#$ does not significantly depend on the initial voltage, as different initial voltage experiments with same step heights ΔV result in almost identical current peak heights. The global validity of the induction motor load's

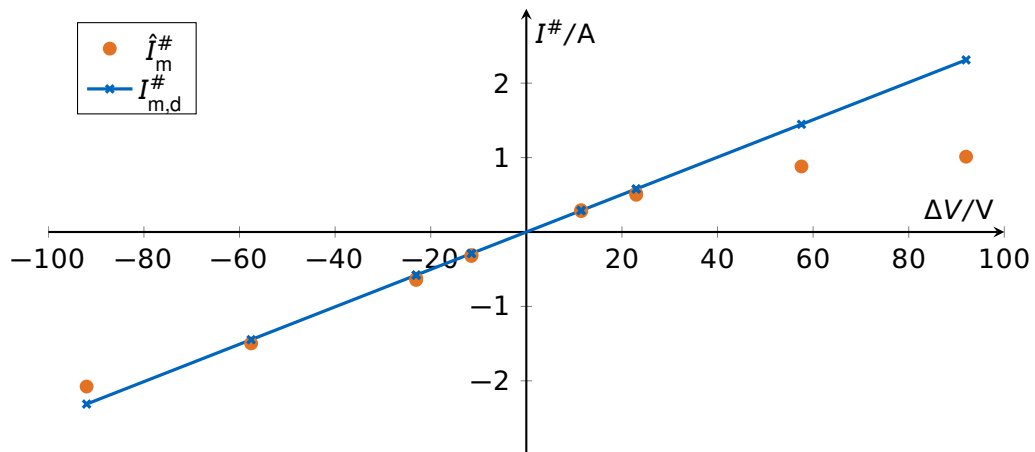


Figure 5.17: Current peaks $I_m^{\#} = I_m^* - \text{peak}(I_m)$ of the vacuum cleaner from Tab. 5.1, depending on voltage step $\Delta V = V_0 - V^*$: Measured $\hat{I}_m^{\#}$ and modeled $I_{m,d}^{\#}$ values

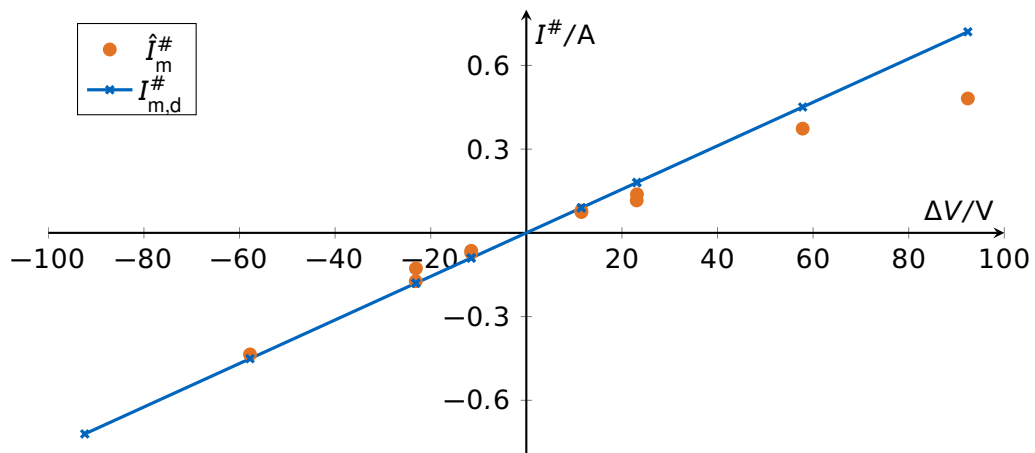


Figure 5.18: Current peaks $I_m^{\#} = I_m^* - \text{peak}(I_m)$ of the waste water pump from Tab. 5.1, depending on voltage step $\Delta V = V_0 - V^*$: Measured $\hat{I}_m^{\#}$ and modeled $I_{m,d}^{\#}$ values

frequency dependency is illustrated in Fig. 5.19. Especially for frequency steps larger than $\Delta f = \pm 5$ Hz significant model deviations are observable. All significant model deviations are in the negative direction, which means that peak heights after increasing frequency steps are overestimated, and after decreasing frequency steps are underestimated by the model. A significant dependency on the initial frequency I_0 is observed for a frequency step of $\Delta f = 5$ Hz, which includes one step from $f_0 = 50$ Hz to $f^* = 45$ Hz and a step from $f_0 = 55$ Hz to $f^* = 50$ Hz.

Provision layer coupled dynamic analysis

This subsection illustrates the behavior of the overall provision layer model, by simulating the measured behavior of multiple different household devices from Tab. 5.1 as an emulated household load. The only used model parameters are listed in Tab. 5.9. These parameters are heuristically optimized for the overall behavior. The steady state voltage

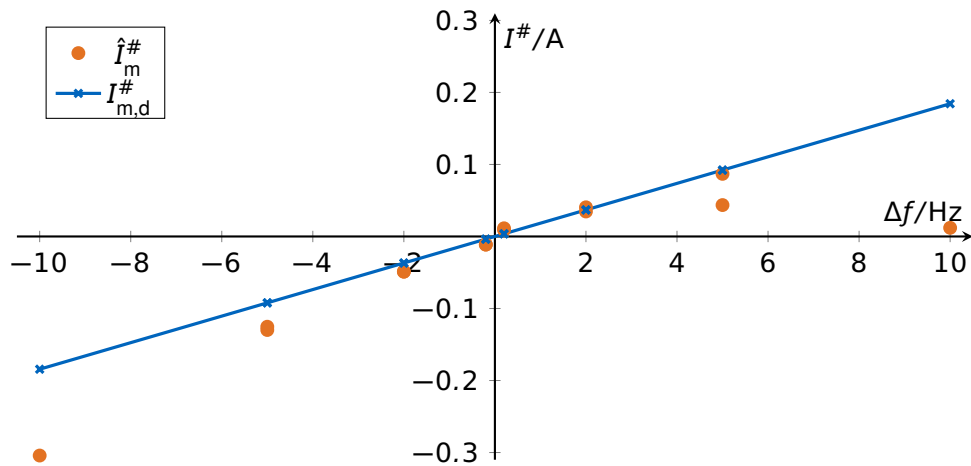


Figure 5.19: Current peaks $I_m^{\#} = I_m^* - \text{peak}(I_m)$ of the waste water pump from Tab. 5.1, depending on frequency step $\Delta f = f_0 - f^*$: Measured $\hat{I}_m^{\#}$ and modeled $I_{m,d}^{\#}$ values

Table 5.9: List of parameters for the provision layer's multiple different household devices from Tab. 5.1 as an emulated household load, as illustrated in Fig. 5.20 et seqq.

variable	value	variable	value
$P_{r,d}$	60 W	$P_{s,d}$	19 W
T_s	190 W/mF	ρ	1700 Ω /W
pf	0.58	$\varphi_{s,n}$	-16 deg
$P_{m,d}$	273 W	$\varphi_{m,n}$	3 deg
$K_{m,V}^*$	0.13	$K_{m,\omega}^*$	0.5
$K_{m,V}$	7.5 Ams/V	$K_{m,\omega}$	2.5 Ams/rad
$T_{m,V}$	20 ms	$T_{m,\omega}$	25 ms

and frequency dependency is illustrated in Fig. 5.20. Noticeable results are an almost flat voltage dependency and a significantly bent frequency dependency \hat{I}^* . Significant model deviations are mainly at extreme low frequencies with a relative modeling error of about 11% at 40 Hz, which causes even higher currents than at 50 Hz. Other significant deviations, at a frequency of 55 Hz and voltages beyond 200 V, are at a magnitude of about 5%.

The dynamic voltage behavior, analyzed through step response investigations, is illustrated in Fig. 5.21. Noticeable is the significant different behavior of positive and negative steps. Negative steps show an initial peak and a delayed step to its steady state current. Positive steps only show an initial peak. Peak heights and the delay time of the step to its steady state current correlate with step height. Besides steady state deviations and measurement noise, slight deviations of the peak shape are observed. The dynamic frequency dependency is illustrated in Fig. 5.22. Noticeable is the initial peak to be significantly lower than the voltage caused peaks, and the higher impact of measurement noise. The clear shape of the measured current peak is blurred.

The global validity of the dynamic model accuracy is evaluated by comparing peak heights. The measurement and simulation results are illustrated in Fig. 5.23. Noticeable

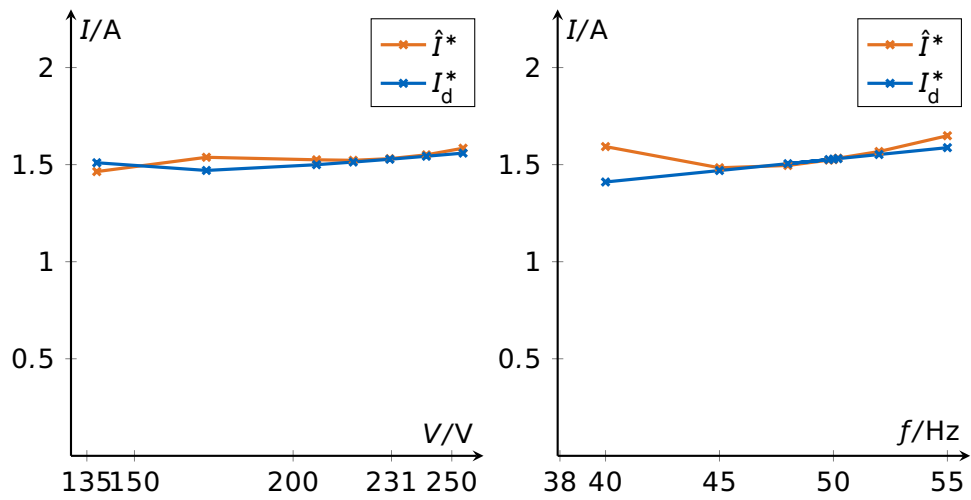


Figure 5.20: Measured steady state current I^* depending on given voltage V and frequency f of multiple different household devices from Tab. 5.1 as an emulated household load

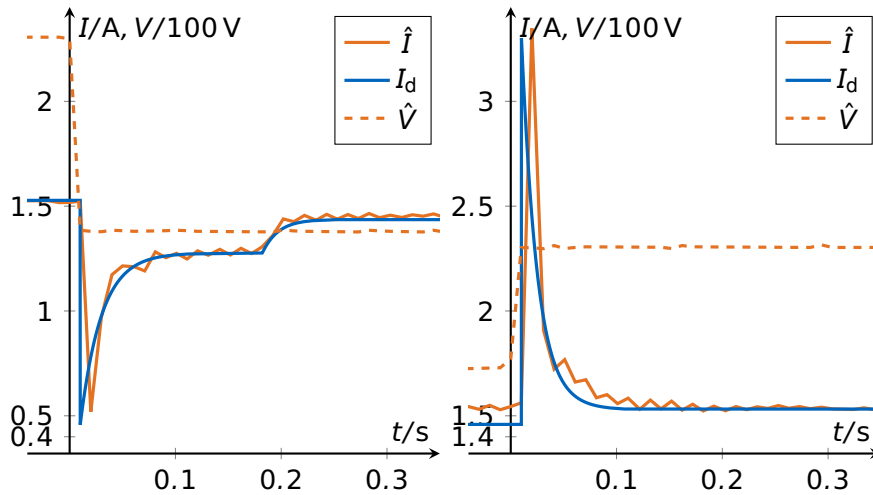


Figure 5.21: Step response of the multiple different household devices from Tab. 5.1 as an emulated household load: A -40% and a $+25\%$ voltage step \hat{V} and the appropriate measured \hat{I} and modeled I_d current responses

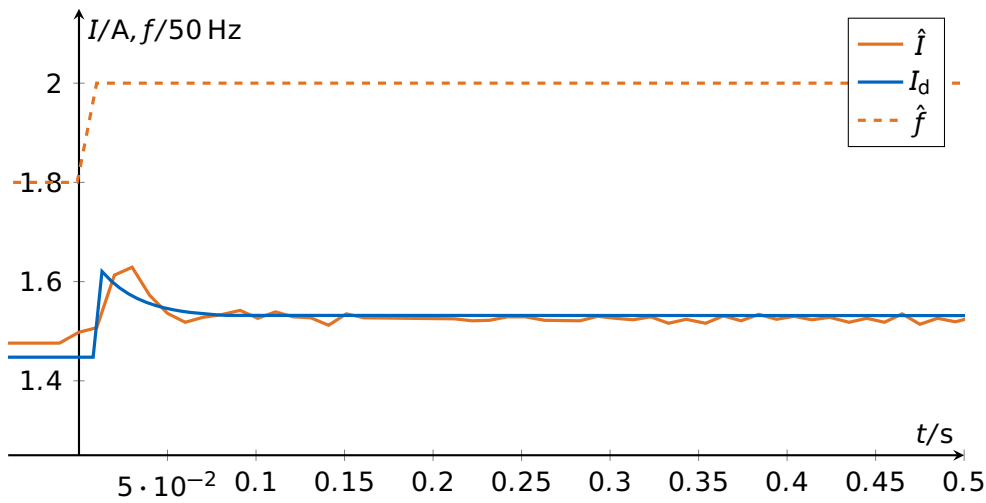


Figure 5.22: Step response of the multiple different household devices from Tab. 5.1 as an emulated household load: A +10% frequency step \hat{f} and the appropriate measured \hat{I} and modeled I_d current responses

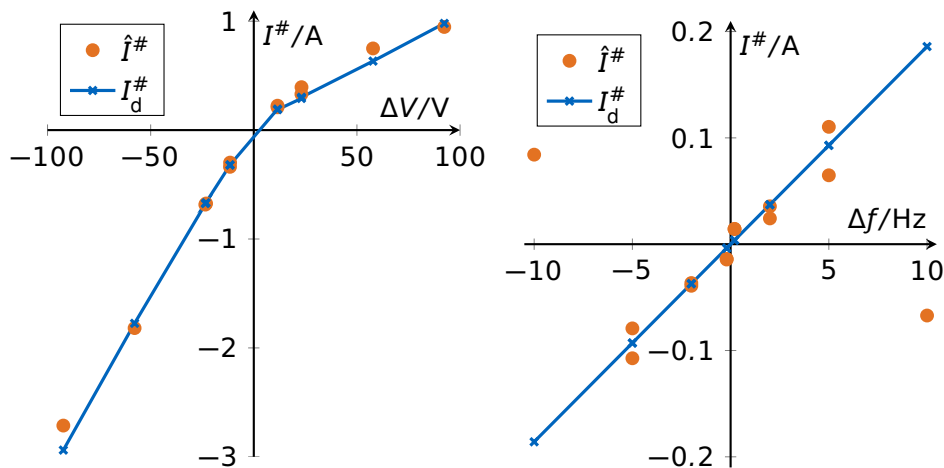


Figure 5.23: Current peak $I^\# = I^* - \text{peak}(I)$ of the multiple different household devices from Tab. 5.1 as an emulated household load, depending on voltage step $\Delta V = V_0 - V^*$ and on frequency step $\Delta f = f_0 - f^*$: Measured $\hat{I}^\#$ and modeled $I_d^\#$ values

is the significant different peak height of positive and negative peaks caused by voltage steps and the model error of high frequency steps of ± 10 Hz, where the sign of the step height changes. This model error results from the measured steady state current that is higher at 40 Hz than at 50 Hz, as illustrated in Fig. 5.20. This causes a reversed modeled step response in comparison to the measured one. Other model deviations are in a range of measurement noise.

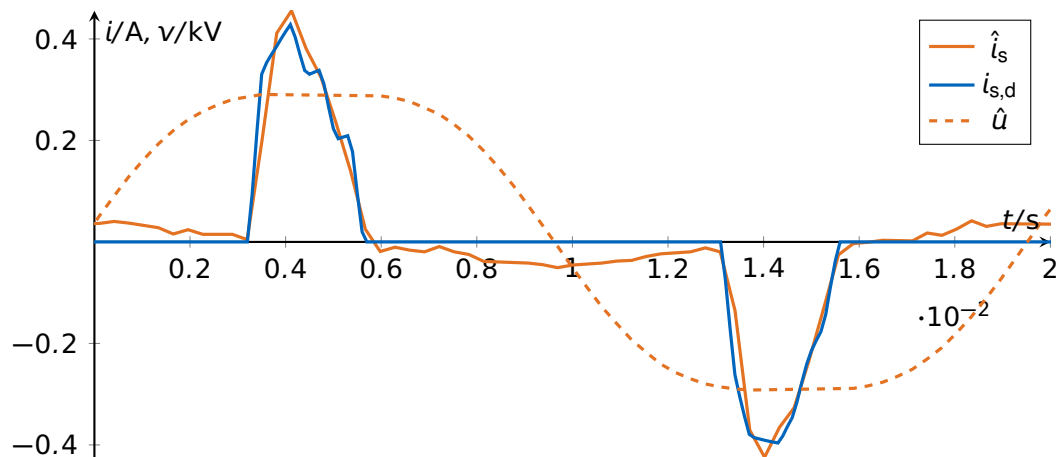


Figure 5.24: Notebook charger's modeled and simulated current reaction on nominal voltages disturbed by a 10% in-phase 3rd order harmonic oscillation

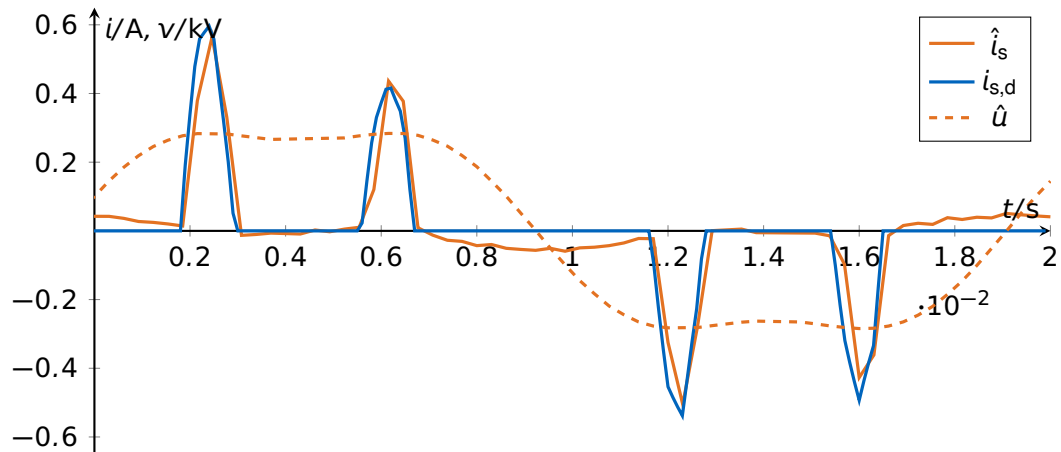


Figure 5.25: Notebook charger's modeled and simulated current reaction on nominal voltages disturbed by a 20% in-phase 3rd order harmonic oscillation

System layer analysis

The dynamic behavior of the system layer's model components is analyzed for aforementioned individual appliances and the multiple different household devices. Results are explicitly shown for the notebook charger as an SMPS device, the waste water pump as a machine load device and the multiple different household devices. Resistive devices have trivial behaviors and show ideal simulation results. The model accuracy is evaluated based on comparing the measured and simulated instantaneous current reactions on differently shaped voltage oscillations. The systematic analyses are based on nominal voltage oscillations, with a 10%, a 20% and a 50% 3rd harmonic oscillation, a 20% 5th harmonic oscillation and a 20% 3rd and 20% 5th harmonic oscillation. All harmonics are in phase with the fundamental oscillation.

The real and the simulated behavior of pure SMPS devices are exemplary illustrated in Fig. 5.24 to 5.26 based on the notebook charger from Tab. 5.1. The typical current

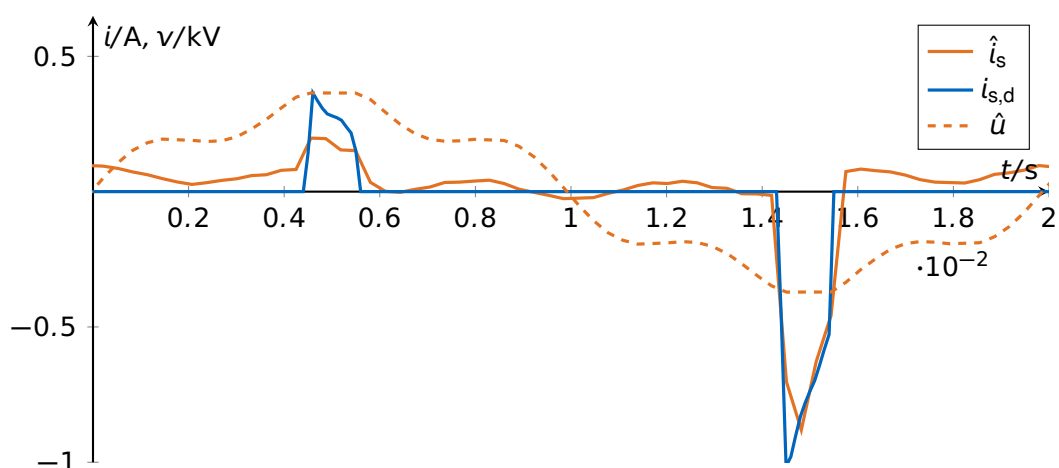


Figure 5.26: Notebook charger's modeled and simulated current reaction on nominal voltages disturbed by a 20% in-phase 5th order harmonic oscillation

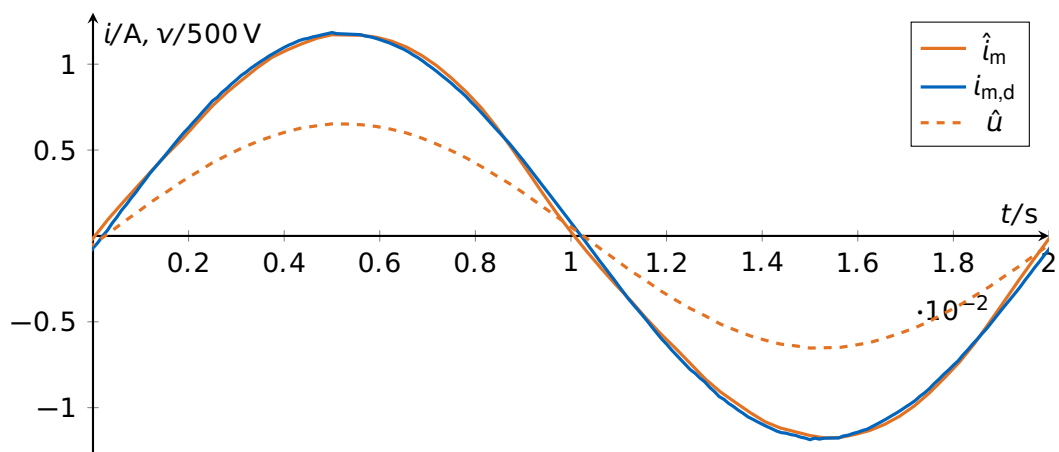


Figure 5.27: Waste water pump's modeled and simulated current reaction on nominal voltages

peaks of SMPS devices during voltage peaks are replicated without significant deviations. The real measured current contains a lagging sinusoidal component with an amplitude of about 10% of the peak height which is not replicated by the model. The result of Fig. 5.26 shows asymmetric peak heights, such that positive peaks are about 20 – 40% the height of the negative peaks. Positive peaks show a significant modeling deviation. The underlying voltage signal contains a significant negative DC component.

The real and the simulated behavior of pure motor devices is exemplarily illustrated in Fig. 5.27 to 5.29 based on the waste water pump from Tab. 5.1. The shape of the simulated and the measured current reactions on nominal voltages in Fig. 5.27 show no significant deviations. Harmonic voltage disturbances cause significant model deviations in varying magnitudes and characteristics. Harmonic distortions of the 5th order show significantly higher modeling accuracies than 3rd order harmonic distortions, as illustrated in Fig. 5.28 and Fig. 5.29. Especially asymmetric distortions which cause differently

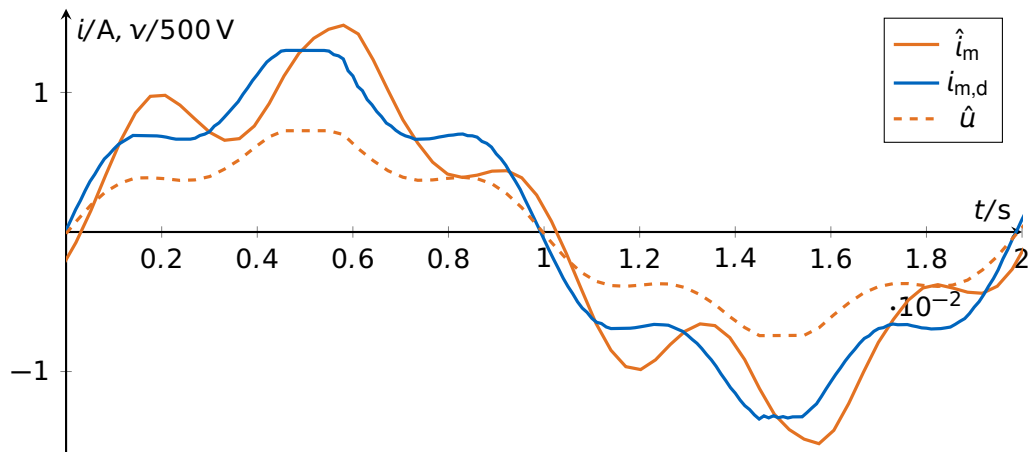


Figure 5.28: Waste water pump's modeled and simulated current reaction on nominal voltages disturbed by a 20% in-phase 5th order harmonic oscillation

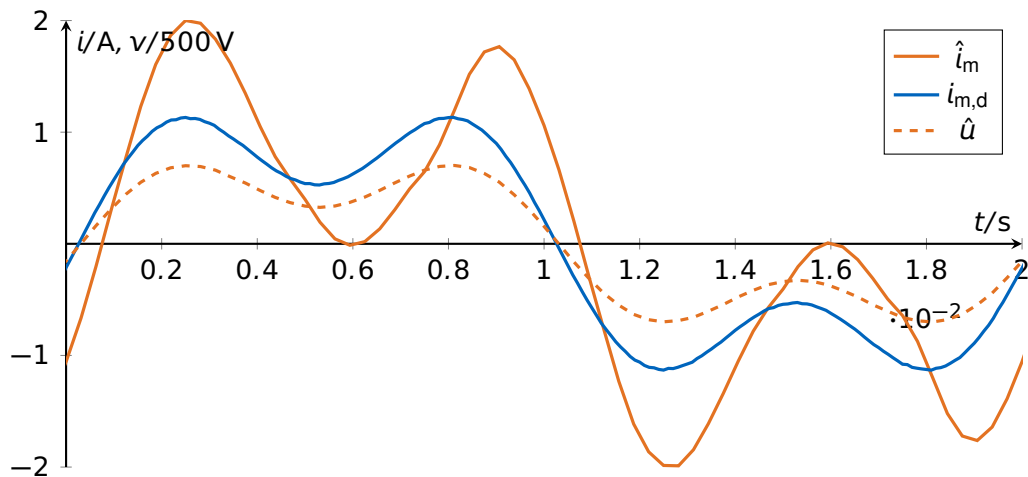


Figure 5.29: Waste water pump's modeled and simulated current reaction on nominal voltages disturbed by a 50% in-phase 3rd order harmonic oscillation

shaped increasing and decreasing oscillation quarters are not replicated.

The real and the simulated behavior of an overall household are exemplarily illustrated in Fig. 5.30 to 5.32 based on multiple different household devices from Tab. 5.1. The fundamental behavior is replicated for all different scenarios, with significant individual modeling deviations. A significant result is, that 5th order harmonics as illustrated in Fig. 5.32 cause less modeling deviations than 3rd order harmonic distortions, as illustrated in Fig. 5.31. Remarkable is the phase shift of the peak with almost sinusoidal voltages in Fig. 5.30, which is not contained in the other results in Fig. 5.31 and 5.32.

5.1.3 Analysis and interpretation of the results

The analysis and interpretation of the model accuracy, based on the previous described experimental results, are based on different fundamental principles. Dynamic effects, like

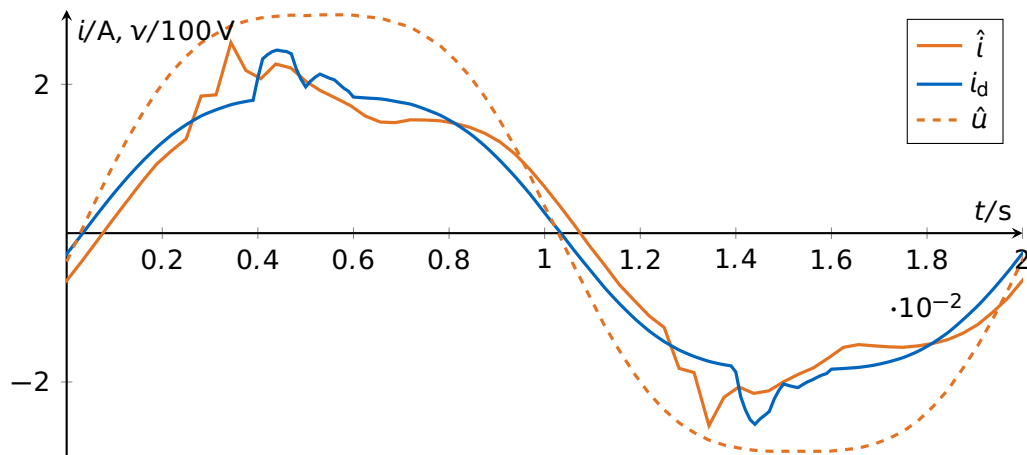


Figure 5.30: Multiple different household devices' modeled and simulated current reaction on nominal voltages disturbed by a 10% in-phase 3rd order harmonic oscillation

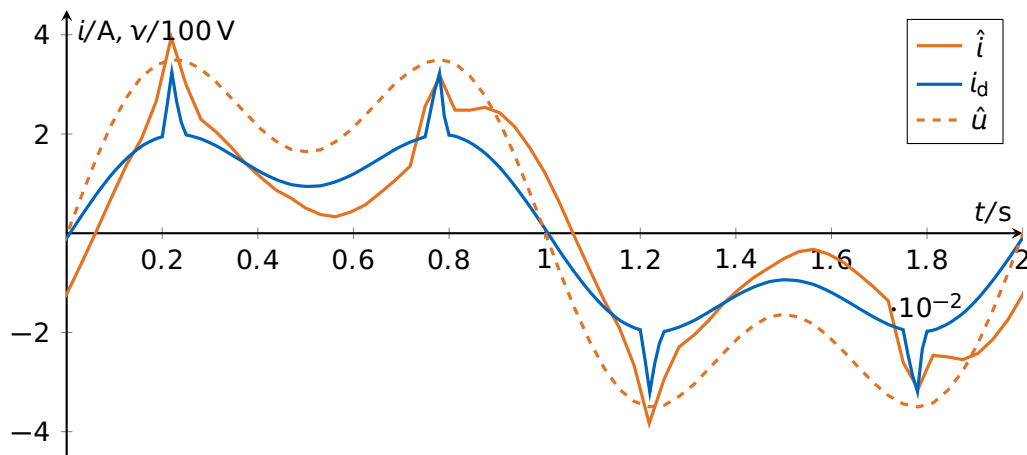


Figure 5.31: Multiple different household devices' modeled and simulated current reaction on nominal voltages disturbed by a 50% in-phase 3rd order harmonic oscillation

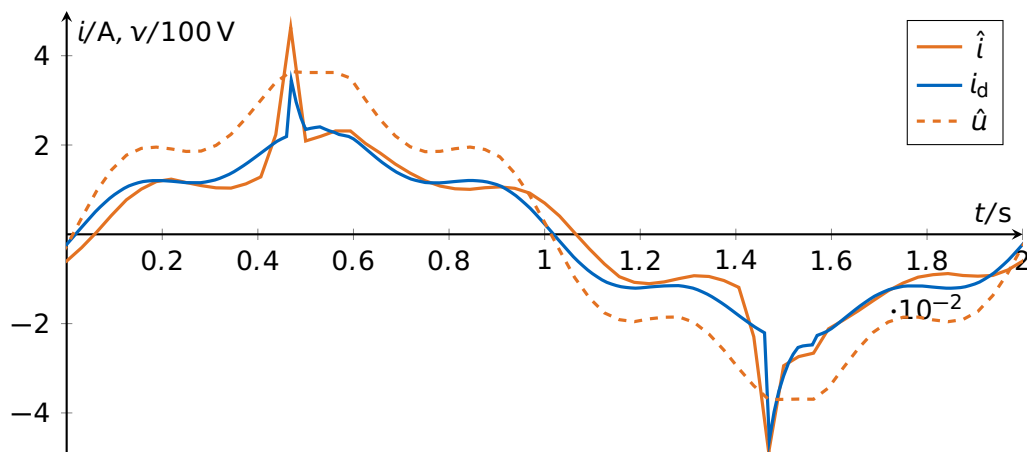


Figure 5.32: Multiple different household devices' modeled and simulated current reaction on nominal voltages disturbed by a 20% in-phase 5th order harmonic oscillation (a dc component of 2 V has been compensated for the model calculation)

the recovery dynamics, can exactly be evaluated based on step responses. This means two linear systems are identical if they show an identical step response, which means the closer the step response the better the model. This principle does not hold for nonlinear systems, which energy system components typically are. But step response analysis of nonlinear systems, especially good natured ones, is still a good indication for the dynamic model accuracy and hence reasonable to be applied.

Static model accuracy, which refers to deviations of the model to the reference steady state, has to be validated over the entire defined state space. Often nonlinear system components, especially good natured ones, cause primary steady state deviations, like distorting deviations of the linearized system response, and less often the dynamic settling process itself. This requires to at least investigate the entire work space, which in practice means to analyze several points in the workspace.

Supply layer

The supply layer's model component, as shown in the previous section and especially in Fig. 5.1, shows entirely good and accurate results. The important aspect of this result is the stochastic nature of the model, which means that basic principles are replicated, but without direct connection between the modeled and the reference behavior. The way of application of the reference mean and standard deviation, and the further model calculations in (4.38)(4.39) ensure that the mean and the standard deviation of multiple trials of the model and the reference behavior are identical. The applied base load ensures that no unrealistic peaks close to zero, or negative values occur. Fundamental model inaccuracies are the not applied time variance of the base load, which could be implemented easily, as it is an explicit parameter. A further inaccuracy is the assumed Weibull distribution of the individual load values. This means that especially high peaks could show significantly different behaviors than the peaks in the reference behavior. Specific time dependent or time variant processes, like regularly repeating uniform load fragments caused by regularly switching of certain appliances, cannot be emulated with this model, due to its stochastic nature. But the typical steep gradients of switching events, as well as the typical duration of peaks can be replicated by the model based on individual parameters. Summing up, this model replicates the stochastic properties of the load well, but specific individual load components are not included to reach a good compromise between accuracy and complexity.

Distribution layer

The distribution layer's recovery dynamics model shows sufficiently accurate results, as shown in the previous section and especially in Fig. 5.2 and Fig. 5.3. Simple experiments show the basic principle of the recovery dynamic process. Consumer applications, which require a specific amount of energy initially react on voltage drops, but will recover the power demand after a while. For example cooking a specific amount of water lasts longer, if the power supply is lower due to voltage variations. An oven will activate the heating element longer or more often to adapt to voltage variations. This means that the energy demand of such processes is independent of the power flow, which leads to the recovery

of the power demand. Other processes like light bulbs typically do not recover their power demand, the slightly weaker light due to voltage variations is typically accepted.

The initial experiment illustrated in Fig. 5.2 shows the fundamental principle of power recovery, by considering several identical water cookers operating at the same time. This leads to a considerable impact of the switching events, which are not implemented in the recovery dynamic model proportion. The settling process of this reference experiment shows a straight recovery trajectory, in contrast to the model with an exponential trajectory. The second experiment, illustrated in Fig. 5.3, adds three fundamental properties. The higher amount of individual devices causes a smoother trajectory. The difference of the devices' types causes an alignment of the reference behavior to the exponential model behavior. The consideration of the light bulbs as non-recovering applications leads to only a partial recovering of the reference behavior, which is emulated accurately by the model. A different share of recovering and non-recovering applications causes a different recovery proportion, which would require an adaption of the recovery proportion parameter K_p . The recovery dynamics model proportion fundamentally emulates the overall behavior of many different appliances with a constant share of recovering and non-recovering ones, very accurately. Individual appliances' behaviors are emulated weakly. This means by considering the model for one single family house, the real recovery dynamic behavior is fundamentally implemented, but details are blurred over multiple different individual consumers, like the entire MG. Due to the stochastic nature with high individual uncertainties, this inaccuracy has negligible impact on most investigations.

The other important aspect of the distribution layer's model is the random process, which up-samples the 15 min energy consumption to a 1 s-based power consumption. The initial experiment in the context of Fig. 5.4 to Fig. 5.6 shows good results. The obvious characteristics of the reference measurements is a switching behavior, which results in steps, peaks and flat trajectory segments, which is caused by the switching of individual consumer devices. Especially stoves and cookers cause the fast pulsing, a frequent on-off switching to control the temperature, similar as illustrated in Fig. 5.6 in the first 4 minutes. The partly marginally stable model causes also such stochastic pulsing behaviors, which realistically represent realistic behavioral patterns. As stated above, the fundamental property of this stochastic model is to emulate the mathematical physical properties of electricity load behavior, while device specific behavioral details are blurred over multiple different individual consumers. The aim to track the reference energy consumption leads to the observed model drifting during flat trajectory segments, which is not observed in the measured data. This won't have significant impact on model accuracy due to its accurate magnitude and low gradient. This tracking finally causes the similarity of the true energy consumption and the reference energy consumption.

The model stochastically emulates many different events, like different high load peaks with various widths, steps and noisy elements. The results in the context of the model variation show that the underlying model properties, being reference tracking, amount of spike and step events, duration of spike and step events, height of spike and step events and the flatness, can be adjusted. These properties are not time variant, as the parameters are not time dependent. The consequences of time dependent parameter implementations are not analyzed, but fundamentally imaginable. This would increase

model complexity significantly. A fundamental limitation is that some parameters influence different properties. This generates an interdependency of individual properties, which can be solved by a sequential parametrization. Starting with the energy tracking stiffness $K_{\Delta E}$ increases the overall tracking of the reference, but causes increased amounts of spike and step events which last shorter. Continuing with the switching height parameter P_{Δ} mainly adapts the height of the spike and step events, but decreases the spike width. The switching rate parameter β adapts the amount of peak and step events and finally the blur parameter α increases the flatness. The width respectively the duration of spikes are directly dependent on the step height, and cannot be independently adapted. This leads to the probably largest limitation of this model, which always depends on a compromise between spike height and spike width. Additionally the shape of the stochastic distribution of the model properties cannot be actively adapted.

The entire conclusion of the distribution layer model is that it emulates the stochastic nature and the fundamental model properties well. Limitations are very detailed properties, like the shape of the distribution of spike height, or time dependent events, like a spike at a specific point in time. Also limitations have to be mentioned for small systems with a significant impact of individual devices, like a constant pulsing is also hardly emulateable.

Provision layer

The provision layer's load model component shows accurate results with some limitations. Resistive loads show high model accuracies, and are not separately discussed. The steady state model behavior of the SMPS devices tends to overestimate the impact of voltage variations. Measurements show a slight increase in power consumption with higher voltages, the model's nature with losses occurring in the resistor causes a decreasing power consumption with higher voltages. This effect can be compensated by considering a higher impact of the resistive model component. Such shifts between the three different groups of devices allow to compensate several individual modeling inaccuracies, like deviations in the steady state voltage dependency of the universal and the induction motor. The steady state frequency dependency is for most individual devices less accurate, especially for both motor types. The measured current drop for higher frequencies of the universal motors could be caused by the interaction of zero crossings and the commutator. Especially the induction motor shows only locally linear steady state behaviors, especially by considering the frequency dependency. This is caused by the complex mechanisms in the induction motor, which cause it to behave more and more nonlinear for increasing deviations to the nominal working space. The worst case example of the pure induction motor, which is operated at idle, shows that at least rare extreme examples exist, which cannot be realistically modeled. As these devices are typically only rarely used, they entirely play only a subordinate role.

The dynamic behavior of the individual components is evaluated based on step responses. As the real device and the model both are based on nonlinearities, the step response analysis is only an indicator for the modeling accuracy. It is extended by the aforementioned steady state analysis and the peak height analysis to indicate the global validity of the individual step response analysis. The SMPS model shows unreliable responses to extreme increasing voltage steps, which are caused by the assumed constant

power factor, which is increasing for high differences between grid and capacity voltages. Several shown deviations, especially the step responses of the waste water pump, are caused by measurement noise and the lower measurement sampling, in contrast to the specified model sampling. Complex behaviors like the shown step response of the artificial worst case example of the pure induction motor at idle shows that devices exist with highly complicated behavioral patterns, which are not included in the model. Furthermore deviations, especially of the peak analyses, are finally noticeable in the working space limits. The negligence of nonlinearities demonstrates at these limits its neglected impact. A further noticeable property is that also dynamic frequency dependent behavioral patterns are typically less accurate than voltage dependent patterns.

The fundamental results of the overall provision layer analysis shows an accurate model behavior. The largest model error of 11% steady state deviation at a frequency of 40 Hz in Fig. 5.20 is caused by the fan, the reason for the unexpected steep increase of its current consumption for frequencies lower than about 43 Hz is not easily accountable. This also causes the errors of peak heights for steps of $\Delta f = \pm 10$ Hz in Fig. 5.23 which is measured through steps between the error containing 40 Hz and 50 Hz. Deviations of peaks, especially the different peak times is caused by the low available measurement sampling and the asynchronous current and frequency measurement. It is obvious that individual inaccuracies of individual devices balance each other.

The overall model accuracy is rated high, by considering the aim to generate a simple model which covers all behavioral patterns of all typically used consumption devices. Model deviations are estimated typically at a magnitude of about 5% for large operating ranges, and significantly lower for smaller operating ranges, by considering a composition of multiple different devices. There exist individual devices which have significantly different behavioral patterns than the model. The noticeable limitations of the provision layer model component are modeling errors at extremely steep and high increasing voltage steps, decreasing modeling accuracies for large deviations of the typical working spaces, especially for frequency deviations and for individual special devices. A further limitation are the assumed constant model parameters, which causes time invariant shares of SMPS, resistive and motor loads, and time invariant properties like settling or peak heights. Additionally, the delayed step to the steady state current as illustrated in Fig. 5.21 (left, at $t = 0.2$ s) can be blurred by multiple different SMPS devices with differently sized capacitors.

System layer

The system layer's load model component replicates the fundamental behavioral patterns, with significant individual modeling deviations. The analysis of model accuracy based on harmonics has the advantage of analyzing the behavior at different conditions, which incorporates dynamical behavioral patterns. Step response analyses require steady state conditions, which would not be realistic operation conditions in AC systems. The difference between positive and negative peak heights of the SMPS component, especially in Fig. 5.26, can only be explained by undesired DC voltage components, which have a high sensitivity due to the high SMPS capacity voltage, which directly enables the SMPS current flow. Modeling deviations considering electric motors are caused by the simple RL-

Table 5.10: List of parameters for the illustrated results of the weather model, based on the reference measurement of Garching

variable	value	variable	value
T_s	1 h		
$A_{0,\mu,\mathcal{I}}$	-0.8	$A_{0,\sigma,\mathcal{I}}$	0.9
$A_{d,\mu,\mathcal{I}}$	1.3	$A_{d,\sigma,\mathcal{I}}$	0.5
$A_{y,\mu,\mathcal{I}}$	0.4	$A_{y,\sigma,\mathcal{I}}$	0.1
$A_{dy,\mu,\mathcal{I}}$	0.0	$A_{dy,\sigma,\mathcal{I}}$	0.0
$\varphi_{d,\mathcal{I}}$	3.3 rad	$\varphi_{y,\mathcal{I}}$	3.9 rad
$T_{\mathcal{I}}$	23 h	ρ	0.83
$A_{0,\mu,\mathcal{A}}$	6.9 deg	$A_{0,\sigma,\mathcal{A}}$	5.1 deg
$A_{d,\mu,\mathcal{A}}$	3.2 deg	$A_{d,\sigma,\mathcal{A}}$	0.8 deg
$A_{y,\mu,\mathcal{A}}$	10.6 deg	$A_{y,\sigma,\mathcal{A}}$	-1.3 deg
$A_{dy,\mu,\mathcal{A}}$	2 deg	$A_{dy,\sigma,\mathcal{A}}$	-0.2 deg
$\varphi_{d,\mathcal{A}}$	2.6 rad	$\varphi_{y,\mathcal{A}}$	2.8 rad
$T_{\mathcal{A}}$	30 h	$\zeta_{\mathcal{I}/\mathcal{A}}$	0.59
$A_{0,\mu,\mathcal{W}}$	2.3 m/s	$A_{0,\sigma,\mathcal{W}}$	2.0 m/s
$A_{d,\mu,\mathcal{W}}$	0.8 m/s	$A_{d,\sigma,\mathcal{W}}$	-0.1 m/s
$A_{y,\mu,\mathcal{W}}$	-0.5 m/s	$A_{y,\sigma,\mathcal{W}}$	-0.8 m/s
$A_{dy,\mu,\mathcal{W}}$	0.1 m/s	$A_{dy,\sigma,\mathcal{W}}$	0.0 m/s
$\varphi_{d,\mathcal{W}}$	2.6 m/s	$\varphi_{y,\mathcal{W}}$	2.4 m/s
$T_{\mathcal{W}}$	20 h	$\zeta_{\mathcal{A}/\mathcal{W}}$	0.23

model, which allows to model all different kinds of motor devices with significant modeling limitations.

The entire modeling accuracy is rated high considering fundamental behavioral patterns, but low considering specific individual behavioral patterns. This allows to use the model as a realistic emulation of household behavior in grid focused analyses, which focus on the mean behavior of multiple households, which is finally allocated to individual households. Model improvements are likely, especially by using more complicated individual model components. Finally, this model allows to be used as the load model in the laboratory. To the best of our knowledge, literature does not provide any nearly comparable alternative to this model, which combines all fundamental behavioral patterns from the time variant energy consumption to the dynamic creation of signal shapes.

5.2 Weather model

The performance of the weather model is hardly measurable due to its stochastic nature. A detailed analysis with multiple specific measures to quantify the modeling accuracy is postponed to future work. The following subsections are based on an emulation of the measurement of the weather station in Garching, Germany and the illustration of its results. Further satellite based data sets' modeling results are subtextually incorporated into the results of the following sections. The model parameters of the illustrated weather model from Garching are listed in Tab. 5.10.

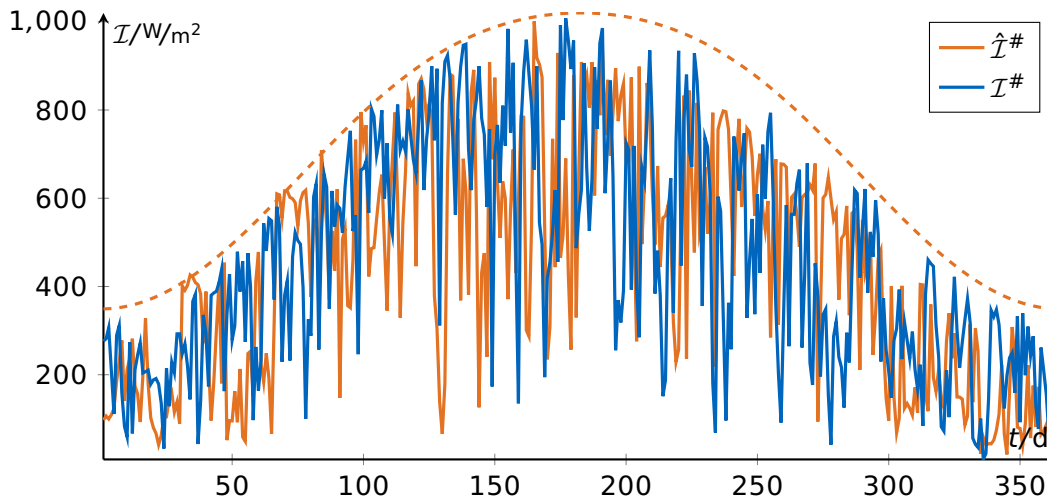


Figure 5.33: Maximum daily global horizontal irradiation $\mathcal{I}^\#$: Measured data $\hat{\mathcal{I}}^\#$ from Garching, Germany and model output $\mathcal{I}^\#$ based on parameters from Tab. 5.10 through a random process. The dashed line shows the maximum possible daily radiation.

5.2.1 Experimental results

The performance of the weather model, especially for the local data set of Garching, are illustrated in this subsection. The comparison of measured and modeled data has to show differences due to the model's stochastic nature. A high model accuracy means that the characteristics of the modeled and the measured reference data are similar, but not necessarily their absolute magnitudes. Their characteristics mainly consist of the time dependent expectation value and standard deviation, as well as the rate of change, the interdependency of irradiation \mathcal{I} , ambient temperature \mathcal{A} and wind speed \mathcal{W} , and further properties, like peak shapes, or radiation at night, etc.

The measured and modeled global horizontal radiation of Garching is illustrated in Fig. 5.33 and Fig. 5.34. The first illustration Fig. 5.33 shows the seasonal behavior through the daily maximum values and the maximum possible daily radiation throughout one entire year. The high impact of stochasticity causes deviations between model and measurement, but in a similar range. There are no significant violations of the maximum possible radiation, individual peaks are randomly distributed but show similar heights. The continuity of weather phenomena, like the duration of sunny weather is similar. The diurnal behavior in Fig. 5.34 shows days with measured high radiation, e.g. day 243, and with measured low radiation like day 244, similarly as the model with high radiation at day 245 and low at day 246. Fluctuations within one day, like some small prongs during the day, show no significant difference between model and measured data.

The seasonal behavior of the measured and modeled ambient temperature \mathcal{A} is illustrated through the daily maximum and minimum values in Fig. 5.35. The obvious result is the higher temperature in summer than in winter, which is accurately consistent. Fluctuations of maximum and minimum temperatures are higher in winter than in summer, similarly for measurement and model results. The measured temperature shows a warm period in January until about day 15 and around day 265 which lasts significantly long.

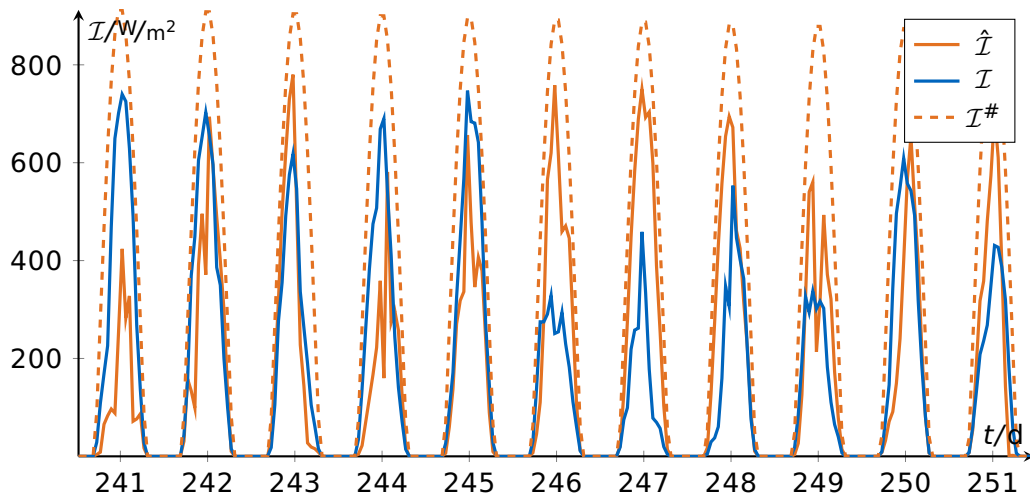


Figure 5.34: Hourly global horizontal irradiation \mathcal{I} end of August to beginning of September: Measured data $\hat{\mathcal{I}}$ from Garching, Germany and model output \mathcal{I} based on parameters from Tab. 5.10 through a random process. The dashed line shows the maximum possible radiation.

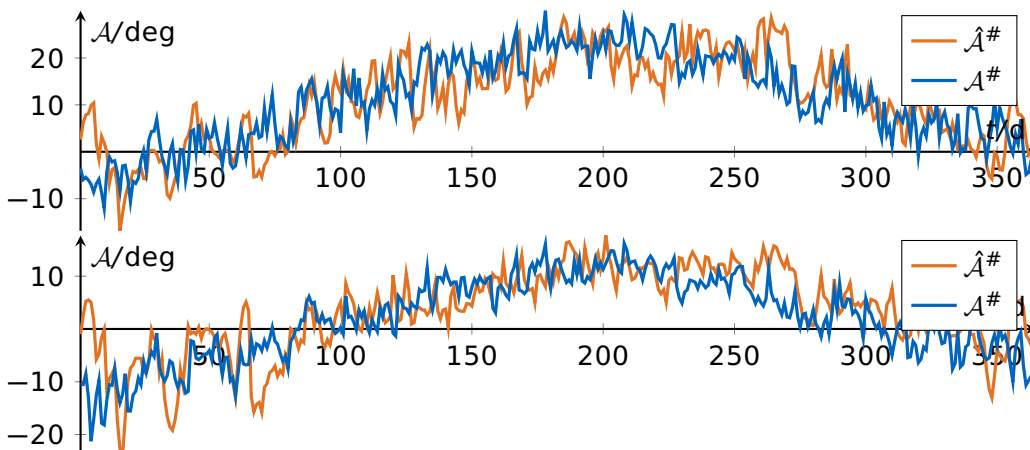


Figure 5.35: Maximum (top graph) and minimum (bottom graph) daily ambient temperature $\mathcal{A}^\#$: Measured data $\hat{\mathcal{A}}^\#$ from Garching, Germany and model output $\mathcal{A}^\#$ based on parameters from Tab. 5.10 through a random process.

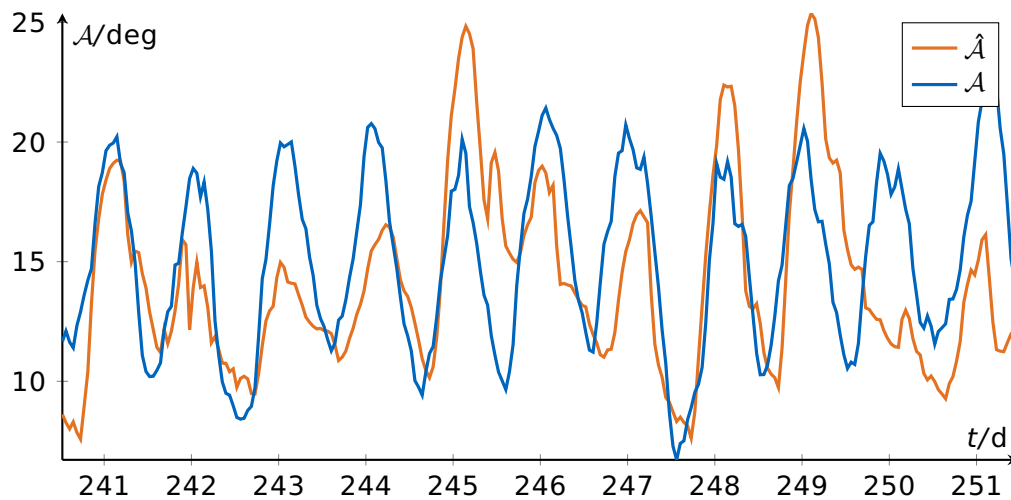


Figure 5.36: Hourly ambient temperature \mathcal{A} end of August to beginning of September: Measured data $\hat{\mathcal{A}}$ from Garching, Germany and model output \mathcal{A} based on parameters from Tab. 5.10 through a random process.

Simulation shows a mainly constant weather period around day 50. Other measured and simulated data show different numbers of such specific weather events, such that no significant deviations are observed. The diurnal variation illustrated in Fig. 5.36 also shows similar measured and modeled characteristics. Both graphs show warm and cold days, as well as typically higher temperatures during the day. Multiple simulations show, beneath higher temperatures and radiations in summer and during the day, a loose relation between radiation and temperature, for instance a high modeled radiation period around day 50 correlates with a relative high ambient temperature at the same time. On the other hand, a relatively low radiation and high temperatures around day 5 shows also deviations from that correlation in reality.

Windspeed is naturally highly fluctuating, as illustrated in Fig. 5.37 and Fig. 5.38. Seasonality leads to higher wind speeds in winter with higher fluctuations than in summer, consistently for simulated and measured data. The range of fluctuations, especially at a diurnal scale in Fig. 5.38 shows wind speeds from about 0 m/s up to 5 m/s, with significant fluctuations in one day.

Global locations are evaluated based on satellite based reference data. These data are averaging over significantly large regions, which has an impact on individual behavior. Fundamental modeling inaccuracies are for instance, that measured weather data close to the equator typically show not simply sinusoidal expectation value trajectories, which is assumed for the model. Especially wind speed shows worse results than irradiation and temperature. Especially for temperate regions the model shows high accuracies.

5.2.2 Analysis and interpretation of the results

The analysis of the weather model accuracy is based on comparisons of measured and modeled data. Averaged data from satellites are only considered to investigate the impact of global locations, as the averaging has a significant impact on the resulting behavior.

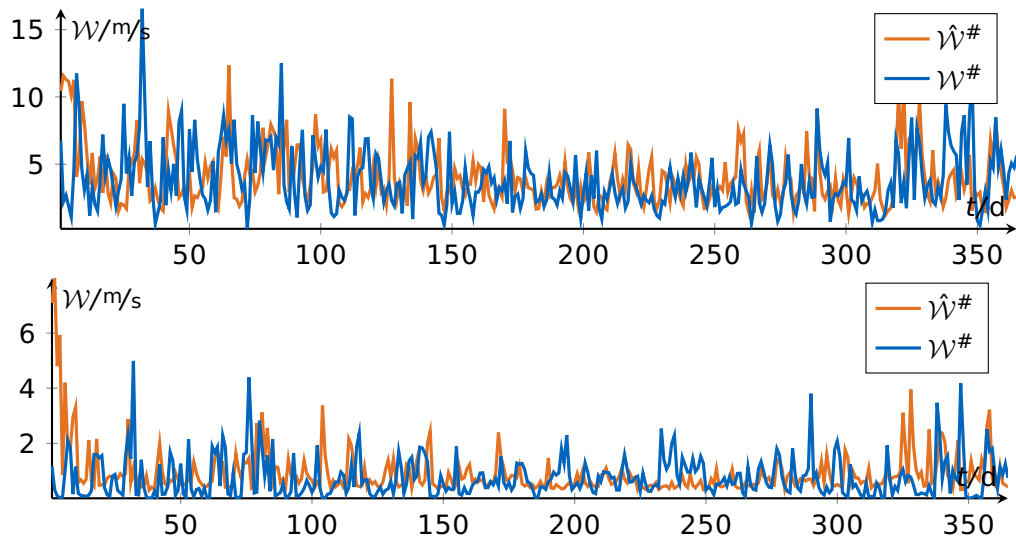


Figure 5.37: Maximum (top graph) and minimum (bottom graph) daily horizontal wind speed $\mathcal{W}^\#$: Measured data $\hat{\mathcal{W}}^\#$ from Garching, Germany and model output $\mathcal{W}^\#$ based on parameters from Tab. 5.10 through a random process.

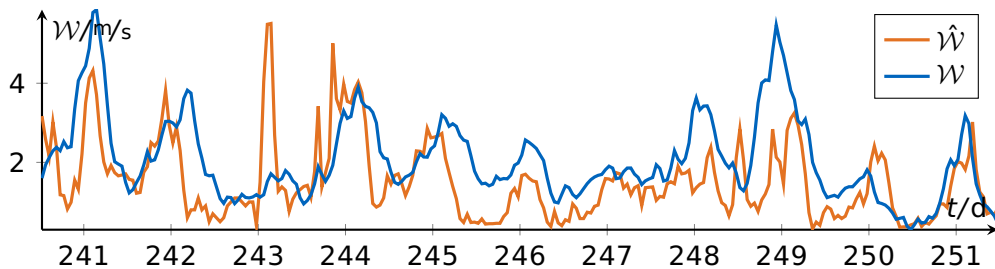


Figure 5.38: Hourly horizontal wind speed \mathcal{W} end of August to beginning of September: Measured data $\hat{\mathcal{I}}$ from Garching, Germany and model output \mathcal{I} based on parameters from Tab. 5.10 through a random process.

Especially the suggested methodology to transform global horizontal radiation to plane-to-array radiation is not analyzed, as it is identical to mechanisms suggested in literature. Future work with the CoSES weather station should elaborate this in detail, through the good measurability of direct, diffuse and global radiation at diverse angles. The overall accuracy appears high through multiple different emulated locations, especially by focusing on temperate regions. The important characteristics, like time variance of expectation value and standard deviation, the interdependency and rate of change of different weather magnitudes can be adjusted through individual parameters. Especially using recorded mean and standard deviation trajectories allows to increase the accuracy of time variance, especially for regions close to the equator.

5.3 Model based laboratory scenario analysis

This section describes the standard laboratory electricity grid configuration and three operating scenarios to illustrate challenges and potentials to solve these challenges. The fundamental focus is set on line voltage drops and on transmission capacity limitations. The standard DIN VDE 50160 allows $\pm 10\%$ voltage deviations for the end consumer at his network interconnection point. Traditionally, the last active voltage control ability is at the substation, the transition from the high to the mean voltage. That transformer's tap changer has a control hysteresis of typically 2%. Calculating 7% voltage drop for the mean voltage grid allows a remaining $\pm 5.5\%$ voltage drop for the low voltage transformer and the low voltage grid.

The standard electricity grid topology is illustrated in Fig. 5.39. It is designed based on multiple heuristic analyses with the aim to be realizable in the laboratory, to show interesting challenges which have to be solvable and which represents a realistic scenery. An exemplary scenery in which this standard grid topology could be realized realistically is shown in Fig. 5.40 as an exemplary landscape. The scenery is based on a rural region, with a small settlement with five houses close to the transformer and two larger remote houses.

The following subsections describe each one possible operation state of the grid. The standard configuration is investigated based on only one active transformer and the open ring, such that the grid topology is radial. The presented system behaviors are obtained based on simulations with the professional grid simulation software PSS@SINCAL of the Siemens group. This simulation is based on optimal power flow calculations with pure resistive-inductive cable models. Typically in low voltage cable grids, the cable capacities have a significant impact, which are typically neglected in professional grid simulation softwares. The mean voltage feeder with the id [0] is considered as slack bus and the seven houses' buses are considered as load buses. Node voltages are analyzed as per unit values based on nominal voltages of $V_n = 400$ V. Edge loads are analyzed as per unit currents, based on nominal currents I_n as specified in Sec. 3.2.2. Additionally, capacity limits are mentioned based on the PSS@SINCAL's database values. Voltage deviations larger than 1% outside the specified limits are considered as critical. Current limit violations are counted as critical if larger than the capacity limit.

5.3.1 Full load scenario

The first system behavior investigation is based on an extreme scenario of maximum load. Each of the five houses and the two EXTs consume nominal load as active power, plus reactive power to get a power angle of 0.9. There is no distributed generation. The resulting current flows of the full load scenario are illustrated in Fig. 5.41. Noncritical and critical limit violations are illustrated in the grid topology diagram in Fig. 5.43 as orange and red elements. Capacity violations occur mainly in the connection from the transformer to the settlement, in cable (1) of 275% and (2) of 186%. The transformer is overloaded at 106%. These overloads would be critical and would lead quickly to the destruction of the infrastructure or to the tripping of the protection devices causing a black-out of the grid. Uncritical violations are the cable (5) and all consumer's connections of 18% to 25%,

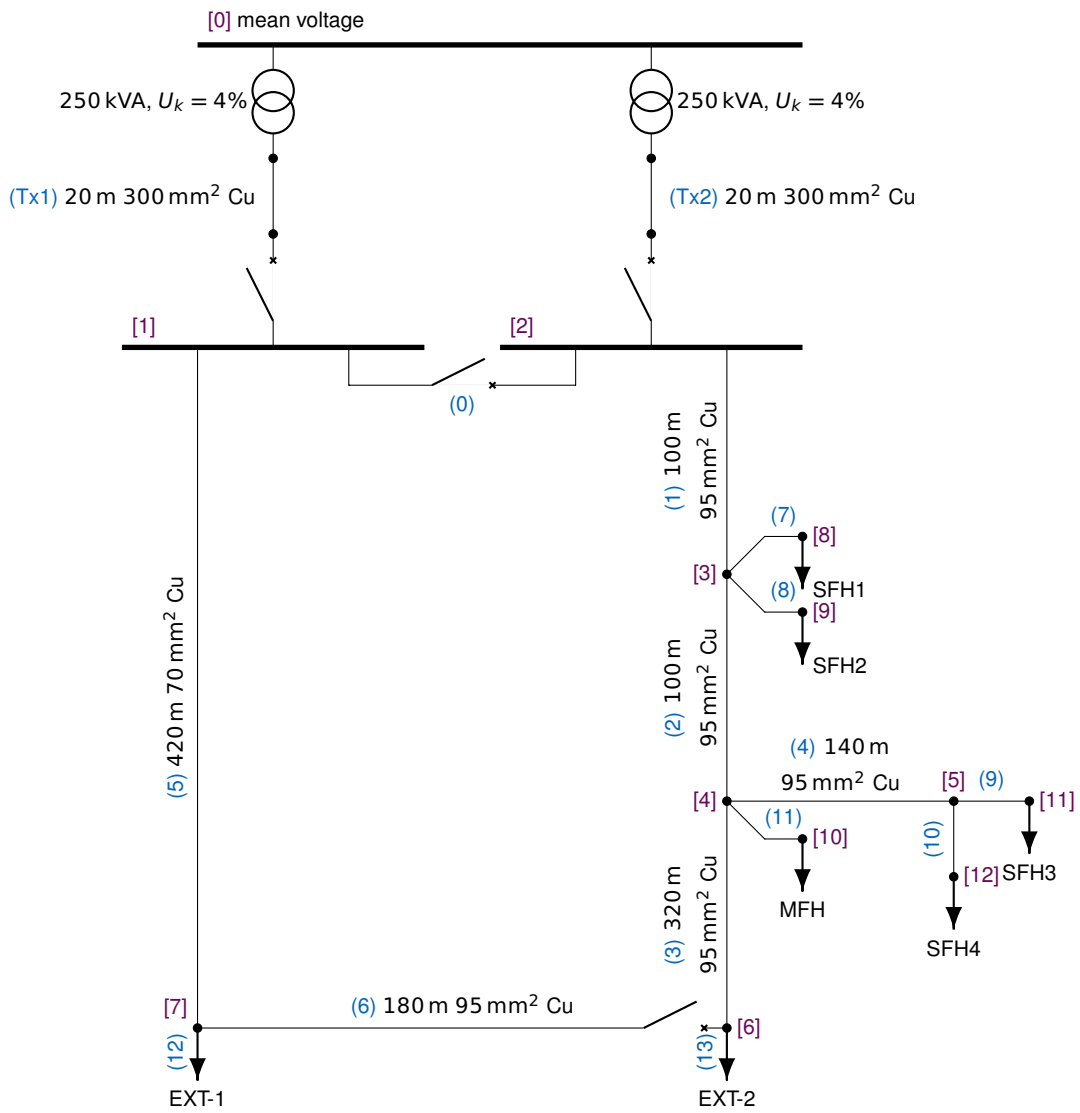


Figure 5.39: Illustration of the CoSES standard electricity grid topology, including cable specifications, node ids [x] and edge ids (y).

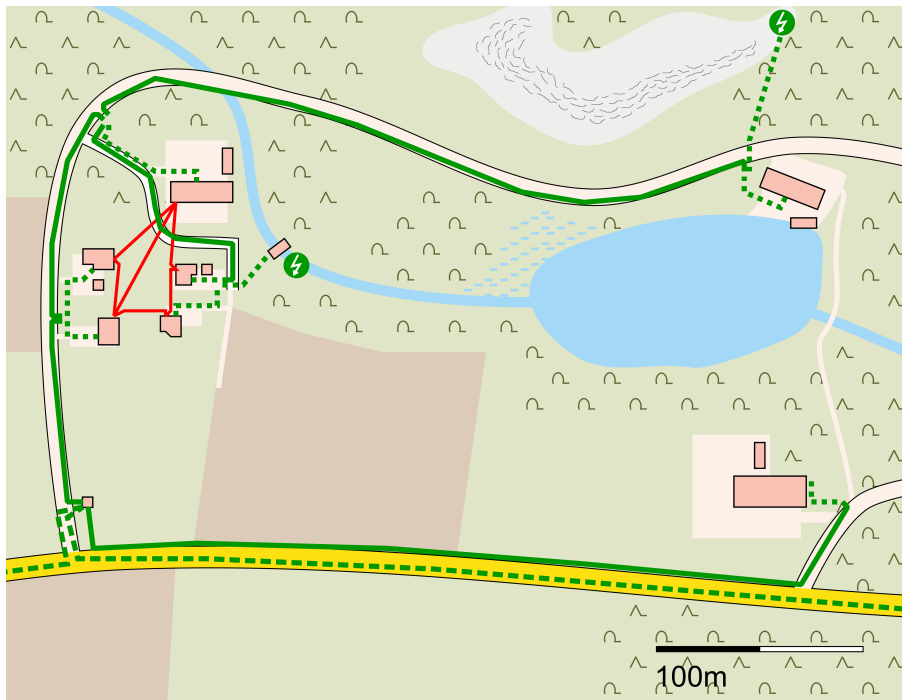


Figure 5.40: Illustration of a possible scenery based on the standard grid topology. Green lines are electricity lines, green dashed line is mean voltage line, green dotted lines are house connection cables, red lines are heat distribution grid pipes, two green marked generators, two houses on the right side are the extensions, small house on the bottom left is the transformer house.

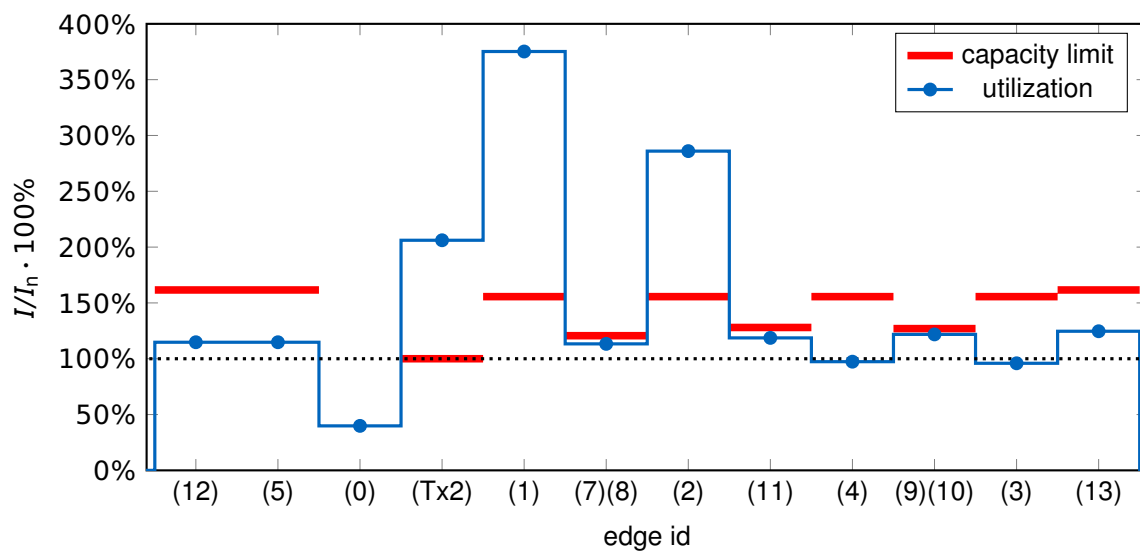


Figure 5.41: Per unit current flows I/I_n of the full load scenario and the capacity limits.

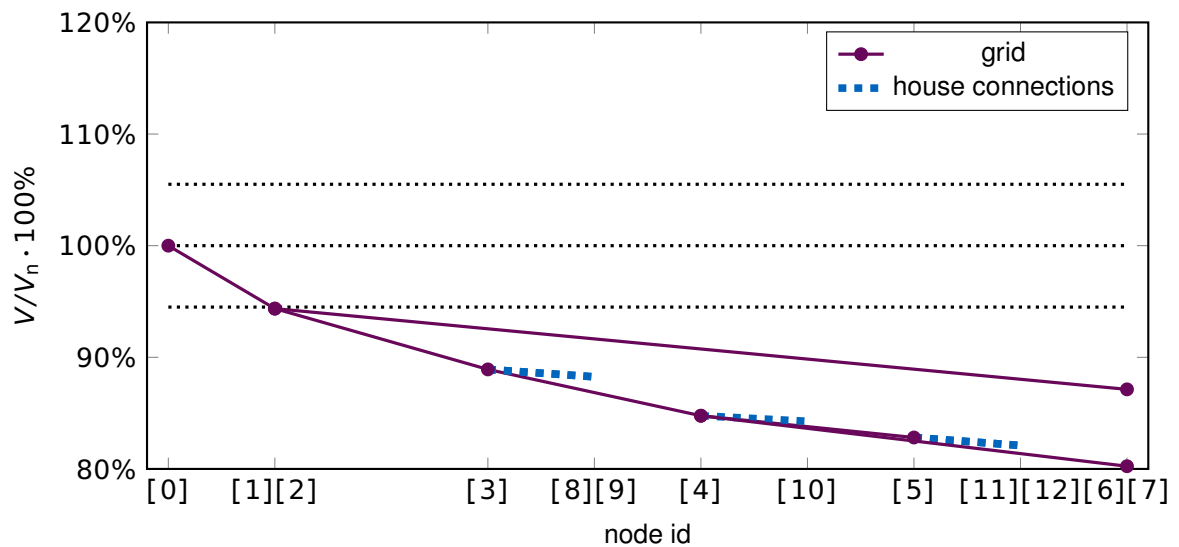


Figure 5.42: Per unit grid voltages V/V_n of the full load scenario including the acceptable voltage band

which would cause the tripping of protection devices after a while. These capacity limits occur due to constant power loads by considering voltage drops.

Occurring line voltage drops are illustrated in Fig. 5.42. All grid voltages are critically violated, except directly at the transformer at busbar [2], which is only marginally violated. The extreme scenario causes these voltage drops of up to 20%, which means a voltage band violation of 14%, which would cause besides legal and economic consequences mainly disturbances in the operation of distributed facilities. One of the fundamental observations is that the main limiting aspect of grid capacity are typically voltage drops, current limitations play a subordinate role. Current limitations of the house connection cables have a major impact, as high peak generation or high consumption due to BEV charging and electric heating can occur.

5.3.2 Generation and consumption feeder scenario

The second scenario is based on one generation and one consumption feeder at the transformer. Each of the five houses and the EXT-2 which is connected to the five houses consume half nominal load as active power. The EXT-1 at the other transformer feeder generates half nominal active power. No reactive powers are consumed in accordance with the actual trend towards more capacitive consumption due to more and more used SMPS devices. The resulting current flows of the generation and consumption feeder scenario are illustrated in Fig. 5.44. Noncritical and critical limit violations are illustrated in the grid topology diagram in Fig. 5.46 as orange and red elements. Capacity violations occur mainly in the connection from the transformer to the settlement, in cable (1) of 65% and (2) of 24%. The overload of the grid segment (1) would be critical and would lead quickly to the destruction of that cable or to the tripping of protection devices causing a black-out of that grid feeder. The uncritical violation of the cable current rating (2)

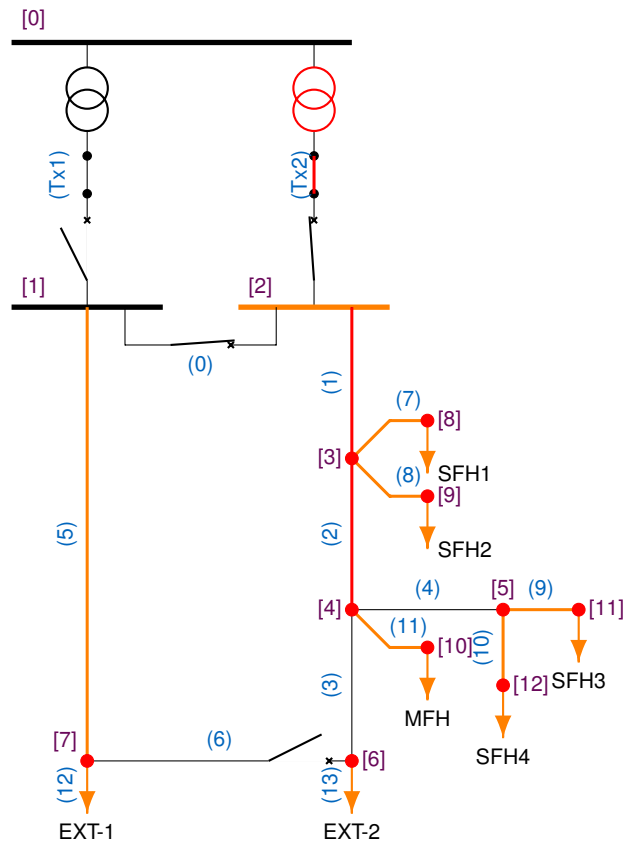


Figure 5.43: Grid configuration and limit violations of the full load scenario: red means critical violations, orange means uncritical violations, of line capacity limits (edges) and of voltages (nodes)

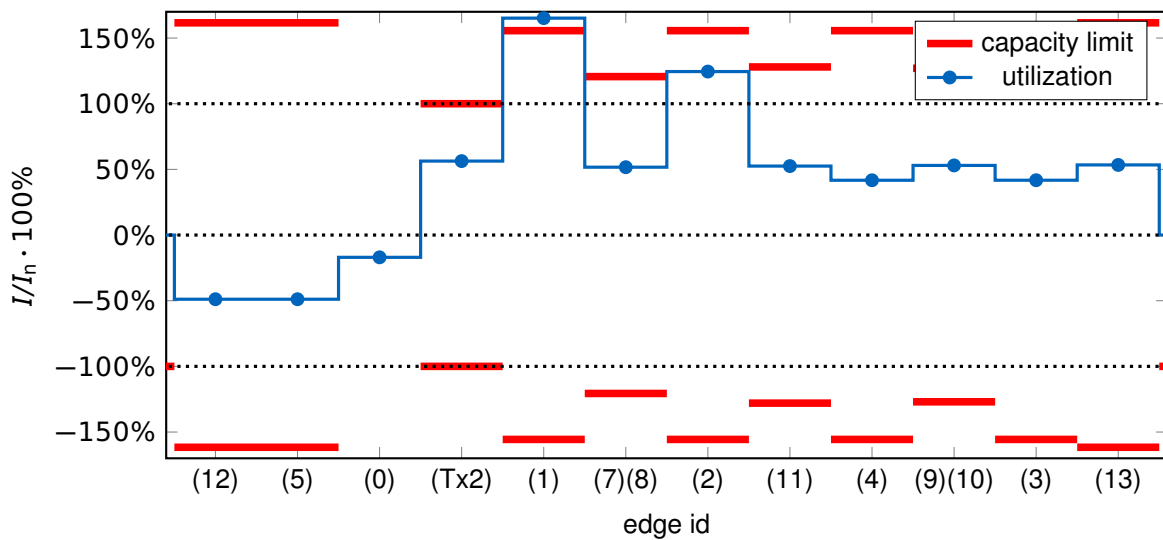


Figure 5.44: Per unit current flows I/I_n of the generation and consumption feeder scenario and the capacity limits.

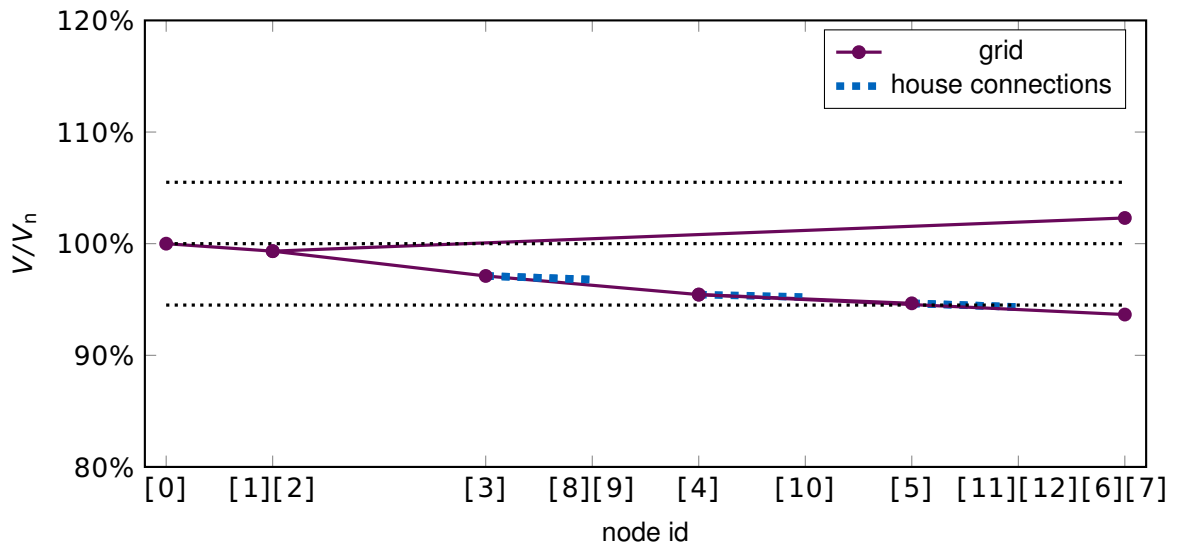


Figure 5.45: Per unit grid voltages V/V_n of the generation and consumption feeder scenario including the acceptable voltage band

would cause the tripping of protection devices, a quicker aging or in worst case also its destruction after a while.

Occurring line voltage drops of the generation and consumption feeder scenario are illustrated in Fig. 5.45. The grid voltages of node [11], [12] and [6] are violated for about 0.5% to 1%. This could cause mainly legal and economic consequences. This scenario shows, that the switching of an OLTC transformer of about 2.5% would allow to hold all grid voltages. Increasing the generation and consumption powers from actually 50% to values close to 100% would cause an increasing of the voltage difference of node [6] and [7], which would mean that an OLTC switching action would improve the conditions for one node, but would corrupt the conditions for the other node. This shows that an OLTC cannot solve all voltage problems.

5.3.3 Mixed generation and consumption scenario

The behavior of the mixed generation and consumption scenario shows that an intelligent coordination of generation and consumption could solve voltage and current limit challenges, even under higher power ratings. Each of the four SFHs consumes 75% of their nominal power rating as active power. The two EXTs and the MFH generate 75% of their nominal power rating as active power. The resulting current flows of the mixed generation and consumption scenario are illustrated in Fig. 5.47. There are no current limit violations, as also shown in the network diagram in Fig. 5.49.

The resulting line voltage drops are illustrated in Fig. 5.48. All grid voltages are in between the specified limits. The fundamental observation of this scenario is that distributed generation and consumption in the close neighborhood balance each other. Consumptions' positive voltage drops and generations' negative voltage drops eliminate each other even under high power ratings and cause only few flowing grid currents. That

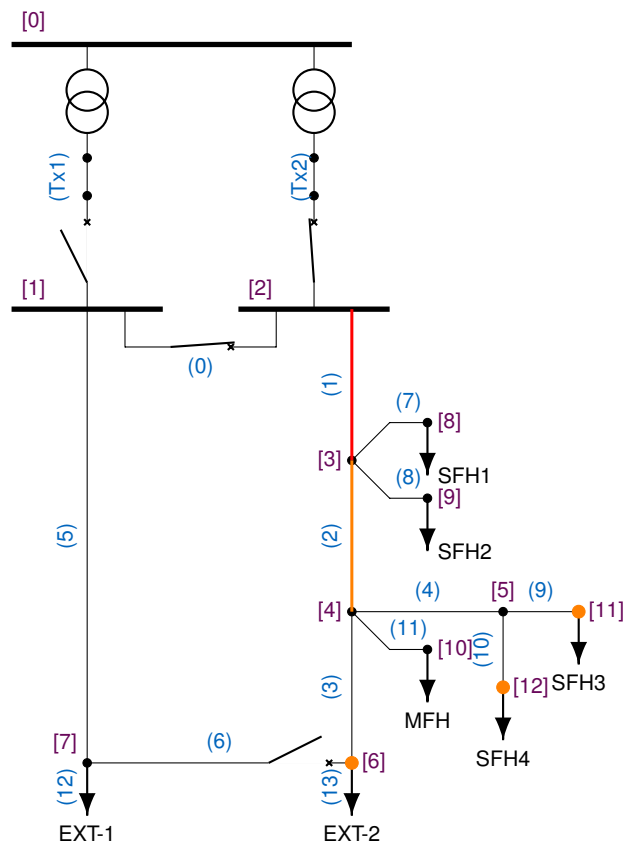


Figure 5.46: Grid configuration and limit violations of the generation and consumption feeder scenario: red means critical violations, orange means uncritical violations, of line capacity limits (edges) and of voltages (nodes)

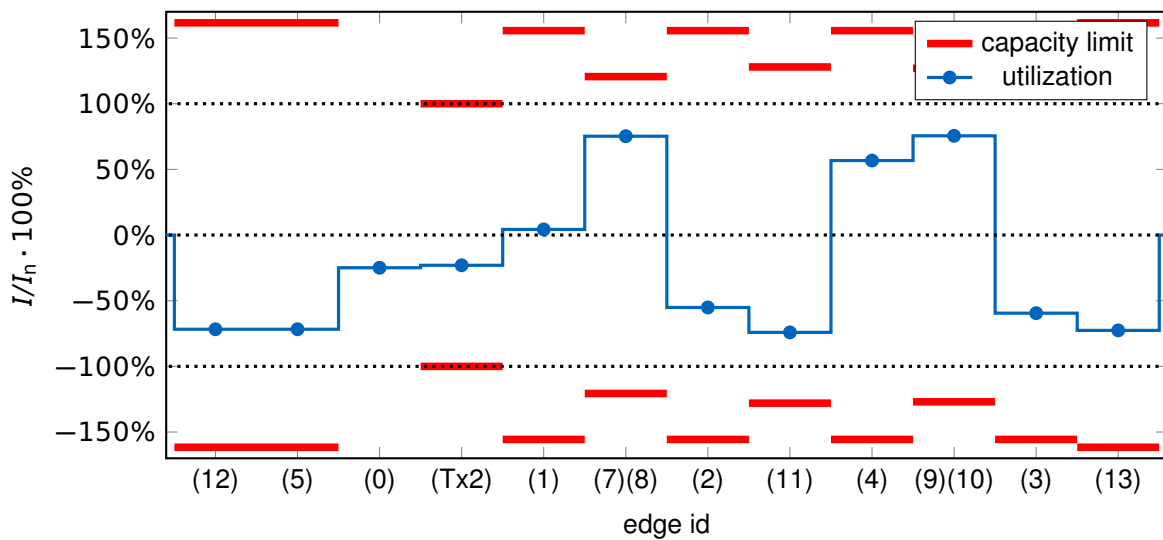


Figure 5.47: Per unit current flows I/I_n of the mixed generation and consumption scenario and the capacity limits.

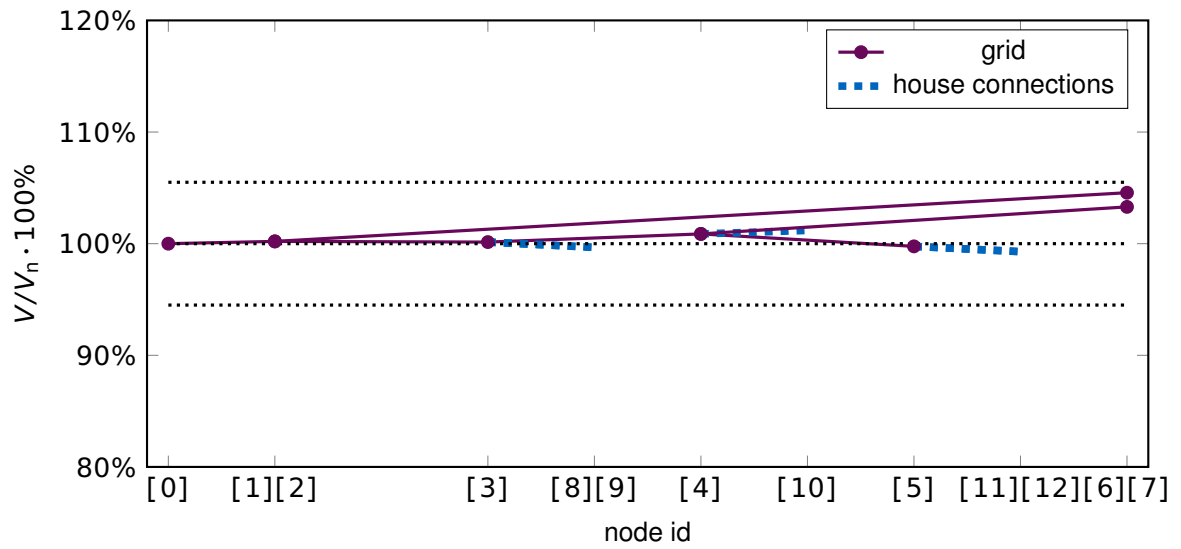


Figure 5.48: Per unit grid voltages V/V_n of the mixed generation and consumption scenario including the acceptable voltage band

is one of the fundamental aims of MG control, to coordinate available flexible generation, storage and consumption devices, such that these balance each other and the grid is relieved.

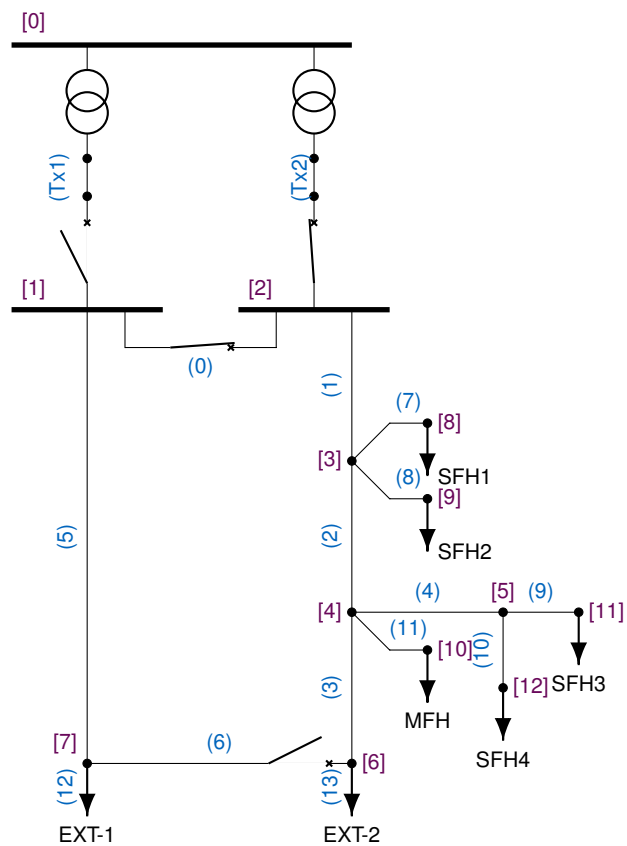


Figure 5.49: Grid configuration and limit violations of the mixed generation and consumption feeder scenario: red means critical violations, orange means uncritical violations, of line capacity limits (edges) and of voltages (nodes)

Chapter 6

Conclusions

The present work addresses challenges of the transition from a centralized, power plant controlled electricity system to an intelligent decentralized network controlled system. This work focuses on LV distribution systems as MGs, by considering heating and the connection to the traffic sector by BEV charging. The context of this work are practical challenges which have to be investigated in a laboratory, the construction of a MG laboratory and technical concepts to operate fundamental parts of the laboratory.

6.1 Summary of contributions

The present work is based on three fundamental contributions. The first contribution is the systematic analysis of the physical-technical principles of energy system operation and their systematic structuring to derive technical laboratory requirements. The ESMIF concept describes a multilayer approach which structures the technical processes and their affiliated challenges in five consecutive layers. This allows to explicitly distinguish specific challenges, like energy provision, powerflow, voltage control, instantaneous processes or the real technological impact and indicates temporal process requirements to avoid undesired cross-layered interactions. This allows to systematically analyze technical requirements for a MG laboratory as a multi-functional tool for investigating challenges across all layers.

The second fundamental contribution is the technical laboratory concept. The fundamental principle is that the laboratory components should allow to actively influence all processes of each layer. Only this realistic consideration of the entire processes of energy system operation allows to generate reliable and viable investigation results. Especially at high levels, referring to energy management challenges, the coupling of heating, electricity and BEV charging is important to be considered in a laboratory. Using heat pumps and CHP units as promising technologies for future sustainable heating supply cause that the requirements and processes of the entire domestic heat system interact with the electricity system. This motivates to incorporate the entire heating and in future the cooling system including a local heat network as a key feature in the laboratory. To allow to investigate multiple different scenarios, the laboratory concept focuses on a modular design and flexible configurations, like the flexible grid configuration system, which allows to flexibly

configure multiple different LV grid topologies. The sophisticated measurement and control system allows to gather and record the detailed system state.

The third fundamental contribution is the design of HIL models for the electricity consumption and for artificial weather behavior. The challenge that no humans live in the laboratory and consume energy makes realistic models necessary, to emulate that behavior. The key feature of this work's model is to incorporate all fundamental processes of conventional electricity consumption, from the dynamic interaction of instantaneous voltages and currents through the consumer devices which can cause the formation of harmonic disturbances, until the time variant energy consumption. The present weather model allows to flexibly configure the virtual weather conditions and hence the location and allows to specifically investigate the individual impact of specific weather phenomena, like higher fluctuating irradiation or a stronger coupling between irradiation and temperature. Both HIL models are critically analyzed by emulating reference measurements. These analyses show accurate results with some limitations, which allow the model to be used in the laboratory.

6.2 Future research

The obvious future work is the final construction and the commissioning of the laboratory and the execution of energy system investigations and research projects. Especially investigations in the context of system modeling, system operation under realistic conditions and the reliable validation of operation strategies are of great interest, where the laboratory can exploit its strengths. An interesting specific topic is for instance to design new electricity grid models with accurate cable models, especially under transient and harmonic conditions. Especially the consideration of the ESMIF layers in such a model could offer a crucial added value.

A further field for future research is the detailed investigation and validation of the accuracy of the presented HIL models, including possible improvements. The weather station with differently sloped pyranometers allows to investigate specifically the transformation of global radiation for differently sloped plains. A further specific future work could be the validation of the weather model for multiple different regions, especially by using reference data from local weather stations. Open questions in the context of the conventional electricity consumption are the impact of the constant share of resistive, motor and SMPS devices, the impact of considering mainly the mean behavior of multiple consumers and the impact of not including non-stochastic time dependent processes. Furthermore it would be interesting to mathematically validate the entire model with multiple different reference measurements, and to define accuracy measures to mathematically quantify the model accuracy.

6.3 Concluding remarks

This work integrates into the research context to find realistic solutions for the challenges of sustainable energy supply mainly at the distribution grid level. This work fundamentally provides the prerequisites for the investigation of such solutions. Furthermore, the present

ESMIF multilayer approach could play a crucial role in future research as a concept to systematically analyze different questions of energy system operation and to combine these at the differently abstracted layers.

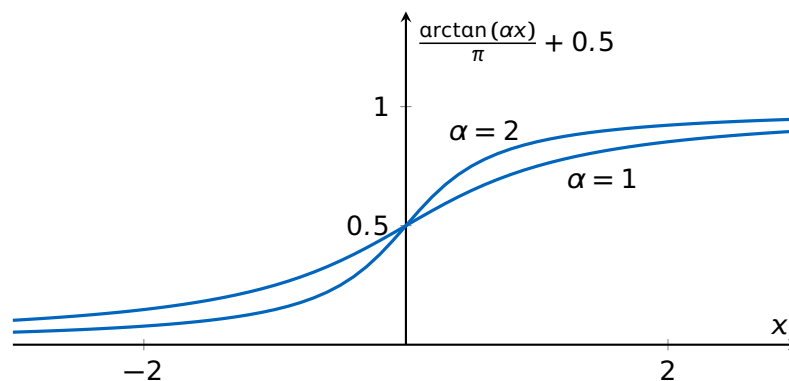
This work could open a new perspective of energy system operation, by opening the view to all system processes, including the realistic and practical aspects. In this view the critical contribution of this work is the idea to reliably investigate the entire process of energy system operation, which reflects in the ESMIF concept as a basis for the laboratory design and the conventional electricity consumption model.

Appendix A

Mathematical Derivations

A.1 Derivation of the electricity load switching behavior process equation

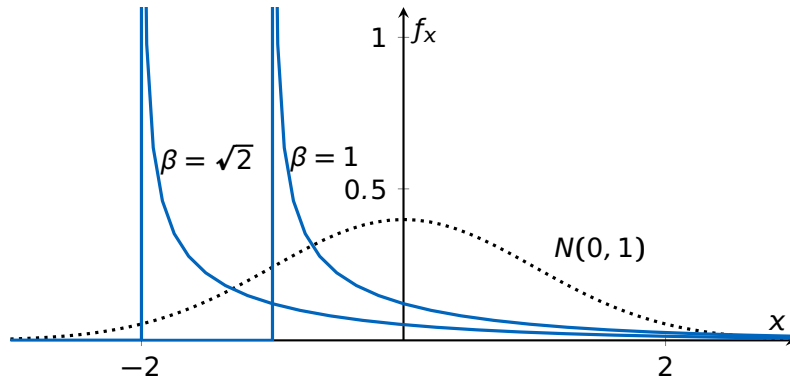
- First aim is to focus on the power increment
- Model a process equation with a certain probability to keep the power consumption constant or to switch it
- Using arctan-function as a blurred switch between 0 (constant event) and 1 (switch event), similarly as the heaviside function $\mathbb{1}(x)$



$$\frac{\arctan(\alpha x)}{\pi} + 0.5 \approx \mathbb{1}(x)$$

- Blur parameter α allows to adapt the steepness of the transition between 0 and 1, which affects the clarity of the distinction between constant and switch event
- Creating a random variable x with a specific probability to keep the power consumption constant for negative values or to switch it for positive values
- Input is the standard normal distributed white noise samples $\zeta'[k]$

- Creating a sign independent random variable by squaring $\zeta'[k]$
- Shifting the probability density function by the switching rate parameter β^2 to modify the probability for switching events $\mathcal{P}(x > 0)$



$$x = \zeta'^2[k] - \beta^2$$

- Multiplying the random variable $\zeta'[k]$ and the switching height parameter P_Δ to specify the typical switching height and the positive or negative direction of it

$$P_\Delta \cdot \zeta'[k] \left(\frac{\arctan(\alpha(\zeta'^2[k] - \beta^2))}{\pi} + 0.5 \right)$$

- Adding this power increment to the previous power sample $P'_d[k-1]$ results in the final process equation (4.35)

$$P'_d[k] = P'_d[k-1] + P_\Delta \cdot \zeta'[k] \left(\frac{\arctan(\alpha(\zeta'^2[k] - \beta^2))}{\pi} + 0.5 \right)$$

A.2 Transformation from normal to Weibull distribution

- Assuming a normal distributed random variable x , with an expectation value μ and a standard deviation σ
- Its probability density function is

$$f_N(x) = \frac{1}{\sigma\sqrt{2\pi}} e^{-0.5\left(\frac{x-\mu}{\sigma}\right)^2}$$

- Its cumulative distribution function is

$$F_N(x) = \frac{1}{2} + \frac{1}{2} \operatorname{erf}\left(\frac{x-\mu}{\sqrt{2}\sigma}\right)$$

- erf is the Gaussian error function
- Assuming a Weibull distributed random variable y , with a shape parameter k and a scale parameter λ
- Its probability density function is

$$f_W(y) = \lambda k (\lambda y)^{k-1} e^{-(\lambda y)^k}$$

- Its cumulative distribution function is

$$F_W(y) = 1 - e^{-(\lambda y)^k}$$

- The aim is a transformation N2W to transform normal to Weibull distributed random variables with identical expectation values and standard deviations

$$x \mapsto y = \text{N2W}(x; \mu, \sigma)$$

- Probabilities have to coincide:

$$\begin{aligned} P(x < X_0) &= P(y < \text{N2W}(X_0; \mu, \sigma)) \\ \Rightarrow \int_{-\infty}^x f_N(x') dx' &= \int_{\text{N2W}(-\infty; \mu, \sigma)}^{\text{N2W}(x; \mu, \sigma)} f_W(y') dy' \\ \Rightarrow F_N(x) - F_N(-\infty) &= F_W(\text{N2W}(x; \mu, \sigma)) - F_W(-\infty) \\ \Rightarrow \frac{1}{2} + \frac{1}{2} \operatorname{erf}\left(\frac{x - \mu}{\sqrt{2}\sigma}\right) &= 1 - e^{-(\lambda \text{N2W}(x; \mu, \sigma))^k} \\ \Rightarrow -(\lambda \text{N2W}(x; \mu, \sigma))^k &= \ln \left\{ \frac{1}{2} - \frac{1}{2} \operatorname{erf}\left(\frac{x - \mu}{\sqrt{2}\sigma}\right) \right\} \\ \Rightarrow \text{N2W}(x; \mu, \sigma) &= \frac{1}{\lambda} \sqrt[k]{-\ln \left\{ \frac{1}{2} - \frac{1}{2} \operatorname{erf}\left(\frac{x - \mu}{\sqrt{2}\sigma}\right) \right\}} \end{aligned}$$

- The following part shows how to compute the shape parameter k and the scale parameter λ to get identical expectation values and standard deviations
- Expectation value of Weibull distribution is

$$\mu(y) = \lambda^{-1} \Gamma\left(1 + \frac{1}{k}\right)$$

- Standard deviation of Weibull distribution is

$$\sigma(y) = \sqrt{\lambda^{-2} \left(\Gamma\left(1 + \frac{2}{k}\right) - \Gamma^2\left(1 + \frac{1}{k}\right) \right)}$$

– $\mu(y) \stackrel{!}{=} \mu$ and $\sigma(y) \stackrel{!}{=} \sigma$ and dividing $\frac{\mu(y)}{\sigma(y)}$

$$\begin{aligned} \Rightarrow \frac{\mu}{\sigma} &= \frac{\lambda^{-1}\Gamma\left(1 + \frac{1}{k}\right)}{\lambda^{-2}\left(\Gamma\left(1 + \frac{2}{k}\right) - \Gamma^2\left(1 + \frac{1}{k}\right)\right)} \\ &= \frac{\Gamma\left(1 + \frac{1}{k}\right)}{\sqrt{\left(\Gamma\left(1 + \frac{2}{k}\right) - \Gamma^2\left(1 + \frac{1}{k}\right)\right)}} \\ \Rightarrow k = k' : \frac{\mu}{\sigma} &= \frac{\lambda^{-1}\Gamma\left(1 + \frac{1}{k'}\right)}{\lambda^{-2}\left(\Gamma\left(1 + \frac{2}{k'}\right) - \Gamma^2\left(1 + \frac{1}{k'}\right)\right)} \end{aligned}$$

– Inserting in expectation value

$$\begin{aligned} \mu &= \lambda^{-1}\Gamma\left(1 + \frac{1}{k}\right) \\ \Rightarrow \lambda &= \frac{\Gamma\left(1 + \frac{1}{k}\right)}{\mu} \end{aligned}$$

A.3 Derivation of the amplitude error compensation factor for filtered white noise

– A white noise signal gets filtered with a first order low-pass filter with a time constant T , a gain K and the transfer function

$$G(s) = \frac{K}{1 + Ts}$$

- The aim is to determine the gain K , such that the signal energy is not affected.
- The standard normal distributed white noise signal is sampled at T_s
- Its Nyquist frequency is

$$\omega_0 = \frac{\pi}{T_s}$$

- White noise has the signal energy content 1
- White noise has up to the Nyquist frequency a uniformly distributed energy density h
- This means in frequency domain

$$\int_0^{\omega_0} h^2 d\omega \stackrel{!}{=} 1$$

$$\Rightarrow h^2 \frac{\pi}{T_s} \stackrel{!}{=} 1$$

$$\Rightarrow h = \sqrt{\frac{T_s}{\pi}}$$

– The frequency response of the filter is

$$|G(\omega)| = \frac{K}{\sqrt{1 + T^2 \omega^2}}$$

– The resulting filtered signal in frequency domain is

$$|G(\omega)| \cdot h = \frac{K}{\sqrt{1 + T^2 \omega^2}} \cdot \sqrt{\frac{T_s}{\pi}}$$

– Signal energy content has to equal 1

$$\int_0^{\omega_0} \left(\frac{K}{\sqrt{1 + T^2 \omega^2}} \cdot \sqrt{\frac{T_s}{\pi}} \right)^2 d\omega \stackrel{!}{=} 1$$

– Assuming $T > 10T_s$ means the filter suppresses energy of frequencies higher than the Nyquist frequency

– This allows to consider the white noise's amplitude to be constant until infinite frequencies, as these energy parts are highly damped and do not affect the final result:

$$\int_0^{\infty} \left(\frac{K}{\sqrt{1 + T^2 \omega^2}} \cdot \sqrt{\frac{T_s}{\pi}} \right)^2 d\omega \stackrel{!}{=} 1$$

$$\Rightarrow K^2 \frac{T_s}{\pi} \left[\frac{\text{atan}(T\omega)}{T} \right]_0^{\infty} \stackrel{!}{=} 1$$

$$\Rightarrow K^2 \frac{T_s}{2T} \stackrel{!}{=} 1$$

$$\Rightarrow K = \sqrt{\frac{2T}{T_s}}$$

Appendix B

Irradiation Factors

B.1 Normal-to-horizontal factor

- φ latitude of the location
- δ solar declination
- h hour angle
- According to [45] the normal-to-horizontal factor results in

$$\eta_{h/n} = \sin \varphi \sin \delta + \cos \varphi \cos \delta \cos h$$

- Solar declination depends on the inclination of the Earth's axis, and 81 d offset until spring breakthrough
- Hour angle depends on the daytime

$$\delta = 0.405 \text{ rad} \sin \left(\frac{2\pi}{1 \text{ y}} (t - 81 \text{ d}) \right)$$

$$h = \frac{2\pi \text{ rad}}{1 \text{ d}} t$$

B.2 Horizontal-to-sloped factor

- α slope angle
- b slope's azimuth angle
- a solar azimuth angle
- According to [45] the horizontal-to-sloped factor results in

$$\eta_{s/h} = \eta_{h/n} \cos \alpha + \sin \alpha \sin(\alpha \cos \eta_{h/n}) \cos(\alpha - b)$$

B.3 Scattering factor

- η_0 atmospheric transmission, equals anisotropy index from [45]
- According to [45] the scattering factor results in

$$\eta_{sc} = \eta_0 \frac{\eta_{s/h}}{\eta_{h/n}} + 0.5(1 - \eta_0)(1 + \cos \alpha)$$

Appendix C

Impressions of the Laboratory Realization



Figure C.1: View into the MV room

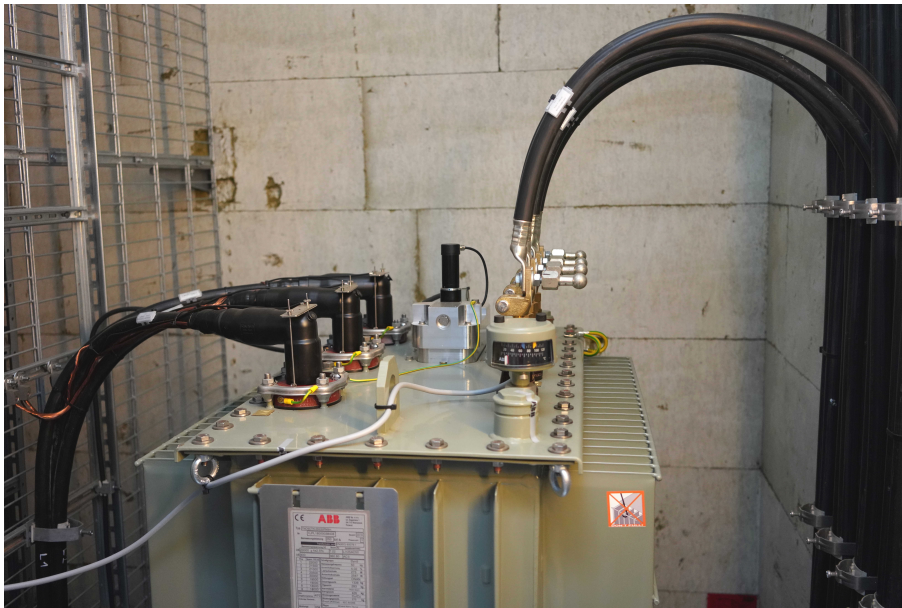


Figure C.2: View into the OLTC room



Figure C.3: View into the patch-panel system to configure the electricity grid



Figure C.4: Overview about the PHIL load emulator.



Figure C.5: Overview about electricity and control system of SFH-3: Left are the sockets, center is the house's electricity distribution cabinet, right is the RT control system.

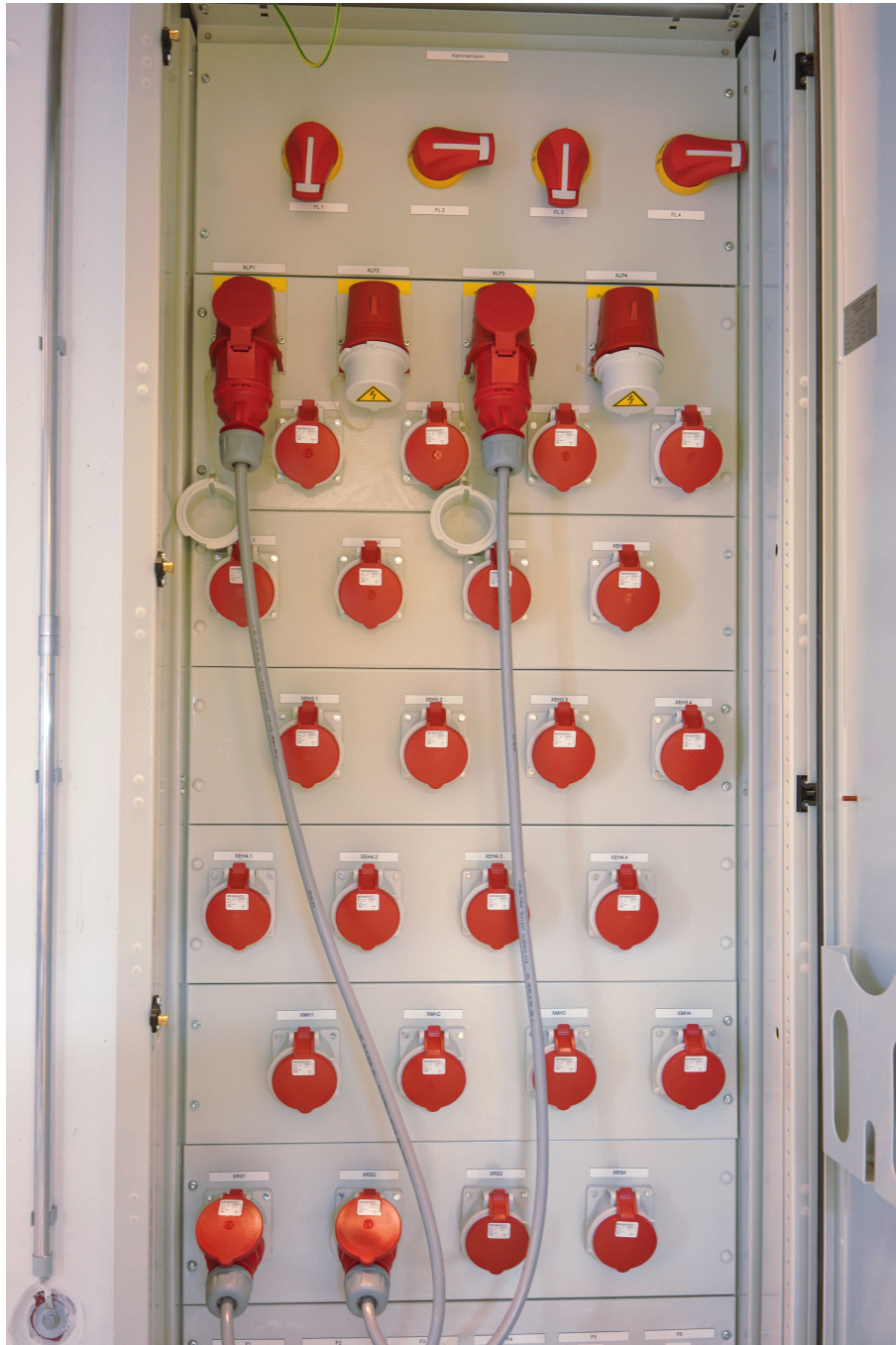


Figure C.6: Overview about the patch-panel system to allocate the BEV charging stations to specific houses



Figure C.7: Overview about heat modules of SFH-2: Left background is the air heat pump, right foreground is the gas boiler, center left is the grid transfer station module.



Figure C.8: Overview about heat modules of MFH: Left is the heat tank, right is the largest CHP, right top is the connection for exhaust, natural gas and cooling water (pipes without insulation).



Figure C.9: Overview about the brine heat pump: Left center is the brine tank, center is the heat pump itself, right is the pipe circuitry.

Bibliography

- [1] Center for grid integration and storage technologies, institute for high voltage technology, rwth aachen university. <http://www.ifht.rwth-aachen.de/cms/IFHT/Forschung/Infrastruktur-Tools/~qdjf/Zentrum-fuer-Netzintegration-und-Speiche/?lidx=1>. Accessed: 2019-07-25. 22
- [2] EPFL Smart Grid Project EPFLSMARTGRID. <https://smartgrid.epfl.ch/>. Accessed: 2019-07-25. 22
- [3] Smart and Efficient Local Heating Supply in a City District. <https://www.german-energy-solutions.de/GES/Redaktion/EN/News/2019/20190711-bestheatnet.html>. Accessed: 2019-08-03. 23
- [4] Smart Heat Grid Hamburg. <https://www.hamburgenergie.de/ueber-uns/unternehmen/forschungsprojekte/smart-heat-grid-hamburg-en/>. Accessed: 2019-08-03. 23
- [5] T. Aboul-Seoud and J. Jatskevich. Dynamic Modeling of Induction Motor Loads for Transient Voltage Stability Studies. In *2008 IEEE Canada Electric Power Conference*, pages 1–5. IEEE, 2008. 77
- [6] A.-C. Agricola, B. Höflich, P. Richard, J. Völker, C. Rehtanz, M. Greve, B. Gwisdorf, J. Kays, T. Noll, J. Schwippe, A. Seack, J. Teuwsen, G. Brunekreeft, R. Meyer, and V. Liebert. dena-Verteilnetzstudie. Ausbau-und Innovationsbedarf der Stromverteilnetze in Deutschland bis 2030. *Deutsche Energie-Agentur GmbH (dena). Energiesysteme und Energiedienstleistungen.*, 2012. 15, 17, 18, 19
- [7] P. Ailliot, D. Allard, P. Naveau, C. D. Beaulieu, and R. Cedex. Stochastic Weather Generators: An Overview of Weather Type Models. pages 1–14, 2015. 93
- [8] P. Anderer, U. Dumont, S. Heimerl, A. Ruprecht, and U. Wolf-Schumann. Potenzialermittlung für den Ausbau der Wasserkraftnutzung in Deutschland als Grundlage für die Entwicklung einer geeigneten Ausbaustrategie. *Studie im Auftrag des Bundesministerium für Umwelt, Naturschutz und Reaktorsicherheit*, 2010. 15, 18
- [9] S. Apipattanavis, G. Podesta, B. Rajagopalan, and R. W. Katz. A Semiparametric Multivariate and Multisite Weather Generator. 43(2), 2007. 93

- [10] Arbeitsgemeinschaft Energiebilanzen. Energiedaten: Gesamtausgabe. URL: <https://www.bmwi.de/Redaktion/DE/Artikel/Energie/energiedaten-gesamtausgabe.html>, 2018. 15, 16, 17, 18
- [11] A. Arif, Z. Wang, J. Wang, B. Mather, H. Bashualdo, and D. Zhao. Load Modeling—A Review. *IEEE Transactions on Smart Grid*, 9(6):5986–5999, 2018. 77
- [12] A. Bagherian and S. M. Tafreshi. A Developed Energy Management System for a Microgrid in the Competitive Electricity Market. In *2009 IEEE Bucharest PowerTech*, pages 1–6. IEEE, 2009. 21
- [13] G. A. Baigorria and J. W. Jones. GiST: A Stochastic Model for Generating Spatially and Temporally Correlated Daily Rainfall Data. *Journal of Climate*, 23(22):5990–6008, 2010. 93
- [14] M. Barnes, A. Dimeas, A. Engler, C. Fitzer, N. Hatziaargyriou, C. Jones, S. Papathanassiou, and M. Vandenberg. Microgrid Laboratory Facilities. In *2005 International Conference on Future Power Systems*, pages 6–pp. IEEE, 2005. 22
- [15] B. P. Bhattarai, M. Lévesque, M. Maier, B. Bak-Jensen, and J. R. Pillai. Optimizing Electric Vehicle Coordination over a Heterogeneous Mesh Network in a Scaled-Down Smart Grid Testbed. *IEEE Transactions on Smart Grid*, 6(2):784–794, 2015. 22
- [16] R. Billinton. Consideration of Multi-State Weather Models in Reliability Evaluation of Transmission and Distribution System. (May):619–622, 2005. 93
- [17] M. Bindi, F. Miglietta, and G. Zipoli. Different Methods for Separating Diffuse and Direct Components of Solar Radiation and their Application in Crop Growth Models. *Climate Research*, pages 47–54, 1992. 98
- [18] Bundesministerium für Verkehr und digitale Infrastruktur. Verkehr in Zahlen 2017/2018 46. Jahrgang. URL: <https://www.bmwi.de/Redaktion/DE/Artikel/Energie/energiedaten-gesamtausgabe.html>, 2018. 17
- [19] Bundesnetzagentur. EEG in Zahlen 2017. 2018. 18
- [20] F. Cappello, E. Caron, M. Dayde, F. Desprez, Y. Jégou, P. Primet, E. Jeannot, S. Lanteri, J. Leduc, N. Melab, et al. Grid'5000: A Large Scale and Highly Reconfigurable Grid Experimental Testbed. In *The 6th IEEE/ACM International Workshop on Grid Computing, 2005.*, pages 8–pp. IEEE, 2005. 22
- [21] R. Cespedes. A Reference Model for the Electrical Energy System Based on Smart Grids. In *2012 Sixth IEEE/PES Transmission and Distribution: Latin America Conference and Exposition (T&D-LA)*, pages 1–6. IEEE, 2012. 20
- [22] F. Christange. ESMIF: Energy-System-Model Interconnection Framework Concept. In *technical report for MSE Colloquium 'Advances in Energy Transition'*, 2018. 20, 25, 28

- [23] F. Christange and T. Hamacher. Analytical Modeling Concept for Weather Phenomena as Renewable Energy Resources. In *2016 IEEE International Conference on Renewable Energy Research and Applications (ICRERA)*, pages 273–278. IEEE, 2016. 93, 94, 99
- [24] F. Christange, A. Stadler, and T. Hamacher. Mathematical Description of a Fundamental Transient Electric Load Model of Households. In *2019 IEEE Milan PowerTech*, pages 1–6. IEEE, 2019. 76, 77
- [25] M. H. Cintuglu, O. A. Mohammed, K. Akkaya, and A. S. Uluagac. A Survey on Smart Grid Cyber-Physical System Testbeds. *IEEE Communications Surveys & Tutorials*, 19(1):446–464, 2017. 22
- [26] R. De Coninck and L. Helsen. Quantification of Flexibility in Buildings by Cost Curves—Methodology and Application. *Applied Energy*, 162:653–665, 2016. 20
- [27] R. W. De Doncker. Power Electronic Technologies for Flexible DC Distribution Grids. In *2014 International Power Electronics Conference (IPEC-Hiroshima 2014-ECCE ASIA)*, pages 736–743. IEEE, 2014. 22
- [28] P. Donner, F. Christange, and M. Buss. Fundamental Dynamics Based Adaptive Energy Control for Cooperative Swinging of Complex Pendulum-Like Objects. In *2015 54th IEEE Conference on Decision and Control (CDC)*, pages 392–399. IEEE, 2015. 77
- [29] W. El-Baz, F. Sänger, and P. Tzscheutschler. Hardware in the Loop (HIL) for Micro CHP Systems. In *Proceedings of the Fourth International Conference on Microgeneration and related Technologies, Tokyo, Japan*, pages 28–30, 2015. 23
- [30] W. El-Baz, P. Tzscheutschler, and U. Wagner. Experimental Study and Modeling of Ground-Source Heat Pumps with Combi-Storage in Buildings. *Energies*, 11(5):1174, 2018. 23
- [31] A. Engler. Applicability of Droops in Low Voltage Grids. *International Journal of Distributed Energy Resources*, 1(1):1–6, 2005. 21
- [32] J. Eto, R. Lasseter, B. Schenkman, J. Stevens, D. Klapp, H. Volkommer, E. Linton, H. Hurtado, and J. Roy. Overview of the CERTS Microgrid Laboratory Test Bed. In *2009 CIGRE/IEEE PES Joint Symposium Integration of Wide-Scale Renewable Resources Into the Power Delivery System*, pages 1–1. IEEE, 2009. 22
- [33] S. Eyerer, C. Schiffelechner, S. Hofbauer, C. Wieland, K. Zosseder, W. Bauer, T. Baumann, F. Heberle, C. Hackl, M. Irl, et al. Potential der hydrothermalen Geothermie zur Stromerzeugung in Deutschland. Technical report, Lehrstuhl für Energiesysteme, 2017. 15, 18
- [34] G. Ferruzzi, G. Cervone, L. Delle Monache, G. Graditi, and F. Jacobone. Optimal Bidding in a Day-Ahead Energy Market for Micro Grid under Uncertainty in Renewable Energy Production. *Energy*, 106:194–202, 2016. 21

- [35] L. G. Franquelo, M. A. Prats, R. C. Portillo, J. I. L. Galvan, M. A. Perales, J. M. Carrasco, E. G. Díez, and J. L. M. Jiménez. Three-Dimensional Space-Vector Modulation Algorithm for Four-Leg Multilevel Converters Using abc Coordinates. *IEEE Transactions on Industrial Electronics*, 53(2):458–466, 2006. 21
- [36] T. Funabashi and R. Yokoyama. Microgrid Field Test Experiences in Japan. In *2006 IEEE Power Engineering Society General Meeting*, pages 2–pp. IEEE, 2006. 22
- [37] N. Gerhardt, F. Sandau, A. Scholz, H. Hahn, P. Schumacher, C. Sager, F. Bergk, C. Kämper, W. Knörr, J. Kräck, et al. Interaktion EE-Strom, Wärme und Verkehr. *Endbericht. Fraunhofer IWES*, 2015. 18
- [38] J. C. Gómez and M. M. Morcos. Impact of EV Battery Chargers on the Power Quality of Distribution Systems. *IEEE Transactions on Power Delivery*, 18(3):975–981, 2003. 22
- [39] J. M. Guerrero, J. Matas, L. G. de Vicuña, M. Castilla, and J. Miret. Decentralized Control for Parallel Operation of Distributed Generation Inverters Using Resistive Output Impedance. *IEEE Transactions on industrial electronics*, 54(2):994–1004, 2007. 21
- [40] J. M. Guerrero, J. C. Vasquez, J. Matas, L. G. De Vicuña, and M. Castilla. Hierarchical Control of Droop-Controlled AC and DC Microgrids—A General Approach Toward Standardization. *IEEE Transactions on industrial electronics*, 58(1):158–172, 2011. 20, 21
- [41] F. Guo, L. Herrera, M. Alsolami, H. Li, P. Xu, X. Lu, A. Lang, J. Wang, and Z. Long. Design and Development of a Reconfigurable Hybrid Microgrid Testbed. In *2013 IEEE Energy Conversion Congress and Exposition*, pages 1350–1356. IEEE, 2013. 23
- [42] C. M. Hackl and M. Landerer. Modified Second-Order Generalized Integrators with Modified Frequency Locked Loop for Fast Harmonics Estimation of Distorted Single-Phase Signals. *arXiv preprint arXiv:1902.04653*, 2019. 21
- [43] S. Hanif, M. Barati, A. Kargarian, H. B. Gooi, and T. Hamacher. Multiphase Distribution Locational Marginal Prices: Approximation and Decomposition. In *2018 IEEE Power & Energy Society General Meeting (PESGM)*, pages 1–5. IEEE, 2018. 21, 31
- [44] N. D. Hatziargyriou, A. Dimeas, A. G. Tsikalakis, J. P. Lopes, G. Karniotakis, and J. Oyarzabal. Management of Microgrids in Market Environment. In *2005 International Conference on Future Power Systems*, pages 7–pp. IEEE, 2005. 21
- [45] J. E. Hay. Calculating Solar Radiation for Inclined Surfaces: Practical Approaches. *Renewable Energy*, 3(4-5):373–380, 1993. 99, 151, 152
- [46] H.-M. Henning and A. Palzer. Was kostet die Energiewende? Wege zur Transformation des deutschen Energiesystems bis 2050. *Fraunhofer ISE*, page 89, 2015. 18

- [47] E. Hossain, E. Kabalci, R. Bayindir, and R. Perez. Microgrid Testbeds Around the World: State of Art. *Energy Conversion and Management*, 86:132–153, 2014. 22
- [48] M. Huber, D. Dimkova, and T. Hamacher. Integration of Wind and Solar Power in Europe: Assessment of Flexibility Requirements. *Energy*, 69:236–246, 2014. 22
- [49] F. Huerta, J. Gruber, M. Prodanovic, and P. Matatagui. A Power-HIL Microgrid Testbed: Smart Energy Integration Lab (SEIL). In *2014 IEEE Energy Conversion Congress and Exposition (ECCE)*, pages 3998–4003. IEEE, 2014. 22
- [50] E. Kabalci, E. Hossain, and R. Bayindir. Microgrid Test-Bed Design with Renewable Energy Sources. In *2014 16th International Power Electronics and Motion Control Conference and Exposition*, pages 907–911. IEEE, 2014. 22
- [51] G. Kerber. *Aufnahmefähigkeit von Niederspannungsverteilnetzen für die Einspeisung aus Photovoltaikkleinanlagen*. PhD thesis, Technische Universität München, 2011. 19
- [52] T. Kietzke. Recent Advances in Organic Solar Cells. *Advances in OptoElectronics*, 2007, 2007. 21
- [53] J.-H. Kim and S.-K. Sul. A Carrier-Based PWM Method for Three-Phase Four-Leg Voltage Source Converters. *IEEE transactions on power electronics*, 19(1):66–75, 2004. 21
- [54] S. Kouro, P. Cortés, R. Vargas, U. Ammann, and J. Rodríguez. Model Predictive Control—A Simple and Powerful Method to Control Power Converters. *IEEE Transactions on industrial electronics*, 56(6):1826–1838, 2009. 21
- [55] B. Lasseter. Microgrids [Distributed Power Generation]. In *2001 IEEE power engineering society winter meeting. Conference proceedings (Cat. No. 01CH37194)*, volume 1, pages 146–149. IEEE, 2001. 19
- [56] R. H. Lasseter. Microgrids. In *2002 IEEE Power Engineering Society Winter Meeting. Conference Proceedings (Cat. No. 02CH37309)*, volume 1, pages 305–308. IEEE, 2002. 19, 20
- [57] R. H. Lasseter, J. H. Eto, B. Schenkman, J. Stevens, H. Vollkommer, D. Klapp, E. Linton, H. Hurtado, and J. Roy. CERTS Microgrid Laboratory Test Bed. *IEEE Transactions on Power Delivery*, 26(1):325–332, 2011. 22
- [58] R. H. Lasseter and P. Piagi. Microgrid: A Conceptual Solution. In *IEEE Power Electronics Specialists Conference*, volume 6, pages 4285–4291. Citeseer, 2004. 20
- [59] N. Lidula and A. Rajapakse. Microgrids Research: A Review of Experimental Microgrids and Test Systems. *Renewable and Sustainable Energy Reviews*, 15(1):186–202, 2011. 22

- [60] G. Lu, D. De, and W.-Z. Song. Smartgridlab: A Laboratory-Based Smart Grid Testbed. In *2010 First IEEE International Conference on Smart Grid Communications*, pages 143–148. IEEE, 2010. 23
- [61] N. Lu, P. Du, P. Paulson, F. L. Greitzer, X. Guo, and M. Hadley. The Development of a Smart Distribution Grid Testbed for Integrated Information Management Systems. In *2011 IEEE Power and Energy Society General Meeting*, pages 1–8. IEEE, 2011. 22
- [62] N. Mahmud and A. Zahedi. Review of Control Strategies for Voltage Regulation of the Smart Distribution Network with High Penetration of Renewable Distributed Generation. *Renewable and Sustainable Energy Reviews*, 64:582–595, 2016. 21
- [63] L. Meng, A. Luna, E. R. Díaz, B. Sun, T. Dragicevic, M. Savaghebi, J. C. Vasquez, J. M. Guerrero, M. Graells, and F. Andrade. Flexible System Integration and Advanced Hierarchical Control Architectures in the Microgrid Research Laboratory of Aalborg University. *IEEE Transactions on industry applications*, 52(2):1736–1749, 2016. 20, 21, 22
- [64] E. A. Mohamed and Y. G. Hegazy. A Novel Probabilistic Strategy for Modeling Photovoltaic Based Distributed Generators. 9(8):864–867, 2015. 93, 94
- [65] N. A. Mohamed and M. A. Salama. A Review on the Proposed Solutions to Microgrid Protection Problems. In *2016 IEEE Canadian Conference on Electrical and Computer Engineering (CCECE)*, pages 1–5. IEEE, 2016. 21
- [66] S. R. Mohanty, S. Sen, N. Kishor, P. K. Ray, and V. P. Singh. Harmonic Compensation in Distributed Generation Based Micro-Grid Using Droop Control Technique. In *2011 5th International Power Engineering and Optimization Conference*, pages 233–237. IEEE, 2011. 21
- [67] S. Monesha, S. G. Kumar, and M. Rivera. Microgrid Energy Management and Control: Technical Review. In *2016 IEEE International Conference on Automatica (ICA-ACCA)*, pages 1–7. IEEE, 2016. 20, 21
- [68] D. E. Olivares, A. Mehrizi-Sani, A. H. Etemadi, C. A. Cañizares, R. Iravani, M. Kazerani, A. H. Hajimiragha, O. Gomis-Bellmunt, M. Saeedifard, R. Palma-Behnke, et al. Trends in Microgrid Control. *IEEE Transactions on smart grid*, 5(4):1905–1919, 2014. 19, 20, 21
- [69] S. Palm and P. Schegner. Static and Transient Load Models Taking Account Voltage and Frequency Dependence. In *2016 Power Systems Computation Conference (PSCC)*, pages 1–7. IEEE, 2016. 77
- [70] D. Papadaskalopoulos, G. Strbac, P. Mancarella, M. Aunedi, and V. Stanojevic. Decentralized Participation of Flexible Demand in Electricity Markets—Part II: Application with Electric Vehicles and Heat Pump Systems. *IEEE Transactions on Power Systems*, 28(4):3667–3674, 2013. 20

- [71] G. Papaefthymiou and B. Kl. MCMC for Wind Power Simulation. *23(1):234–240*, 2008. 93, 94
- [72] R. Pardatscher. *Planungskriterien und Spannungsqualität in Mittel- und Niederspannungsnetzen mit hoher Photovoltaik-Einspeisung*. Dissertation, Technische Universität München, München, 2015. 18, 52
- [73] M. B. Parlange and R. W. Katz. An Extended Version of the Richardson Model for Simulating Daily Weather Variables. pages 610–622, 2000. 93
- [74] F. Z. Peng. Z-Source Inverters. *Wiley Encyclopedia of Electrical and Electronics Engineering*, pages 1–11, 1999. 21
- [75] M. L. Perry and A. Z. Weber. Advanced Redox-Flow Batteries: A Perspective. *Journal of The Electrochemical Society*, 163(1):A5064–A5067, 2016. 21
- [76] E. Planas, A. Gil-de Muro, J. Andreu, I. Kortabarria, and I. M. de Alegría. General Aspects, Hierarchical Controls and Droop Methods in Microgrids: A Review. *Renewable and Sustainable Energy Reviews*, 17:147–159, 2013. 20, 21, 22
- [77] W. Price, H. Chiang, H. Clark, C. Concordia, D. Lee, J. Hsu, S. Ihara, C. King, C. Lin, Y. Mansour, et al. Load Representation for Dynamic Performance Analysis. *IEEE Transactions on Power Systems (Institute of Electrical and Electronics Engineers);(United States)*, 8(2), 1993. 76
- [78] W. Price, C. Taylor, and G. Rogers. Standard Load Models for Power Flow and Dynamic Performance Simulation. *IEEE Transactions on power systems*, 10(CONF-940702-), 1995. 76
- [79] R. C. Qiu, Z. Hu, Z. Chen, N. Guo, R. Ranganathan, S. Hou, and G. Zheng. Cognitive Radio Network for the Smart Grid: Experimental System Architecture, Control Algorithms, Security, and Microgrid Testbed. *IEEE Transactions on Smart Grid*, 2(4):724–740, 2011. 22
- [80] I. T. F. Report. Load Representation for Dynamic Performance Analysis (Of Power Systems). *IEEE Transactions on Power Systems*, 8(2):472–482, May 1993. 22
- [81] K. Roe, D. Stevens, and C. Mccord. High Resolution Weather Modeling for Improved Fire Management. (November), 2001. 93
- [82] M. Saleh, Y. Esa, Y. Mhandi, W. Brandauer, and A. Mohamed. Design and Implementation of CCNY DC Microgrid Testbed. In *2016 IEEE Industry Applications Society Annual Meeting*, pages 1–7. IEEE, 2016. 23
- [83] B. Satish and S. Bhuvanewari. Control of Microgrid—A Review. In *2014 International Conference on Advances in Green Energy (ICAGE)*, pages 18–25. IEEE, 2014. 20, 21

- [84] M. J. Stanovich, I. Leonard, K. Sanjeev, M. Steurer, T. P. Roth, S. Jackson, and M. Bruce. Development of a Smart-Grid Cyber-Physical Systems Testbed. In *2013 IEEE PES Innovative Smart Grid Technologies Conference (ISGT)*, pages 1–6. IEEE, 2013. 22
- [85] S. Talari, M. Yazdaninejad, and M.-R. Haghifam. Stochastic-Based Scheduling of the Microgrid Operation Including Wind Turbines , Photovoltaic Cells, Energy Storages and Responsive Loads. 9:1498–1509, 2015. 94
- [86] G. Turner, J. P. Kelley, C. L. Storm, D. A. Wetz, and W.-J. Lee. Design and Active Control of a Microgrid Testbed. *IEEE Transactions on Smart Grid*, 6(1):73–81, 2015. 23
- [87] C. Wang, X. Yang, Z. Wu, Y. Che, L. Guo, S. Zhang, and Y. Liu. A Highly Integrated and Reconfigurable Microgrid Testbed with Hybrid Distributed Energy Sources. *IEEE Transactions on Smart Grid*, 7(1):451–459, 2016. 22
- [88] H. Wirth and K. Schneider. Aktuelle Fakten zur Photovoltaik in Deutschland. *Fraunhofer ISE*, 2019. 15, 17
- [89] B. Xiao, M. Starke, G. Liu, B. Ollis, P. Irminger, A. Dimitrovski, K. Prabakar, K. Dowling, and Y. Xu. Development of Hardware-in-the-Loop Microgrid Testbed. In *2015 IEEE Energy Conversion Congress and Exposition (ECCE)*, pages 1196–1202. IEEE, 2015. 22
- [90] R. Zamora and A. K. Srivastava. Controls for Microgrids with Storage: Review, Challenges, and Research Needs. *Renewable and Sustainable Energy Reviews*, 14(7):2009–2018, 2010. 20, 21
- [91] A. Zeh, M. Müller, M. Naumann, H. Hesse, A. Jossen, and R. Witzmann. Fundamentals of Using Battery Energy Storage Systems to Provide Primary Control Reserves in Germany. *Batteries*, 2(3):29, 2016. 21
- [92] R. Zhang, V. H. Prasad, D. Boroyevich, and F. C. Lee. Three-Dimensional Space Vector Modulation for Four-Leg Voltage-Source Converters. *IEEE Transactions on power electronics*, 17(3):314–326, 2002. 21
- [93] B. Zhao, X. Zhang, and J. Chen. Integrated Microgrid Laboratory System. *IEEE Transactions on power systems*, 27(4):2175–2185, 2012. 22
- [94] Y. Zhou and C. N.-M. Ho. A Review on Microgrid Architectures and Control Methods. In *2016 IEEE 8th International Power Electronics and Motion Control Conference (IPEMC-ECCE Asia)*, pages 3149–3156. IEEE, 2016. 20, 21
- [95] Y. Zhu, J. Wang, and K. Wu. Open System Interconnection for Energy: A Reference Model of Energy Internet. In *2017 IEEE International Conference on Energy Internet (ICEI)*, pages 314–319. IEEE, 2017. 19